

Polyaniline based Composite for Gas Sensors

Dr. Muktikanta Panigrahi, Dr. Arpan Kumar Nayak

Dr. Muktikanta Panigrahi

Assistant Professor,
PG Department of Materials Science,
Maharaja Sriram Chandra Bhanja Deo
University (MSCBDU),
Keonjhar campus, Keonjhar, Odisha,

Dr. Arpan Kumar Nayak

Assistant Professor,
School of Advanced Sciences,
Vellore Institute of Technology Vellore
(VIT Vellore),
Vellore, 632014, Tamil Nadu, India.



ISBN 978-93-90853-97-7

E-ISBN 978-93-90853-40-3

<https://doi.org/10.34256/ioriip212>

© IOR INTERNATIONAL PRESS. This book is an open access publication. **Open Access** This book is licensed under the terms of the Creative Commons Attribution 4.0 International License (<http://creativecommons.org/licenses/by/4.0/>), which permits use, sharing, adaptation, distribution and reproduction in any medium or format, as long as you give appropriate credit to the original author(s) and the source, provide a link to the Creative Commons license and indicate if changes were made.

The images or other third party material in this book are included in the book's Creative Commons license, unless indicated otherwise in a credit line to the material. If material is not included in the book's Creative Commons license and your intended use is not permitted by statutory regulation or exceeds the permitted use, you will need to obtain permission directly from the copyright holder.

The use of general descriptive names, registered names, trademarks, service marks, etc. in this publication does not imply, even in the absence of a specific statement, that such names are exempt from the relevant protective laws and regulations and therefore free for general use.

The publisher, the authors and the editors are safe to assume that the advice and information in this book are believed to be true and accurate at the date of publication. Neither the publisher nor the authors or the editors give a warranty, expressed or implied, with respect to the material contained herein or for any errors or omissions that may have been made. The publisher remains neutral with regard to jurisdictional claims in published maps and institutional affiliations.

This IOR INTERNATIONAL PRESS imprint is published by the registered company IOR PRESS. The registered company address is: 5/11, Perumal Kovil St, Naickenpalayam, Coimbatore-641020 Tamil Nadu, India.

Preface

In this research work, we have demonstrated the synthesis, spectroscopic characteristics, thermal behaviour and DC conductivity of a few nanostructured composites, substituted conducting polymers (ICPs) and composites of ICPs. The physical properties of aforementioned composites are significantly changed by the doping with HCl, H₂SO₄, HNO₃, H₃PO₄, or acrylic acid. The charge transport properties of these polymeric materials have been studied in detail because of their potential application in gas sensors. In the current work, varieties of conducting polymer based materials such as PANI-ES/Cloisite 20A nanostructured composite, acrylic acid (AA) doped PANI polymer, N-substituted conducting polyaniline polymer, DL-PLA/PANI-ES composites, poly methyl methacrylate (PMMA) based polyaniline composite, and inorganic acid doped polyaniline are successfully synthesized using aniline/aniline hydrochloride as precursors in acidic medium. Particularly, AA based synthesised PANI polymer was found with higher solubility. The spectroscopic, thermal stability, enthalpy of fusion, room temperature DC conductivity and temperature dependent DC conductivity measurements with and without magnetic field was carried out with as-synthesized materials. The FTR/ATR-FTIR spectra indicated the presence of different functional groups in the as-prepared composite materials. The UV-Visible absorption spectroscopic analysis showed the presence of polaron band suggesting PANI-ES form. The Room temperature DC conductivity, temperature variation DC conductivity (in presence and absence of magnetic field), and magnetoresistance (MR) of as-prepared conducting polyaniline based were analysed. The highest room temperature DC conductivity value was obtained from H₂SO₄ doped based composite materials and all prepared conductive composites were followed ohms law. The low temperature DC conductivity was carried out in order to study the semiconducting nature of prepared materials. The Mott type VRH model was found to be well fitted the conductivity data and described the density of states at the Fermi level which is constant in this temperature range. From MR plots, a negative MR was observed, which described the quantum interference effect on hopping conduction. We discuss different gas analytes *i.e.*, NO₂, LPG, H₂, NH₃, CH₄, and CO of conducting polymer based materials.

Editors

Dr. Muktikanta Panigrahi working as an **Assistant Professor** of PG Department of **Materials Science** in Maharaja Sriram Chandra Bhanja Deo University (MSCBDU) Keonjhar campus, Keonjhar, Odisha, India. He has more than 7 years of Teaching and **13 years R & D Experience**. He has completed **M.Sc.** (Chemistry, Ravenshaw University), **M. Tech.** (School of Materials Science & Engineering, IIT BHU, Varanasi) and **PhD degree** (Materials Science Centre, IIT Kharagpur). He has successfully completed **two sponsored project** which is funded by **Government of India**. He has organised **five International/National conferences**. He has guided many more BTech/MTech students. and published **Book Chapters,/SCI Journals,/Proceedings/etc.** He has **six patents** which is credit to the research. He has skilled in the field of Geopolymer; Basification of Industrial wastes Organic Semiconductor, Nanocomposites, Ceramic/Thermoplastic polymer composites, Biodegradable polymer, Gas sensor.



Dr. Arpan Kumar Nayak earned his M.Sc from Jadavpur University, India. Then, he completed his PhD degree from Indian Institute of Technology Kharagpur (IIT-KGP), India under the guidance of Prof. Debabrata Pradhan. He was a post-doctoral fellow at Hanyang University, South Korea. Currently he is working as Assistant Professor at Vellore Institute of Technology, Vellore, India. His current research mainly focuses on the synthesis of various nanostructured materials towards environment and energy applications. He has published more than 40 articles in various international journals. He was assigned as Editor-in-chief in the Journal of Applied Physics and Engineering and Associate editor in Nanoscale report.



Table of Contents

1. Fundamentals on Polyaniline based Composites

Muktikanta Panigrahi, Basudam Adhikari.....1-43

2. Synthesis Methods of Polyaniline Based Composites

Muktikanta Panigrahi, Basudam Adhikari.....44-76

3. Acrylic Acid (AA) Based Polyaniline Composite for Liquified Petroleum Gas (LPG) Sensors

Muktikanta Panigrahi, Basudam Adhikari.....77-105

4. Acrylic Acid (AA) Based Polyaniline Composite for Liquified Petroleum Gas (LPG) Sensors

Muktikanta Panigrahi, Basudam Adhikari.....106-148

5. DL-Polylactide (DL-PLA) Based Polyaniline Composite for Hydrogen Gas Sensor

Muktikanta Panigrahi, Basudam Adhikari.....149-171

6. Poly Methyl Methacrylate (Pmma) Based Polyaniline Composite for Ammonia (Nh3) Gas Sensors

Muktikanta Panigrahi, Basudam Adhikari.....172-190

7. Inorganic Doped DI-Polylactide Polyaniline Based Composite for Methane (Ch4) Gas Sensing

Muktikanta Panigrahi, Basudam Adhikari.....191-201

8. Inorganic Acid Doped Polyaniline Based Carbon Monoxide (Co) Sensor

Muktikanta Panigrahi, Basudam Adhikari.....202-230

Chapter 1

Fundamentals on Polyaniline based Composites

Muktikanta Panigrahi ^{1, *}, Basudam Adhikari ¹

¹ Materials Science Centre, Indian Institute of Technology, Kharagpur, West Bengal, India

*Corresponding author: muktikanta2@gmail.com

Abstract

The background of work carried out highlighting on polyaniline, N-substituted polyaniline and acid-doped polyaniline. The problems associated with this polymer and promises it hold are also discussed. It also provides introduction to the nanocomposites of polyaniline/nanoclays, and polyaniline/polyacrylic acid. As well, we have described the polymer stabilized intrinsically conducting polymer composites. The state of the art polymer stabilised intrinsically conducting composites have been reviewed. At last, we have reviewed on the CH₄ gas sensing since it has been recognized as one of the inflammable gas sensors. The main problem on the CH₄ gas sensor lies on its room temperature operation and detection of low ppm level concentration.

Keywords

Polyaniline, Nanocomposites, N-substituted polymer, Doping, Conductivity, Variable range hopping (VRH), Magnetoresistance, Gas sensor

Introduction

In recent times, polymers are widely used multipurpose materials in different fields due to the some advantageous nature. These are flexibility, tailorability, processability, environmental stability, low cost, light weight, etc. [1]. Polymers are used as electrically insulating materials in various electronic devices such as covering insulating materials on electrical wire, switches, insulating coating on electronic circuit board, etc. [1]. The band gap of these polymers are reported more than 10 eV and also, the surface resistivity is higher than 10¹² ohm.cm [1].

The work on the discovery of conducting polymers began in the year of 1975. First, polyacetylene was discovered by Shirakawa [2] as conducting polymer, which

is called a linear conjugated organic polymer. On the other hand, the material showed metallic conductivity after the doping by iodine, which was reported after the discovery of polyacetylene (PA) [2]. This gave rise to a surge of activity directed towards the exploration of synthesis and characterization of this class of materials, also known as ‘Synthetic Metals’ [3]. The desirable properties of the conducting polymeric materials can be achieved among other processability at the molecular level by modifying the parent monomers.

1. Conducting Polymer

In the conducting polymeric system, it contains a highly delocalized π -electronic structure with alternate single and double bonds. The alternation of bonds generates energy difference between highest occupied molecular orbitals (HOMO) and lowest unoccupied molecular orbitals (LUMO) and it can be readily oxidized or reduced [4]. Intrinsically conducting polymers (ICPs) are also known as ‘synthetic metal’ or simply called ‘synmet’ because of their metallic or near metallic conductivity. The scientific community has shown much interest in this field after the award of Nobel Prize (2000) for the discovery and development of ICPs. ICPs contain alternatively single bond and double bond in the backbone. The π -electrons are loosely bound and it can delocalise throughout the polymer chain [5]. In neutral state, the ICPs become insulator and they become conducting only after incorporation of electron acceptor or electron donator through a process known as ‘doping’. Most of the ICPs show conductivity in semiconducting region (Fig. 1).

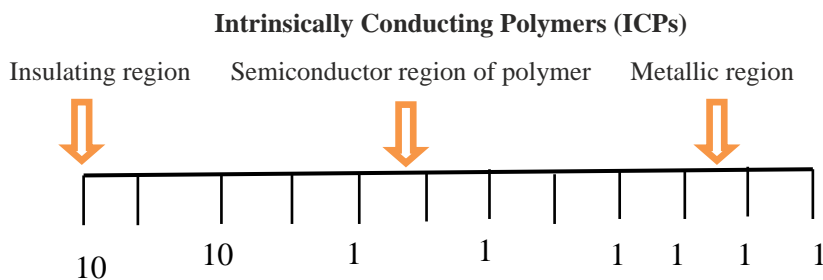
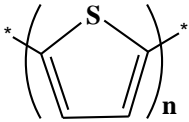
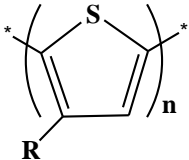
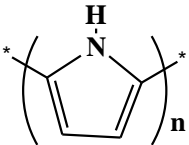
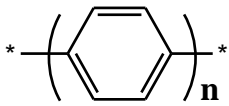
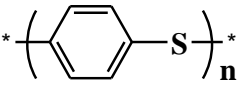
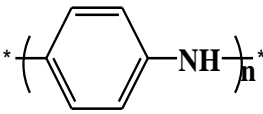


Figure 1. Conductivity of electronic polymeric materials [3]

In the ICP family, PA is the first member and exhibit high conductivity. Although, PA is not environmentally stable but it has led to the discovery of other conducting polymers such as polypyrrole, polythiophene, polyphenylene, polyphenylene vinylene, polyaniline, etc. The molecular structure, doping materials and conductivity (S/cm) of a few ICPs are shown in **Table 1**.

The electrical behavior of these polymers and their derivatives is similar to that of polyacetylene. Moreover, they show higher stability and better processability [3,6]. Of all these conducting polymers, polyaniline (PANI) is now establishing itself as a novel material due to its potential technological applications and low cost of synthesis [7].

Table 1. List of some ICPs with doping materials and conductivity value (S/cm) [5]

Polymer type	Structure	Doping materials	σ (S/cm)
Polyacetylene	$*-(CH)-_n^*$	I ₂ , Br ₂ , Li, Na, AsF ₅	10000
Polythiophene		BF ₄ ⁻ , ClO ₄ ⁻	1000
Poly(3-alkylthiophene)		BF ₄ ⁻ , ClO ₄ ⁻	10000-1000
Polypyrrole		BF ₄ ⁻ , ClO ₄ ⁻	7500-500
Polyphenylene		Li, Na, AsF ₅	1000
Polyphenylene Sulfide		AsF ₅	500
Polyaniline		HCl	200

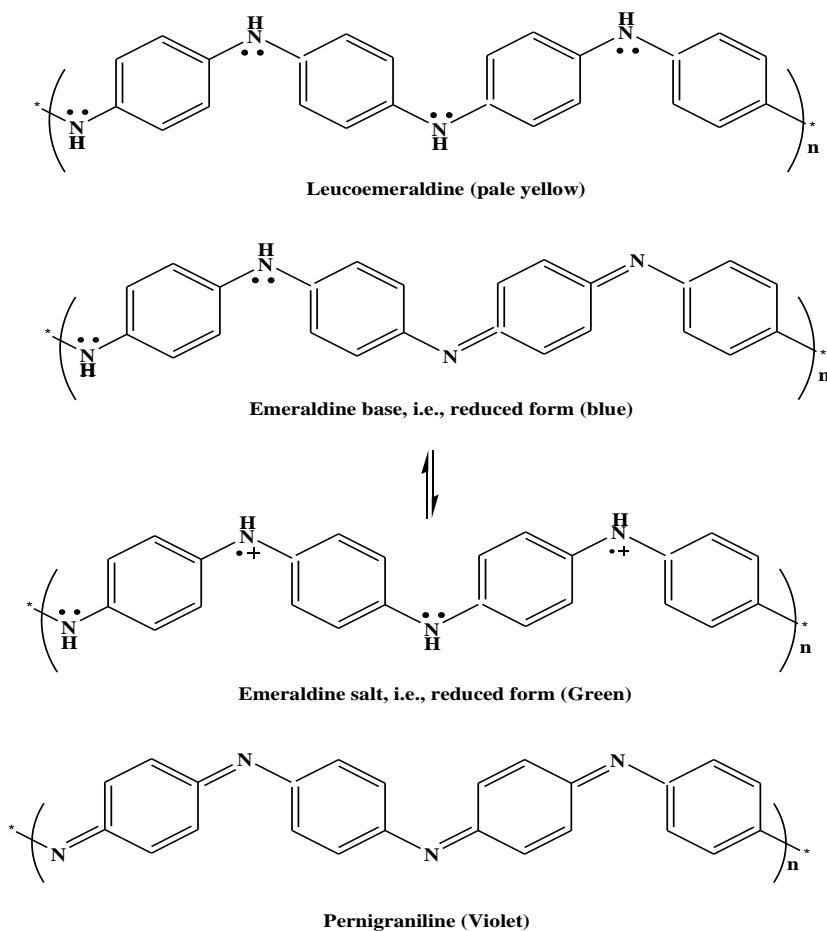
2. Polyaniline (Pani)

PANI has been investigated extensively for few decades. It has attracted special attention towards scientific community/technologist as a conducting material for several important reasons. These are inexpensive; polymerization reaction is straightforward and proceeds with high yield and excellent stability. In early discovery, this product was known as ‘aniline black’ [8]. An attention has been focused on processing, *i.e.*, synthesized easily both by electrochemical and chemical

oxidation processes and sensitivity towards environment due to the proton activity [9].

2.1 Structure of Polyaniline

Green and Woodhead [10,11] have shown PANI as a chain structure which is obtained from aniline molecules and coupled head-to-tail manner at the para position of the phenyl ring. The diversity in physicochemical properties of PANI is attributed to the $-NH-$ group. These properties come from the combination of amine and imine segments present in PANI chains. Amine and imine segments generate several oxidation states and produce different forms of PANI materials. These are fully reduced leucoemeraldine, fully oxidized pernigraniline states, and also other form, which is shown in **Scheme 1**. The different forms of PANI can be readily converted to one another by simple redox methods (Scheme 1.1). Out of several possible oxidation states, the 50 % oxidized emeraldine salt state shows electrical conductivity [12].



Scheme 1. Various possible oxidation states of PANI [12]

2.2. Synthesis Of Polyaniline

There are two principal methods for the synthesis of PANI. The first one is the direct oxidation of aniline by chemical oxidation, *i.e.*, chemical method and the second way is through electro-oxidation on an inert electrode, *i.e.*, electrochemical method. [9, 13-32].

3. Mechanism of Conductivity

The electrical conductivity of doped conducting polymers can be varied up to more than ten orders of magnitude. Charge transport in these polymers has been extensively investigated [29]. All conducting polymers have intrinsic defects which are introduced during polymerization. Removal of a charge from the valance band generates a radical cation whose energy lies in the band gap. Such radical cation which is partially delocalised over some polymer segments is called a 'polaron' Formation of polaron is associated with the distortion of lattice and the presence of two localized electronic states in the gap. According to the model proposed by Brazovski-Kirova [33], formation of a polaron leads to the possibility of three new optical transitions. A bipolaron is also associated with structural deformation and the two charges are not independent but act as a pair. Application of an external electric field makes both polaron and bipolaron mobile via the rearrangement of conjugation.

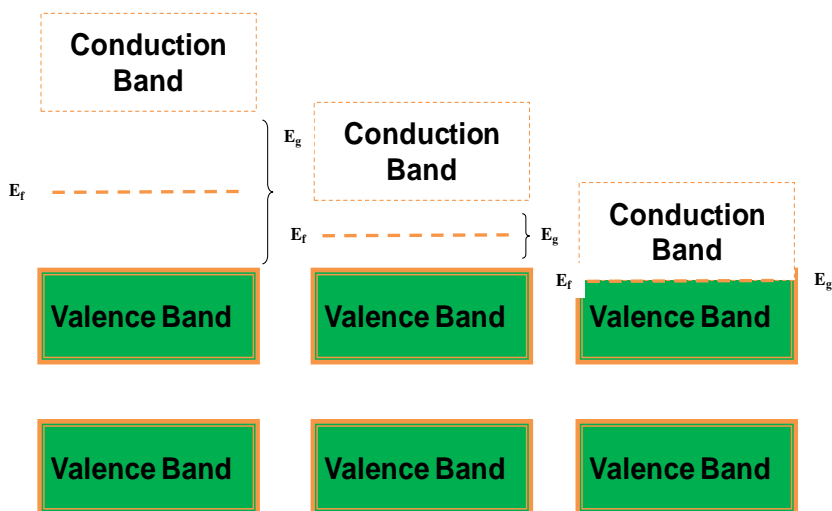
In the case of PANI polymer, the charged species are formed during protonation of the polymer, which are subsequently responsible for the increase in conductivity [20]. Several other mechanisms are also proposed for the conductivity of PANI polymer. Salaneck and co-workers [34,35] studied a one-dimensional variable range hopping or three-dimensional fluctuation-induced tunnelling models.

3.1. Metal-Insulator (M-I) Transition In Doped Conducting Polymer

Heavily doped conducting polymers show many electrical properties. These are electrical conductivity, Pauli temperature independent magnetic susceptibility, etc. The doping of conducting polymers produces in inhomogeneity or phase-segregated regions. Therefore, the conducting polymer contains both crystalline and amorphous regions. The amorphous region affects the transport. As a result, the metallic features in the bulk transport are severely limited due to strong disorder [36]. The disorder can result in localization of states. If the magnitude of the disordered potential is large compared with the bandwidth, all states become localized, and the system will be an insulator. In such a state, there is no gap in the density of states. In insulating state, Fermi level (E_f) lies in an energy interval in which all density of states are localized and is known as Fermi glass. In a Fermi glass, the conductivity is activated. The energy band gap of materials is shown in **Scheme 2**. At high temperatures, the activation energy is a measure of the energy difference between E_f (which lies in the region of localized states) and the mobility edge, whereas, at lower temperatures, variable-range-hopping transport results from the existence of unoccupied localized electronic states near E_f . The M-I transition occurs when the disorder is sufficiently weak that

the mobility edges move away from the center of the band toward the band tails such that E_f lies in a region of extended states.

In M-I transition, the mean free path becomes less than the inter-atomic spacing. This is due to increase in disorder in a metallic system and the coherent metallic transport is not possible [36]. When the disorder is sufficiently weak, the metal shows a transition from the metallic state to insulating state. This transition is known as the Anderson transition, *i.e.*, all the states in a conductor become localized and it converts into a "Fermi glass" [37] with a continuous density of localized states occupied according to Fermi statistics. Although there is no energy gap in a Fermi glass but due to the spatially localized energy states a Fermi glass behaves as an insulator [37]. It has been found that electrical conductivity of a material near the critical regime of Anderson transition obeys power law temperature dependence [36,37].



Scheme 2. Energy band gap of materials

Variety of conducting polymers, *viz.*, polyacetylene, polyaniline, polypyrrole, poly (p-phenylene vinylene), etc. have shown M-I transition. It is very interesting observation because the critical behaviour has been observed over a relatively wide temperature range [36-41]. In the metallic region, the zero temperature conductivity (σ_0) remains finite, and $\sigma(T)$ remains constant as T approaches zero [36-44]. In the critical region, the conductivity follows a power law, whereas in the insulator region, transport occurs through VRH among localized states. The disorder is generally recognized in the physics of "metallic" polymers. Till now, the disorder of the metallic polymer and the nature of the M-I transition are not resolved [36-44].

4. Application of Polyaniline

Depending on the conductivity and electroactivity character, conducting

polymers are being used various applications. They are described as follows;

Group I

In group applications, conductivity of the polymers is the key parameter. Also, the polymers have some characteristics *i.e.*, lightweight, biological compatibility for ease of manufacturing or cost. Therefore, conducting polymer is employed in electrostatic materials, conducting adhesives, electromagnetic shielding, printed circuit boards, artificial nerves, antistatic clothing, piezoceramics, active electronics (diodes, transistors), aircraft structures. These applications discussed briefly as follows;

Electrostatic materials: It is prepared by thin layer coating of conducting polymer on an insulator. it is used to prevent the build-up of static electricity. This is particularly important where such a discharge is undesirable. Such a discharge can be dangerous in an environment with flammable gasses and liquids. It is also dangerous in the explosives industry.

Conducting adhesives: it is prepared by insertion of monomer between two conducting surfaces which is allowed to polymerize. The polymerised monomer is promising to stick between them. It is used to stick the conducting objects and is allowed to pass the electric current through them.

Electromagnetic shielding: Several electrical devices such as computers, generate electromagnetic radiation, often radio and microwave frequencies can cause malfunctions. This problem can be overcome by inside coating of the plastic casing with a conductive surface. So, the emitted radiation can be absorbed by inside coated with conducting surface.

Printed circuit boards: Numerous electrical appliances are used printed circuit boards. In printed circuited board, copper coated epoxy-resins are used. The copper is selectively etched. It is produced conducting lines. These lines are used to connect various devices. The device is placed in holes cut into the resin. In order to get a good connection the holes need to be lined with a conductor. Copper has been used but there is several problems. Therefore, coating method is used. Now, the process is being replaced by the polymerization of monomer. The monomer is formed conducting polymer. Initially the board is etched by potassium permanganate solution. A thin layer of manganese dioxide is formed on the surface of resin. The resin is polymerized by suitable monomer and is produced a layer of conducting polymer.

Artificial nerves: Because of biocompatibility nature of some conducting polymers, they may be used to transport small electrical signals through the body. Therefore, it act as an artificial nerves.

Aircraft structures: In the present scenario, planes and spacecraft are made up with lightweight composites. The structure makes them weak and is to be damaged from lightning bolts. The damaged part can be saved by coating with a conducting polymer. The electricity can be directed away from the vulnerable internals of the

aircraft.

Group II

In group II applications, conducting polymer utilizes the electroactive behaviour. Numerous applications such as molecular electronics, electrical displays, sensors (Chemical, biochemical and thermal), rechargeable batteries, solid electrolytes, drug release systems, optical computers, ion exchange membranes, electromechanical actuators, 'smart' structures, switches are mainly based on electroactive behaviour. Some are discussed below;

Rechargeable batteries: In rechargeable batteries, conducting polymers are potentially used. This is why the conducting polymers have a commercial impact. Some leading companies like BASF/VARTA and Allied Signal are investigated conducting polymer in batteries. The conducting polymers *viz.*, polyacetylene, polyaniline Polythiophene, polypyrrole, etc have been used as electrode materials in rechargeable batteries.

Sensors: Because of electrical nature, conducting polymers are widely used in different sensors (chemical sensors or as gas sensors). In its simplest form of mechanism, sensor materials are absorbed, a particular vapour and affect the conductivity. The change in electrical signal may be due to the presence analytes.

Electrochromic devices: The device convert optical properties of a material by the action of an electric field, the phenomenon is called **Electrochromic devices**. Conducting polymers have an electronic band structure. There is a gap between two energy bands such as valence band and the conduction band. The energy gap determines the optical properties of the conducting polymers. The color changes are produced by doping. Doping is modified the conducting polymer band structure. The first electrochromic materials are used in display panels, sun energy crossing a window, automotive industry, rear view mirrors, etc.

Electromechanical Actuators: Actuation is one of the behaviour of conducting polymers. This means change in volume of conducting polymer by the change of their oxidation state. So, conducting polymers have ability to convert electrical energy into mechanical work.

Drug release systems: Conducting polymers is also used as drug release system by controlled manner. Ions can be selectively released *i.e.*, biologically active ions such as adenosine 5-triphosphate (ATP) and Heparin. The Principle used in the system is potential dependence ion transport. It is an interesting way to deliver ionic drugs to certain biological systems.

Catalyst: Generally, conducting polymers show redox property. So, these are expected to act as redox catalyst. The catalytic behaviour has been controlled by doping. In case of polyaniline and polypyrrole, bonding between transition metal(s) to the nitrogen atoms makes them complexes. This may possible by the interaction between transition metals and a conjugated chain. The characteristics of conjugated

polymers are expected to provide novel catalytic system.

5. Limitation of Conducting Polymer

Though, the conducting polymer has potential application in the different fields as an optoelectronic material instead of inorganic materials, still, it has some limitations. The problems of conducting polymers are related to their synthesis, reproducibility, types of dopant used, processability, and stability. Among these problems, the processability and stability are most prominent.

6. Polymer Nanocomposites

The emergence of polymer nanocomposites is largely based on a consideration in which polymer matrix is reinforced by uniformly dispersed nano-sized particles [51,52]. Polymer nanocomposites can be prepared using a variety of nanomaterials including disk-like nanoparticles (*e.g.*, clay platelets), spherical and polyhedral nanoparticles (*e.g.*, colloidal silica) and nanofibers (*e.g.*, nanotubes, whiskers). There are many reports on polymer nanocomposites with improved properties other than individual components or their macro- and micro-counterpart [51-53].

7. Clay Minerals

The layered clays which can be used for the preparation of polymer nanocomposites may be divided into two types.

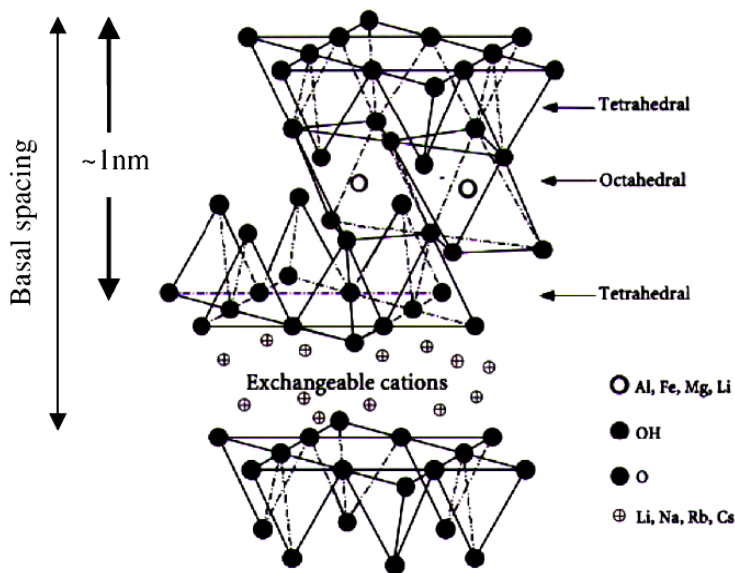


Figure 2. Schematic representation of the clay structure [51]

Table 2. Classification of nanoclays (Phallosilicate) [54,55]

Type of clay	Formula	Origin	Substitution	Layer charge
<u>2:1 type</u>				
MMT	$M_x(Al_{2-x}Mg_xSi_4O_{10}(OH)_2nH_2O$	N	Octahedral	-ve
Hectorite	$M_x(Mg_{3-x}Li_x)Si_4O_{10}(OH)_2nH_2O$	N	Octahedral	-ve
Saponite	$M_xMg_3(Si_{4-x})Al_xO_{10}(OH)_2nH_2O$	N	Tetrahedral	-ve
Fluorohectorite	$M_x(Mg_{3-x}Li_x)Si_4O_{10}F_2nH_2O$	S	Octahedral	-ve
Laponite	$M_x(Mg_{3-x}Li_x)Si_4O_{10}(OH)_2nH_2O$	S	Octahedral	-ve
Fluoromica	$NaMg_{2.5}Si_4O_{10}F_2$	S	Octahedral	-ve
<u>1:1 type</u>				
Kaolinite	$Al_2Si_2O_5(OH)_4$	N	---	Neutral
Halloysite	$Al_2Si_2O_5(OH)_4H_2O$	N	---	Neutral
Hydrotalcite	$Mg_6Al_2(CO_3)(OH)_{16}4H_2O$	S	Octahedral	+ve
<u>Layered silicic acid</u>				
Kanemite	$NaHSi_2O_5.7H_2O$	N/S	Tetrahedral	-ve
Makatite	$Na_2Si_4O_9.5H_2O$	N/S	Tetrahedral	-ve
Octasilicate	$Na_2Si_8O_{17}.9H_2O$	S	Tetrahedral	-ve
Magadiite	$Na_2Si_{14}O_{29}10H_2O$	N/S	Tetrahedral	-ve
Kenyaite	$Na_2Si_{20}O_{44}.10H_2O$	N/S	Tetrahedral	-ve

M indicates exchangeable ions represented by monovalent ions. **Symbols:** *N* (Natural), *S* (Synthetic), -ve and +ve.

One is natural clays (e.g., montmorillonite, hectorite and saponite etc.) and other one is synthesized clays (e.g., fluorohectorite, laponite, mica, magadiite and hydrotalcite). These are presented in **Table 2**. Out of them, both MMT and hectorite are the most commonly used. The hydrotalcite clays are called anionic clay because the layered clay bears negative clay layers. Among the large amount of layered solids, clay minerals especially the members of smectite group are most suitable for the reinforcement of polymer matrix. For the fabrication of clay based polymer nanocomposites, clay materials are used because of their unique structure and high aspect ratio of each clay platelet. The basic structures of nanoclays are composed of layered silicate network. The silanol groups contains hydroxy group in the inter layer

regions, which favour the organic modification by grafting organic functional groups in the interlayer regions (**Fig. 2**) [51-53].

8. Modification of Clay Minerals

Purification and surface modification is essential for the preparation of polymer nanocomposites. This is essential because of their hydrophilic and incompatible nature to most polymers. Therefore, the dispersion of clay minerals in polymer matrix is very difficult. Some parameters of MMT and organically modified nanoclays are presented in **Table 3**.

Table 3. Some parameters of MMT and organically modified nanoclays

OMLS code	Pristine Layered Silicate	d ₀₀₁ (nm)	CEC meq /100g	Modifying group name	Reference No.
MEE	Synthetic clay	2.2	120	Dipoly oxy ethylene alkyl methyl ammonium cation	56
MAE		3.3	120	Dimethyl dialkyl ammonium cation	56
ME100		0.95	120	Unmodified mica	57
30B	Southern clay (Natural clay)	1.85	90	Methyl, tallow, bis-2-hydroxyethyl quaternary ammonium chloride	57
15A		3.15	125	Dimethyl, dihydrogenated tallow quaternary ammonium chloride	58
20A		2.42	95	Dimethyl-2-dihydrogenated tallow, quaternary ammonium	57
25A		1.86	95	Dimethyl, dihydrogenated tallow, 2-ethylhexyl quaternary ammonium	59
93A		2.36	95	Dimethyl, dihydrogenated tallow, ammonium	60
NC		1.17	92	Unmodified MMT	51

MMT indicates montmorillonite. **Abbreviation:** *OMLS* (Organically modifying layered silicate), *CEC* (Chemical exchange cation), *nm* (nano meter), *meq.* (Miliequivalent), and *d* (basal distance), and *NC* (Nanoclay which is unmodified)

9. Conducting Polymer Nanocomposite

When clay minerals are added to a polymer matrix, they form three types of structures, which depend on the nature of the components and processing condition. These are conventional composite, intercalated, and exfoliated nanocomposites. In conventional composite, the components are separated, *i.e.*, phase separated. The properties of such composite are similar to that of micro-particles reinforced polymer composites. In intercalated nanocomposites, the polymer chain is inserted into the clay gallery resulting in a well ordered multilayer stacking morphology. **Fig. 3** shows a diagram of three broad classes of thermodynamically achievable polymer/layered silicate nanocomposites [51].

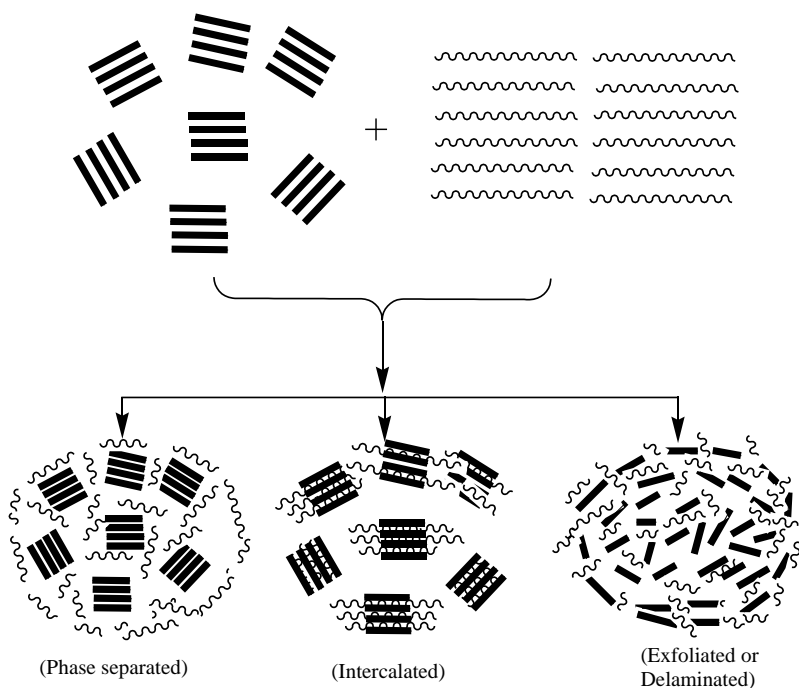


Figure 3. Three typical nanocomposites prepared from conducting polymer and clay minerals: (a) phase separated nanocomposite; (b) intercalated nanocomposite; (c) exfoliated or delaminated nanocomposite [51]

Several techniques are followed for the preparation of nanocomposites, which predominantly includes chemical and electrochemical techniques [61]. Nanomaterials are encapsulated in various ways *viz.*, *ex situ*, *in situ*, and *core-shell*.

9.1. *Ex Situ* Nanocomposites

In *ex situ* technique the inorganic nanoparticles are dispersed in a monomer and then polymerised to form conducting polymer nanocomposites [62]. The

inorganic nanoparticles are encapsulated in the conducting polymer matrix during polymerization in the same reaction vessel [62]. Variety of conducting polymer nanocomposites have been prepared using polyaniline (PANI) [63], polypyrrole (PPy) [64], polyphenylene vinylene (PPV) [65], poly (3,4-ethylenedioxythiophene) (PEDOT) [66] as hosts for inorganic metal, metal oxide and ceramic nanoparticles as guest materials.

9.2. Core-Shell Conducting Polymer Nanocomposites

Among the inorganic-organic nanocomposites, the *core-shell* structures have attracted much more scientific interest and have become more popular leading to some interesting nanocomposite synthesis.

Table 4. Selected conducting polymer/clay nanocomposites

Polymer	Layered clay	Synthesis method	Structure of nanocomposite	Reference No.
olyaniline	MMT CdS	Emulsion	intercalation	70
		Micro-emulsion	intercalation	71
		<i>in situ</i>	intercalation	61
		<i>ex situ</i>	Not mention	61
		Chemical-oxidation	Not mention	61
	Om-MMT	Dispersion	Exfoliation/ intercalation	51
	Maghnite-H+	<i>in situ</i>	intercalation	72
	Cloisite 15A	<i>in situ</i>	Not mention	73
Polypyrrole	MMT	Chemical-oxidation		74
	Bentonite	Chemical-oxidation	intercalation	75
	Hydroxy appatite	Electropoly-merization	Not mention	76
	VMT	Chemical-oxidation	intercalation	77
Polythiophene	Modified MMT	<i>in situ</i>	intercalation	64

In this technique, different metal and metal oxide nanoparticles are encapsulated in the core of conducting polymers. *Core-shell* structured silica (SiO_2) nanoparticles based PANI and Ppy nanocomposites were synthesized in stable colloidal forms, where SiO_2 was used as the core [67]. Colloidal PPy-Au *core-shell* structured nanocomposites have been synthesized by a template-guided polymerization technique [68]. Deng and co-workers have reported the synthesis of *core-shell* structured ferromagnetic (Fe_3O_4)-cross linked PANI nanocomposites. This composite shows *core-shell* morphology in aqueous solution [69]. Layered clays, synthesis method, structure of nanocomposites of selected conducting polymer/clay based nanocomposites are presented in **Table 4**.

Hematite/silica/polypyrrole ($\text{Fe}_2\text{O}_3/\text{SiO}_2/\text{PPy}$) ellipsoidal sandwich composite spheres as well as SiO_2/PPy ellipsoidal hollow capsules with movable hematite as cores and Ppy as shell were successfully fabricated by *core-shell* technique [67]. Polypyrrole-coated silver nanocomposite have been synthesized by one step aqueous chemical oxidation dispersion polymerization technique from pyrrole monomer using silver nitrate as an oxidant [78]. Electromagnetic functionalized *core-shell* nanocomposites of polypyrrole (PPy) were prepared by a self-assembly process [78]. Yang *et al.* have reported that they prepared novel sunflower-like organic-inorganic composites using smaller conductive polypyrrole and spherical silica particles through an *in situ* route by self-assembly polymerization process. For this preparation chitosan was employed as a modifying agent on silica surface [79]. Polypyrrole (PPy)-coated Ag composites were synthesized by interfacial polymerization process in the presence of polyvinyl pyrrolidone (PVP) by Feng *et al.* [78]. *Core-shell* nanocomposites of CuO/PANI [80], $\text{Fe}_2\text{O}_3/\text{PANI}$ [80], $\text{In}_2\text{O}_3/\text{PANI}$ [80] and $\text{Fe}_2\text{O}_3/\text{SiO}_2/\text{PANI}$ [80] were successfully prepared using a double-surfactant-layer assisted polymerization method. Chuang and Yang [81] have reported the preparation of CeO_2/PANI (CeO_2/PANI) *core-shell* nanocomposites via chemical oxidation method using aniline as monomer and CeO_2 as an oxidant as well as nanomaterials. Synthesis of metallic copper nanoparticle coated with polypyrrole was very recently reported by Kobayashi *et al.* [82].

9.3. Solution Casting

In this technique, homogenous dispersion of organoclay (Na^+ MMT) was added to solution of ammonium salt of hexadecylamine. The solution was spread onto a glass plate and the solvent was evaporated by taking appropriate time for drying to form nanocomposite [83].

10. Solubility of Polyaniline

10.1. Solubility

The acid doped form of PANI is insoluble in aqueous solutions as well as in most common organic solvents, but soluble in concentrated sulphuric acid [84]. When the emeraldine salt of PANI is deprotonated to form the insulating emeraldine base of

PANI, it can be solubilized in a number of organic solvents [85], such as N-methyl pyrrolidone (NMP), dimethyl formamide (DMF), dimethyl sulphoxide (DMSO), m-cresol, chloroform (CHCl_3) and tetrahydrofuran (THF). The process of dedoping effectively removes the cationic charges upon the conducting polymer backbone and that reduces the ionic character, which is more amenable to dissolution. Gelation of the conducting polymer commonly occurs at high concentrations of the EB solutions. This result helps to increase viscosity due to formation of strong interchain hydrogen bonding between the amine hydrogens and nearest neighbour imine nitrogens. A novel route to solubilize the ES form is by the use of functionalized protonic acid dopants such as sulphonic acids (camphor sulphonic acid, dodecyl benzene sulphonic acid) [86].

10.2. Substituted Polyanilines

Solubility of PANI can be improved by polymerizing a derivative of aniline, particularly by choosing the substituent which has solubilising effect. There are two types of substituents. One substituent occurs at N-atom and other is on the ortho- and meta-position of benzene ring. The different substituents are alkyl [87], alkoxy [88] groups, phosphoric and sulphonic acid [89] groups. The acid group substituted PANI was found to be more soluble, some of them being water soluble and also showing higher thermal stability. Polymerization of substituted anilines can also be carried out either chemically [87] or electrochemically [87]. The major drawback of these rings substituted PANIs is the fact that solubility is achieved at the cost of conductivity [87].

10.3. Functionalized Protonic Acid As Dopant

Cao, Smith, and Heeger [90] synthesised metallic form of PANI using functionalized protonic acids and simultaneously resulted PANI complex soluble in common organic solvents. The functionalized counter ion acts as 'surfactant' and the charged head group is ionically bound to the oppositely charged protonated PANI chain, and the 'tail' is chosen to be compatible with non-polar or weakly polar organic liquids [90]. This is called 'counter-ion' induced processability.

10.4. Blends Of Polyaniline

Conducting blend is another kind of conducting materials, which supports to improve the solubility and that, is found from literatures [91-93]. It is a physical mixture of two or more polymers with different chemical compositions. Improvement of the PANI processability resulted in the fabrication of several types of conductive blends of PANI [91-93]. The main purpose of making blends is to introduce flexibility and toughness to PANI thereby making it melt processable. A phase separation between the two components of the blends leads to decrease of mechanical strength of the material [94]. However, by keeping the PANI composition less than 16 wt%, materials with good flexibility blend can be obtained. Several conductive blends of PANI salt with thermoplastic polymers such as polystyrene [92], polyamides [95],

poly (vinyl alcohol) [96], poly (vinyl chloride) [97], and so forth have been extensively studied.

10.5 Copolymers

Copolymer is another class of materials with improved solubility. It is generally carried out to combine the diverse physicochemical properties of different polymers to form a single polymeric system. Copolymerization of aniline with ring or N-substituted anilines leads to polymers which have conductivity like PANI and solubility of substituted anilines [89,88].

11. Polyaniline Dispersions

Dispersion polymerization is a well known technique for the synthesis of conventional polymer in both aqueous and non-aqueous media [18,98,99]. Colloidal dispersion is one of the widely used and technologically important ways for tackling the problem of poor solubility of PANI [100,101]. Dispersion of PANI is used in the preparation of blend with thermoplastic polymers [47].

12. Polymer Stabilized Polyaniline Dispersions

Various polymeric steric stabilizers such as ethyl cellulose [102], carboxymethyl cellulose [103], poly (vinyl alcohol) [96], poly (vinyl methyl ether) [104], poly (N-vinylpyrrolidone) [105], etc. are employed for the synthesis of PANI in colloidal form or as suspension by chemical polymerization using aniline precursors. According to Armes and co-workers [100], they have synthesized colloidal PANI by chemical grafting of PANI onto several tailor made copolymer surfactants. The resulting polymer (PANI) is insoluble in solvents and its macroscopic coagulation is prevented by steric stabilizers [102]. The possible synthetic routes and the properties of PANI colloids have been reviewed by Stejskal [102]. The morphology and the size of colloidal particles are strongly depended on the steric stabilizer, oxidizing agent and reaction conditions [106]. On the other hand, the use of polymeric stabilizers in PANI drastically lowers the electrical conductivity of PANI [107].

13. Processability

Processability is one of the major issues in the synthesis of conducting polymers for commercial applications in different areas. These applications of conducting polymers like PANIs are limited due to the lacking of solubility and processability. A number of approaches have been investigated to improve the processability of PANI.

Generally, alkyl and alkoxy substituted aniline monomer is polymerized to improve the solubility of the polymer in organic solvents. But, it has a negative influence on the conductivity [87,88]. The first known examples of water soluble

conducting polymers reported in 1987 are the sodium salts of poly -3-(2-ethane sulfonate) thiophene and poly -3-(4-butane sulfonate) thiophene [108]. These polymers are self-doped Polythiophenes. The electrochemical polymerization of aniline carboxylic acid isomers has been recently reported [109]. Poly (o-amino benzyl phosphoric acid) is another type of self-doped conducting polyaniline synthesised and the polymer was soluble in dilute ammonia solution but insoluble in water [110]. Electro-co-polymerization of aniline and o-aminobenzenesulphonic acid formed sulfonated PANI which was soluble in neutral pH [111].

Introduction of sulphonic acid group to the PANI chain makes soluble PANI which is self-doped and is known as Sulfonated PANI (SPAN). By chemical and electrochemical method, methoxyaniline sulphonic acid is polymerized [112-114]. Another type of conducting PANI was synthesised for improving the processability as well as redox-activity over a wide pH range [115-117]. However, these conducting polymers have low electrical conductivity.

In a solution processing route, nanostructured materials were prepared from colloidal dispersions with reasonable conductivity using a range of steric stabilizers. These used different surfactant micelles such as dodecyl benzene sulfonic acid [118], naphthalene sulphonic acid [119], polyethylene oxide (PEO) [120], water soluble polymers such as poly (N-vinyl pyrrolidone) [121], organic dopants [122] and silica colloids [123].

Polyanilines can also be formed using aniline as monomer and polyelectrolytes such as polystyrenesulphonic acid [124], polyacrylic acid [125] and poly (2-acryloamido-2-methyl-1-propane sulphonic acid) [126] as template. The role of the polyelectrolyte template is to align aniline monomer and promote head-to-tail coupling. The polyacid template was thought to provide a low pH for growth of water soluble PANI and also the necessary counter ions for doping PANI to the conducting form [124]. The polymerization reaction rate was faster compared to ordinary chemical polymerization owing to the high local concentration of aniline and hydrogen ions on the template matrix (polyamide) [126]. The use of these non-conducting polyelectrolytes resulted in low electrical conductivity of the water dispersible PANI [127-129].

Recently, PANI nanofibers were synthesised by using interfacial polymerization at aqueous/organic interface or rapid mixing of monomer and oxidant aqueous solutions in controlled ratio [130]. These methods have the advantage of stabilizer-template free polymerization and ease of purification. The nanofibers have diameters between 30 and 50 nm and make relatively stable dispersion at pH around 2-3 [131].

14. POLYANILINE COMPOSITES

The preparation of conducting polymer composite blends with common polymers in order to improve the mechanical properties and processability of ICPs has been investigated [132]. In general, there are two main methods used to produce

composites: synthetic method based on polymerization of aniline in a matrix polymer and blending methods via mixing a previously synthesised polyaniline with a matrix polymer.

15. Gas Sensor

Gas sensor plays an important role in the monitoring and controlling the environment for detection of test gas/analytes present in the environment. The detection of test gas is very important in today's life in many different sectors like industrial, medical, environmental, and domestic to detect toxic and flammable gases [133]. The specific applications of gas sensors are presented in **Table 5**. It provides early warning against harmful agents present in the environment for safety [133]. Without sensors, significant advances in industrial and environmental monitoring, control and instrumentation will not be possible. Hence, the development of reliable and economically fabricated devices is essential. Directly, this allows to sense these species with high efficiency and rapid analysis, which help the mankind for healthy life. The interaction between the test gas and the sensor surface can be detected measurement of change in resistance, capacitance, work function, mass, optical characteristics, etc.

Table 5. Specific applications of gas sensors in different areas

Application Areas	Purpose of Gas sensing
Indoor air quality monitoring	Cooking gas leakage monitoring, air quality control, monitoring heat ventilation and air conditioning (HVAC) system
Human safety	Inflammable and toxic gas detection, smoke detection, hydrogen detection in aerospace, methane leak detection, detection of explosive materials
Food industries	Monitoring microbial, fungal attack of food, packaging quality control
Automobile industries	Fuel to oxygen ratio determination, car ventilation system control, NOx detection, HVAC control
Health care	Breath analysis, disease detection

Environment may contain corrosive or contaminating species, which can seriously interfere with sensor operation and ultimately it reduces the sensor performances. Accordingly, sensor technology has continued to achieve adequate sensitivity, selectivity, reproducibility, and stability at reasonable cost [134,135].

Gases are key targets in many industrial and domestic activities requiring the precise measurement or control. This has been stimulated by a series of clean air laws, which have or are being legislative on the international, national, state and local levels. To meet these demands, the sensitivity, selectivity and stability of conventional

sensors need to be drastically improved. To achieve these goals, attention is being focused on several approaches such as research on novel sensing materials, use of catalysts and promoters, surface modification of sensor, multi-sensor array systems, data processing methods (FFT and wavelet transform, pattern recognition), fabrication techniques, optimization of sensor performance with the use of nanotechnology.

Conducting polymers are of increasing importance in the development of sensors due to their potential nature. These are room temperature operation, low fabrication cost, ease of deposition onto a wide variety of substrates and their rich structural modification chemistry [136]. Among the conducting polymer family, PANI is one of the most highly studied gas sensing materials because of its simple synthesis, environmental stability and straightforward redox doping/dedoping chemistry to control conductivity [137]. PANI nanofibers possess higher aspect ratio, *i.e.*, surface to volume ratios [138] and permit easier addition of surface functionality and interaction compared with traditional PANI which is highly agglomerated. In addition, PANI nanofibers have a cylindrical morphology and form porous structures when deposited as thin films. This structure allows the diffusion of gas molecules into and out of the PANI film. As a result, most reports indicate that nanostructured PANI performs the gas sensing applications [139].

The sensitivity of conventional PANI film-based sensor depends on the film thickness [140]. On the other hand, sensitivity of a PANI nanofiber-based sensor is independent of film thickness. This is due to the porous structure of the PANI film which leads to diffuse gas molecules on the surface of sensor and dominating the sensor response. The thickness plays the important role in the fabrication of sensor and produces the reproducible responses [140]. A gas sensor can be described as a device, which upon exposure to a gas alters one or more of its physical properties (*e.g.*, mass, electrical conductivity or capacitance) in a way that can be measured and quantified directly or indirectly [141]. Structurally, every gas sensor consists of a physical transducer and a sensitive layer. Usually, the sensitive layer which is in contact with the environment is laid down on top of the transducer platform. At the sensitive layer, the gas molecules interact chemically with the surface, producing a change in physical/chemical properties. These changes are measured by the transducer resulting in the output electrical signals [142]. Gas sensors can be classified according to their operating principle or material use, each class having different parameters.

15.1 Types of Gas Sensor

There are a huge number of sensors using a wide variety of methods and technologies with which gas species can be analysed both quantitatively and qualitatively. All of these methods aim to provide accurate, stable, high resolution, low cost sensing. Therefore, when selecting an approach, it is essential to account for temperature, humidity, shock and vibrations. All these factors can greatly impact on the sensors' performance [143]. Gas sensors can be classified according to the materials used on the surface of the transducer, such as metal oxide semiconductor (MOS), conducting polymer, etc.

15.2 Conductometric Gas Sensors

Conducting polymers are widely used in gas sensor, based on the electrical conduction mechanism (*e.g.*, chemoresistors) [144,145]. They consist of two electrodes with the polymer film in between. They are usually operated at room temperature (low-power). Many commercialized sensors are based on this principle. The related technologies such as fabrication technique and measuring type are established. Thick films, thin films, fibers and bulk materials can be utilized as the sensing elements of a chemiresistor and the output signal is resistance or current or which are facile to measure. The chemiresistor is formed by patterning metal interdigitated transducers (IDTs) on any insulating substrate such as alumina and silicon. The chemiresistor also contains a micro-heater fabricated on the opposite side of the IDT pattern for semiconducting metal oxides. Both semiconducting metal oxides and conducting polymers are chosen for the sensing materials as their conductivity is changed in presence of specific gas molecules. Conductometric sensors have very good linearity and can measure large or small gas concentrations (ppm to ppb ranges) as well as requiring less calibration than other sensors and ability to operate in the continuous presence of a gas.

15.3 Conducting Polymer (Cp) Based Sensors

Polymer based gas sensors measure resistance changes in thin film structures. Among the conducting polymer family, PANI and PPy are possibly the most studied polymers for sensor applications due to their simple synthesis, environmental stability and straightforward doping/dedoping characteristics to control the conductivity [137]. For sensing applications, the suitable polymers have conjugated π -electron system along the polymer backbone. However, the choice of the polymer is limited to ICPs or those which can be made conducting by doping the polymer with counter ions using reducing or oxidising processes. Conducting polymeric layers can be incorporated in many different types of transducers, including conductometric, SAW and optical transducers [146,147]. For sensing measurement, usually a thin polymer film is directly deposited onto the sensor substrate by electrochemical or chemical polymerization. Drop casting, dip and spin coating, screen printing, layer by layer self assembled and Langmuir-Blodgett (LB) technique can also be used to deposit thin films onto the substrates [147]. Conducting polymer sensors operate at room temperature. Their advantages also include high sensitivity, small size, low production costs and ease of deposition on a wide variety of substrates [148]. Disadvantages include the reproducibility of fabrication, strong humidity interference, and base line drift over time due to oxidation processes or changes in the conformation by exposure to inappropriate compounds. The sensitivity of these type of sensors can be altered over a wide range by incorporating functional side groups to the polymer backbone, the selection of doping ions, variation of polymer chain length, condition of the polymerization and the use of nanostructured forms [148]. Among these options, the nanostructured forms of polymer appear to be the most promising to develop highly sensitive and stable gas sensor.

More attention has been devoted to increase the sensitivity, response time and stability of the gas sensors by modifying the sensing materials. Varieties of conducting polymers such as PPy, PTh and PANI have been used as the active materials in the sensors and are mentioned in **Table 6**.

Table 6. Conducting polymer composite used in gas sensors

Conducting polymer	Second component	Texture	Reference
PPy	PS	Blend	[157]
	High density polyethylene (HDPE)	Blend	[158]
	PEO	Blend	[159]
	PVA	Blend	[160]
	PMMA	Coated	[161]
	PMMA	Coated	[162]
	Poly(etheretherketone) (PEEK)	Blend	[162]
	PVDF	Blend	[163]
	PVAc	Blend	[164]
	PVC	Coated	[164]
	Poly (acrylonitrile-co-butadiene-co-stryrene) (ABS)		[158]
PTh	4-t-butyl-Cu-phthalocyanine	Blend	[165]
PANI	PS	Blend	[166]
	PVA	Blend	[167]
	PMMA	Blend	[168]
	PVDF	Coated	[169]
	Poly (butyl acrylate-co-vinyl acetate) (PBuA-VAc)	Blend	[170]
	PP + Carbon black + Thermoplastic PU	Blend	[171]
	PS + Carbon black + Thermoplastic PU	Blend	[172]
	Ethylene vinyl acetate copolymer (EVA)/copolyamide (CoPA)		[173]
	Nylon 6		[174]

The introduction of side chains to the backbones of conducting polymers has two effects. Firstly, most of the side chains are able to increase the solubility of conducting polymers. This helps to process into the sensing film by LB technology, spin coating, ink-printing or other solution-assistant method. Secondly, the functional chains can regulate the properties of conducting polymers as well as it creates space

between molecules [149] or dipole moments [150], or bring additional interactions with analytes. Because of this, it may enhance the response, shorten the response time, or produce sensitivity to other gases. Many sensors employ substituted or copolymerized conducting polymers as the active materials. Dopants can influence the physical and chemical properties of the conducting polymers. Conducting polymers doped with different ions may give distinct responses to a specific analyte. PANI doped with small inorganic ions showed a resistance increase to ammonia, while acrylic acid doped PANI exhibited an inverse response [151]. It should be mentioned that different dopants in a sensing system shows the different dopants activity. The % Response is estimated by the ratio of change of resistance ($\Delta R = R - R_0$) and initial resistance (R_0). High conductivity resulted in a low initial resistance R_0 and high relative response ($\Delta R/R_0$) [152]. Camphorsulphonic acid (CSA) doped PANI shows better response compared to those doped with diphenyl phosphate (DPPH) and maleic acid (Mac) for the detection of water vapor [153]. Hong et al. [154] studied the reversibility of PANI based chemiresistor, and found that strong acid dopants resulted in better reversibility, while a worse response. Differences in sensing performances between Cl^- , SO_4^- and NO_3^- doped Ppy composites were also studied [155]. Further, de Souza et al. [156] tried to find the relationship between the response and the molecular sizes of dopants.

The functions of incorporating another component into the conducting polymers are manifold. We can classify these sensors according to sensing mechanisms. In the composites, the second components play an important role in sensing process. They may improve the properties of sensing film (*i.e.*, partition coefficient [175]), help in electron or proton transfer [176], or directly interact with analytes by swelling [177] or electron/proton exchange [177]. As well, the second components are introduced only to improve the device configuration, *e.g.*, change the morphology of the film, which is expected to influence the performance of the sensors [178,179], improve the mechanical property [180] or protect sensing film [170]. The content of the conducting polymer will also influence the performance of the sensor [181-183].

16. Device Fabrication

For sensors, a thin film active layer is most suitable. However, morphology change of sensing layer can strongly influence the performances of sensor. These effects are usually attributed to be the results of changing the ratio of surface area to volume (aspect ratio) [184]. A film with higher aspect ratio makes analyte molecules to diffuse and interact with the sensing layer more easily, which lead to a higher sensitivity and shorter response time. The materials used in the device may be in the form of thin or porous film [185-187]. In porous film, the volume ratio of micropores increases and is able to enhance the response [179]. The reverse effect is insensitive to its thickness [186]. Thin film fabricated by LB technique was also used [188,189]. Other than the LB technique, spin coating, dip coating, sputtering technique were employed. Fibers, wires, tubes, etc. in nanoregime have high aspect values. So, they

are perfect candidates for preparing sensors with high sensitivities and fast responses [190-197]. Chemical modification of the surface of PANI can be done by grafting onto Si with good adherence [198]. These technologies are useful in the fabrication of electrochemical sensors.

17. Working Environment

The temperature at which a sensor can perform is most important. Like semiconductors, the conductance of conducting polymers increases with the increase of temperature. For a chemiresistor, the initial conductance of conducting polymer is changed as the temperature alters [199,200]. However, the change of initial value is not the key issue. Other than the temperature, the influence of humidity, pressure, introducing hydrophobic substituted groups on polymer backbone reduces the sensor performance [201,202]. When designing a chemiresistor, the influence of current also should not be neglected. Stronger current flow through conducting polymer will produce heat, which can affect the response as described above [203].

18. Sensing Principle

The proposed sensing mechanism of PANI for CH₄ is mainly based on the interaction phenomenon due to the presence of active sites in PANI chains. Still the mechanism is not fully clear. It is believed that CH₄ interacts with oxygen which is present in the environment to form H₂O and the presence of H₂O ruins the ability of PANI to sense the CH₄ [204,205]. This causes the resistance to change. It is detected by transducer by signal as resistance. Understanding the sensing properties of PANI depends on the reversible binding of the target molecule with the sensing film and the minimal interaction between sensing material and the chemical species which may be present in the sensed environment. Therefore, a molecular level understanding of the sensing mechanism can provide adequate information for the sensitivity and selectivity issues induced by analyte, moisture and temperature changes.

19. Measurement of The Gas Sensing Characteristics

In *dynamic* method, the sensors are kept in a chamber with continuous flow of gases, this leads more gas molecules over the sensing surface. At elevated temperature (sensor operating temperature) first the sensor is allowed to be exposed in a continuous flow of air (usually controlled by mass flow controllers) to attain a constant base resistance in air. After achieving a fixed sensor resistance in air (R_a) a calculated amount of test / carrier gas mixture is passed through the chamber with same flow rate until it attains a fixed resistance (R_g). Generally the sensor recovery is attained by flushing the sensor with the flow of air. The characteristic sensor parameters and their significance are presented in **Table 7**.

Table 7. Characteristic sensor parameters and their significance

Sensor parameters	Significance
Response (R) (%)	$(R_a - R_g)/R_a$ % or R_a/R_g where R_a and R_g is the resistance of the sensor in presence of air and test gas respectively
Selectivity	Maximum response to a particular gas over other test gases
Response range	The minimum and maximum gas concentration can be detected by a sensing element
Stability	Minimal variation of the base resistance (measured in ambient condition) after repeated response-recovery cycles

20. Advantages of Using Conducting Polymers

The advantages of using conducting polymers as the sensing layers are listed as following.

Room Temperature Operations

For conducting polymer based sensor, the interaction between conducting polymer and gas analyte is rather strong at room temperature. Therefore, this sensor can give remarkable signals. This endows conducting polymer sensors with low energy consumption and simple device configuration.

Facile Property Adjustment

The backbones of common conducting polymers are built up with aromatic rings, which are easy to attach various grafts through electrophilic substitutions. Both substituted conducting polymer, presence of variety of substituents and copolymerizing with different monomers, it is facile to adjust both the chemical and physical properties of conducting polymers. These are useful for promoting selectivity of sensors, and convenient in fabricating sensor arrays. Detection limits of conducting polymers and their composites used for gas sensing are shown in **Table 8**.

High Sensitivity and Short Response Time

The detection limits are rather low for conducting polymer based sensors. For inorganic analytes such as CO, CO₂, NO_x, etc., the detection limit is smaller than 1 ppm, and for organic analytes (CH₄, n-Hexane, etc.), the limit is found about several ppm or lower. The response times of these sensors are usually hundreds of seconds. The response obtained from ultra thin film sensors may be as low as few seconds [206-210].

Easy Device Fabrication

The fabrication of sensors based on conducting polymers is much easier than that based on other sensing materials. Furthermore, by introducing longer side chains on conducting polymer backbone, the solubility of conducting polymers can be greatly improved, which make them to be processed into films from their solutions. The different techniques are employed for making films by casting, layer-by-layer deposition, spin-coating or LB technique.

Long Time Instability and Irreversibility

Stability of the conducting polymer based sensors is a major issue.

Table 8. Detection limits of sensors based on conducting polymers and their composites to several gases

Analyte	Sensing material	Detect limit	Sensor type	Reference
NO ₂	PPy/PET PTh/CuPc	<20 ppm	Chemresistor	[189]
	PANI/In ₂ O ₃	4.3 ppm	Chemresistor	[176]
	PANI/FeAl	<0.5 ppm	SAW	[206]
	PANI/heavy CO]	0.2 ppm	Chemresistor	[207]
	PANI/FeAl	<10 ppm	Chemresistor	[192]
HCl	PANI/In ₂ O ₃	10 ppm	Chemresistor	[208]
H ₂ S	PANI	<60 ppm	SAW	[206]
CO	PANI/Pd	< 25 ppm	Chemresistor	[209]
	Poly(3-methylthiophene)/	<1 ppm	Chemresistor	[210]
Water		Several ppm	Chemresistor	[183]
Methanol	MWNT	<10 ppm	Chemresistor	[211]
Methane halide	PANI/Cu			

The efficiency of the sensors decreased significantly as they were stored in open environment or air for a relatively long time. Many conducting polymers like PANIs are easy to be dedoped when they are exposed to air. This may be considered when designing sensing materials. Another problem is the irreversibility of these sensors, *i.e.*, the response of sensors gradually fall down in the sensing cycles, or the signal cannot return to the original value after exposed to analytes. The mechanism of irreversibility is still not clear now.

The growing areas of conducting polymer based materials are generating many exciting new materials with novel properties. It is therefore, of immense significance to explore whether nanostructures of conducting polymers can lead to better performance and whether reliable and scalable synthetic methods can be developed in order to provide the necessary materials base for both research and applications.

21. Conclusions

Now-a-days, conducting polymer composites are being studied extensively due to their potential applications in sensors, and actuators. For the commercial applications of polymer composites, the synthesis, and processability must be simple, direct and cost-effective, along with improved material properties. In the present work, a variety of materials, *viz.*, hydrophobic nanomaterials (Cloisite 20A), dopants such as HCl, HNO₃, H₂SO₄, H₃PO₄ acrylic acid (AA), polyacrylic acid (PAA), substituted form of aniline, aniline, aniline hydrochloride and thermoplastic polymer as base materials (DL-PLA) are used to prepare several composites.

Acknowledgment

The author conveys their sincere thanks to Materials Science Centre, IIT Kharagpur, West Bengal, India for providing facilities to gather the research work.

References

- [1] Forrest, S.R. (2004), The Path to Ubiquitous and Low-Cost Organic Electronic Appliances on Plastic, *Nature*, Vol. 428, pp. 911-919.
- [2] Shirakawa, H. (2001), Nobel Lecture: The Discovery of Polyacetylene Film-the Dawning of an era of Conducting Polymers, *Reviews of Modern Physics*, Vol. 73, pp. 713-718.
- [3] MacDiarmid, A. G. (2001), Synthetic Metals: A Novel Role for Organic Polymers (Nobel Lecture), *Angewandte Chemie International Edition*, Vol. 40, pp. 2581-2590.
- [4] Moliton, A., and Hiorns, R. C. (2004), Featured Article Review of Electronic and Optical Properties of Semiconducting π -Conjugated Polymers: Applications in Optoelectronics, *Polymer International*, Vol. 53, pp. 1397-1412.
- [5] Bakhshi, A. K., and Bhalla, G. (2004), Electrically Conducting Polymers: Materials of the Twenty-first Century, *Journal of Scientific & Industrial Research*, Vol. 63, pp. 715-728.
- [6] Kumar, D., and Sharma, R. C. (1998), Advance in Conductive Polymers, *European Polymer Journal*, Vol. 34, pp. 1053-1060.
- [7] Miras, M. C., Acevedo, D. F., Monge, N., Frontera, E., Rivarola, C. R., and Barbero, C. A. (2008), Organic Chemistry of Polyanilines: Tailoring Properties to Technological Applications, *The Open Macromolecules Journal*, Vol. 1, pp. 58-73.
- [8] Shao, Z., Rannou, P., Sadki, S., Fey, N., Lindsay, D. M., and Faul, C. F. J. (2011), Delineating Polyachtungtrenung (Aniline) Redox Chemistry by

- Using Tailored Oligo (Aryleneamine)s: Towards Oligo Achtungtrenung (Aniline)-Based Organic Semiconductors with Tunable Optoelectronic Properties, *Chemistry of European Journal*, Vol. 17, pp. 12512–12521.
- [9] Macdiarmid, A. G., Chiang J. C., Richter, A. F. (1987), *Polyaniline: A New Concept in Conducting Polymers*, *Synthetic Metals*, Vol. 18, pp. 285-290.
- [10] Green A. G., and Woodhead A. E. (1910), CCXLIII.-Aniline-black and allied compounds, Part I, *Journal of Chemical Society Transaction*, Vol. 97, pp. 2388-2403.
- [11] Green A. G., and Woodhead A. E. (1912), CXVII.-Aniline-black and allied compounds, Part II, *Journal of Chemical Society Transaction*, Vol. 101, pp. 1117-1123.
- [12] MacDiarmid, A. G. (1992), "The Polyanilines: A Novel Class of Conducting Polymers", *Conjugated Polymers and Related Materials: The Interconnection of Chemical and Electronic Structure*, W.R. Salaneck and I. Lundstrom, Eds., Oxford Scientific Press, UK, (1992).
- [13] Vatani, Z., and Eisazadeh, H. (2012), Synthesis of polyaniline/polystyrene and polyaniline/poly (vinyl chloride) nanocomposite using hydroxy propylcellulose as a surfactant, *Proceedings of the 4th International Conference on Nanostructures (ICNS4) 12-14 March, 2012, Kish Island, I.R. Iran*, pp. 129-131.
- [14] Surwade, S. P., Agnihotra, S. R., Dua, V., Manohar, N., Jain, S., Ammu, S., and Manohar, S. K. (2009), Catalyst-Free Synthesis of Oligoanilines and Polyaniline Nanofibers Using H₂O₂, *Journal of American Chemical Society*, Vol. 131, pp. 12528-12529.
- [15] Chowdhury, P., and Saha, B. (2005), Potassium Dichromate initiated Polymerization of Aniline, *Indian Journal of Chemical technology*, Vol. 12, pp. 671-675.
- [16] Svoboda, J., Bláha, M., Sedláček, J., Vohlidal, J., Balcar, H., Mav-Golež, I., Žigon, M. (2006), (Minireview), *New Approaches to the Synthesis of Pure Conjugated Polymers*, *Acta Chiica Slovenica*, Vol. 53, pp. 407-416.
- [17] Osterholm, J.-E., Cao, Y., Klavetter, F., and Smith, P. (1994), Emulsion Polymerization of Aniline, *Polymer*, Vol. 35, pp. 2902-2906.
- [18] Namgoong, H., Woo, D. J., and Lee, S.-H. (2007), Micro-Chemical Structure of Polyaniline Synthesized by Self-Stabilized Dispersion Polymerization, *Macromolecular Research*, Vol. 15, pp 633-639.
- [19] Zhang, X., Chan-Yu-King, R., Jose, A., Manohar, S. K. (2004), Nanofibers of Polyaniline Synthesized by Interfacial Polymerization, *Synthetic Metals*, Vol. 145, pp. 23-29.
- [20] K. Wilbourn, K., Murray, R.W. (1988), *Electrochemical Doping Reactions*

- of the Conducting Ladder Polymer Benzimidazobenzophenanthroline (BBL), *Macromolecules*, Vol. 21, pp. 89-96.
- [21] Athawale, A. A., Kulkarni, M. V., Chabukswar, V. V. (2002), Studies on Chemically Synthesized Soluble Acrylic Acid Doped Polyaniline, *Materials Chemistry and Physics*, Vol. 73, pp. 106-110.
- [22] Ding, H, Wan, M., and Wei, Y. (2007), Controlling the Diameter of Polyaniline Nanofibers by Adjusting the Oxidant Redox Potential, *Advanced Materials*, Vol. 19, pp. 465-469.
- [23] Shreepathi, S., and Holze, R. (2005), Spectroelectrochemical Investigations of Soluble Polyaniline Synthesized via New Inverse Emulsion Pathway, *Chemistry of Materials*, Vol. 17, pp. 4078-4085.
- [24] Meng, F., Yan, X., Zhu, Y., and Pengchao Si, P. (2013), Controllable synthesis of MnO₂/Polyaniline Nanocomposite and its Electrochemical Capacitive Property, *Nanoscale Research Letters*, Vol. 8, pp. 179-187.
- [25] Lin, Y.-W., and Wu, T.-M. (2009) Synthesis and Characterization of Externally Doped Sulfonated Polyaniline/Multi-Walled Carbon Nanotube Composites, *Composites Science and Technology*, Vol. 69, pp. 2559–2565.
- [26] Nalwa, H. S. (2001), Holze In *Advanced Functional Molecules and Polymers*, (ed.), Gordon and Breach, Tokyo, Vol. 2, pp. 171-xxx.
- [27] Genis, E. M., Boyle, A., Lapkowsky, M. Tsintavis, C. (1990), Polyaniline: A Historical Survey, *Synthetic Metals*, Vol. 36, pp. 139-182.
- [28] Yang, H., and Bard, A. J. (1992), The Application of Fast Scan Cyclic Voltammetry. Mechanistic Study of the Initial Stage of Electropolymerization of Aniline in Aqueous Solutions, *Journal of Electroanalytical Chemistry*, Vol. 339, pp. 423-449.
- [29] Rao, P. S., Sathyanarayana, D. N., and Jeevananda, T. (2001), In *Advanced Functional Molecules and Polymers*, H. S. Nalwa (ed.), Gordon and Breach, Tokyo, Vol.3, p. 79-xxx.
- [30] Bredas, J. L., Street, G. B. (1985), Polarons, Bipolarons, and Solitons of Conducting Polymer, *Accounts of Chemical Research*, Vol. 18, pp. 309-315.
- [31] Heeger, A. J. (2001), Semiconducting and Metallic Polymers: The Fourth Generation of Polymeric Materials (Nobel Lecture) *Angewandte Chemie International Edition*, Vol. 40, pp. 2591-2611.
- [32] Chiang, J. C., and MacDiarmid, A. G. (1986), 'Polyaniline': Protonic Acid Doping of the Emeraldine form to the Metallic Regime, *Synthetic Metals*, Vol. 13, (1986) pp. 193-205.
- [33] Brazovskii, S. A., and Kirova, N. N. (1981), Excitations, Polarons, and Bipolarons in Conducting Polymers, *Soviet Physics: Journal of Experimental*

- and Theoretical Physics Letter, Vol. 33, pp.4-8.
- [34] Wnek, G. E. (1986), A Proposal for the Mechanism of Conduction in Polyaniline Synthetic Metals, Vol. 15, pp. 213-218.
- [35] Lundberg, B., Salaneck, W. R., and Lundström, I. (1987), Pressure, Temperature and Field Dependence of Hopping Conduction in Polyaniline, Synthetic Metals, Vol. 21, pp. 143-147.
- [36] Salaneck, W. R., Lundström, I., Hjertberg, T., Duke, C. B., Paton, A., Conwell, E. M., Huang, W. S., Somasri, N. L. D., Richter, A. F. and MacDiarmid, A. G. (1987), Electronic Structure of some Polyanilines, Synthetic Metals, Vol. 18, pp. 291-296.
- [37] Menon, R., Yoon, C. O., Moses, D., Heeger, A. J., and Cao, Y. (1993), Transport in Polyaniline Near the Critical Regime of the Metal-Insulator Transition, Physical Review B: Condensed matter, Vol. 48, pp. 17685-17694.
- [38] Cho, S., Park, S. H., and Lee, K. (2005), Reflectance Study on the Metal-Insulator Transition Driven by Crystallinity Change in Poly(3,4-Ethylenedioxythiophene)/ Poly(Stylenesulfonate) Films, Journal of the Korean Physical Society, Vol. 47, pp. 474-478.
- [39] Aleshin, A. N. (2010), Charge Carrier Transport in Conducting Polymers on the Metal Side of the Metal-Insulator Transition: A Review, Physics of the Solid State, Vol. 52, pp. 2307-2332.
- [40] Heeger, A. J., (2001), Disorder-Induced Metal-Insulator Transition in Conducting polymers, Journal of Superconductivity: Incorporating Novel Magnetism, Vol.14, pp. 261-268.
- [41] Levyy, O., and Stroudz, D. (1997), Macroscopic Disorder and the Metal-Insulator Transition in Conducting Polymers, Journal of Physics: Condensed Matter, Vol. 9, pp. L599-L605.
- [42] Li, J., Fang, K., Qiu, H., Li, S., and Mao, W. (2004), Micromorphology and Electrical Property of the HCl-doped and DBSA-doped Polyanilines, Synthetic Metals, Vol. 142, pp. 107-111.
- [43] Sheng, P., Abeles, B., and Arie, Y. (1973), Hopping Conductivity in Granular Metals, Physical Review Letters, Vol. 31, pp. 44-47.
- [44] G. T. Kim, M. Burghard, D. S. Suh, K. Liu, J. G. Park, S. Roth, Y. W. Park. 1999. Conductivity and magnetoresistance of polyacetylene fiber network. Synthetic Metals 105, 207-210.
- [45] Ghosh, M., Barman, A., Meikap, A. K., De, S. K., Chatterjee, S., and Chattopadhyay, S. K. (2000) Electrical Resistivity and Magnetoresistivity of Protonic Acid (H₂SO₄ and HCl)-Doped Polyaniline at Low Temperature, Journal of Applied Polymer Science, Vol. 75, pp. 1480-1486.

- [46] Zhang, G., Chu, V., and Conde, J. P. (2007), Electrostatically Actuated Conducting Polymer Microbridges, *Journal of Applied Physics*, Vol. 101, pp. 064507-064514.
- [47] Ouyang, J., and Yang, Y. (2006), Conducting Polymer as Transparent Electric Glue, *Advanced Materials*, Vol. 18, pp. 2141–2144.
- [48] Kim, Y.-Y., Yun, J., Lee, Y.-S., and Kim, H.-Il. (2011), Preparation and Characteristics of Conducting Polymer-Coated MWCNTs as Electromagnetic Interference Shielding Materials, *Carbon Letters*, Vol. 12, pp. 48-52.
- [49] Zheng, Y., He, Z., Gao, Y., and Liu, J. (2013), Direct Desktop Printed-Circuits-on-Paper Flexible Electronics, *Scientific Reports*, Vol. 3, pp. 1-7.
- [50] Cortés, M. T., Moreno, J. C. (2003), Artificial Muscles Based on Conducting Polymers: Review, *e-Polymer*, Vol. xxx, pp. 1-42.
- [51] Das, T. K., and Prusty, S. (2012), Review on Conducting Polymers and Their Applications, *Polymer-Plastics Technology and Engineering*, Vol. 51, pp. 1487–1500.
- [52] Alexandre, M., and Dubois, P. (2000), Polymer-Layered Silicate Nanocomposites: Preparation, Properties and Uses of a New Class of Materials, *Materials Science and Engineering (R)*, Vol. 28, pp. 1-63.
- [53] Binitha, N. N., and Sugunan, S. (2008), Polyaniline/Pillared Montmorillonite Clay Composite Nanofibers, *Journal of Applied Polymer Science*, Vol. 107, pp. 3367–3372.
- [54] Garai, A., Kuila, B.K. and Nandi, A.K. (2006), Montmorillonite Clay Nanocomposites of Sulfonic Acid Doped Thermoreversible Polyaniline Gel: Physical and mechanical Properties, *Macromolecules*, Vol. 39, pp. 5410-5418.
- [55] Uddin, F. (2008), Clays, Nanoclays, and Montmorillonite Minerals, *Metallurgical and Materials Transactions A*, Vol. 39A, pp. 2804-2814.
- [56] Floody, M. C., Theng, B. K. G., Reyes, P., and Mora, M. L. (2009), Natural Nanoclays: Applications and Future Trends–A Chilean Perspective, *Clay Minerals*, Vol. 44, pp.161–176.
- [57] Panigrahi, M., Singh, N. K., Gautam, R. K., Banik, R. M., and Maiti, P. (2010), Improved Biodegradation and Thermal Properties of Poly(lactic acid)/Layered Silicate Nanocomposites, *Composite Interfaces*, Vol. 17, pp. 143–158.
- [58] Peeterbroeck, S., Alexandre, M., Jerome, R., and Dubois, Ph. (2005), Poly(ethylene-co-vinyl acetate)/Clay Nanocomposites: Effect of Clay Nature and Organic Modifiers on Morphology, Mechanical and Thermal Properties, *Polymer Degradation and Stability*, Vol. 90, pp. 288-294.

- [59] Kiliaris, P., and Papaspyrides, C. D. (2010), Polymer/Layered Silicate (Clay) Nanocomposites: An Overview of Flame Retardancy, *Progress in Polymer Science*, Vol. 35, pp. 902-958.
- [60] Lee, S. K., Seong, D. G., and Youn, J. R. (2005), Degradation and Rheological Properties of Biodegradable Nanocomposites Prepared by Melt Intercalation Method, *Fibers and Polymers*, Vol.6, pp. 289-296.
- [61] Wang, K., Chen, L., Wu, J., Toh, M. L., He, C., and Yee, A. F. (2005), Epoxy Nanocomposites with Highly Exfoliated Clay: Mechanical Properties and Fracture Mechanisms, *Macromolecules*, Vol. 38, pp. 788-800.
- [62] Basnayaka, P. A., Ram, M. K., Stefanakos, L., Kumar, A. (2013), Graphene/Polypyrrole Nanocomposite as Electrochemical Supercapacitor Electrode: Electrochemical Impedance Studies, *Graphene*, Vol.2, pp. 81-87.
- [63] Nascimento, G. M. do, Constantino, V. R. L., and Temperini, M. L. A. (2002), Spectroscopic Characterization of a New Type of Conducting Polymer-Clay Nanocomposite, *Macromolecules*, Vol. 35, pp. 7535-7537.
- [64] Kondawar, S. B., Agrawal, S. P., Nimkar, S. H., Sharma, H. J. and Patil P. T. (2012), Conductive Polyaniline-Tin Oxide Nanocomposites for Ammonia Sensor, *Advanced Materials Letter*, Vol. 3, pp. 393-398.
- [65] Meguedad, A, and Benharrats, N. (2012), Thermal Degradation Behavior of Polythiophene-modified Montmorillonite Nanocomposite, *Journal of Analytical Science & Technology*, Vol. 3, pp. 193-201.
- [66] Yoon, S., and Park, H.-H., (2010), Enhancement of the Electrical Properties of Poly (pphenylene vinylene) by the Incorporation of Silicon Dioxide Nanoparticles, *Journal of Applied Polymer Science*, Vol. 117, pp. 700–705.
- [67] Murugan, A.V., Gopinath, C. S., and Vijayamohanan, K. (2005), Electrochemical Studies of Poly (3,4-thylenedioxythiophene) PEDOT/VS₂ Nanocomposite as a Cathode Material for Rechargeable Lithium Batteries, *Electrochemistry Communications*, Vol. 7, pp. 213–218.
- [68] Goswami, L., Sarma, N. S., and Chowdhury, D. (2011), Determining the Ionic and Electronic Contribution in Conductivity of Polypyrrole/Au Nanocomposites, *Journal of Physical Chemistry C*, Vol. 115, pp. 19668–19675.
- [69] Hao, L.-Y., Zhu, C.-L., Jiang, W.-Q., Chen, C.-N., Hu, Y. and Chen, Z.-Y. (2004), Sandwich Fe₂O₃@SiO₂@PPy Ellipsoidal Spheres and Four Types of Hollow Capsules by Hematite Olivary Particles, *Journal Materials Chemistry*, Vol. 14, pp. 2929–2934.
- [70] Deng, J. G., Ding, X. B., Zhang, W. C., Peng, Y. X., Wang, J. H., Long, X. P., Li, P., and Chan, A. S. C. (2002), Magnetic and Conducting Fe₃O₄-Cross-Linked Polyaniline Nanoparticles with Core-shell Structure, *Polymer*, Vol.

43, pp. 2179-2184.

- [71] Ashraf, S. M., Ahmad, S., and Riaz, U. (2006), Synthesis and Characterization of Novel Poly(1-Naphthylamine)-Montmorillonite Nanocomposites Intercalated by Emulsion Polymerization, *Journal of Macromolecular Science, Part B: Physics*, Vol. 45, pp. 1109–1123.
- [72] Khiew, P. S., Huang, N. M., Radiman, S. and Ahmad, M. S. (2004), Synthesis and Characterization of Conducting Polyaniline-Coated Cadmium Sulphide Nanocomposites in Reverse Microemulsion, *Materials Letters*, Vol. 58, pp. 516– 521.
- [73] Abdelkader, A., Amine, H., and Mohammed, B. (2013), Maghnite-H⁺, An Eco-catalyst layered for Synthesis of Polyaniline/Maghnite Nanocomposites, *International Journal of Basic and Applied Sciences*, Vol. 2, pp. 193-199.
- [74] Olad, A., and Rashidzadeh, A. (2008), Preparation and Anticorrosive Properties of PANI/Na-MMT and PANI/O-MMT Nanocomposites, *Progress in Organic Coatings*, Vol. 62, pp. 293–298.
- [75] Rizvi, T. Z., and Shakoar, A. (2009), Electrical Conductivity and Dielectric Properties of Polypyrrole/Na⁺–Montmorillonite (PPy/Na⁺–MMT) Clay Nanocomposites, *Journal of Physics D: Applied Physics*, Vol. 42, pp. 095415-095420.
- [76] Demets, G. J.-F., Anaissi, F. J., Toma, H. E., and Fontes, M. B. A. (2002), Preparation and Properties of Polypyrrole/Bentonite/Vanadium (V) Oxide Ternary Composites, *Materials Research Bulletin*, Vol. 37, pp. 683-695.
- [77] Ma, R., Sask, K. N., Shi, C., Brash, J. L., and Zhitomirsky, I. (2011), Electrodeposition of Polypyrrole-Heparin and Polypyrrole-Hydroxyapatite Films, *Materials Letters*, Vol. 65, pp. 681–684.
- [78] Yang, C., Liu, P., Guo, J., and Wang, Y. (2010), Polypyrrole/Vermiculite Nanocomposites via Self-Assembling and *in situ* Chemical Oxidative Polymerization, *Synthetic Metals*, Vol. 160, pp. 592–598.
- [79] Feng, X., Huang, H., Ye, Q., Zhu, J.-J., and Hou, W. (2007), Ag/Polypyrrole Core-Shell Nanostructures: Interface Polymerization, Characterization, and Modification by Gold Nanoparticles, *Journal of Physical Chemistry C*, Vol. 111, pp. 8463-8468.
- [80] Yang, X. Dai, T., and Lu. Y. (2006), Synthesis of Novel Sunflower-like Silica/Polypyrrole Nanocomposites via Self-assembly Polymerization, *Polymer*, Vol. 47, pp. 441–447.
- [81] Zhu, C.-L., Chou, S.-W., He, S.-F., Liao, W.-N., and Chen, C.-C. (2007), Synthesis of Core/shell Metal Oxide/PANI Nanocomposites and Hollow PANI Capsules, *Nanotechnology*, Vol. 18, pp. 275604-275609.
- [82] Chuang, F.-Y. and Yang S.-M. (2008), Cerium dioxide/polyaniline core–

- shell nanocomposites, *Journal of Colloid and Interface Science*, Vol. 320, pp. 194–201.
- [83] Kobayashi, Y., Ishida, S., Ihara, K., Yasuda, Y., Morita, T., and Yamada, S. (2009), Synthesis of Metallic Copper Nanoparticles Coated with Polypyrrole, *Colloidal Polymer Science*, Vol. 287, pp. 877–880.
- [84] Kuila, B. K., and Nandi, A. K. (2004), Physical, Mechanical, and Conductivity Properties of Poly(3-hexylthiophene)-Montmorillonite Clay Nanocomposites Produced by the Solvent Casting Method, *Macromolecules*, Vol. 37, pp. 8577-8584.
- [85] Ryu, K. S., Chang, S. H., Kang, S.-G., Oh, E. J., and Yo, C. H. (1999), Physicochemical and Electrical Characterization of Polyaniline Induced by Cross linking, Stretching, and Doping, *Bulletin of Korean Chemical Society*, Vol. 20, pp. 333-336.
- [86] Ahmad, N., Naseer, S. and Norman, M. (2005), Polyaniline Octyl Benzene Sulphonic Acid; Characterization and Synthesis in Normal and Reverse Phase, *Indian Journal of Chemistry*, Vol. 44B, pp. 1536-1537.
- [87] Wang, Y. Z., Joo, j., Hsu, C.-H., and Epstein. A. J. (1995), Charge Transport of Camphor Sulfonic Acid-Doped Polyaniline and Poly (o-Toludine) Fibers: Role of Processing, *Synthetic Metals*, Vol. 68, pp. 207-211.
- [88] Yue, J., Wang, Z. H., Cromack, K. R., Epstein, A. J., and Macdiarmid, A. G. (1991), Effect of Sulfonic Acid Group on Polyaniline Backbone, *Journal of American chemical society*, Vol. 113, pp. 2665-2671.
- [89] Chevalier, J.-W., Bergeron, J.-Y., and Dao, L. H. (1992), Synthesis, Characterization, and Properties of Poly (N-alkylanilines), *Macromolecules*, Vol. 25, pp. 3325-3331.
- [90] Ardsley, N. Y., (1978), Methods of Using N-substituted-N-alkoxy Carbonyl Anilino compounds, US Patent, Appl. No.: 885718, Adolf Hubele, Magden, Switzerland Ciba-Geigy Corporation.
- [91] Cao, Y., Smith P., and Heeger, A. J. (1992), Counter-ion Induced Processability of Conducting Polyaniline and of Conducting Polyblends of Polyaniline in Bulk Polymers, *Synthetic Metals*, Vol. 48, pp. 91-97.
- [92] Ananda, J., Palaniappanb, S., and Sathyanarayana, D. N. (1998), Conducting Polyaniline Blends and Composites, *Progress in Polymer Science*, Vol. 23, pp. 993–1018.
- [93] Jousseau, V., Morsli, M., Bonnet, A., and Lefrant, S. (1998), X-Ray Photoelectron Spectroscopy of Conducting Polyaniline and Polyaniline–Polystyrene Blends, *Journal of Applied Polymer Science*, Vol. 67, pp. 1209–1214.
- [94] Banerjee, P., and Mandal, B. M. (1995), Conducting Polyaniline

- Nanoparticle Blends with Extremely Low Percolation Thresholds, *Macromolecules*, Vol. 28, pp. 3940-3943.
- [95] Nair, B. P., and Pavithran, C. (2010), Micropatterned Surfaces through Moisture-Induced Phase-Separation of Polystyrene-Clay Nanocomposite Particles, *Langmuir*, Vol. 26, pp. 12948–12952.
- [96] Rska, M. Z., Taler, E., Kulszewicz-Bajer, I., Pron, A., and Nizioł, J. (1999), Conductive Polyaniline–Polyamide 6 Blends Processed from Formic Acid with Improved Stability against Deprotonation, *Journal of Applied Polymer Science*, Vol. 73, pp. 1423–1426.
- [97] Rao, P. S., Subrahmanya, S., and Sathyanarayana, D. N. (2005), Water-Soluble Conductive Blends of Polyaniline and Poly (vinyl alcohol) Synthesized by Two Emulsion Pathways, *Journal of Applied Polymer Science*, Vol. 98, pp. 583–590.
- [98] Banerjee, P., and Mandal, B. M. (1995) Blends of HCl-doped Polyaniline Nanoparticles and Poly(vinyl chloride) with Extremely Low Percolation Threshold- a Morphology Study, *Synthetic Metals*, Vol. 74, pp. 257-261.
- [99] Hussain, F., Hojjati, M., Okamoto, M., and Gorga, R. E. (2006), Review article: Polymer-matrix Nanocomposites, Processing, Manufacturing, and Application: An Overview, *Journal of Composite Materials*, Vol. 40, pp. 1511-1575.
- [100] Basavaiah, K., Kumar, Y. P., and Rao, A. V. P. A Facile One-pot Synthesis of Polyaniline/Magnetite Nanocomposites by Micelles-assisted Method, *Applied Nanoscience*, Vol. xxx, pp. 1-7.
- [101] Armes, S. P., Aldissi, M., Agnew, S., and Gottesfeld, S. (1990), Aqueous Colloidal Dispersions of Polyaniline Formed by Using Poly(vinylpyridine) -Based Steric Stabilizers, *Langmuir*, Vol. 6, pp. 1745-1749.
- [102] Stejskal, J., Kratochvil, P., Armes, S. P., Lascelles, S. F., Riede, A., Helmstedt, M., Prokes, J., and Krivka, I. (1996), Polyaniline Dispersions: Stabilization by Colloidal Silica Particles, *Macromolecules*, Vol. 29, pp. 6814-6819.
- [103] Chattopadhyay, D., Banerjee, S., Chakravorty, D., and Mandal, B. M. (1998), Ethyl(hydroxyethyl) Cellulose Stabilized Polyaniline Dispersions and Destabilized Nanoparticles Therefrom, *Langmuir*, Vol. 14, pp. 1544-1547.
- [104] Banerjee, P. (1998), Carboxy Methylcellulose Stabilized Polyaniline Dispersions and Conducting Copolymer Latex Composites, *European Polymer Journal*, Vol. 34, pp. 841-847.
- [105] Banerjee, P., Bhattacharyya, S. N., and Mandal, B. M. (1996), Poly(vinyl methyl ether) Stabilized Colloidal Polyaniline Dispersions, *Langmuir*, Vol. 11, pp. 2414-2418.

- [106] Stejskal, J., Kratochvíl, P., and Helmstedt, M. (1996), Polyaniline Dispersions. 5. Poly(vinyl alcohol) and Poly(*N*-vinylpyrrolidone) as Steric Stabilizers, *Langmuir*, Vol. 12, pp. 3389-3392.
- [107] Yan, F., and Xue, G. (1999), Synthesis and Characterization of Electrically Conducting Polyaniline in Water-oil Microemulsion, *Journals of Materials Chemistry*, Vol. 9, pp. 3035-3039.
- [108] Dearmitt, C., and Armes, S. P. (1992), Synthesis of Novel Polyaniline Colloids Using Chemically Grafted Poly (*N*-vinylpyrrolidone)-Based Stabilizers, *Journal of Colloids and Interface Science*, Vol. 150, pp. 134-142.
- [109] Patil, A. O., Ikenoue, Y., Basescu, N., Colaneri, N. Chen, J., F. Wudl, and Heeger, A. J. (1987), Self-doped Conducting Polymers, *Synthetic Metals*, Vol. 20, 151–159.
- [110] Thiemann, C., and Brett, C. M. A. (2002), Electropolymerization and Properties of Conducting Polymers Derived from Aminobenzenesulphonic Acid and from Mixtures with Aniline, *Synthetic metal*, Vol. 125 pp. 445-451.
- [111] Chan, H. S. O., Ho, P. K. H., Ng, S. C., Tan, B. T. G., and Tan, K. L. (1995), A New Water-Soluble, Self-Doping Conducting Polyaniline from Poly(*o*-aminobenzyl phosphonic acid) and Its Sodium Salts: Synthesis and Characterization, *Journal of American chemical society*, Vol. 117, pp. 8517-8523.
- [112] Kilmartin, P. A., and Wright, G. A. (1997), Photoelectrochemical and Spectroscopic Studies of Sulfonated Polyaniline Part I. Copolymers of Orthanilic Acid and Aniline, *Synthetic Metals*, Vol. 88, pp. 153-162.
- [113] Shimizu, S., Saitoh, T., Uzawa, M., Yuasa, M., Yano, K., Maruyama, T., and Watanabe, K. (1997), Synthesis and Applications of Sulfonated Polyaniline, *Synthetic Metals*, Vol. 85, pp. 1337-1338.
- [114] Guo, R., Barisci, J. N., Innis, P. C., Too, C. O., Wallace, G.G., and Zhou, D. (2000), Electrohydrodynamic Polymerization of 2-Methoxyaniline-5-Sulfonic acid, *Synthetic Metals*, Vol. 114, pp. 267–272.
- [115] Zhou, D., Innis, P. C., Wallace, G. G., Shimizu, S., Maeda, S.-I. (2000), Electrosynthesis and Characterisation of Poly (2-methoxyaniline-5-sulfonic acid) Effect of pH Control, *Synthetic Metals*, Vol. 114, pp. 287–293.
- [116] Wei, X.-L., Wang, Y. Z., Long, S. M., Bobeczko, C., and Epstein, A. J. (1996), Synthesis and Physical Properties of Highly Sulfonated Polyaniline, *Journal of American Chemical Society*, Vol. 118, pp. 2545-2555.
- [117] Kitani, A., Satoguchi, K., Tang, H.-Q., Ito, S., and Sasaki, K. (1995), Electrosynthesis and Properties of Self-doped Polyaniline, *Synthetic Metals*, Vol. 69, pp. 129-130.
- [118] Wei, X., and Epstein, A. J. (1995), Synthesis of Highly Sulfonated

- Polyaniline, Synthetic Metals, Vol. 74, Vol. 123-125.
- [119] Han, M. G., Cho, S. K., Oh, S. G., and Im, S. S. (2002), Preparation and Characterization of Polyaniline Nanoparticles Synthesised from DBSA Micellar Solution, Synthetic Metal, Vol. 126, pp.53-60.
- [120] Kinlen, P. J., Liu, J., Ding, Y., Graham, C. R., and Remsen, E. E. (1998), Emulsion Polymerization Process for Organically Soluble and Electrically Conducting Polyaniline, Macromolecules, Vol. 31, pp. 1735-1744.
- [121] Kim, D., Choi, J., Kim, J.-Y., Han, Y.-K., and Sohn, D. (2002), Size Control of Polyaniline Nanoparticle by Polymer Surfactant, Macromolecules, Vol. 35, pp. 5314-5316.
- [122] Stejskal, J., and Sapurina, I. (2004), On the Origin of Colloidal Particles in the Dispersion Polymerization of Aniline, Journal of Colloid and Interface Science, Vol. 274, pp. 489-495.
- [123] Qiu, H., and Wan, M. (2001), Conducting Polyaniline Nanotubes by Template-Free Polymerization, Macromolecules, Vol. 34, pp. 675-677.
- [124] Aboutanos, V., Barisci, J. N., Kane-Maguire, L. A. P., and Wallace, G. G. (1999), Electrochemical Preparation of Chiral Polyaniline Nanocomposites, Synthetic Metals, Vol. 106, pp. 89-95.
- [125] Liu, W., Cholli, A. L., Nagarajan, R., Kumar, J., Tripathy, S., Bruno, F. F., and Samuelson, L. (1999), The Role of Template in the Enzymatic Synthesis of Conducting Polyaniline, Journal of American chemical society, Vol. 121, pp. 11345-11355.
- [126] Liu, J.-M., and Yang, S. C. (1991), Novel Colloidal Polyaniline Fibrils Made by Template Guided Chemical Polymerization, Journal of Chemical Society: Chemical Communication, Vol. xxx, pp. 1529-1531.
- [127] Ivanov, V. F., Gribkova, O. L., Cheberyako, K. V., Nekrasov, A. A., Tverskoi, V. A., and Vannikov, A. V. (2004), Template Synthesis of Polyaniline in the Presence of Poly-(2-acrylamido-2-methyl-1-propanesulfonic Acid), Russian Journal of Electrochemistry, Vol. 40, pp. 299-304.
- [128] Stejskal, J., Omastova, M., Fedorova, S., Prokes, J., and Trchova, M. (2003), Polyaniline and Polypyrrole Prepared in the Presence of Surfactants: A Comparative Conductivity Study, Polymer, Vol. 44, pp. 1353-1358.
- [129] Jayanty, S., Prasad, G. K., Sreedhar, B., and Radhakrishnan, T. P. (2003), Polyelectrolyte Templated Polyaniline-Film Morphology and Conductivity, Polymer, Vol. 44, pp. 7265-7270.
- [130] Yuan, G.-L., Noriyuki Kuramoto N., and Su, S.-J. (2002), Template Synthesis of Polyaniline in the Presence of Phosphomannan, Synthetic Metals, Vol. 129, pp. 173-178.

- [131] Huang, J., and Kaner, R. B. (2004), A General Chemical Route to Polyaniline Nanofibers, *Journal of American Chemical Society*, Vol. 126, pp. 851-855.
- [132] Li, D., and Kaner, R. B. (2005), Processable Stabilizer-free Polyaniline Nanofiber Aqueous Colloids, *Chemical Communication*, Vol. 26, pp. 3286-3288.
- [133] Pud, A., Ogurtsov, N., Korzhenko, A., and Shapoval, G. (2003), Some Aspects of Preparation Methods and Properties of Polyaniline Blends and Composites with Organic Polymers, *Progress in Polymer Science*, Vol. 28, pp. 1701-1753.
- [134] Capone, S., Forleo, A., Francioso, L., Rella, R., Siciliano, P., Spadavecchia, J., Presicce, D. S., and Taurino, A. M. (2003), Solid State Gas Sensors: State of the Art and Future Activities, *Journal of Optoelectronics and Advanced Materials*, Vol. 5, pp.1335-1348.
- [135] Moseley, P. T., and Tofield, B. C. (1987), *Solid State Gas Sensor*, Bristol and Philadelphia: Adam Hilger.
- [136] Tuller, H. L., and Micak, R. (2000), Advanced Sensor Technology Based on Oxide thin Film MEMS Integration, *Journal of Electroceramics*, Vol. 4, pp. 415-425.
- [137] Janata J., and Josowicz, M. (2003), Conducting Polymers in Electronic Chemical Sensors, *Nature Materials*, Vol. 2, pp. 19-24.
- [138] Huang, W. S., Humphrey, B. D., and MacDiarmid, A. G. (1986), Polyaniline, A Novel Conducting Polymer: Morphology and Chemistry of its Oxidation and Reduction in Aqueous Electrolytes, *Journal of the Chemistry Society Faraday Transactions*, Vol. 82, pp. 2385-2400.
- [139] Kang, U., and Wise, K. D. (2000), A High-speed Capacitive Humidity Sensor with On-chip Thermal Reset, *IEEE Transactions Electron Devices*, Vol. 47, pp. 702-710.
- [140] Virji, S., Huang, J., Kaner, R. B., and Weiller, B. H. (2004), Polyaniline Nanofiber Gas Sensors: Examination of Response Mechanisms, *Nano Letters*, Vol. 4, pp. 491-496.
- [141] Huang, J., Viriji, S., Weiller, B. H., and Kaner, R. B. (2004), Nanostructured Polyaniline Sensors, *Chemistry of European Journal*, Vol. 10, pp. 1314-1319.
- [142] Gopel, W., Jones, T. A., Kleitz, M., Lundstrom, I., and Seiyama Eds., T. (1991), Chemical and Biochemical Sensors: Part I, in: *Sensors: A Comprehensive Survey*, W. Gopel, J. Hesse, J. N. Zemel, Eds. Weinheim: Wiley-VCH, 1991, Vol. 2.
- [143] Stetter J., and Penrose, W. (2002), "Understanding Chemical Sensors and Chemical Sensor Arrays (electronic noses): Past, Present, and Future", *Sensors Update*, Vol. 10, pp. 189-229.

- [144] Gopel, W., Hesse, J. and Zemel, J. N. (1989), *Sensors, A Comprehensive Survey*, New York: VCH Publishing, Vol. 1.
- [145] Bidan, G. (1992), "Electroconducting Conjugated Polymers: New Sensitive Matrices to Build up Chemical or Electrochemical Sensors: A Review", *Sensors and actuators B*, Vol. 6, pp. 45-56.
- [146] Deng, Z., Stone, D. C., and Thompson, M., (1996), Selective Detection of Aroma Components by Acoustic Wave Sensors Coated with Conducting Polymer Films, *The Analyst*, Vol. 121, pp. 671-679.
- [147] Porter, T. L., Eastman, M. P., Pace, D. L., and Bradley, M. (2000), Polymer-based Materials to be used as the Active Element in Microsensors: A Scanning Force Microscopy Study, *The Journal of Scanning Microscopies*, Vol. 22, pp. 304-309.
- [148] Bai, H., and Shi, G. (2007), Gas Sensors Based on Conducting Polymers, *Sensors*, Vol. 7, pp. 267-307.
- [149] Roh, J. G., Hwang, H. R., Yu, J. B., Lim, J. O., and Huh, J. S. (2002), Oxidant Effects on Polypyrrole and Polyaniline Sensor for Several Volatile Organic Gases, *Journal of Macromolecular Science, Pure Applied Chemistry*, Vol. A39, pp. 1095-1105.
- [150] Li, B., Sauve, G., Iovu, M. C., Jeffries-El, M., Zhang, R., Cooper, J., Santhanam, S., Schultz, L., Revelli, J. C., Kusne, A. G., Kowalewski, T., Snyder, J. L., Weiss, L. E., Fedder, G. K., McCullough, R. D., and Lambeth, D. N. (2006), Volatile Organic Compound Detection Using Nanostructured Copolymers, *Nano Letter*, Vol. 6, pp. 1598-1602.
- [151] Torsi, L., Tanese, M. C., Cioffi, N., Gallazzi, M. C., Sabbatini, L., Zambonin, P. G., Raos, G., Meille, S. V., and Giangregorio, M. M. (2003), Side-chain Role in Chemically Sensing Conducting Polymer Field Effect Transistors, *Journal of Physical Chemistry B*, Vol. 107, pp. 7589-7594.
- [152] Chabukswar, V. V., Pethkar, S., and Athawale, A. A. (2001), Acrylic Acid Doped Polyaniline as an Ammonia Sensor, *Sensors and Actuators B*, Vol. 77, pp. 657-663.
- [153] Brie, M., Turcu, R., Neamtu, C., and Pruneanu, S. (1996), The Effect of Initial Conductivity and Doping Anions on Gas Sensitivity of Conducting Polypyrrole Films to NH₃, *Sensors and Actuators B*, Vol. 37, pp. 119-122.
- [154] Jain, S., Chakane, S., Samui, A. B., Krishnamurthy, V. N., and Bhoraskar, S. V. (2003), Humidity Sensing with Weak Acid-doped Polyaniline and its Composites, *Sensors and Actuators B*, Vol. 96, pp. 124-129.
- [155] Hong, K. H., Oh, K. W., and Kang, T. J. (2004), Polyaniline-nylon 6 Composite Fabric for Ammonia Gas sensor, *Journal of Applied Polymer Science*, Vol. 92, pp. 37-42.

- [156] Guernion, N., Costello, B. P. J. D., and Ratcliffe, N. M. (2002), The Synthesis of 3-octadecyl- and 3-docosylpyrrole, Their Polymerisation and Incorporation into Novel Composite Gas Sensitive Resistors, *Synthetic Metals*, Vol. 128, pp. 139-147.
- [157] De Souza, J. E. G., dos Santos, F. L., Barros-Neto, B., dos Santos, C. G., and de Melo, C. P. (2001), Polypyrrole Thin Films Gas Sensors, *Synthetic Metals*, Vol. 119, pp. 383-384.
- [158] Freund, M. S., and Lewis, N. S. (1995), A Chemically Diverse Conducting Polymer-Based Electronic Nose, *Proceedings of the National Academy Science United State of America*, Vol. 92, pp. 2652-2656.
- [159] Ruangchuay, L., Sirivat, A., and Schwank, J. (2004), Selective Conductivity Response of Polypyrrole-based Sensor on Flammable Chemicals, *Reactive and Functional Polymer*, Vol. 61, pp. 11-22.
- [160] Unde, S., Ganu, J., and Radhakrishnan, S. (1996), Conducting Polymer-based Chemical Sensor: Characteristics and Evaluation of Polyaniline Composite Films, *Advanced Materials for Optics and Electronics*, Vol. 6, pp. 151-157.
- [161] Lin, C. W., Hwang, B. J., and Lee, C. R. (1998), Methanol Sensors Based on the Conductive Polymer Composites from Polypyrrole and Poly(vinyl alcohol), *Materials Chemistry and Physics*, Vol. 55, pp. 139-144.
- [162] Bhat, N. V., Gadre, A. P., and Bambole, V. A. (2003), Investigation of Electropolymerized Polypyrrole Composite Film: Characterization and Application to Gas Sensors, *Journal of Applied Polymer Science*, Vol. 88, pp. 22-29.
- [163] Guernion, N., Ewen, R. J., Pihlainen, K., Ratcliffe, N. M., and Teare, G. C. (2002), The Fabrication and Characterisation of a Highly Sensitive Polypyrrole Sensor and its Electrical Responses to Amines of Differing Basicity at High Humidities, *Synthetic Metals*, Vol. 126, pp. 301-310.
- [164] Bhat, N., Geetha, P., and Pawde, S. (1999), Preparation and Characterization of Composites of Polypyrrole, *Polymer Engineering and Science*, Vol. 39, pp. 1517-1524.
- [165] Hosseini, S. H., and Entezami, A. A. (2003), Conducting Polymer Blends of Polypyrrole with Polyvinyl acetate, Polystyrene, and Polyvinyl chloride Based Toxic Gas Sensors, *Journal of Applied Polymer Science*, vol. 90, pp. 49-62.
- [166] Chyla, A., Lewandowska, A., Soloducho, J., Gorecka-Drzazga, A., and Szablewski, M. (2001), 4-t-butyl-CuPc-PODT Molecular Composite Material for an Effective Gas Sensor, *IEEE Transactions Dielectric and Electrical Insulation*, Vol. 8, pp. 559-565.

- [167] Matsuguchi, M., Io, J., Sugiyama, G., and Sakai, Y. (2002), Effect of NH₃ Gas on the Electrical Conductivity of Polyaniline Blend Films, *Synthetic Metals*, Vol. 128, pp. 15-19.
- [168] Ogura, K., Shiigi, H., Nakayama, M., and Ogawa, A. (1999), Thermal Properties of Poly (anthranilic acid) (PANA) and Humidity-sensitive Composites Derived from Heat-treated PANA and Poly (vinyl alcohol), *Journal of Polymer Science A*, Vol. 37, pp. 4458-4465.
- [169] Ogura, K., Shiigi, H., Oho, T., and Tonosaki, T. (2000), A CO₂ Sensor with Polymer Composites Operating at Ordinary Temperature, *Journal of the Electrochemical Society*, Vol. 147, pp. 4351-4355.
- [170] Hu, H., Trejo, M., Nicho, M. E., Saniger, J. M., and Garcia-Valenzuela, A. (2002), Adsorption Kinetics of Optochemical NH₃ Gas Sensing with Semiconductor Polyaniline Films, *Sensors and Actuators B*, Vol. 82, pp. 14-23.
- [171] McGovern, S. T., Spinks, G. M., and Wallace, G. G. (2005), Micro-humidity Sensors Based on a Processable Polyaniline Blend, *Sensors and Actuators B*, Vol. 107, pp. 657-665.
- [172] Segal, E., Tchoudakov, R., Mironi-Harpaz, I., Narkis, M., and Siegmman, A. (2005), Chemical Sensing Materials Based on Electrically-conductive Immiscible Polymer Blends, *Polymer International*, Vol. 54, pp. 1065-1075.
- [173] Cooper, H., Segal, E., Srebnik, S., Tchoudakov, R., Narkis, M., and Siegmman, A. 2006, Electrically Conductive Sensors for Liquids Based on Quaternary Ethylene Vinyl Acetate (EVA)/Copolyamide/Maleated-EVA/Polyaniline Blends, *Journal of Applied Polymer Science*, Vol. 101, pp. 110-117.
- [174] Hong, K. H., Oh, K. W., and Kang, T. J. (2004), Polyaniline-nylon 6 Composite Fabric for Ammonia Gas Sensor, *Journal of Applied Polymer Science*, Vol. 92, pp. 37-42.
- [175] Watcharaphalakorn, S., Ruangchuay, L., Chotpattahanont, D., Sirivat, A., and Schwank, J. (2005), Polyaniline/Polyimide Blends as Gas Sensors and Electrical Conductivity Response to CO-N₂ Mixtures, *Polymer International*, Vol. 54, pp. 1126-1133.
- [176] Hwang, . J., Yang, J. Y., and Lin, C. W. (1999), A Microscopic Gas-sensing Model for Ethanol Sensors Based on Conductive Polymer Composites from Polypyrrole and Poly (ethylene oxide), *Journal of the Electrochemical Society*, Vol. 146, pp. 1231-1236.
- [177] Tongpool, R., and Yoriya, S. (2005), Kinetics of Nitrogen Dioxide Exposure in Lead Phthalocyanine Sensors, *Thin Solid Films*, Vol. 477, pp. 148-152.
- [178] Silverstein, M. S., Tai, H. W., Sergienko, A., Lumelsky, Y. L., and

- Pavlovsky, S. (2005), Poly (HIPE): IPNs, Hybrids, Nanoscale Porosity, Silica Monoliths and ICP-based Sensors, *Polymer*, Vol. 46, pp. 6682-6694.
- [179] Matsuguchi, M., Okamoto, A., and Sakai, Y. (2003), Effect of Humidity on NH₃ Gas Sensitivity of Polyaniline Blend Films, *Sensors and Actuators B*, Vol. 94, pp. 46-52.
- [180] Brady, S., Lau, K. T., Megill, W., Wallace, G. G., and Diamond, D. (2005), The Development and Characterisation of Conducting Polymeric-based Sensing Devices, *Synthetic Metals*, Vol. 154, pp. 25-28.
- [181] Sharma, S., Nirkhe, C., Pethkar, S., Athawale, A. A. (2002), Chloroform Vapour Sensor Based on Copper/Polyaniline Nanocomposite, *Sensors and Actuators B*, Vol. 85, pp. 131-136.
- [182] Hao, Q. L., Wang, X., Lu, L. D., Yang, X. J., and Mirsky, V. M. (2005), Electropolymerized Multilayer Conducting Polymers with Response to Gaseous Hydrogen Chloride, *Macromolecular Rapid Communications*, Vol. 26, pp. 1099-1103.
- [183] Santhanam, K. S. V., Sangoi, R., and Fuller, L. (2005), A Chemical Sensor for Chloromethanes Using a Nanocomposite of Multiwalled Carbon Nanotubes with Poly(3-methylthiophene), *Sensors and Actuators B*, Vol. 106, pp. 766-771.
- [184] Milella, E., Musio, F., and Alba, M. B. (1996), Polypyrrole LB Multilayer Sensitive Films for Odorants, *Thin Solid Films*, Vol. 285, pp. 908-910.
- [185] Stussi, E., Stella, R., and De Rossi, D. (1997), Chemiresistive Conducting Polymer-based Odour Sensors: Influence of Thickness Changes on their Sensing Properties, *Sensors and Actuators B*, Vol. 43, pp. 180-185.
- [186] Huang, J., Virji, S., Weiller, B. H., and Kaner, R. B. (2004), Nanostructured Polyaniline Sensors, *Chemistry of European Journal*, Vol. 10, pp. 1315-1319.
- [187] Xing, S. X., Zhao, C., Jing, S. Y., Wu, Y., and Wang, Z. C. (2006), Morphology and Gas-Sensing Behavior of *in situ* Polymerized Nanostructured Polyaniline Films, *European Polymer Journal*, Vol. 42, pp. 2730-2735.
- [188] Prasad, G. K., Radhakrishnan, T. P., Kumar, D. S., and Krishna, M. G. (2005), Ammonia Sensing Characteristics of Thin Film Based on Polyelectrolyte Templated Polyaniline, *Sensors and Actuators B*, Vol. 106, pp. 626-631.
- [189] Xie, D., Jiang, Y. D., Pan, W., Li, D., Wu, Z. M., Li, Y. R. (2002), Fabrication and Characterization of Polyaniline-based Gas Sensor by Ultra-thin Film Technology, *Sensors and Actuators B*, Vol. 81, pp. 158-164.
- [190] Yoon, H., Chang, M., and Jang, J. (2006), Sensing Behaviors of Polypyrrole Nanotubes Prepared in Reverse Microemulsions: Effects of Transducer Size

- and Transduction Mechanism, *Journal of Physical Chemistry*, Vol. 110, pp. 14074-14077.
- [191] Virji, S., and Huang, J. X., Kaner, R. B., and Weiller, B. H. (2004), Polyaniline Nanofiber Gas Sensors: Examination of Response Mechanisms, *Nano Letter*, Vol. 4, pp. 491-496.
- [192] Virji, S., Fowler, J. D., Baker, C. O., Huang, J. X., Kaner, R. B., and Weiller, B. H. (2005), Polyaniline Nanofiber Composites with Metal Salts: Chemical Sensors for Hydrogen Sulfide, *Small*, Vol. 1, pp. 624-627.
- [193] Li, G. F., Martinez, C., Janata, J., Smith, J. A., Josowicz, M., and Semancik, S. (2004), Effect of Morphology on the Response of Polyaniline-based Conductometric Gas Sensors: Nanofibers vs. Thin Films, *Electrochemistry Solid State Letter*, Vol. 7, pp. 44-47.
- [194] Ma, X. F., Li, G., Wang, M., Cheng, Y. N., Bai, R., and Chen, H. Z. (2006), Preparation of a Nanowire Structured Polyaniline Composite and Gas Sensitivity Studies, *Chemistry of European Journals*, Vol. 12, pp. 3254-3260.
- [195] Zhang, X. Y., Goux, W. J., and Manohar, S. K. (2004), Synthesis of Polyaniline Nanofibers by "Nanofiber Seeding", *Journal of American Chemical Society*, Vol. 126, pp. 4502-4503.
- [196] Jang, J., Chang, M., and Yoon, H. (2005), Chemical Sensors Based on Highly Conductive Poly (3,4-ethylenedioxythiophene) Nanorods, *Advanced Materials*, Vol. 17, pp. 1616-1620.
- [197] Chen, Y. J., Kang, E. T., Neoh, K. G., and Tan, K. L. (2001), Oxidative Graft Polymerization of Aniline on Modified Si (100) Surface, *Macromolecules*, Vol. 34, pp. 3133-3141.
- [198] Kemp, N. T., Flanagan, G. U., Kaiser, A. B., Trodahl, H. J., Chapman, B., Partridge, A. C., and Buckley, R. G. (1999), Temperature-dependent Conductivity of Conducting Polymers Exposed to Gases, *Synthetic Metals*, Vol. 101, pp. 434-435.
- [199] Krutovertsev, S. A., Ivanova, O. M., and Sorokin, S. I. (2001), Sensing Properties of Polyaniline Films Doped with Dawson Heteropoly Compounds, *Journal of Analytical Chemistry*, Vol. 56, pp. 1057-1060.
- [200] Bissell, R. A., Persaud, K. C., and Travers, P. (2002), The Influence of Non-specific Molecular Partitioning of Analytes on the Electrical Responses of Conducting Organic Polymer Gas Sensors, *Physical Chemistry Chemical Physics*, Vol. 4, pp. 3482-3490.
- [201] Fedorko, P., and Skakalova, V. (1998), Low Pressure Effect in the Electrical Conductivity of Doped Polypyrrole, *Synthetic Metals*, Vol. 94, pp. 279-283.
- [202] Harris, P. D., Arnold, W. M., Andrews, M. K., and Partridge, A. C. (1997), Resistance Characteristics of Conducting Polymer Films Used in Gas

- Sensors, Sensors and Actuators B, Vol. 42, pp. 177-184.
- [203] Al-Mashat, L., Shin, K., Kalantar-zadeh, K., Plessis, J. D., Han, S. H. Kojima, R. W., Kaner, R. B., Li, D., Gou, X., Ippolito, S. J., and Wlodarski, W. (2010), Graphene/Polyaniline Nanocomposite for Hydrogen Sensing, *Journal of Physical Chemistry C*, Vol. 114, pp. 16168–16173.
- [204] Wu, Z., Chen, X., Zhu, S., Zhou, Z., Yao, Y., Quan, W., and Liu, B. (2013), Room Temperature Methane Sensor Based on Graphene Nanosheets/Polyaniline Nanocomposite Thin Film, *IEEE Sensors Journal*, Vol. 13, pp. 777-782.
- [205] Misra, S. C. K., Mathur, P., Yadav, M., Tiwari, M. K., Garg, S. C., and Tripathi, P. (2004), Preparation and Characterization of Vacuum Deposited Semiconducting Nanocrystalline Polymeric Thin Film Sensors for Detection of HCl, *Polymer*, Vol. 45, pp. 8623-8628.
- [206] Dixit, V., Misra, S. C. K., and Sharma, B. S. (2005), Carbon Monoxide Sensitivity of Vacuum Deposited Polyaniline Semiconducting Thin Films, *Sensors and Actuators B*, Vol. 104, pp. 90-93.
- [207] Li, G. F., Martinez, C., and Semancik, S. (2005), Controlled Electrophoretic Patterning of Polyaniline from a Colloidal Suspension, *Journal of American Chemical Society*, Vol. 127, pp. 4903-4909.
- [208] Athawale, A. A., Bhagwat, S. V., and Katre, P. P. (2006), Nanocomposite of Pd-polyaniline as a Selective Methanol Sensor, *Sensors and Actuators B*, Vol. 114, pp. 263-267.
- [209] Sharma, S., Nirkhe, C., Pethkar, S., and Athawale, A. A. (2002), Chloroform Vapour Sensor Based on Copper/Polyaniline Nanocomposite, *Sensors and Actuators B*, Vol. 85, pp. 131-136.

Chapter 2

Synthesis Methods of Polyaniline Based Composites

Muktikanta Panigrahi^{1,*}, Basudam Adhikari¹

¹ Materials Science Centre, Indian Institute of Technology, Kharagpur, West Bengal, India

*Corresponding author: muktikanta2@gmail.com

Abstract

Polymer composites synthesized in the present work have been studied extensively. Polymer composites are investigated using sophisticated analytical tools. Electron microscopy was used to study the surface morphology by SEM/FESEM and dispersion of nanoparticles in the polymer matrix by HRTEM. The structural details, i.e., crystallite size, crystallinity, types of nano structure were studied by X-ray diffraction. H1-NMR, ESI-MS and FTIR have been used to elucidate chemical structure of synthesised monomers. The conformational variations in the polymeric materials have been studied using vibrational spectroscopy employing Fourier Transform Infrared (FTIR) spectroscopy. The UV-Visible absorption spectroscopy was used to study the optical properties of the monomers, and as-prepared polymeric samples. The DC conductivity measurement was carried out to study the electronic properties and charge transport mechanisms of the prepared polymeric samples. The gas sensing response was found by electrical measurement. Thermal study has been used to study the stability of prepared materials.

Introduction

The fundamental requisite in the synthesis of conducting polymers is the conjugated nature of the monomer. That is conserved the synthesis process of conducting polymer. Choices of monomer and polymerization method are two main parameters for synthesizing conducting polymer. It is great difficult to synthesize conducting polymer from monomers. Also, there is great challenge to develop a polymerization process by considering appropriate functionality of monomer(s). Generally, most of the monomers are electron-rich molecules. Some of contains simple electron rich molecules i.e., acetylene and other some molecules contains electron rich molecules with pendant groups i.e., aniline, pyrrole, thiophene, or 3,4-ethylenedioxythiophenes. Polymerization reaction occurred of a given monomer in

© IOR INTERNATIONAL PRESS, 2021

Muktikanta Panigrahi & Basudam Adhikari, *Synthesis Methods of Polyaniline Based Composites*,
<https://doi.org/10.34256/ioriip2122>

many routes. Numerous methods are used to polymerize the given monomer. Both monomer and polymer in polymerization reactions are completely soluble and there is possibility for forming high molecular weight polymer. There are two principal methods for the synthesis of PANI. The first one is the direct oxidation of aniline by chemical oxidation, *i.e.*, chemical method and the second way is through electro-oxidation on an inert electrode, *i.e.*, electrochemical method and is discussed below;

Chemical Synthesis

PANI-ES can be easily obtained as dark green powder by polymerization of aniline in aqueous acid medium using ammonium persulfate (APS) oxidant [1 10], potassium iodate [2 14], hydrogen peroxide [3 15], potassium dichromate [4 16], etc. The possible polymerization routes and availability of list of oxidant is shown in **Table 1**. The reaction is mainly carried out in acid medium at low pH (pH ~ 0 and 2). The concentration of the monomer used varies from 0.01 to 1 M. Generally, a stoichiometric equivalent of oxidant is used to carry the polymerisation and also to avoid degradation of the polymer [5 17]. Chemical oxidation polymerization is generally carried out at low temperature (–5 to 0 °C) in order to achieve high molecular weight PANI. One of the disadvantages of this method stems from the experimental observation that an excess of the oxidant and higher ionic strength of the acid medium leads to materials that are essentially intractable.

In a typical synthesis of PANI Emeraldine salt (ES), aniline (0.1 M) is dissolved in 1 M solution of protonic acid such as HCl, H₂SO₄, HClO₄, etc. and is cooled to 0–5 °C. A precooled solution of oxidant (0.1 M) with or without protonic acid is added drop wise for 30–60 min. After about 10–15 min, the solution gradually develops a green tint. The dark green/blue-green precipitate (ES) formed after 12 h and then it is filtered, washed with excess of dilute acid and then with organic solvents. After that the products are dried in vacuum for 24 h. Emeraldine salt (ES) form of PANI can be obtained. PANI Emeraldine base (EB) can be obtained by stirring PANI-ES powder in 0.05 M solution of NH₄OH for 10–12 h. The dark blue powder of EB is further washed with 0.05 M NH₄OH and dried under vacuum. Other than the chemical oxidation method [1 10], emulsion polymerization [6 18], dispersion polymerization [7 19], interfacial polymerization [8 20], and etc. are also available for the polymerization of aniline. The possible polymerization routes and availability of list of oxidants have been thoroughly reviewed in the literature mentioned in **Table 1**.

Electrochemical Synthesis

In this route, polymerization of aniline is carried out in a three electrode system to produce good yield of PANI. The anodic oxidation of aniline is generally carried out on an inert electrode material which is usually platinum (counter electrode). However, other electrode materials such as iron, copper are employed as working electrode [9 21], whereas Ag/AgCl electrode is used as reference electrode. Homogeneous polymer is obtained when synthesized *via* potential cycling [9 21]. The

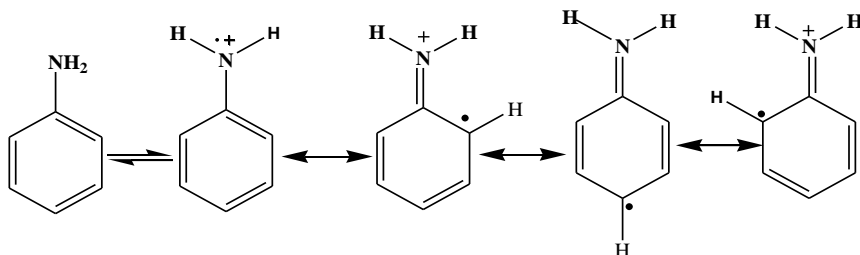
anodic oxidation of aniline is normally carried out in an inert atmosphere at ambient temperature. For many conceivable applications, deposition of the PANI as a thin film or thick coating is desirable which can be easily achieved using electrochemical polymerization.

Table 1. Types of polymerisation processes, oxidants and dopants

Types of Conducting polymers	Pol merization process	Types of Oxidant	Dopants	Reference
PANI-ES	Chemical-oxidation	APS	HCl	[1 10]
PANI- S	hemical-oxidation	APS	AA	[10 22]
PANI-ES	Chem ca - oxidation	APS FeCl ₃ CuCl ₂	---	[11 23]
PANI-ES	Emulsion route	APS	HCl	[6 18]
PANI-ES	Inverse emulsion	APS	DBSA	[12 24]
PANI-ES	Electrochemical	---	HClO ₄	[13 25]
PANI-ES	Electrochemical	---	HCl	[9 21]
PANI-ES	Electrochemical	---	HNO ₃	[14 26]

Polymerization of aniline

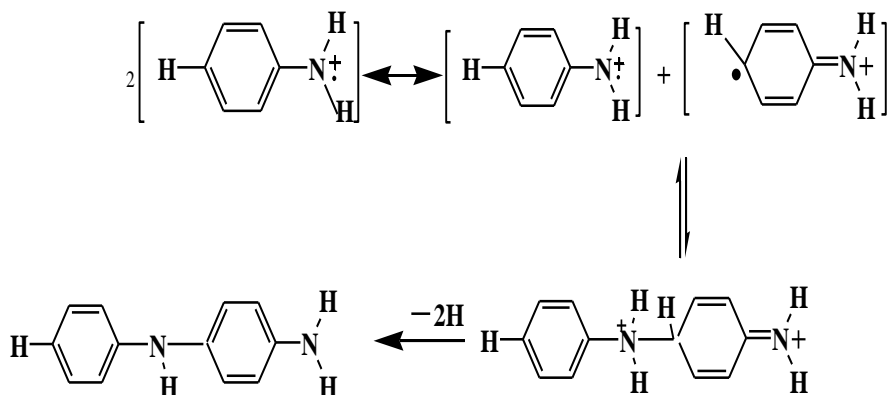
The mechanism and kinetics of PANI formation have been extensively studied for the identification of intermediates and steps involved [15 27]. Various polymerization mechanisms and electrochemical aspects of the formation of PANI have been proposed by different authors depending on the protocol used in the synthesis of PANI [15, 16 27,28]. The first step in the reaction is the formation of a radical cation which is resonance stabilized by several canonical forms (Scheme 1)



Scheme 1. Formation of radical cation and its resonance stabilized canonical forms

This dimer, further leads to higher intermediates and finally to emeraldine form (Scheme 2) [17, 18 29, 30].

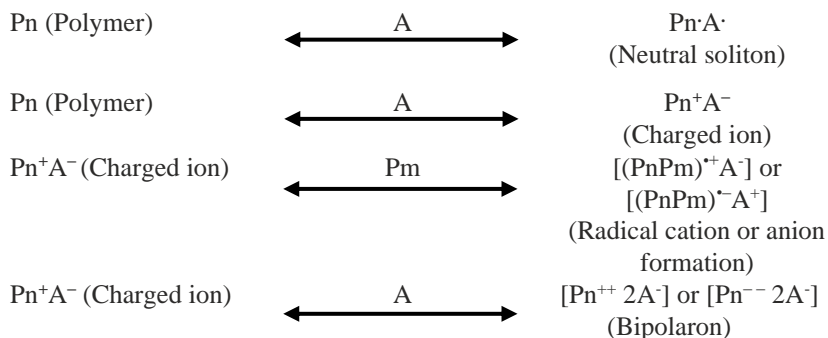
The polymerization mechanism is characterized as 'autocatalytic'. This may occur due to less positive potentials of the oligomers compared to aniline monomer. Such an autocatalytic effect is observed only in aqueous solutions with significant acidity [27].



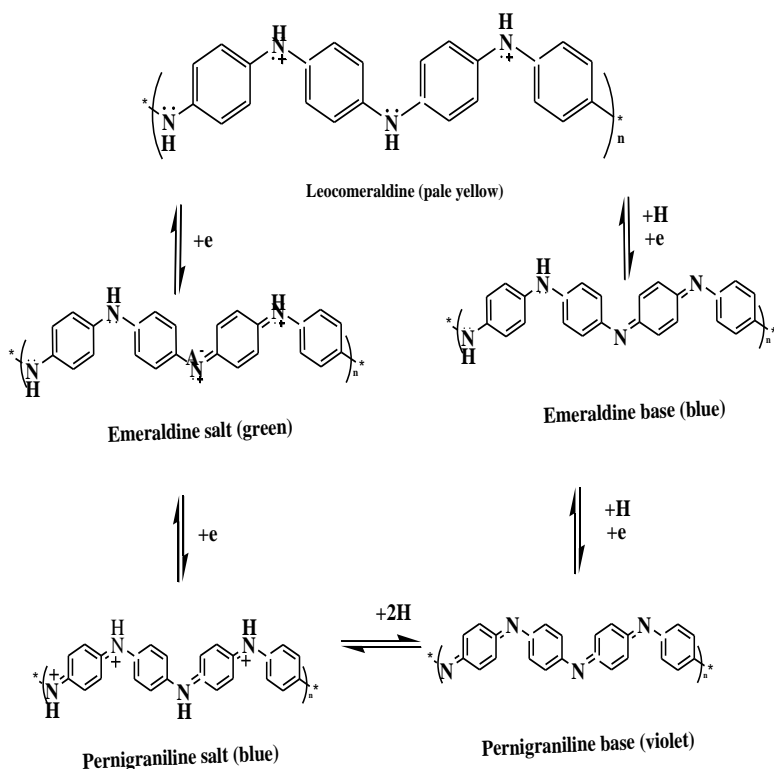
Scheme 1.3. Formation of p-amino diphenylamine from the monomeric radical cation

Doping in Polyaniline: Acid Doping

Usually, the conductivity of undoped state of the conjugated polymers is low (10^{-7} – 10^{-11} S cm⁻¹) [19 3]. One of the effective ways to improve the conductivity is doping. When the conjugated polymers are doped, the electrical conductivity of the polymers increases to several folds [19 3]. Doping in most of the known conducting polymers is achieved by partial oxidation by electron donor or partial reduction by electron acceptor of the π -systems polymer which leads to either increase or decrease in the number of electrons associated with it [20 32]. Generally, doping process can occur either by electron donation or acceptance to the polymer by the dopant (donor) and the resultant species is known as neutral soliton [1, 21 10,33]. If both the electrons are accepted (cation) or donated (anion) by the dopant then the charged soliton is formed [1, 21 10,33]. After the first redox process, charge transfer complex may form between the charged soliton and neutral segment of the polymer. As a result, radical cation or radical anion is formed, which is called polaron [1, 21 10, 33]. Alternatively, charged soliton formation may be followed by a second electron transfer with the dopant. This process results the formation of a dication or dianion, which is known as bipolaron [21 33]. Formation of soliton, polaron, bipolaron is shown in Scheme 3.



Scheme 3. Formation of soliton, polaron and bipolaron



Scheme 4. Interconversion of different oxidation states of polyaniline via redox procedure [22-34]

After doping, non-conducting form of PANI, *i.e.*, emeraldine base (EB) forms conducting PANI, *i.e.*, emeraldine salt (ES) [22-34]. Such a doping behaviour is achieved by the introduction of protonic acids (mineral or organic) and is known as ‘acid doping’ (Scheme 1.5). In this doping process, the conductivity of PANI increases

more than eight orders of magnitude [23–35]. Positive charges accumulated on the polymeric backbone during protonation of PANI are neutralized by the negatively charged counter ions of the dopant, called polymeric organic salts. The protonation changes the electronic structure, crystallinity, solubility, etc. of the polymer [20–32]. The degree of protonation and the conductivity can be controlled by changing the concentration of the dopant acid solution. Mineral acids such as HCl, H₂SO₄, etc are the most frequently used as dopants.

Limitation of conducting polymer

Though, the conducting polymer has potential application in the different fields as an optoelectronic material instead of inorganic materials, still, it has some limitations. The problems of conducting polymers are related to their synthesis, reproducibility, types of dopant used, processability, and stability. Among these problems, the processability and stability are most prominent.

Polymer nanocomposites

The emergence of polymer nanocomposites is largely based on a consideration in which polymer matrix is reinforced by uniformly dispersed nano-sized particles [24, 25–51,52]. Polymer nanocomposites can be prepared using a variety of nanomaterials including disk-like nanoparticles (*e.g.*, clay platelets), spherical and polyhedral nanoparticles (*e.g.*, colloidal silica) and nanofibers (*e.g.*, nanotubes, whiskers). There are many reports on polymer nanocomposites with improved properties other than individual components or their macro- and micro-counterpart [24–26–51–53].

Clay minerals

The layered clays which can be used for the preparation of polymer nanocomposites may be divided into two types. One is natural clays (*e.g.*, montmorillonite, hectorite and saponite etc.) and other one is synthesized clays (*e.g.*, fluorohectorite, laponite, mica, magadiite and hydrotalcite). These are presented in **Table 2**. Out of them, both MMT and hectorite are the most commonly used. The hydrotalcite clays are called anionic clay because the layered clay bears negative clay layers. Among the large amount of layered solids, clay minerals especially the members of smectite group are most suitable for the reinforcement of polymer matrix. For the fabrication of clay based polymer nanocomposites, clay materials are used because of their unique structure and high aspect ratio of each clay platelet. The basic structures of nanoclays are composed of layered silicate network. The silanol groups contains hydroxy group in the inter layer regions, which favour the organic modification by grafting organic functional groups in the interlayer regions (**Fig. 1**) [24–26–51–53].

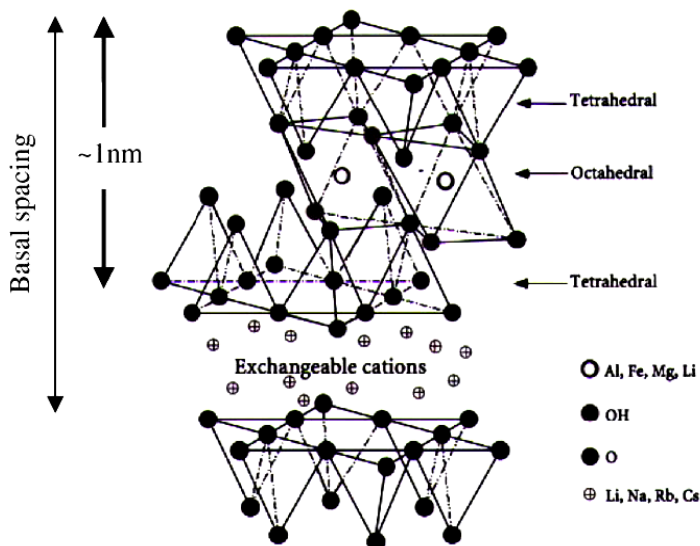


Figure 1. Schematic representation of the clay structure [24 51]

Table 2. Classification of nanoclays (Phallosilicate) [27, 28 54,55]

Type of clay	Formula	Origin	Substitution	Layer charge
2:1 type				
MMT	$M_x (Al_{2-x}Mg_xSi_4O_{10}(OH)_2nH_2O$	N	Octahedral	-ve
Hectorite	$M_x (Mg_{3-x}Li_x) Si_4O_{10}(OH)_2nH_2O$	N	Octahedral	-ve
Saponite	$M_xMg_3(Si_{4-x}Al_xO_{10}(OH)_2nH_2O$	N	Tetrahedral	-ve
Fluorohectorite	$M_x (Mg_{3-x}Li_x) Si_4O_{10}F_2nH_2O$	S	Octahedral	-ve
Laponite	$M_x (Mg_{3-x}Li_x) Si_4O_{10}(OH)_2nH_2O$	S	Octahedral	-ve
Fluoromica	$NaMg_{2.5}Si_4O_{10}F_2$	S	Octahedral	-ve
1:1 type				
Kaolinite	$Al_2Si_2O_5(OH)_4$	N	---	Neutral
Halloysite	$Al_2Si_2O_5(OH)_4 \cdot 2H_2O$	N	---	Neutral
Hydrotalcite	$Mg_6Al_2(CO_3)(OH)_{16} \cdot 4H_2O$	S	Octahedral	+ve
Lavered silicic acid				
Kanemite	$NaHSi_2O_5 \cdot 7H_2O$	N/S	Tetrahedral	-ve
Makatite	$Na_2Si_4O_9 \cdot 5H_2O$	N/S	Tetrahedral	-ve
Octasilicate	$Na_2Si_8O_{17} \cdot 9H_2O$	S	Tetrahedral	-ve
Magadiite	$Na_2Si_{14}O_{29} \cdot 10H_2O$	N/S	Tetrahedral	-ve
Kenyaite	$Na_2Si_{20}O_{44} \cdot 10H_2O$	N/S	Tetrahedral	-ve

M indicates exchangeable ions represented by monovalent ions. **Symbols:** N (Natural), S (Synthetic), -ve and +ve

Modification of clay minerals

Purification and surface modification is essential for the preparation of polymer nanocomposites. This is essential because of their hydrophilic and incompatible nature to most polymers. Therefore, the dispersion of clay minerals in polymer matrix is very difficult. Some parameters of MMT and organically modified nanoclays are presented in **Table 3**.

Table 3. Some parameters of MMT and organically modified nanoclays

OMLS code	Pristine Layered Silicate	d ₀₀₁ (nm)	CEC meq /100g	Modifying group name	Reference No.
MEE	Synthetic clay	2.2	120	Dipoly oxy ethylene alkyl methyl ammonium cation	29 56
MAE		3.3	120	Dimethyl dialkyl ammonium cation	29 56
ME100		0.95	120	Unmodified mica	30 57
30B	Southern clay (Natural clay)	1.85	90	Methyl, tallow,bis-2-hydroxyethyl quaternary ammonium chloride	30 57
15A		3.15	125	Dimethyl, dihydrogenated tallow quaternary ammonium chloride	31 58
20A		2.42	95	Dimethyl-2-dihydrogenated tallow, quaternary ammonium	30 57
25A		1.86	95	Dimethyl, dihydrogenated tallow, 2-ethylhexyl quaternary ammonium	32 59
93A		2.36	95	Dimethyl, dihydrogenated tallow, ammonium	33 60
NC		1.17	92	Unmodified MMT	24 51

MMT indicates montmorillonite. **Abbreviation:** **OMLS** (Organically modifying layered silicate), **CEC** (Chemical exchange cation), **nm** (nano meter), **meq.** (Miliequivalent), and **d** (basal distance), and **NC** (Nanoclay which is unmodified)

Conducting polymer nanocomposite

When clay minerals are added to a polymer matrix, they form three types of structures, which depend on the nature of the components and processing condition. These are conventional composite, intercalated, and exfoliated nanocomposites. In conventional composite, the components are separated, *i.e.*, phase separated. The properties of such composite are similar to that of micro-particles reinforced polymer composites. In intercalated nanocomposites, the polymer chain is inserted into the clay gallery resulting in a well ordered multilayer stacking morphology. **Fig. 2** shows a diagram of three broad classes of thermodynamically achievable polymer/layered silicate nanocomposites [24 51].

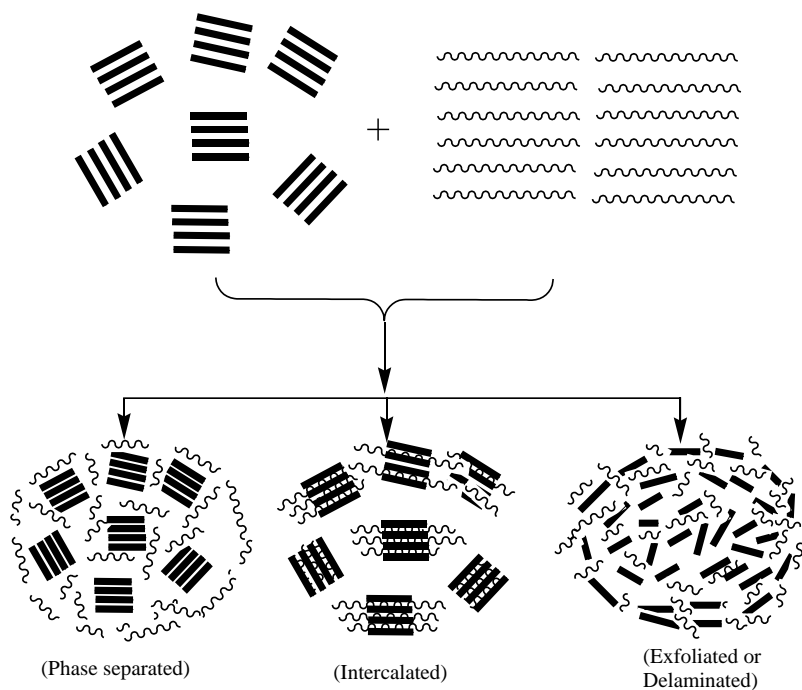


Figure 2. Three typical nanocomposites prepared from conducting polymer and clay minerals: (a) phase separated nanocomposite; (b) intercalated nanocomposite; (c) exfoliated or delaminated nanocomposite [24 51]

Several techniques are followed for the preparation of nanocomposites, which predominantly includes chemical and electrochemical techniques [34 61]. Nanomaterials are encapsulated in various ways *viz.*, *ex situ*, *in situ*, and *core-shell*.

Ex situ nanocomposites

In *ex situ* technique the inorganic nanoparticles are dispersed in a monomer and then polymerised to form conducting polymer nanocomposites [35 62]. The

inorganic nanoparticles are encapsulated in the conducting polymer matrix during polymerization in the same reaction vessel [35 62]. Variety of conducting polymer nanocomposites have been prepared using polyaniline (PANI) [36 63], polypyrrole (PPy) [37 64], polyphenylene vinylene (PPV) [38 65], poly (3,4-ethylenedioxythiophene) (PEDOT) [39 66] as hosts for inorganic metal, metal oxide and ceramic nanoparticles as guest materials.

Core-shell conducting polymer nanocomposites

Among the inorganic-organic nanocomposites, the *core-shell* structures have attracted much more scientific interest and have become more popular leading to some interesting nanocomposite synthesis. In this technique, different metal and metal oxide nanoparticles are encapsulated in the core of conducting polymers.

Table 4. Selected conducting polymer/clay nanocomposites

Polymer	Layered clay	Synthesis method	Structure of nanocomposite	Reference No.
olyaniline	MMT CdS	Emulsion	intercalation	43 70
		Micro-emulsion	intercalation	44 71
		<i>in situ</i>	intercalation	34 61
		<i>ex situ</i>	Not mention	34 61
		Chemical-oxidation	Not mention	34 61
	Om-MMT	Dispersion	Exfoliation/ intercalation	24 51
	Maghnite-H+	<i>in situ</i>	intercalation	45 72
	Cloisite 15A	<i>in situ</i>	Not mention	46 73
Polypyrrole	MMT	Chemical-oxidation		47 74
	Bentonite	Chemical-oxidation	intercalation	48 75
	Hydroxy appatite	Electropoly-merization	Not mention	49 76
	VMT	Chemical-oxidation	intercalation	50 77
Polythiophene	Modified MMT	<i>in situ</i>	intercalation	37 64

Core-shell structured silica (SiO₂) nanoparticles based PANI and Ppy nanocomposites were synthesized in stable colloidal forms, where SiO₂ was used as the core [40 67]. Colloidal PPy-Au *core-shell* structured nanocomposites have been synthesized by a template-guided polymerization technique [41 68]. Deng and co-workers have reported the synthesis of *core-shell* structured ferromagnetic (Fe₃O₄)-cross linked

PANI nanocomposites. This composite shows *core-shell* morphology in aqueous solution [42–69]. Layered clays, synthesis method, structure of nanocomposites of selected conducting polymer/clay based nanocomposites are presented in **Table 4**.

Hematite/silica/polypyrrole ($\text{Fe}_2\text{O}_3/\text{SiO}_2/\text{PPy}$) ellipsoidal sandwich composite spheres as well as SiO_2/PPy ellipsoidal hollow capsules with movable hematite as cores and Ppy as shell were successfully fabricated by *core-shell* technique [40–67]. Polypyrrole-coated silver nanocomposite have been synthesized by one step aqueous chemical oxidation dispersion polymerization technique from pyrrole monomer using silver nitrate as an oxidant [51–78]. Electromagnetic functionalized *core-shell* nanocomposites of polypyrrole (PPy) were prepared by a self-assembly process [51–78]. Yang *et al.* have reported that they prepared novel sunflower-like organic-inorganic composites using smaller conductive polypyrrole and spherical silica particles through an *in situ* route by self-assembly polymerization process. For this preparation chitosan was employed as a modifying agent on silica surface [52–79]. Polypyrrole (PPy)-coated Ag composites were synthesized by interfacial polymerization process in the presence of polyvinyl pyrrolidone (PVP) by Feng *et al.* [51–78]. *Core-shell* nanocomposites of CuO/PANI [53–80], $\text{Fe}_2\text{O}_3/\text{PANI}$ [53–80], $\text{In}_2\text{O}_3/\text{PANI}$ [53–80] and $\text{Fe}_2\text{O}_3/\text{SiO}_2/\text{PANI}$ [53–80] were successfully prepared using a double-surfactant-layer assisted polymerization method. Chuang and Yang [54–81] have reported the preparation of CeO_2/PANI (CeO_2/PANI) *core-shell* nanocomposites via chemical oxidation method using aniline as monomer and CeO_2 as an oxidant as well as nanomaterials. Synthesis of metallic copper nanoparticle coated with polypyrrole was very recently reported by Kobayashi *et al.* [55–82].

Solution casting

In this technique, homogenous dispersion of organoclay (Na^+ MMT) was added to solution of ammonium salt of hexadecylamine. The solution was spread onto a glass plate and the solvent was evaporated by taking appropriate time for drying to form nanocomposite [56–83].

Solubility of polyaniline

Solubility

The acid doped form of PANI is insoluble in aqueous solutions as well as in most common organic solvents, but soluble in concentrated sulphuric acid [57–84]. When the emeraldine salt of PANI is deprotonated to form the insulating emeraldine base of PANI, it can be solubilized in a number of organic solvents [58–85], such as N-methyl pyrrolidone (NMP), dimethyl formamide (DMF), dimethyl sulfoxide (DMSO), m-cresol, chloroform (CHCl_3) and tetrahydrofuran (THF). The process of dedoping effectively removes the cationic charges upon the conducting polymer backbone and that reduces the ionic character, which is more amenable to dissolution. Gelation of the conducting polymer commonly occurs at high concentrations of the

EB solutions. This result helps to increase viscosity due to formation of strong interchain hydrogen bonding between the amine hydrogens and nearest neighbour imine nitrogens. A novel route to solubilize the ES form is by the use of functionalized protonic acid dopants such as sulphonic acids (camphor sulphonic acid, dodecyl benzene sulphonic acid) [59 86].

Substituted Polyaniline

Solubility of PANI can be improved by polymerizing a derivative of aniline, particularly by choosing the substituent which has solubilising effect. There are two types of substituents. One substituent occurs at N-atom and other is on the ortho- and meta-position of benzene ring. The different substituents are alkyl [60 87], alkoxy [61 88] groups, phosphoric and sulphonic acid [62 89] groups. The acid group substituted PANI was found to be more soluble, some of them being water soluble and also showing higher thermal stability. Polymerization of substituted anilines can also be carried out either chemically [60 87] or electrochemically [60 87]. The major drawback of these rings substituted PANIs is the fact that solubility is achieved at the cost of conductivity [60 87].

Functionalized protonic acid as dopant

Cao, Smith, and Heeger [63 90] synthesised metallic form of PANI using functionalized protonic acids and simultaneously resulted PANI complex soluble in common organic solvents. The functionalized counter ion acts as 'surfactant' and the charged head group is ironically bound to the oppositely charged protonated PANI chain, and the 'tail' is chosen to be compatible with non-polar or weakly polar organic liquids [63 90]. This is called 'counter-ion' induced processability.

Blends of polyaniline

Conducting blend is another kind of conducting materials, which supports to improve the solubility and that, is found from literatures [64-66 91-93]. It is a physical mixture of two or more polymers with different chemical compositions. Improvement of the PANI processability resulted in the fabrication of several types of conductive blends of PANI [64-66 91-93]. The main purpose of making blends is to introduce flexibility and toughness to PANI thereby making it melt processable. A phase separation between the two components of the blends leads to decrease of mechanical strength of the material [67 94]. However, by keeping the PANI composition less than 16 wt%, materials with good flexibility blend can be obtained. Several conductive blends of PANI salt with thermoplastic polymers such as polystyrene [65 92], polyamides [68 95], poly (vinyl alcohol) [69 96], poly (vinyl chloride) [70 97], and so forth have been extensively studied.

Copolymers

Copolymer is another class of materials with improved solubility. It is generally carried out to combine the diverse physicochemical properties of different polymers to form a single polymeric system. Copolymerization of aniline with ring or N-substituted anilines leads to polymers which have conductivity like PANI and solubility of substituted anilines [61, 62 89,88].

Polyaniline dispersions

Dispersion polymerization is a well-known technique for the synthesis of conventional polymer in both aqueous and non-aqueous media [6, 71, 72 18,98,99]. Colloidal dispersion is one of the widely used and technologically important ways for tackling the problem of poor solubility of PANI [73, 74 100,101]. Dispersion of PANI is used in the preparation of blend with thermoplastic polymers.

Polymer stabilized polyaniline dispersions

Various polymeric steric stabilizers such as ethyl cellulose [75 102], carboxymethyl cellulose [76 103], poly (vinyl alcohol) [69 96], poly (vinyl methyl ether) [77 104], poly (N-vinylpyrrolidone) [78 105], etc. are employed for the synthesis of PANI in colloidal form or as suspension by chemical polymerization using aniline precursors. According to Armes and co-workers [73 100], they have synthesized colloidal PANI by chemical grafting of PANI onto several tailor made copolymer surfactants. The resulting polymer (PANI) is insoluble in solvents and its macroscopic coagulation is prevented by steric stabilizers [75 102]. The possible synthetic routes and the properties of PANI colloids have been reviewed by Stejskal [75 102]. The morphology and the size of colloidal particles are strongly depended on the steric stabilizer, oxidizing agent and reaction conditions [79 106]. On the other hand, the use of polymeric stabilizers in PANI drastically lowers the electrical conductivity of PANI [80 107].

Processability

Processability is one of the major issues in the synthesis of conducting polymers for commercial applications in different areas. These applications of conducting polymers like PANIs are limited due to the lacking of solubility and processability. A number of approaches have been investigated to improve the processability of PANI.

Generally, alkyl and alkoxy substituted aniline monomer is polymerized to improve the solubility of the polymer in organic solvents. But, it has a negative influence on the conductivity [60, 61 87,88]. The first known examples of water soluble conducting polymers reported in 1987 are the sodium salts of poly -3-(2-ethane sulfonate) thiophene and poly -3-(4-butane sulfonate) thiophene [81 108]. These

polymers are self-doped Polythiophenes. The electrochemical polymerization of aniline carboxylic acid isomers has been recently reported [82-109]. Poly (o-amino benzyl phosphoric acid) is another type of self doped conducting polyaniline synthesised and the polymer was soluble in dilute ammonia solution but insoluble in water [83-110]. Electro-co-polymerization of aniline and o-aminobenzenesulphonic acid formed sulfonated PANI which was soluble in neutral pH [84-111].

Introduction of sulphonic acid group to the PANI chain makes soluble PANI which is self-doped and is known as Sulphonated PANI (SPAN). By chemical and electrochemical method, methoxyaniline sulphonic acid is polymerized [85-87-112-114]. Another type of conducting PANI was synthesised for improving the processability as well as redox-activity over a wide pH range [88-90-115-117]. However, these conducting polymers have low electrical conductivity.

In a solution processing route, nanostructured materials were prepared from colloidal dispersions with reasonable conductivity using a range of steric stabilizers. These used different surfactant micelles such as dodecyl benzene sulfonic acid [91-118], naphthalene sulphonic acid [92-119], polyethylene oxide (PEO) [93-120], water soluble polymers such as poly (N-vinyl pyrrolidone) [94-121], organic dopants [95-122] and silica colloids [96-123].

Polyaniline can also be formed using aniline as monomer and polyelectrolytes such as polystyrenesulphonic acid [97-124], polyacrylic acid [98-125] and poly (2-acryloamido-2-methyl-1-propane sulphonic acid) [99-126] as template. The role of the polyelectrolyte template is to align aniline monomer and promote head-to-tail coupling. The polyacid template was thought to provide a low pH for growth of water soluble PANI and also the necessary counter ions for doping PANI to the conducting form [97-124]. The polymerization reaction rate was faster compared to ordinary chemical polymerization owing to the high local concentration of aniline and hydrogen ions on the template matrix (polyamide) [99-126]. The use of these non-conducting polyelectrolytes resulted in low electrical conductivity of the water dispersible PANI [100-102-127-129].

Recently, PANI nanofibers were synthesised by using interfacial polymerization at aqueous/organic interface or rapid mixing of monomer and oxidant aqueous solutions in controlled ratio [103-130]. These methods have the advantage of stabilizer-template free polymerization and ease of purification. The nanofibers have diameters between 30 and 50 nm and make relatively stable dispersion at pH around 2-3 [104-131].

Polyaniline composites

The preparation of conducting polymer composite blends with common polymers in order to improve the mechanical properties and processability of ICPs has been investigated [105-132]. In general, there are two main methods used to produce composites: synthetic method based on polymerization of aniline in a matrix polymer and blending methods via mixing a previously synthesised polyaniline with a matrix

polymer.

Characterization techniques

Generally, the prepared materials are needed three types of characterizations such as spectroscopic analysis, structural analysis, and electrical analysis (DC electrical conductivity, temperature dependent DC conductivity with and without field, and gas sensor measurements).

Spectroscopic characterization for chemical structure

The different non-destructive techniques (NDT) such as NMR (^1H NMR), ESI-MS, FTIR/ATR-FTIR, and UV-Visible are generally required to characterize the prepared materials.

Proton nuclear magnetic resonance (^1H NMR)

^1H NMR technique is one of the NDT. Molecular structure was investigated using Nuclear Magnetic Resonance (NMR) spectrometer (Bruker DRX-500MHz spectrometer). The molecular structure of synthesised salt (AA and Ani) and its polymer was also characterised by NMR technique. In NMR spectrometer, radiofrequency (RF) is used as NMR source and to induce transition between different nuclear spin states of samples in a magnetic field. By the application of strong magnetic field to the samples, their spins are reoriented, *i.e.*, aligned with the field or against the field [106 7].

Furthermore, splitting of the spectra lines arises due to interactions between different nuclei, which provide information about the proximity of different atoms in a molecule. We explored the ^1H NMR to investigate the molecular structure. Orientation parallel to alignment of applied force is lower in energy. When nuclei are irradiated with RF radiation the lower energy nuclei flip to high state and nuclei is said to be in resonance, hence the term NMR.

For this technique, particular deuterated solvent is required and it is called lock solvent. In my thesis work, deuterated chloroform (CDCl_3)/deuterated dimethyl sulphoxide (d_6 -DMSO) was used. Prepared samples were dissolved in a CDCl_3/d_6 -DMSO to form deuterated solution. The prepared NMR samples are run in 5 mm glass NMR tubes. An NMR tube was filled prepared sample and then, the sample tube was exposed to RF radiation in the spectrometer and data were collected. The chemical shifts of the groups are recorded in the range 10-200 ppm with a delay of 2.5 sec. This technique was done to help the analysing the molecular structure.

Mass analysis (ESI-MS)

Mass spectrometry [MS] is an analytical technique which is NDT that

identifies the chemical composition as adduct of a prepared sample on the basis of the mass-to-charge ratio (m/z), called charged ions. Such ionization of mass occurred by electrospray ionization of mass (ESI-MS) technique. The technique is used in both qualitative and quantitative analysis.

Now a days, this technique is more acceptable to identify the large molecules. It fragments the samples [107 8] to form charged ions from relatively non-volatile, thermally labile compounds. ESI-MS had as its first uses, the ionization of intact chemical species but now has found wide acceptance in the identification of large molecules. This instrument has ability to form charged ions from relatively non-volatile, thermally labile compounds. Multiple charged ions are generated which serve to extend the useful mass range of the instrument. A mass spectrometer generates multiple ions from the sample under investigation; it then separates them according to their m/z , and then records the relative abundance of each ion type.

The first step in the ESI-MS spectroscopic analysis of compounds is the production of gas phase ions, basically by electron ionization. This molecular ion undergoes fragmentation. Each primary product ion derived from the molecular ion, in turn, undergoes fragmentation, and so on. The ions are separated in the mass spectrometer according to their m/z ratio and are detected in proportion to their abundance. A mass spectrum of the molecule is produced. It displays the results in the form of a plot of ion abundance verses m/z ratio. Ions provide information concerning the nature and the structure of their precursor molecule. In the spectrum of a pure compound, the molecular ion if present, appears at the highest value of m/z (followed by ions containing heavier isotopes) and gives the molecular mass of the compound. In the thesis work, mass spectra were obtained from AXIMA-CFR laser desorption ionization flying time spectrometer (COMPACT). In this work, we used gel-like (prepared salt) samples. It helped to evaporate solvent easily. Typical solvents for electrospray ionization were prepared by mixing water with volatile organic compounds like methanol and acetonitrile. Acetic acid was added to prepared typical solvent. That was done because to decrease the initial droplet size and increase the conductivity of prepared materials like salt.

Fourier transformation infra-red (FTIR) spectroscopy

Like NMR and ESI-MS, FTIR/ATR-FTIR is a NDT technique. This technique is used to analyse the presence of functional groups, formation of chemical linkage between used materials and interaction between nanomaterials and polymers, metal oxygen bond and removal of organic and other phases with have been investigated using a FTIR/ATR-FTIR spectrometer (Nexus-870, Thermo Nicolet Corp, and USA). The instrument parameters were kept constant (50 scan at 4 cm^{-1} resolution, transmittance/absorbance mode). In this spectrometer [108, 109 9,10], the IR radiations from an IR source are passed through the sample and the amount of energy adsorbed/transmitted was recorded by suitable detector and is guided through an interferometer where a Fourier Transform is performed on the output signal.

For this technique, powder, liquid and solid film samples were used. Solid film samples were analyzed in ATR mode. For this measurement, the powdered samples were prepared by making pellet. At first, dry KBr are grinded using mortar pestle followed by addition of small amount of prepared samples. Further, sample mixture is grinded. Then it put in die and placed inside (appropriate place) the hydraulic pressure and compacted the samples by pressure (5 kg.f).

The pellet (13 mm diameter, 0.3 mm thick) so prepared was used for IR characterization. Liquid samples was directly put on KBr pellet/quartz glass plate and used for this characterization. Before running the samples, a background spectrum was collected. Then pellets samples were put in a sample holder. The pellets are exposed to IR radiation in the spectrometer and data were collected. This technique was done to characterize the bonding type of the molecules and for each type of bonding it produced characteristic absorption bands.

Ultraviolet-visible (UV-Vis) spectroscopy

UV-Vis spectroscopy is also one type of NDT technique. The UV-Vis spectra of the prepared materials were recorded by using a Micropack UV-VIS-NIR, DH 2000. The wave length of spectrum was taken from 200 to 800 nm. Powdered, liquid, and solid film samples were used for doing UV-Vis characterization. Transparent solvent was used within the wavelength range for making required solution. In this spectroscopy, we choose the wave length in the UV and Visible region and expressed in nanometre. For this analysis, transparent solution is required. UV-Vis light is an electromagnetic radiation and obtained from different sources (tungsten lamp or tungsten-halogen lamp or deuterated lamp). The emitted energy was passed through the molecules containing π -electrons or non-bonding electrons. It absorb/reflect and cause excitation from highest occupied molecular orbital to lowest unoccupied molecular orbital, *i.e.*, HOMO to LUMO. It is detected by the detector and spectrum is obtained in computer. In this thesis work, I have prepared desired transparent solution using small amount of synthesized powder as starting materials and DMSO/NMP as solvent.

Such solution was made by taking 5 mg synthesized materials and 20 mL DMSO/NMP. For recording the spectrum, quartz cell (length = 5 cm) is commonly used. These require approx. 3 mL of solution and were placed in the path of light beam and spectrum was recorded by varying the wavelength of incident light. The sample cell should be rinsed three to five times with DMSO/NMP solvent before filling with the pure solvent that will be used in the measurement. Most UV-Vis instruments can analyze solid samples or suspensions with a diffraction apparatus but this is not common. Base line was corrected before recording the spectra. This technique was performed for studying the variety of electronic transitions [110 11].

Structural and Morphological Characterizations

X-ray diffraction (XRD) technique

X-ray diffraction (XRD) is a powerful non-destructive technique to determine crystalline/amorphous structure [111 12], intercalated/exfoliated/delaminated nanostructure [111 12] of clay based composites. It also estimates various structural parameters such as crystallite size (D), interlayered-spacing (d), etc. X-rays are generated from Cu target with a characteristic wavelength (λ) which can be obtained from the expression [112, 113 13,14] as shown in equation (1)

$$E = h\nu = h \frac{c}{\lambda} \dots\dots\dots (1)$$

Where, h is the Planck's constant (6.62×10^{-34} joule), c is the velocity of light (3×10^8 m/s) and E is the energy of the radiation. The wavelength of X-ray is comparable to the size of atoms.

The basic principle of X-ray diffraction is based on constructive interference of X-rays (monochromatic) and prepared samples. The interaction of the incident X-rays with the samples produces constructive interference and the diffracted rays are generated which satisfies the Bragg's law ($n\lambda = 2d\sin\theta$). By scanning the sample through a range of 2θ angles, all possible diffraction directions of the lattice should be attained due to the random orientation of the powdered materials. Conversion of the diffraction peaks to d-spacing allows the identification of the materials because each material has a set of unique d-spacing. Typically, this is achieved by comparison of d-spacing with standard reference patterns.

In the present thesis work, most of the X-ray diffraction patterns were recorded using $\text{CuK}\alpha$ radiation (wavelength, $\lambda = 0.154$ nm). During the operation, XRD was operated at 40 kV and 20 mA. The powder samples were placed on a quartz sample holder at room temperature and were scanned at diffraction angle 2θ from 5° to 45° . The sample is kept in a Perspex holder.

Electron Microscopies (SEM/FESEM or TEM/HRTEM)

Scanning Electron Microscopy or Field Emission Scanning Electron Microscopy

Surface morphologies of prepared materials were analyzed by electron microscopies such as SEM/FESEM or TEM/HRTEM. SEM/FESEM is a microscope that uses electrons in place of light to produce image [114 15]. It is a surface phenomenon. In this measurement, the electron beam produced from electron gun is focused on a small portion of the sample that is kept in vacuum. Detector collects the output signals during the interaction of electrons with the sample and that is sent to a computer. This forms the final image. Two types of electron gun are used. One is

thermionic and the other one is field emission.

The electrons emitted from the electron gun are accelerated by applying a high electric potential. The scanning of the electron beam over the sample surface is controlled by deflecting the electron beam using a scanning coil. In vacuum condition, both FESEM/SEM are used to produce image. Therefore, special preparation technique is needed for the sample to avoid moisture absorption. All nonconducting materials need thin layer of conducting coating. This is done by 'sputter coater'. Operating voltage was 4 kV. Such coater uses an electric field and argon gas. The sample is placed in a small vacuum chamber. The argon gas is ionized in the applied electric field to form argon ion (Ar^+). The argon ions knock gold atoms from the surface of the gold foil and get deposited on sample.

High Resolution Transmission Electron Microscopy (HRTEM)

It is also a special kind of electron microscopic tool that uses highly accelerated beam of electron as illumination for microscopic analysis. Such beams are passed through the electron transparent samples. The interaction occurred between electron and atoms of the sample. The transmitted electrons are then focused by the objective lens into an image. In HRTEM, electromagnetic lenses are used to guide the electron beam through the microscope. The specimen preparation for HRTEM experiment should be important for getting good results. The main criteria of sampling are artifacts free. The detailed sampling procedure was found in the journal [115 16]. In this investigation, pellet samples were used for doing HRTEM.

Thermal Characterization

Thermogravimetric (TG) Analysis

TGA analysis is a type of thermal analysis that measures mass change of materials [116 17] with change of temperature. The purpose of doing such experiment is to measure volatile content, thermal stability, degradation characteristics, etc.

Differential Scanning Calorimetric (DSC) Analysis

Differential scanning calorimetry (DSC) is a technique for measuring the energy necessary to establish a nearly zero temperature difference between a substance and an inert reference material, as the two specimens are subjected to identical temperature regimes in an environment heated or cooled at a controlled rate. The technique provides qualitative and quantitative information about physical and chemical changes that involve endothermic or exothermic processes or changes in heat capacity using minimal amounts of sample. It has many advantages including fast analysis time, typically thirty minutes, easy sample preparation, applicability to both liquids and solids, a wide range of temperature applicability and excellent quantitative capability [117 18].

There are two types of DSC systems in common use. In power compensation

DSC, the temperatures of the sample and reference are controlled independently using separate, identical furnaces. The temperatures of the sample and reference are made identical by varying the power input to the two furnaces; the energy required to do this is a measure of the enthalpy or heat capacity changes in the sample relative to the reference.

DSC has been used in the evaluation of small transitions such as multiple phase transitions in liquid crystals and those due to side chains in polymers which cannot be resolved by most other techniques. It allows accurate determination of temperatures associated with thermal events. Temperature can be calibrated with respect to one or more standards which allow highly accurate, precise and reproducible values. The technique reveals the thermal history imparted to thermoplastics as a result of different processing conditions. The information generated can be used to vary heating rates to deliver the required degree of crystallinity.

Differential scanning calorimetry (DSC, Diamond Perkin-Elmer, USA) was used for determination of crystallization. Samples (5-10 mg) were placed in sealed aluminium pans and scanned under a constant nitrogen purge (20 mL/min). Subsequently, the samples were heated from 30 °C to 200 °C at a rate of 20 °C/min, held at 200 °C for 2 min, cooled to 30 °C at the same rate and held for 2 min to stabilize. Finally a second scan was carried out from room temp to 200°C. The results crystallization temperature (T_c), melting temperature (T_m) and glass transition temperature (T_g) were noted from the second scan.

In the current research work, DSC has been carried out for the PANI-ES/Cloisite 20A nanocomposites and acrylic acid based PANI to investigate the crystallization behavior of the samples. Sample preparation work can greatly affect the results. So, specimen preparation should be as gentle as possible. The vertical specimen has smaller contact area and so it takes longer time to melt. Large contact area promotes heat transfer. Polymers can absorb water, *e.g.*, polyamides and this affects their properties as well as results. For DSC study, specimen mass should be 5-20 mg.

Electrical Characterizations

DC conductivity measurement at Room temperature as well as temperature dependent (presence and absence of magnetic field)

DC conductivity measurement at room temperature as well as temperature dependent (presence and absence of magnetic field) is an important electrical characterization to show the electrical nature of materials at different conditions. For DC conductivity measurement a four probe set-up was used as shown in **Fig. 3**.

Usually, resistivity of semiconductor is measured by four probes technique. It is a one of the standard electrical measurement method. In this investigation, I have used linear four probe technique to measure both room and low temperature resistivity. Pellet and solid film samples were taken for this measurement. Four electrical contacts

were made by attaching copper wires onto the sample surface through silver paste. In this technique, four probes contact points were arranged linearly in a straight line at equal distance (S) from each other. For room temperature measurement, the sample was fixed on insulating plate where four probes are connected.

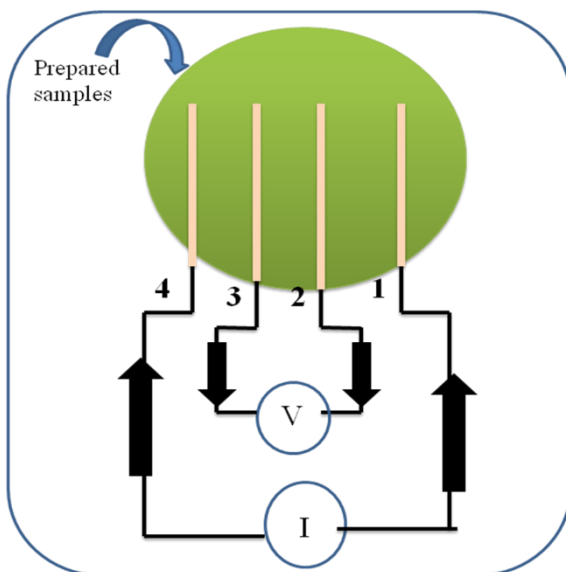


Figure 3. Schematic representation of linear four probe set-up

The output voltage is related proportionally to the applied current. Such type of contacts was called ohmic. According to four point probe method, the resistivity (ρ) was calculated using the relation [118 19]

$$\rho = 2\pi S \left(\frac{V}{I} \right) \dots \dots \dots (2)$$

Where S is the probe spacing in centimetre (cm), which was kept constant, I is the supplied current in millampere (mA) or nanoampere (nA) and the corresponding voltage was measured in volt (V) or millivolt (mV). The conductivity (σ) was calculated using the relation [118 19]

$$\sigma = \frac{1}{\rho} \dots \dots \dots (3)$$

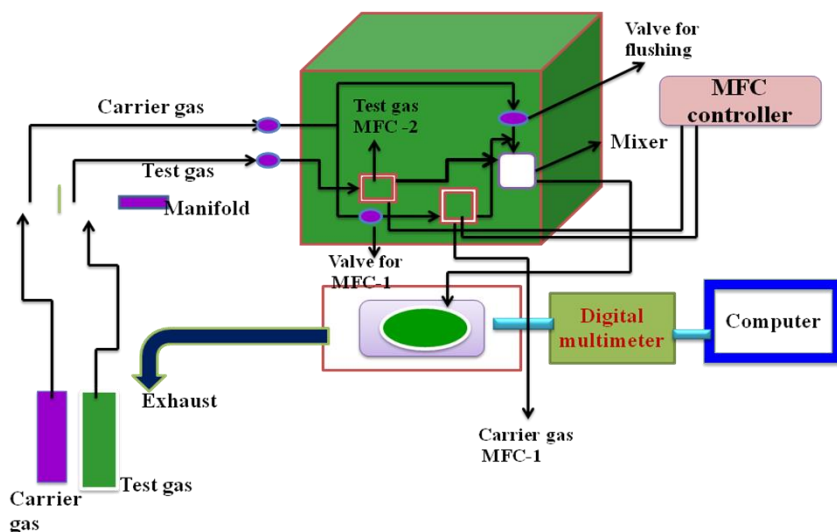
For low temperature resistivity measurement, sample was placed in a specific chamber and the pressure was maintained at 10^{-5} torrs. The Lakeshore (model 331) temperature controller was connected. Then, we measured DC resistivity. A constant current is passed through the two side probes and measured voltage in the two middle probes. A DC current source (Keithley 220 programmable) was taken. Different

millampere/nanoampere current was applied and corresponding voltage was measured. Voltage across the terminals was measured using Keithley nanovoltmeter (model 2182). For In addition, the resistivity measurement with a particular magnetic field is a function of temperature which is important for calculating localization length (L_{loc}). Determination of other different transport parameters [119 20] such as Density of states at Fermi level ($N(E_F)$), Mott's characteristics temperature in Kelvin (T_{Mott}), Mott's hopping distance ($R_{Hop, Mott}$ in nm at 300 K) and the energy difference ($\Delta_{Hop, Mott}$) between the sites in the Mott's limits is calculated using L_{loc} . These are the important parameters to understand the conduction mechanism.

Magnetoresistance (MR) was investigated using a Helium Compressor (HC) (model HC-4E1)–sumitomo cryostat (model Ganis research CO, INC) equipped with 0.8T superconducting magnet (Lake shore electromagnet). For the controlling and measurement of the temperature, we used Lake Shore 331 temperature controller. Magnetoresistance (MR) measurements were performed up to 4000 Gauss (for acid doped membrane based PANI-ES composites) and 5000 Gauss (for Cloisite 20A based composites) and different temperatures 100 K, 200 K, 250 K, 300 K using a computer-controller measuring system.

Gas sensing measurement

For gas sensing studies, the prepared composite film ($\sim 25^\circ\text{C}$) was used. Schematically, gas sensing measuring set up is shown in **Fig. 4**. The set up mainly consists of three sub units and are gas deliver unit, reactor unit and measurement unit.



$$\text{Response (\%)} = \frac{R_a - R_g}{R_a} \times 100 \dots \dots \dots (4)$$

Figure 4. Schematic dynamic gas sensor set- up unit

For the sensing measurements, the surface of the sensing material is electroded with silver paste strip of 8 mm length, 1.5 mm width, and separated from each other by 4 mm. The methane gas sensing behaviour was estimated by measuring the resistance change before and after gas exposure. This measurement was done using an electrometer (6517A, Keithley instruments, USA) in a specially designed sensing-setup [120 21] under dynamic flow of methane gas. The pre-diluted (~10,000 ppm) reducing gases (methane) in nitrogen are mixed with carrier gas (air) using a mixing unit before flowing into the reactor unit. The mass flow controller and electrometer are all interfaced with a PC equipped with a GPIB card (National Instruments) and Labview 8.5 (National Instruments) software.

To evaluate the gas sensing characteristics of the polymer membrane, its planar resistance transient were measured as a function of temperature and gas concentration. From the measured value of equilibrium resistance in air (R_a) and gas (R_g) the response of the sensor surface towards reducing gases was calculated using the relation [120 21].

5. Conclusions

PMMA/PANI composite films are prepared by *insitu* polymerization technique. HCl, H₂SO₄, and H₃PO₄ are used dopants, separately, during the polymerization reaction. Different desired chemical groups of PMMA film, PANI and PMMA/PANI composites are confirmed from ATR-FTIR spectroscopy. Polaron band is shown in UV-Visible data and are confirmed the formation of emeraldine salt (ES). A drastic increment of band gap of the doped samples is found. I-V characteristics without magnetic field of doped PMMA/PANI composites are revealed ohmic behaviour at room temperature. Highest DC conductivity without magnetic field is found to be 0.1421×10^{-2} S/cm for H₂SO₄ doped PMMA/PANI composite. Decreased DC conductivity data with increased magnetic field is observed. Temperature dependent DC conductivity data of HCl doped composite is indicated the semiconducting behaviour.

2.4. Acknowledgments

The author conveys their sincere thanks to the CRF, IIT Kharagpur for their providing testing facilities and Materials Science Centre to do the research work.

2.5. References

- [1] Green A. G., and Woodhead A. E. (1910), CCXLIII.-Aniline-black and allied compounds, Part I, Journal of Chemical Society Transaction, Vol. 97,pp. 2388-2403.

- [2] Surwade, S. P., Agnihotra, S. R., Dua, V., Manohar, N., Jain, S., Ammu, S., and Manohar, S. K. (2009), Catalyst-Free Synthesis of Oligoanilines and Polyaniline Nanofibers Using H_2O_2 , *Journal of American Chemical Society*, Vol. 131, pp. 12528-12529.
- [3] Chowdhury, P., and Saha, B. (2005), Potassium Dichromate initiated Polymerization of Aniline, *Indian Journal of Chemical technology*, Vol. 12, pp. 671-675.
- [4] Svoboda, J., Bláha, M., Sedláček, J., Vohlidal, J., Balcar, H., Mav-Golež, I., Žigon, M. (2006), (Minireview), New Approaches to the Synthesis of Pure Conjugated Polymers, *Acta Chiica Slovenica*, Vol. 53, pp. 407-416.
- [5] Osterholm, J.-E., Cao, Y., Klavetter, F., and Smith, P. (1994), Emulsion Polymerization of Aniline, *Polymer*, Vol. 35, pp. 2902-2906.
- [6] Namgoong, H., Woo, D. J., and Lee, S.-H. (2007), Micro-Chemical Structure of Polyaniline Synthesized by Self-Stabilized Dispersion Polymerization, *Macromolecular Research*, Vol. 15, pp 633-639.
- [7] Zhang, X., Chan-Yu-King, R., Jose, A., Manohar, S. K. (2004), Nanofibers of Polyaniline Synthesized by Interfacial Polymerization, *Synthetic Metals*, Vol. 145, pp. 23-29.
- [8] K. Wilbourn, K., Murray, R.W. (1988), Electrochemical Doping Reactions of the Conducting Ladder Polymer Benzimidazobenzophenanthroline (BBL), *Macromolecules*, Vol. 21, pp. 89-96.
- [9] Athawale, A. A., Kulkarni, M. V., Chabukswar, V. V. (2002), Studies on Chemically Synthesized Soluble Acrylic Acid Doped Polyaniline, *Materials Chemistry and Physics*, Vol. 73, pp. 106-110.
- [10] Ding, H, Wan, M., and Wei, Y. (2007), Controlling the Diameter of Polyaniline Nanofibers by Adjusting the Oxidant Redox Potential, *Advanced Materials*, Vol. 19, pp. 465-469.
- [11] Shreepathi, S., and Holze, R. (2005), Spectroelectrochemical Investigations of Soluble Polyaniline Synthesized via New Inverse Emulsion Pathway, *Chemistry of Materials*, Vol. 17, pp. 4078-4085.
- [12] Meng, F., Yan, X., Zhu, Y., and Pengchao Si, P. (2013), Controllable synthesis of MnO_2 /Polyaniline Nanocomposite and its Electrochemical Capacitive Property, *Nanoscale Research Letters*, Vol. 8, pp. 179-187.
- [13] Lin, Y.-W., and Wu, T.-M. (2009) Synthesis and Characterization of Externally Doped Sulfonated Polyaniline/Multi-Walled Carbon Nanotube Composites, *Composites Science and Technology*, Vol. 69, pp. 2559–2565.
- [14] Nalwa, H. S. (2001), Holze In *Advanced Functional Molecules and Polymers*, (ed.), Gordon and Breach, Tokyo, Vol. 2, pp. 171-xxx.

- [15] Genis, E. M., Boyle, A., Lapkowsky, M. Tsintavis, C. (1990), Polyaniline: A Historical Survey, *Synthetic Metals*, Vol. 36, pp. 139-182.
- [16] Yang, H., and Bard, A. J. (1992), The Application of Fast Scan Cyclic Voltammetry. Mechanistic Study of the Initial Stage of Electropolymerization of Aniline in Aqueous Solutions, *Journal of Electroanalytical Chemistry*, Vol. 339, pp. 423-449.
- [17] Rao, P. S., Sathyanarayana, D. N., and Jeevananda, T. (2001), In *Advanced Functional Molecules and Polymers*, H. S. Nalwa (ed.), Gordon and Breach, Tokyo, Vol.3, p. 79-xxx.
- [18] Bredas, J. L., Street, G. B. (1985), Polarons, Bipolarons, and Solitons of Conducting Polymer, *Accounts of Chemical Research*, Vol. 18, pp. 309-315.
- [19] MacDiarmid, A. G. (2001), *Synthetic Metals: A Novel Role for Organic Polymers (Nobel Lecture)*, *Angewandte Chemie International Edition*, Vol. 40, pp. 2581-2590.
- [20] Chiang, J. C., and MacDiarmid, A. G. (1986), 'Polyaniline': Protonic Acid Doping of the Emeraldine form to the Metallic Regime, *Synthetic Metals*, Vol. 13, (1986) pp. 193-205.
- [21] Brazovskii, S. A., and Kirova, N. N. (1981), Excitations, Polarons, and Bipolarons in Conducting Polymers, *Soviet Physics: Journal of Experimental and Theoretical Physics Letter*, Vol. 33, pp.4-8.
- [22] Wnek, G. E. (1986), A Proposal for the Mechanism of Conduction in Polyaniline *Synthetic Metals*, Vol. 15, pp. 213-218.
- [23] Lundberg, B., Salaneck, W. R., and Lundström, I. (1987), Pressure, Temperature and Field Dependence of Hopping Conduction in Polyaniline, *Synthetic Metals*, Vol. 21, pp. 143-147.
- [24] Das, T. K., and Prusty, S. (2012), Review on Conducting Polymers and Their Applications, *Polymer-Plastics Technology and Engineering*, Vol. 51, pp. 1487-1500.
- [25] Alexandre, M., and Dubois, P. (2000), Polymer-Layered Silicate Nanocomposites: Preparation, Properties and Uses of a New Class of Materials, *Materials Science and Engineering (R)*, Vol. 28, pp. 1-63.
- [26] Binitha, N. N., and Sugunan, S. (2008), Polyaniline/Pillared Montmorillonite Clay Composite Nanofibers, *Journal of Applied Polymer Science*, Vol. 107, pp. 3367-3372.
- [27] Garai, A., Kuila, B.K. and Nandi, A.K. (2006), Montmorillonite Clay Nanocomposites of Sulfonic Acid Doped Thermoreversible Polyaniline Gel: Physical and mechanical Properties, *Macromolecules*, Vol. 39, pp. 5410-5418.

- [28] Uddin, F. (2008), Clays, Nanoclays, and Montmorillonite Minerals, Metallurgical and Materials Transactions A, Vol. 39A, pp. 2804-2814.
- [29] Floody, M. C., Theng, B. K. G., Reyes, P., and Mora, M. L. (2009), Natural Nanoclays: Applications and Future Trends-A Chilean Perspective, Clay Minerals, Vol. 44, pp.161–176.
- [30] Panigrahi, M., Singh, N. K., Gautam, R. K., Banik, R. M., and Maiti, P. (2010), Improved Biodegradation and Thermal Properties of Poly(lactic acid)/Layered Silicate Nanocomposites, Composite Interfaces, Vol. 17, pp. 143–158.
- [31] Peeterbroeck, S., Alexandre, M., Jerome, R., and Dubois, Ph. (2005), Poly(ethylene-co-vinyl acetate)/Clay Nanocomposites: Effect of Clay Nature and Organic Modifiers on Morphology, Mechanical and Thermal Properties, Polymer Degradation and Stability, Vol. 90, pp. 288-294.
- [32] Kiliaris, P., and Papaspyrides, C. D. (2010), Polymer/Layered Silicate (Clay) Nanocomposites: An Overview of Flame Retardancy, Progress in Polymer Science, Vol. 35, pp. 902-958.
- [33] Lee, S. K., Seong, D. G., and Youn, J. R. (2005), Degradation and Rheological Properties of Biodegradable Nanocomposites Prepared by Melt Intercalation Method, Fibers and Polymers, Vol.6, pp. 289-296.
- [34] Wang, K., Chen, L., Wu, J., Toh, M. L., He, C., and Yee, A. F. (2005), Epoxy Nanocomposites with Highly Exfoliated Clay: Mechanical Properties and Fracture Mechanisms, Macromolecules, Vol. 38, pp. 788-800.
- [35] Basnayaka, P. A., Ram, M. K., Stefanakos, L., Kumar, A. (2013), Graphene/Polypyrrole Nanocomposite as Electrochemical Supercapacitor Electrode: Electrochemical Impedance Studies, Graphene, Vol.2, pp. 81-87.
- [36] Nascimento, G. M. do, Constantino, V. R. L., and Temperini, M. L. A. (2002), Spectroscopic Characterization of a New Type of Conducting Polymer-Clay Nanocomposite, Macromolecules, Vol. 35, pp. 7535-7537.
- [37] Kondawar, S. B., Agrawal, S. P., Nimkar, S. H., Sharma, H. J. and Patil P. T. (2012), Conductive Polyaniline-Tin Oxide Nanocomposites for Ammonia Sensor, Advanced Materials Letter, Vol. 3, pp. 393-398.
- [38] Meguedad, A, and Benharrats, N. (2012), Thermal Degradation Behavior of Polythiophene-modified Montmorillonite Nanocomposite, Journal of Analytical Science & Technology, Vol. 3, pp. 193-201.
- [39] Yoon, S., and Park, H.-H., (2010), Enhancement of the Electrical Properties of Poly (pphenylene vinylene) by the Incorporation of Silicon Dioxide Nanoparticles, Journal of Applied Polymer Science, Vol. 117, pp. 700–705.
- [40] Murugan, A.V., Gopinath, C. S., and Vijayamohanam, K. (2005), Electrochemical Studies of Poly (3,4-thylenedioxythiophene) PEDOT/VS₂

- Nanocomposite as a Cathode Material for Rechargeable Lithium Batteries, *Electrochemistry Communications*, Vol. 7, pp. 213–218.
- [41] Goswami, L., Sarma, N. S., and Chowdhury, D. (2011), Determining the Ionic and Electronic Contribution in Conductivity of Polypyrrole/Au Nanocomposites, *Journal of Physical Chemistry C*, Vol. 115, pp. 19668–19675.
- [42] Hao, L.-Y., Zhu, C.-L., Jiang, W.-Q., Chen, C.-N., Hu, Y. and Chen, Z.-Y. (2004), Sandwich $\text{Fe}_2\text{O}_3/\text{SiO}_2/\text{PPy}$ Ellipsoidal Spheres and Four Types of Hollow Capsules by Hematite Olivary Particles, *Journal Materials Chemistry*, Vol. 14, pp. 2929–2934.
- [43] Deng, J. G., Ding, X. B., Zhang, W. C., Peng, Y. X., Wang, J. H., Long, X. P., Li, P., and Chan, A. S. C. (2002), Magnetic and Conducting Fe_3O_4 -Cross-Linked Polyaniline Nanoparticles with Core-shell Structure, *Polymer*, Vol. 43, pp. 2179–2184.
- [44] Ashraf, S. M., Ahmad, S., and Riaz, U. (2006), Synthesis and Characterization of Novel Poly(1-Naphthylamine) -Montmorillonite Nanocomposites Intercalated by Emulsion Polymerization, *Journal of Macromolecular Science, Part B: Physics*, Vol. 45, pp. 1109–1123.
- [45] Khiew, P. S., Huang, N. M., Radiman, S. and Ahmad, M. S. (2004), Synthesis and Characterization of Conducting Polyaniline-Coated Cadmium Sulphide Nanocomposites in Reverse Microemulsion, *Materials Letters*, Vol. 58, pp. 516–521.
- [46] Abdelkader, A., Amine, H., and Mohammed, B. (2013), Maghnite- H^+ , An Eco-catalyst layered for Synthesis of Polyaniline/Maghnite Nanocomposites, *International Journal of Basic and Applied Sciences*, Vol. 2, pp. 193–199.
- [47] Olad, A., and Rashidzadeh, A. (2008), Preparation and Anticorrosive Properties of PANI/Na-MMT and PANI/O-MMT Nanocomposites, *Progress in Organic Coatings*, Vol. 62, pp. 293–298.
- [48] Rizvi, T. Z., and Shakoor, A. (2009), Electrical Conductivity and Dielectric Properties of Polypyrrole/ Na^+ -Montmorillonite (PPy/ Na^+ -MMT) Clay Nanocomposites, *Journal of Physics D: Applied Physics*, Vol. 42, pp. 095415–095420.
- [49] Demets, G. J.-F., Anaissi, F. J., Toma, H. E., and Fontes, M. B. A. (2002), Preparation and Properties of Polypyrrole/Bentonite/Vanadium (V) Oxide Ternary Composites, *Materials Research Bulletin*, Vol. 37, pp. 683–695.
- [50] Ma, R., Sask, K. N., Shi, C., Brash, J. L., and Zhitomirsky, I. (2011), Electrodeposition of Polypyrrole-Heparin and Polypyrrole-Hydroxyapatite Films, *Materials Letters*, Vol. 65, pp. 681–684.
- [51] Yang, C., Liu, P., Guo, J., and Wang, Y. (2010), Polypyrrole/Vermiculite

- Nanocomposites via Self-Assembling and *in situ* Chemical Oxidative Polymerization, *Synthetic Metals*, Vol. 160, pp. 592–598.
- [52] Feng, X., Huang, H., Ye, Q., Zhu, J.-J., and Hou, W. (2007), Ag/Polypyrrole Core-Shell Nanostructures: Interface Polymerization, Characterization, and Modification by Gold Nanoparticles, *Journal of Physical Chemistry C*, Vol. 111, pp. 8463-8468.
- [53] Yang, X. Dai, T., and Lu. Y. (2006), Synthesis of Novel Sunflower-like Silica/Polypyrrole Nanocomposites via Self-assembly Polymerization, *Polymer*, Vol. 47, pp. 441–447.
- [54] Zhu, C.-L., Chou, S.-W., He, S.-F., Liao, W.-N., and Chen, C.-C. (2007), Synthesis of Core/shell Metal Oxide/PANI Nanocomposites and Hollow PANI Capsules, *Nanotechnology*, Vol. 18, pp. 275604-275609.
- [55] Chuang, F.-Y. and Yang S.-M. (2008), Cerium dioxide/polyaniline core-shell nanocomposites, *Journal of Colloid and Interface Science*, Vol. 320, pp. 194–201.
- [56] Kobayashi, Y., Ishida, S., Ihara, K., Yasuda, Y., Morita, T., and Yamada, S. (2009), Synthesis of Metallic Copper Nanoparticles Coated with Polypyrrole, *Colloidal Polymer Science*, Vol. 287, pp. 877–880.
- [57] Kuila, B. K., and Nandi, A. K. (2004), Physical, Mechanical, and Conductivity Properties of Poly(3-hexylthiophene)-Montmorillonite Clay Nanocomposites Produced by the Solvent Casting Method, *Macromolecules*, Vol. 37, pp. 8577-8584.
- [58] Ryu, K. S., Chang, S. H., Kang, S.-G., Oh, E. J., and Yo, C. H. (1999), Physicochemical and Electrical Characterization of Polyaniline Induced by Cross linking, Stretching, and Doping, *Bulletin of Korean Chemical Society*, Vol. 20, pp. 333-336.
- [59] Ahmad, N., Naseer, S. and Norman, M. (2005), Polyaniline Octyl Benzene Sulphonic Acid; Characterization and Synthesis in Normal and Reverse Phase, *Indian Journal of Chemistry*, Vol. 44B, pp. 1536-1537.
- [60] Wang, Y. Z., Joo, j., Hsu, C.-H., and Epstein. A. J. (1995), Charge Transport of Camphor Sulfonic Acid-Doped Polyaniline and Poly (o-Toludine) Fibers: Role of Processing, *Synthetic Metals*, Vol. 68, pp. 207-211.
- [61] Yue, J., Wang, Z. H., Cromack, K. R., Epstein, A. J., and Macdiarmid, A. G. (1991), Effect of Sulfonic Acid Group on Polyaniline Backbone, *Journal of American chemical society*, Vol. 113, pp. 2665-2671.
- [62] Chevalier, J.-W., Bergeron, J.-Y., and Dao, L. H. (1992), Synthesis, Characterization, and Properties of Poly (N-alkylanilines), *Macromolecules*, Vol. 25, pp. 3325-3331.
- [63] Ardsley, N. Y., (1978), *Methods of Using N-substituted-N-alkoxy Carbonyl*

- Anilino compounds, US Patent, Appl. No.: 885718, Adolf Hubele, Magden, Switzerland Ciba-Geigy Corporation.
- [64] Cao, Y., Smith P., and Heeger, A. J. (1992), Counter-ion Induced Processability of Conducting Polyaniline and of Conducting Polyblends of Polyaniline in Bulk Polymers, *Synthetic Metals*, Vol. 48, pp. 91-97.
- [65] Ananda, J., Palaniappanb, S., and Sathyanarayana, D. N. (1998), Conducting Polyaniline Blends and Composites, *Progress in Polymer Science*, Vol. 23, pp. 993–1018.
- [66] Jousseau, V., Morsli, M., Bonnet, A., and Lefrant, S. (1998), X-Ray Photoelectron Spectroscopy of Conducting Polyaniline and Polyaniline–Polystyrene Blends, *Journal of Applied Polymer Science*, Vol. 67, pp. 1209–1214.
- [67] Banerjee, P., and Mandal, B. M. (1995), Conducting Polyaniline Nanoparticle Blends with Extremely Low Percolation Thresholds, *Macromolecules*, Vol. 28, pp. 3940-3943.
- [68] Nair, B. P., and Pavithran, C. (2010), Micropatterned Surfaces through Moisture-Induced Phase-Separation of Polystyrene-Clay Nanocomposite Particles, *Langmuir*, Vol. 26, pp. 12948–12952.
- [69] Rska, M. Z., Taler, E., Kulszewicz-Bajer, I., Pron, A., and Nizioł, J. (1999), Conductive Polyaniline–Polyamide 6 Blends Processed from Formic Acid with Improved Stability against Deprotonation, *Journal of Applied Polymer Science*, Vol. 73, pp. 1423–1426.
- [70] Rao, P. S., Subrahmanya, S., and Sathyanarayana, D. N. (2005), Water-Soluble Conductive Blends of Polyaniline and Poly (vinyl alcohol) Synthesized by Two Emulsion Pathways, *Journal of Applied Polymer Science*, Vol. 98, pp. 583–590.
- [71] Banerjee, P., and Mandal, B. M. (1995) Blends of HCl-doped Polyaniline Nanoparticles and Poly (vinyl chloride) with Extremely Low Percolation Threshold- a Morphology Study, *Synthetic Metals*, Vol. 74, pp. 257-261.
- [72] Hussain, F., Hojjati, M., Okamoto, M., and Gorga, R. E. (2006), Review article: Polymer-matrix Nanocomposites, Processing, Manufacturing, and Application: An Overview, *Journal of Composite Materials*, Vol. 40, pp. 1511-1575.
- [73] Basavaiah, K., Kumar, Y. P., and Rao, A. V. P. A Facile One-pot Synthesis of Polyaniline/Magnetite Nanocomposites by Micelles-assisted Method, *Applied Nanoscience*, Vol. xxx, pp. 1-7.
- [74] Armes, S. P., Aldissi, M., Agnew, S., and Gottesfeld, S. (1990), Aqueous Colloidal Dispersions of Polyaniline Formed by Using Poly (vinylpyridine) -Based Steric Stabilizers, *Langmuir*, Vol. 6, pp. 1745-1749.

- [75] Stejskal, J., Kratochvil, P., Armes, S. P., Lascelles, S. F., Riede, A., Helmstedt, M., Prokes, J., and Krivka, I. (1996), *Polyaniline Dispersions: Stabilization by Colloidal Silica Particles, Macromolecules*, Vol. 29, pp. 6814-6819.
- [76] Chattopadhyay, D., Banerjee, S., Chakravorty, D., and Mandal, B. M. (1998), *Ethyl(hydroxyethyl) Cellulose Stabilized Polyaniline Dispersions and Destabilized Nanoparticles Therefrom, Langmuir*, Vol. 14, pp. 1544-1547.
- [77] Banerjee, P. (1998), *Carboxy Methylcellulose Stabilized Polyaniline Dispersions and Conducting Copolymer Latex Composites, European Polymer Journal*, Vol. 34, pp. 841-847.
- [78] Banerjee, P., Bhattacharyya, S. N., and Mandal, B. M. (1996), *Poly (vinyl methyl ether) Stabilized Colloidal Polyaniline Dispersions, Langmuir*, Vol. 11, pp. 2414-2418.
- [79] Stejskal, J., Kratochv, P., and Helmstedt, M. (1996), *Polyaniline Dispersions. 5. Poly (vinyl alcohol) and Poly(N-vinylpyrrolidone) as Steric Stabilizers, Langmuir*, Vol. 12, pp. 3389-3392.
- [80] Yan, F., and Xue, G. (1999), *Synthesis and Characterization of Electrically Conducting Polyaniline in Water-oil Microemulsion, Journals of Materials Chemistry*, Vol. 9, pp. 3035-3039.
- [81] Dearnitt, C., and Armes, S. P. (1992), *Synthesis of Novel Polyaniline Colloids Using Chemically Grafted Poly (N-vinylpyrrolidone)-Based Stabilizers, Journal of Colloids and Interface Science*, Vol. 150, pp. 134-142.
- [82] Patil, A. O., Ikenoue, Y., Basescu, N., Colaneri, N. Chen, J., F. Wudl, and Heeger, A. J. (1987), *Self-doped Conducting Polymers, Synthetic Metals*, Vol. 20, 151-159.
- [83] Thiemann, C., and Brett, C. M. A. (2002), *Electropolymerization and Properties of Conducting Polymers Derived from Aminobenzenesulphonic Acid and from Mixtures with Aniline, Synthetic metal*, Vol. 125 pp. 445-451.
- [84] Chan, H. S. O., Ho, P. K. H., Ng, S. C., Tan, B. T. G., and Tan, K. L. (1995), *A New Water-Soluble, Self-Doping Conducting Polyaniline from Poly (o-aminobenzyl phosphonic acid) and Its Sodium Salts: Synthesis and Characterization, Journal of American chemical society*, Vol. 117, pp. 8517-8523.
- [85] Kilmartin, P. A., and Wright, G. A. (1997), *Photoelectrochemical and Spectroscopic Studies of Sulfonated Polyaniline Part I. Copolymers of Orthanilic Acid and Aniline, Synthetic Metals*, Vol. 88, pp. 153-162.
- [86] Shimizu, S., Saitoh, T., Uzawa, M., Yuasa, M., Yano, K., Maruyama, T., and Watanabe, K. (1997), *Synthesis and Applications of Sulfonated Polyaniline, Synthetic Metals*, Vol. 85, pp. 1337-1338.

- [87] Guo, R., Barisci, J. N., Innis, P. C., Too, C. O., Wallace, G.G., and Zhou, D. (2000), Electrohydrodynamic Polymerization of 2-Methoxyaniline-5-Sulfonic acid, *Synthetic Metals*, Vol. 114, pp. 267–272.
- [88] Zhou, D., Innis, P. C., Wallace, G. G., Shimizu, S., Maeda, S.-I. (2000), Electrosynthesis and Characterisation of Poly (2-methoxyaniline-5-sulfonic acid) Effect of pH Control, *Synthetic Metals*, Vol. 114, pp. 287–293.
- [89] Wei, X.-L., Wang, Y. Z., Long, S. M., Bobeczko, C., and Epstein, A. J. (1996), Synthesis and Physical Properties of Highly Sulfonated Polyaniline, *Journal of American Chemical Society*, Vol. 118, pp. 2545-2555.
- [90] Kitani, A., Satoguchi, K., Tang, H.-Q., Ito, S., and Sasaki, K. (1995), Electrosynthesis and Properties of Self-doped Polyaniline, *Synthetic Metals*, Vol. 69, pp. 129-130.
- [91] Wei, X., and Epstein, A. J. (1995), Synthesis of Highly Sulfonated Polyaniline, *Synthetic Metals*, Vol. 74, Vol. 123-125.
- [92] Han, M. G., Cho, S. K., Oh, S. G., and Im, S. S. (2002), Preparation and Characterization of Polyaniline Nanoparticles Synthesised from DBSA Micellar Solution, *Synthetic Metal*, Vol. 126, pp.53-60.
- [93] Kinlen, P. J., Liu, J., Ding, Y., Graham, C. R., and Remsen, E. E. (1998), Emulsion Polymerization Process for Organically Soluble and Electrically Conducting Polyaniline, *Macromolecules*, Vol. 31, pp. 1735-1744.
- [94] Kim, D., Choi, J., Kim, J.-Y., Han, Y.-K., and Sohn, D. (2002), Size Control of Polyaniline Nanoparticle by Polymer Surfactant, *Macromolecules*, Vol. 35, pp. 5314-5316.
- [95] Stejskal, J., and Sapurina, I. (2004), On the Origin of Colloidal Particles in the Dispersion Polymerization of Aniline, *Journal of Colloid and Interface Science*, Vol. 274, pp. 489–495.
- [96] Qiu, H., and Wan, M. (2001), Conducting Polyaniline Nanotubes by Template-Free Polymerization, *Macromolecules*, Vol. 34, pp. 675-677.
- [97] Aboutanos, V., Barisci, J. N., Kane-Maguire, L. A. P., and Wallace, G. G. (1999), Electrochemical Preparation of Chiral Polyaniline Nanocomposites, *Synthetic Metals*, Vol. 106, pp. 89–95.
- [98] Liu, W., Cholli, A. L., Nagarajan, R., Kumar, J., Tripathy, S., Bruno, F. F., and Samuelson, L. (1999), The Role of Template in the Enzymatic Synthesis of Conducting Polyaniline, *Journal of American chemical society*, Vol. 121, pp. 11345-11355.
- [99] Liu, J.-M., and Yang, S. C. (1991), Novel Colloidal Polyaniline Fibrils Made by Template Guided Chemical Polymerization, *Journal of Chemical Society: Chemical Communication*, Vol. xxx, pp. 1529-1531.

- [100] Ivanov, V. F., Gribkova, O. L., Cheberyako, K. V., Nekrasov, A. A., Tverskoi, V. A., and Vannikov, A. V. (2004), Template Synthesis of Polyaniline in the Presence of Poly-(2-acrylamido-2-methyl-1-propanesulfonic Acid), *Russian Journal of Electrochemistry*, Vol. 40, pp. 299–304.
- [101] Stejskal, J., Omastova, M., Fedorova, S., Prokes, J., and Trchova, M. (2003), Polyaniline and Polypyrrole Prepared in the Presence of Surfactants: A Comparative Conductivity Study, *Polymer*, Vol. 44, pp. 1353–1358.
- [102] Jayanty, S., Prasad, G. K., Sreedhar, B., and Radhakrishnan, T. P. (2003), Polyelectrolyte Templated Polyaniline-Film Morphology and Conductivity, *Polymer*, Vol. 44, pp. 7265–7270.
- [103] Yuan, G.-L., Noriyuki Kuramoto N., and Su, S.-J. (2002), Template Synthesis of Polyaniline in the Presence of Phosphomannan, *Synthetic Metals*, Vol. 129, pp. 173–178.
- [104] Huang, J., and Kaner, R. B. (2004), A General Chemical Route to Polyaniline Nanofibers, *Journal of American Chemical Society*, Vol. 126, pp. 851–855.
- [105] Li, D., and Kaner, R. B. (2005), Processable Stabilizer-free Polyaniline Nanofiber Aqueous Colloids, *Chemical Communication*, Vol. 26, pp. 3286–3288.
- [106] Pud, A., Ogurtsov, N., Korzhenko, A., and Shapoval, G. (2003), Some Aspects of Preparation Methods and Properties of Polyaniline Blends and Composites with Organic Polymers, *Progress in Polymer Science*, Vol. 28, pp. 1701–1753.
- [107] Edwards, J. C. Principles of NMR, Process NMR Associates LLC, 87A Sand Pit Rd, Danbury CT 06810.
- [108] Mann, M., Hendrickson, R. C., Pandey, A. (2001), Analysis of Proteins and Proteomes by Mass Spectrometry, *Annual Review Biochemistry*, Vol. 70, pp. 437–73.
- [109] FTIR Spectroscopy Attenuated Total Reflectance (ATR), www.perkinelmer.com.
- [110] Smith, W. E., and Dent, G. (2005), *Modern Raman Spectroscopy—A Practical Approach*, John Wiley & Sons, Ltd ISBNs: 0-471-49668-5 (HB); 0-471-49794-0 (PB).
- [111] Thermo Spectronic, Basic UV-Vis Theory, Concepts and Applications.
- [112] Alexandre, M., and Dubois, P. (2000), Polymer-layered Silicate Nanocomposites: Preparation, Properties and Uses of a New Class of Materials, *Materials Science and Engineering R*, Vol. 28, pp. 1–63.
- [113] Klugg, H. P., and Alexander, L. E. (1974), *X-ray Diffraction Procedures*;

John Wiley & Sons: U.S.A.

- [114] Moore, D., and Reynolds, R. Jr. (1997), X-ray Diffraction and Identification and Analysis of Clay Minerals of Clay Minerals; Second Ed.; Oxford University Press, U. K.
- [115] Carl Zeiss Microscopy, 2004, Detection Principles based on GEMINI ® Technology.
- [116] Trayner, S. (2012), Carbon Nanotype Composite Sample Preparation by Using Microtome for TEM Analysis, Honors Theses, Paper 51.
- [117] Anandhan, S. Thermal Analysis, Dept. of Met. and Mat. Engg., NITK.
- [118] Paul Gabbott (Editor), 16 Apr 2008, DOI: 10.1002/9780470697702, Principles and Applications of Thermal Analysis, 1999-2013 John Wiley & Sons, Inc.
- [119] Sengupta, P. P., Kar, P., Adhikari, B. (2009), Influence of Dopant in the Synthesis, Characteristics and Ammonia Sensing Behavior of Processable Polyaniline, Thin Solid Films, Vol. 517, pp. 3770-3775.
- [120] Ghosh, M., Barman, A., De, S. K., and Chatterjee, S. (1998), Electrical Resistivity and Magnetoresistivity of Protonic Acid (H₂SO₄ and HCl)-Doped Polyaniline at Low Temperature, Journal of Applied Physics, Vol. 84, pp. 806–811.
- [121] Mukherjee, K., and Majumder, S. B. (2009), Analysis of Response and Recovery Kinetics of Znc Ferrites as Hydrogen Gas Sensor, Journal of Applied Physics Vol. 106, pp. 064912-064921.

Chapter 3

Cloisite 20A Based Polyaniline Nanocomposites for Nitrogen Dioxide (NO₂) Gas Sensors

Muktikanta Panigrahi ^{1,*}, Basudam Adhikari ¹

¹ Materials Science Centre, Indian Institute of Technology, Kharagpur, West Bengal, India

*Corresponding author: muktikanta2@gmail.com

Abstract

Compacted polyaniline (PANI)/Layered silicate nanocomposites have been successfully prepared by simple *in situ*, *core-shell*, and *ex situ* polymerization routes using AnHCl as a predecessor through chemical oxidation method. The structure, chemical groups, electronic transition and properties were investigated by XRD, SEM, HRTEM, UV Visible, DC electrical conductivity, TGA, and DSC. The XRD results reveals that HCl-treated Cloisite 20A, and PANI-ES/Cloisite 20A nanocomposites are delaminated. Flake-like morphologies were observed in Cloisite 20A and HCl-treated Cloisite 20A, whereas different rate of compacted fibrous morphologies of prepared PANI-ES/Cloisite 20A nanocomposites were observed as evident from SEM images. The Si-O FTIR band position does not change even after HCl treatment of Cloisite 20A, but different FTIR peaks positions of PANI-ES/Cloisite 20A nanocomposites were shifted from pure PANI-ES peaks after using Cloisite 20A nanoclays. UV-Visible spectra indicated the increment of charge carrier within the PANI-ES/Cloisite 20A nanocomposites compared to the pure one. The prepared nanohybrids showed significantly improved thermal property compared to pristine PANI-ES as clear from TGA and DSC analysis. The highest DC electronic conductivity of nanocomposite prepared by *core-shell* route is found to be 5.12 S/cm using linear four probe techniques. In addition, the charge transport mechanism was understood with and without loading Cloisite 20A in PANI-ES. The conductivity data supported the temperature-dependence relationship $\sigma(T) = \sigma_0 \exp[-T_0/T]^{1/4}$ and followed characteristic of three-dimensional variable-range hopping (3D–VRH) mechanism. In addition, we were discussed the response of Nitrogen dioxide (NO₂) gas with polyaniline based sensor materials.

Keywords: PANI-ES, Nanofibers, Delamination, Enthalpy, Electrical conductivity, VRH mechanism

© IOR INTERNATIONAL PRESS, 2021

Muktikanta Panigrahi & Basudam Adhikari, *Fundamentals on Polyaniline based Composites*

<https://doi.org/10.34256/ioriiip2123>

1. Introduction

Conducting polymers have attracted much more attention of scientific community in recent decades because of their prospective application in different fields such as antistatic shielding, light emitting diodes, supercapacitors, rechargeable batteries, sensors, corrosion inhibitors and artificial muscles [1-6]. Among the known conducting polymers, PANI has been extensively studied due to its ease of synthesis *via* chemical and electrochemical routes, good environmental stability, unique acid-base doping-dedoping, oxidation reduction chemistry and low-cost synthesis [7-9]. However, the electrical and physical properties of PANI are not satisfactory for practical purpose. To solve this, development of polymer nanocomposites is one of the effective ways to improve material performance.

Among the large number of layered solids, clay minerals especially the members of smectite group are most suitable for the reinforcement of polymer matrix. Organically modified layered silicates (OMLS) nanoclays have been used to prepare the cost-effective polymer nanocomposite because of their unique structure, reactivity combined with their high strength, stiffness and high aspect ratio of each clay platelet [10,11]. And also layered structured (2:1 smectite minerals) possess a high negative charge density, high anisotropy, which make them of great capacity for surface adsorption and also catalytic activity in organic reactions. The structure of smectite hydrophobic clays (2:1 type) minerals, has received great attention when the PANI confinement is desirable [10]. Chemical structure of smectite clay minerals forms by sandwiching an $\text{MO}_4(\text{OH})_2$ octahedron sheet between two MO_4 tetrahedron sheets producing layers designated by T:O:T which consists of nanometer thick layers. The octahedral sites are occupied by ions such as aluminium, magnesium and iron; while the tetrahedral site accommodates silicon and aluminium. The overall negative charge of individual layer assumes to have a parallel orientation and the electric charge is neutralized by the presence of exchangeable hydrated positive ion in the interlayer space [10-13]. In the present work, Cloisite 20A was chosen as reinforcing filler because the platelets are generally surface modified with surfactants to allow complete dispersion, provide miscibility, *i.e.*, compatibility with the polymer system; and improve the thermal stability and compactness of polymer chains for which they were designed.

There are several literature reports on the preparation of PANI-clay based nanocomposites with different weight percentages of dispersion [14-17]. The majorities of reports show *in situ* polymerization technique to prepare clay based intercalated/exfoliated nanocomposites [14-17]. In addition, emulsion polymerization method was employed to prepare the clay based nanocomposites [18]. Both intercalated and exfoliated conducting polymer nanocomposites show better properties such as stiffness, strength and barrier with few weight percentage of inorganic-organic clay content [14-17]. It is rationalized that higher is the degree of exfoliation between polymer and inorganic-organic hybrid nanocomposites, the greater is the increment of materials properties. Recently, Yeh *et al.* [19] have reported that polyaniline clay-based nanocomposites with exfoliated silicate layers are

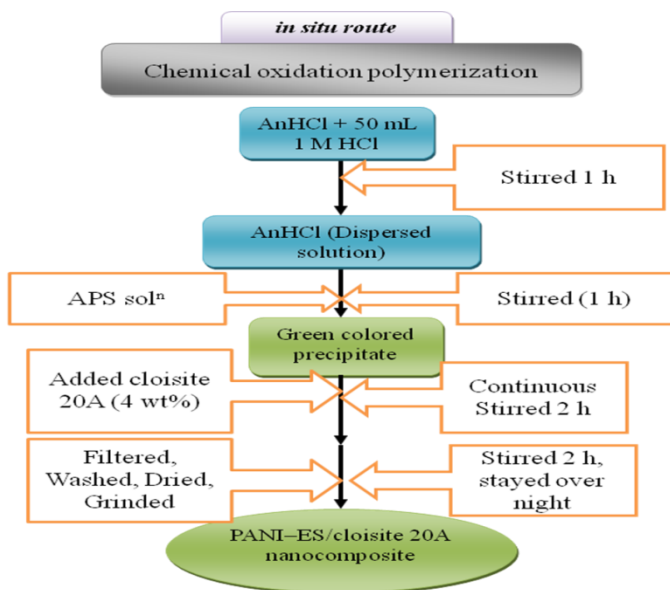
successfully prepared using organically modified clay.

Different spectroscopic analyses such as XRD, FTIR, and UV-Visible *etc.* were used to characterize the prepared layered silicate composite materials [14-17]. Particularly, Raman spectroscopic analysis has been modest discovered to examine the nature of these composite materials [20]. In this paper, we have reported the synthesis of PANI-ES, PANI-ES/Cloisite 20A nanocomposites from aniline hydrochlorides (AnHCl) *via in situ* polymerization route. We analyzed the effect of 4 wt% Cloisite 20A nanoclays on nanostructure, crystallinity, charge transfer spectra, thermal stability, and DC conductivity at room temperature as well as temperature dependent (with and without field) in PANI-ES chains.

2. Experimental Section

2.1. Synthesis of PANI-ES/Cloisite 20a (4 Wt%) Nanocomposites by *In Situ* Route.

PANI-ES was synthesized by a simple chemical oxidation polymerization technique from AnHCl (monomer) at room temperature. For this synthesis, three different types of solutions were required to complete the polymerization. Therefore, Solution 1 was prepared by adding 50 mL of 1 (M) HCl and 2.59 g (0.03 moles) of AnHCl and was stirred to 1 h. Solution 2 was also prepared by mixing 50 mL of 1 (M) HCl and 10.26 g (0.045 moles) ammonium perdisulphate (APS). Solution 2 was added drop wise to the solution 1 to form solution 3.

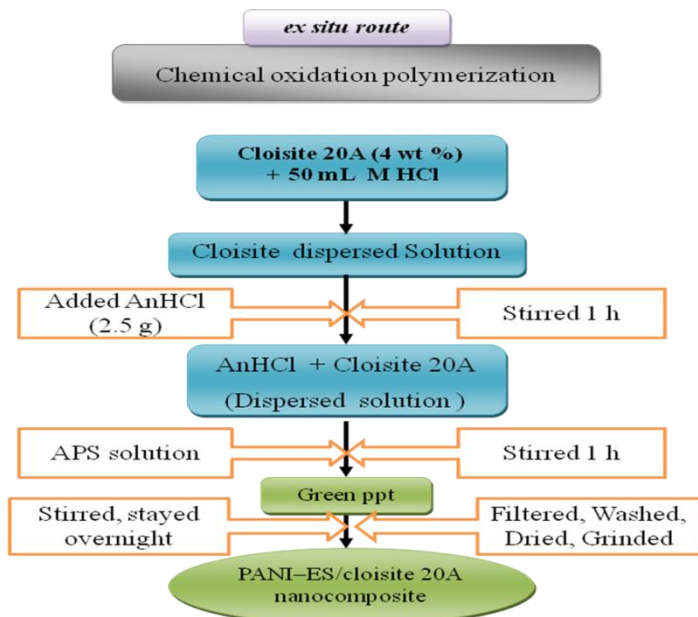


Scheme 1. Summary of the *in-situ* route synthesized PANI-ES/Cloisite 20A (4 wt%) nanocomposites

During this addition, the color of solution 3 changed from slight yellowish to blue to green color. This was observed that the polymerization was continued under constant stirring (2 h).²⁰ Then, 0.1036 g (4 wt%) of Cloisite 20A was added on solution 3 by constant stirring and kept for 12 h for complete reaction and polymerization. The resulting products were filtered and washed with 1 (M) HCl, deionizer water, diethyl ether and dried under vacuum at 60 °C for 6 h. For comparison, pure PANI-ES powders were prepared under conditions similar to those mentioned above up to addition of Cloisite 20A. Summary of the *in situ* route to synthesized PANI-ES/Cloisite 20A nanomaterials is shown as flow chart in **Scheme 1**.

2.2. Synthesis Of PANI-ES/Cloisite 20a (4 Wt%) Nanocomposites by *Ex Situ* Polymerization Process.

In this process, PANI-ES/Cloisite 20A (4 wt%) nanocomposites were synthesized by a simple *ex situ* polymerization route using AnHCl as precursor at room temperature.²¹ The synthesis procedure was slightly modified in the procedure for preparation of nanocomposite. Generally, two type of prepared solutions were required for synthesis of PANI-ES/Cloisite 20A (4 wt%) nanocomposites. Accordingly, solution A was prepared by taking 50 mL of 1 (M) HCl and 4 wt% Cloisite 20A. It was stirred continuously and followed by the addition of 2.59 g of AnHCl for 1 h to form dispersed solution. Solution B was also prepared by mixing 50 mL of 1 (M) HCl and 10.26 g (0.045 moles) of APS as oxidant.

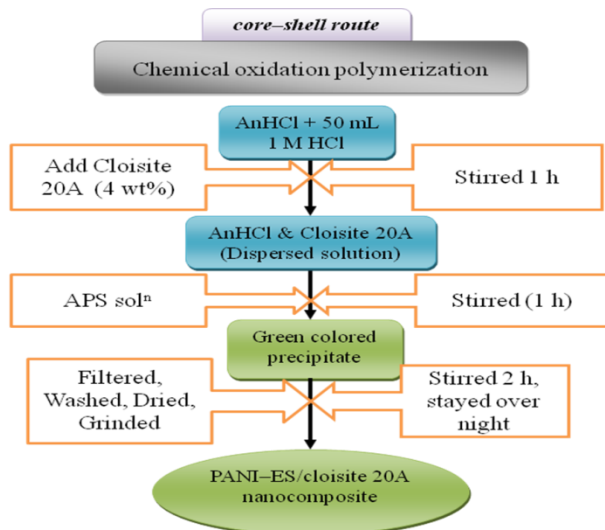


Scheme 2. The flow chart for *ex situ* route synthesized PANI-ES/Cloisite 20A (4 wt%) nanocomposites

Solution B was added drop wise to the solution A to 1 h and the polymerization is carried out. During this addition, the color of the solution changed from slight blackish to blue to green color and then deep green color. It may believe that the polymerization was carried out under constant stirring for 2 h.²¹ The obtained dispersion was kept for overnight for complete reaction and polymerization. The resulting dispersion was filtered and washed with 1(M) HCl, deionized (DI) water, diethyl ether and dried under vacuum at 60 °C for 6 h to get HCl doped PANI-ES/Cloisite 20A (4 wt%) nanocomposites. The flow chart for *ex situ* route synthesis of PANI-ES/Cloisite 20A (4 wt%) nanocomposites is shown in **Scheme 2**.

2.3. Synthesis Of PANI-Es/Cloisite 20a (4 Wt%) Nanocomposites by CORE-SHELL Polymerization Process.

In a typical synthesis route, PANI-ES/Cloisite 20A nanocomposites was synthesized by a simple *core-shell* polymerization route at room temperature using AnHCl as starting materials. The details synthesis procedure is followed as described in the literature.²² For this synthesis, two types of prepared solutions such as Cloisite 20A dispersed in monomer solution (dispersed solution) and oxidant (APS) solution were needed. Accordingly, dispersed solution consisted of 50 mL 1 (M) HCl and AnHCl (2.59 g) in which 4 wt% Cloisite 20A was dispersed. This dispersion was stirred continuously for 1 h. Oxidant solution was also prepared by taking 50 mL of 1 (M) HCl and 10.26 g (0.045 moles) of APS as oxidant.



Scheme 3: The Flow Chart for *CORE-SHELL* Route Synthesized PANI-ES/Cloisite 20a (4 Wt%) Nanocomposites

Oxidant solution was added drop wise to the dispersed solution for 1 h and the polymerization was carried out. At that time, the color of the solution changed

from slight blackish to blue and turned into green color and then deep green color. This was observed when the polymerization is continued under constant stirring to 2 h.²² The obtained dispersion was kept for overnight for complete reaction and polymerization. The resulting dispersion was filtered and washed with 1 (M) HCl, deionized (DI) water, diethyl ether and dried under vacuum at 60 °C for 6 h to get HCl doped PANI-ES/Cloisite 20A nanocomposites. The flow chart for *core-shell* technique synthesis of PANI-ES/Cloisite 20A nanocomposite is shown in **Scheme 3**.

2.4. Pellets Preparation.

Pellets were obtained from as prepared conducting polymeric materials by compression molding using a pelletizer. The assembled plates were first cleaned. A pressure of 124 MPa was applied for five minutes to form pellet. After the removing the pressure, the pelletizer was removed and then the pellet sample was removed. Thicknesses and diameter of prepared pellets were measured to be 1.10 mm and 15.76 mm (pure PANI-ES), 1.09 mm and 15.76 mm (*in situ* nanocomposite), 1.11 mm and 15.75 mm (*ex situ* nanocomposite), 1.10 mm and 15.75 mm (*core-shell* nanocomposite), respectively. These samples were used for characterizations.

2.5. Characterization Techniques.

XRD experiments were performed using a Phillips PW-1710 advance wide angle X-ray diffractometer, Phillips PW-1729 X-ray generator and Cu K α radiation (wavelength, $\lambda = 0.154$ nm). The generator was operated at 40 kV and 20 mA.

FTIR spectra were recorded on a Thermo Nicolet Nexus 870 spectrophotometer in the range of 400-4000 cm⁻¹. The instrument settings were kept constant (50 scan at 4 cm⁻¹ resolution, absorbance mode).

UV-Visible spectra of the pure PANI and its corresponding nanocomposite were recorded by using a Micropack UV-VIS-NIR, DH 2000 in the wave length region 200-1000 cm⁻¹. Base line was corrected before recording the spectra.

Surface morphology of Cloisite 20A, HCl-treated Cloisite 20A, pure PANI-ES, and PANI-ES/Cloisite 20A nanocomposites were analyzed by **SEM** using Carl Zeiss Supra 40 scanning electron microscope. For this experiment, operating voltage was maintained at 30 kV.

To identify the internal structure and dispersion status, the prepared nanocomposite were examined using **HRTEM** at 200 kV acceleration voltages (JEM-2100 HRTEM, JEOL, and Japan). HRTEM experiment specimens of PANI-ES/Cloisite 20A nanocomposites were prepared by microtome technique LEICA Microsystem, GmbH, A-1170) and was transferred them onto Cu TEM grids.

TGA analysis and **DSC** were performed using a Perkin Elmer Pyris Diamond analyzer at a heating rate of 10 °C/min in nitrogen environment.

The room temperature (~30 °C) **DC conductivity** of the prepared pure PANI-

ES and PANI-ES/Cloisite 20A (4 wt%) nanocomposite was measured using linear four-probe technique. Contact was made with silver paste. A constant current (I) from a current source (Keithley 2400 programmable current source) was allowed to pass through two terminal leads of the four probe and the voltage (V) across the other two leads was measured using a multimeter (Keithley 2000 digital multimeter). According to four point-probe method, first the resistivity (ρ) was calculated using the relation²³

$$\rho = 2\pi S \left(\frac{V}{I} \right) \dots\dots\dots (1)$$

where S is the probe spacing in centimetres (cm), which was kept constant, (I) is the supplied current in millamperes (mA) and the corresponding voltage (V) was measured in millivolts (mV). The conductivity (σ) was calculated using the relation as follows²³

$$\sigma = \frac{1}{\rho} \dots\dots\dots (2)$$

Also, resistivity measurement with and without magnetic field as a function of temperature was measured using a linear four-probe technique for understanding of transport phenomenon of prepared pure PANI-ES and PANI-ES/Cloisite 20A (4 wt%) nanocomposite. Resistivity measurement with magnetic field was investigated using a helium compressor (HC) (model HC-4E1)-sumitomo cryostat (model Gains research CO, INC) equipped with 0.8 T superconducting magnet (Lake shore electromagnet). Lake shore 331 temperature controller was used. Such measurements were performed at 5000 gauss and at various temperatures using a computer controlling measuring system. A constant current (I) from a current source (Keithley 220 programmable current source) was allowed to pass through two terminals leads of four probe and the voltage (V) across the other two leads was measured using a multimeter (2182 NANO-VOLTMETER Keithley).

2.6. Results and Discussion

X-Ray Diffraction (XRD) Study

Low angle (1-10°) X-ray diffraction (LXRD) has often been used to determine the degree of intercalation and/or exfoliation and/or delamination of nanoclays in the polymer matrix. XRD patterns for Cloisite 20A and HCl-treated Cloisite 20A, PANI-ES and PANI-ES/Cloisite 20A (4 wt%) nanocomposites are shown in **Fig. 1**. The different parameters (from XRD analysis) of Cloisite 20A, HCl-treated Cloisite 20A, PANI-ES and PANI-ES/Cloisite 20A (4 wt%) nanocomposites are presented in **Table 1**. The d-spacing in (001) plane has been reported to be 2.42 nm for pure Cloisite 20A nanoclay [21], whereas HCl treated Cloisite 20A clay was

found to be 2.315 nm. This has happened due to the presence of aqueous acidic solution. That plays the role for separation of clay layers [14]. That is why, we got lower d-value. No distinct peak was observed for pure PANI-ES, whereas for *in situ*, *core-shell* and *ex situ* prepared nanocomposites, the small intense peak was found at lower angle. According to [14], it is confirmed that the clay layers were delaminated in the polymer matrix. Acidic aqueous medium has played the major role for delamination along with the interaction between positively charged nitrogen centres in PANI-ES chains and negatively charged centres of oxygen in Cloisite 20A layers (Si-O⁻).

Also, the crystallite size (D) of Cloisite 20A, HCl-treated Cloisite 20A, and PANI-ES/Cloisite 20A (4 wt%) nanocomposites (*in situ*, *core-shell* and *ex situ*) was also calculated using the Sherrer's equation 1 [22]

$$D = \frac{0.9\lambda}{\beta \cos \theta} \dots\dots\dots(1)$$

Where D is the crystallite size, λ is wave length of the radiation, θ is the Bragg's angle at (001) reflection and β is the full width at half maxima (FWHM).

In **Fig. 1**, the D-values were found to be 15 nm, 7.88 nm, 9.24 nm and 15.857 nm for PANI-ES, for *in situ*, *core-shell* and *ex situ* prepared nanocomposites, respectively by considering angles between 5 and 45°. FWHM of nanocomposites are significantly lower as compared to pure PANI-ES. Crystallite size and FWHM are inversely related (**Table 1**) [22,23], which has immense impact on property (like crystallinity) enhancement in nanocomposites.

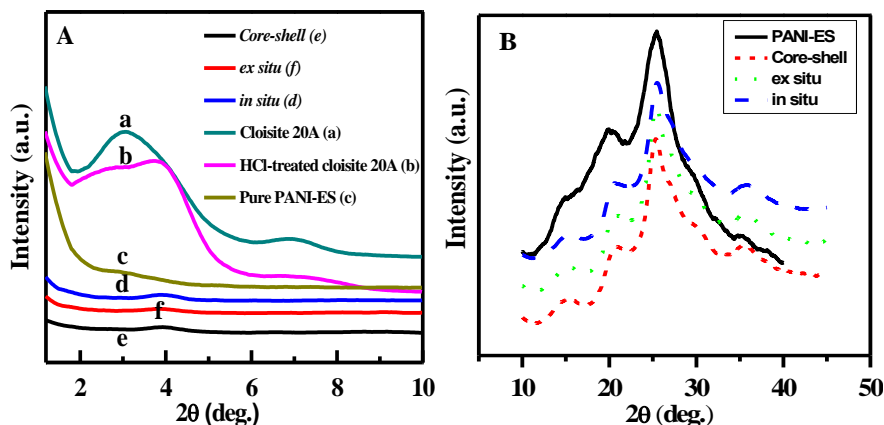


Figure 1. A: Nanostructure study of Cloisite 20A (a), HCl-Cloisite 20A (b), PANI-ES (c), *in situ* nanocomposites (d), *core-shell* nanocomposites (e) and *ex situ* nanocomposite (f); B: Crystallite size study and determination of FWHM of PANI-ES, *in situ* nanocomposites, *ex situ* nanocomposites and *core-shell* nanocomposites

The observed peak positions are found to be at 25.45° for PANI-ES [24],

25.45° for nanocomposite (*in situ*), 25.31° for nanocomposite (*core-shell*) and 25.35° for nanocomposite (*ex situ*). This indicates that the characteristic crystalline phase of the PANI-ES has improved significantly.

Table 1. XRD parameters such as FWHM, crystallite size (D) and nanostructure of Cloisite 20A, HCl-treated Cloisite 20A, PANI-ES, *in situ* nanocomposites, *ex situ* nanocomposites, and *core-shell* nanocomposites

Materials name	FWHM	Crystallite size (D) (nm)	Nanostructure	Referen ce no.
Cloisite 20A	---	---	OMLS	21
HCl treated-cloisite 20A	---	---	Delaminated	14
PANI-ES/20A (<i>in situ</i>)	1.008	7.88	Delaminated	14
PANI-ES/20A (<i>core-shell</i>)	0.8640	9.24	Delaminated	14
PANI-ES/20A (<i>ex situ</i>)	1.1520	15.857	Delaminated	14
PANI-ES	0.582	15	Structure could not assigned	19

Fourier transform infrared (FTIR) spectroscopic analysis

Chemical group analysis of with and without Cloisite 20A, PANI-ES and as prepared nanocomposites (*in situ*, *core-shell* and *ex situ*) was done by FTIR experiment. The presence of chemical groups and shifting of peak positions were observed from FTIR experiment. FTIR spectra of Cloisite 20A [23], HCl-treated Cloisite 20A, PANI-ES [24] and PANI-ES/Cloisite 20A nanocomposites (*in situ*, *core-shell* and *ex situ*) are shown in the **Fig. 2**. The characteristic peak positions and peak assignments are given in the **Table 2**. In Fig. 3.2, the most important Si–O stretching of Cloisite 20A and HCl-treated Cloisite 20A was found to be at 1040 cm⁻¹ [16]. However, there are some extra bands found in Cloisite 20A, whereas these bands are not exhibited in MMT clay. These bands are located at 2924, 2842 and 1475 cm⁻¹ and are assigned for C–H symmetric, asymmetric and bending vibrations of methylene groups, respectively. Similarly for HCl-treated Cloisite 20A, Si–O band position is not changed (it is also clearly evident from SEM images in **Fig. 4**). FTIR spectra of

PANI-ES [20] and PANI-ES/Cloisite 20A (4 wt%) nanocomposites (*in situ*, *core-shell* and *ex situ*) are shown in **Fig. 2**. The important FTIR bands of PANI-ES were found at 1554, 1475 and 1108 cm^{-1} corresponding to quinoid, benzenoid and C=N stretching, respectively [16]. From this observation, the presence of quinoid and benzenoid ring vibrations (at 1475 and 1554 cm^{-1}) indicates the oxidation state of PANI-ES [20].

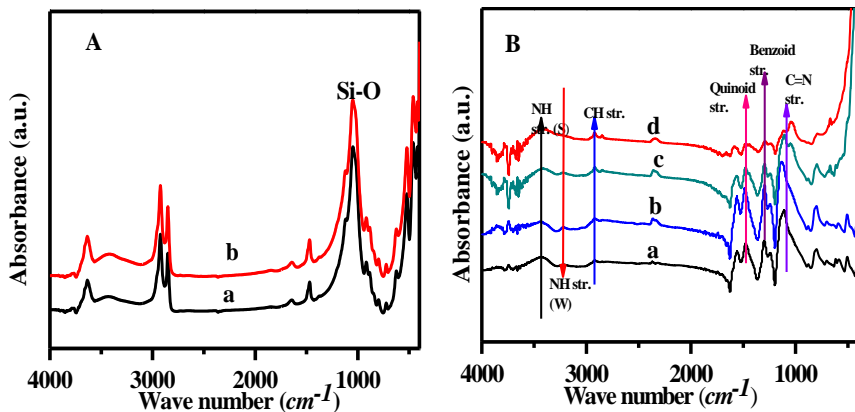


Figure 2. A: FTIR spectra of Cloisite 20A (a) and HCl-treated Cloisite 20A (b); B: PANI-ES, *in situ* nanocomposites, *ex situ* nanocomposites and *core-shell* nanocomposites

The characteristic bands of *in situ* nanocomposites were observed at 1556, 1473, 3441 and 1132 cm^{-1} (**Fig. 2**). These bands are shifted towards higher wave number which indicates the interaction occurring between PANI-ES chains and Cloisite 20A. For *ex situ* nanocomposites (**Fig. 2**), the bands have appeared at 3425, 1567, 1460, and 1107 cm^{-1} . The FTIR bands of *core-shell* nanocomposites are found at 3432, 2926, 1588, 1474, and 1034 cm^{-1} (**Fig. 2**). The C=N bands of prepared PANI-ES/Cloisite 20A (4 wt%) nanocomposites (*in situ*), *core-shell* nanocomposites and *ex situ* nanocomposites were found to be at 1132 cm^{-1} , 1034 cm^{-1} and 1107 cm^{-1} , respectively. It was described as the "electron-like-band". This was considered to be the delocalization of electrons in the polymer chain. The stretching vibrations of the C-N⁺ in the polaron structure of PANI-ES, *in situ* and *ex situ* nanocomposites were found to be at 1236, 1247 and 1244 cm^{-1} , respectively. The peak positions in benzenoid ring of PANI-ES and its corresponding *in situ*, *core-shell* and *ex situ* nanocomposites were observed at 1473, 1479, 1474 and 1489 cm^{-1} , respectively. Similarly, the stretching vibrations of C=C in the quinoid ring of PANI-ES, *in situ* nanocomposites, *core-shell* nanocomposites and *ex situ* nanocomposites were found to be at 1556 cm^{-1} , 1560 cm^{-1} , 1588 cm^{-1} and 1560 cm^{-1} , respectively. This indicates that the characteristic peaks of PANI-ES chains are shifted to higher wave numbers due to the strong interaction between HCl doped PANI-ES and negatively charged species of used clay platelet [16]. It is well known that the strong interaction between the clay platelet and PANI-ES would facilitate a charge transfer process between the components of the system, which further contributes to the increment of the conductivity of the nanocomposites. Also, this result is clear evidence of the presence

of different chemical groups in Cloisite 20A and PANI-ES chains.

Table 2. FTIR Peak positions and peak assignments of Cloisite 20A, HCl-treated Cloisite 20A, PANI-ES, *in situ* nanocomposites, *ex situ* nanocomposites, and *core-shell* nanocomposites

Peak Assignments	Peak Positions (cm^{-1})					
	Cloisite 20A	HCl treated Cloisite 20A	PANI-ES	PANI-ES/20A (<i>in situ</i>)	PANI-ES/20A (<i>core-shell</i>)	PANI-ES/20A(<i>ex situ</i>)
N–H stretch (weak)	N ^a	N ^a	3217	3220	N ^a	3220
N–H stretch (strong)	N ^a	N ^a	3419	3441	3432	3425
C–H stretch	N ^a	N ^a	2926	2926	2926	2926
Quinoid stretch	N ^a	N ^a	1554	1556	1588	1567
Benzoid stretch	N ^a	N ^a	1475	1473	1474	1460
C=N stretch	N ^a	N ^a	1108	1132	1034	1107
Si–O stretch	1055	1055	N ^a	N ^a	N ^a	N ^a
Reference	16	N ^a	20	N ^a	N ^a	N ^a

^aN stands for no peak

UV-visible (UV-Vis) spectroscopic analysis

Dispersed solution of Cloisite 20A and HCl-treated Cloisite 20A exhibits an absorbing peak at 262 nm, due to the scattering and/or absorption from the clay layers with lateral sizes from 50 to 200 nm [25]. The small band appears at 305 nm for Cloisite 20A and HCl-treated Cloisite 20A due to the presence of organic modified group in Cloisite 20A clays. Also, it is clear from **Fig. 3** and **Table 3** that PANI-ES shows characteristic peaks at 312 and 346 nm correspond to π - π^* transition of the benzenoid ring and 618 nm peak for electronic excitation from benzenoid ring to quinoid ring [16].

UV-Vis spectra of prepared nanocomposites exhibited two characteristic bands similar to the PANI-ES. Peaks were observed at 336 and 635 nm for nanocomposites prepared *via in situ* method, 303 and 588 nm for nanocomposites prepared *via core-shell* route and 349 and 633 nm for nanocomposites prepared *via ex situ* technique.

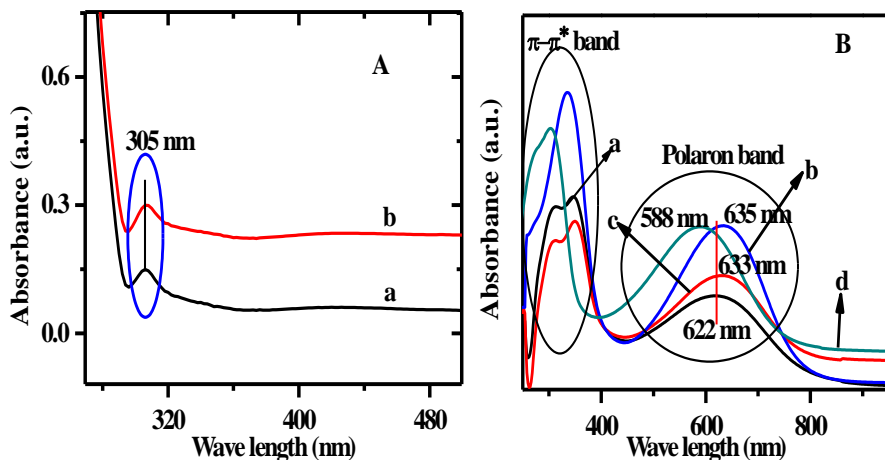


Figure 3. A: UV-Vis spectra of Cloisite 20A (a) and HCl-treated Cloisite 20A (b); B: PANI-ES (a), *in situ* nanocomposite (b), *ex situ* nanocomposite (c) and *core-shell* nanocomposites (d)

Table 3. UV-Vis peak positions and peak assignment of Cloisite 20A, HCl-treated Cloisite 20A, PANI-ES, *in situ* nanocomposites, *ex situ* nanocomposites, and *core-shell* nanocomposites

Materials name	Figure(s)	Peak Positions (nm)	Peak Assignments
Neat Cloisite 20A	3.3A	262 & 305	Scattering of clay platelet & organic modified group
HCl-treated Cloisite 20A		262 & 305	Scattering of clay platelet & organic modified group
PANI-ES	3.3B	327–316 & 618	π - π^* transition & π -polaron transition
<i>in situ</i> nanocomposites		336 & 635	π - π^* transition & π -polaron transition
<i>ex situ</i> nanocomposites		308-349 & 633	π - π^* transition & π -polaron transition
<i>core-shell</i> nanocomposites		303 & 588	π - π^* transition & π -polaron transition

Scanning electron microscopy (SEM)

SEM images with magnification 20 kX for Cloisite 20A, HCl-treated Cloisite 20A, PANI-ES, and PANI-ES/Cloisite 20A (4 wt%) nanocomposites (*in situ*, *core-shell* and *ex situ*) are shown in **Fig. 4**. As evident from SEM images, Cloisite 20A and HCl-treated Cloisite 20A possess similar type of morphology and it is crystal-like (**Fig. 4A and 3.4B**). SEM image of HCl doped PANI-ES is shown **Fig. 4C** which possesses tangled fiber-like morphology. SEM images of PANI-ES/Cloisite 20A (4 wt%) nanocomposites (*in situ*, *core-shell* and *ex situ*) are also shown in **Fig 4D, 4E** and **4F**, respectively) which possess aggregated tangled fiber-like images. These results showed clearly that Cloisite 20A participate in the closing of the PANI-ES Chains. Hence, these nanocomposites become more ordered state. Generally, ordered materials showed better electrical conductivity. The diameters of these compacted tangled fibers were found to nano regime dimension, which is providing higher surface area. Particularly for gas sensor application, it may be helpful to diffuse more gas molecules and show better response.

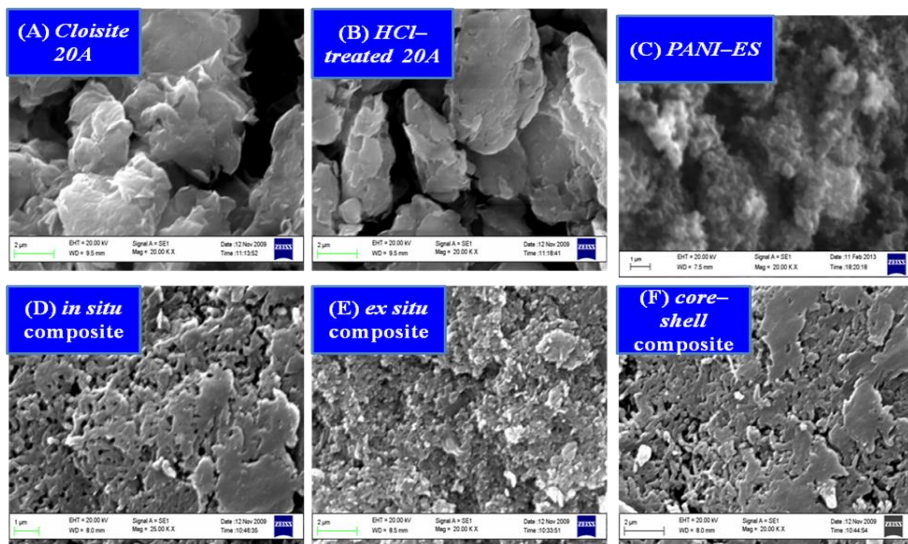


Figure 4. SEM images of Cloisite 20A (A), HCl-treated Cloisite 20A (B), PANI-ES (C), *in situ* nanocomposites (D), *ex situ* nanocomposites (E) and *core-shell* nanocomposites (F)

High resolution transmission electron microscopy (HRTEM)

The morphology of the resulting nanocomposites was observed using high resolution transmission electron microscopy (HRTEM). **Fig. 5** showed the typical HRTEM images of the PANI-ES/Cloisite 20A nanocomposites (*in situ*, *core-shell* and *ex situ*). HRTEM image in **Fig. 5A** showed a distribution of Cloisite 20A in *in situ* nanocomposite. For this nanocomposite, disorder layers in the nanoregime were found in **Fig. 5D**. This indicates that Cloisite 20A layers were delaminated. This result

is supported by XRD analysis. Similar results were found in other two prepared nanocomposites. But the main difference is dispersion and disorder criteria. HRTEM images are shown in **Fig. 5B, 5C, 5D, 5E, 5F**. It was observed that the whole Cloisite 20A particles were covered by uniform PANI-ES Chains, which indicated the formation of apparent *core-shell* structures. This result showed a well dispersion in PANI-ES matrix.

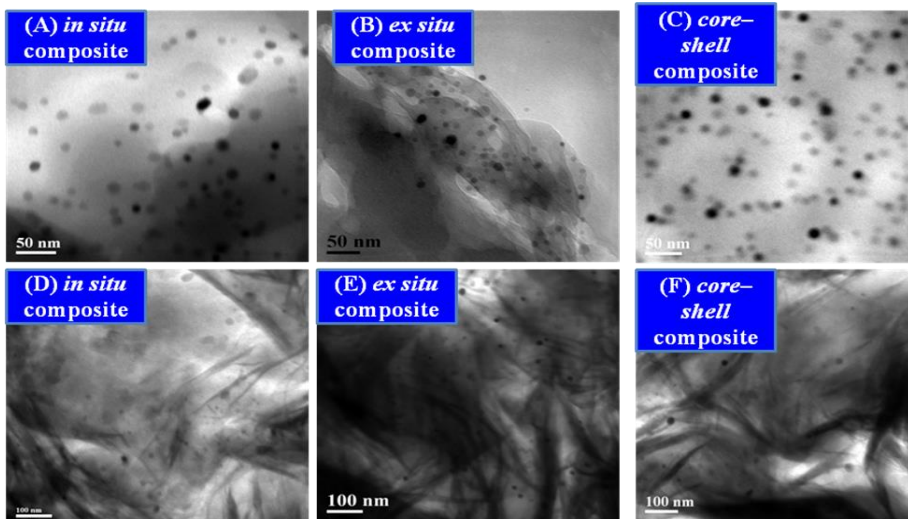


Figure 5. HRTEM image of (A) *in situ* nanocomposites, (B) *ex situ* nanocomposites, (C) *core-shell* nanocomposites for study of dispersion of Cloisite 20A and (D) *in situ* nanocomposites, (E) *ex situ* nanocomposites and (F) *core-shell* nanocomposites for study of disordered structure

DC conductivity measurements

At room temperature, DC conductivity of the PANI-ES and PANI-ES/Cloisite 20A nanocomposites (*in situ*, *core-shell* and *ex situ*) were measured using linear four-probe technique. For this measurement, pellet samples were used. The average DC conductivity values of PANI-ES and as prepared nanocomposites are presented in **Table 4**. The DC conductivity of PANI-ES was found to be 1.92 S/cm. With the addition of 4 wt% Cloisite 20A nanoclays, the conductivity of prepared PANI-ES is increased. The conductivity of as prepared nanocomposites (*in situ*, *core-shell* and *ex situ*) was found to be 3.87, 5.12 and 2.75 S/cm, respectively. $I-V$ Characteristics of PANI-ES and PANI-ES/Cloisite 20A (4 wt%) nanocomposites (*in situ*, *core-shell* and *ex situ*) are shown in **Fig. 6**. It is seen from **Fig. 6** that the applied current(s) and obtained voltage(s) are linearly related, showing ohmic behaviour [28].

The higher compacted PANI-ES chains in PANI-ES/Cloisite 20A (4 wt%) nanocomposites (*in situ*, *core-shell* and *ex situ*) leads more localized site (π -bond to the exciton band) and hence, higher amount of charge carrier occurs.

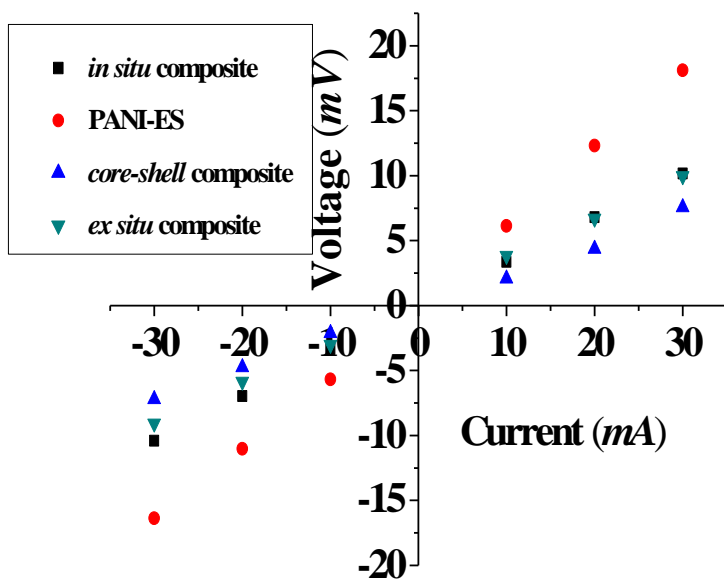


Figure 6. Room temperature I – V characteristics of PANI-ES, *in situ* nanocomposites, *ex situ* nanocomposites and *core-shell* nanocomposites

This indicates the higher carrier path and shows the higher DC conductivity of as prepared nanocomposites than HCl doped PANI-ES. This is really an interesting observation. In *core-shell* structure nanocomposite, the compactness is more than other prepared nanocomposites. That means Cloisite 20A connects more the PANI-ES Chains which increase the carrier paths. Therefore, it gives more DC conductivity [27,28].

Table 4. Room temperature DC conductivity of PANI-ES/MMT, PANI-ES/15A, PANI-ES, *in situ* nanocomposites, *ex situ* nanocomposites, and *core-shell* nanocomposites

Materials Name	PANI-ES /MMT	PANI-ES /15A	PANI-ES	PANI-ES/20A (<i>in situ</i>)	PANI-ES/20A (<i>core-shell</i>)	PANI-ES/20A (<i>ex situ</i>)
σ (S/cm)	1.20	1.650	1.92	3.87	5.12	2.75

The variation of DC conductivity with temperature is shown in **Fig. 7**. It was observed that PANI-ES and prepared nanocomposites showed increase of conductivity with the increase of temperature from 50 to 300 K. This behaviour is similar to the behaviour of inorganic semiconductor. Hence it can be called as organic semiconductor [29,30].

Various models were used to find the probable transport mechanism of conducting polymers which requires below room temperature. DC conductivity was

measured in a temperature range 77–300 K in the present work and fitted the Mott's variable range hopping (Mott's VRH) model and Arrhenius model to analyse the transport mechanism. According to Mott's VRH model, the temperature (T) dependence DC conductivity follows the expression [29,30]

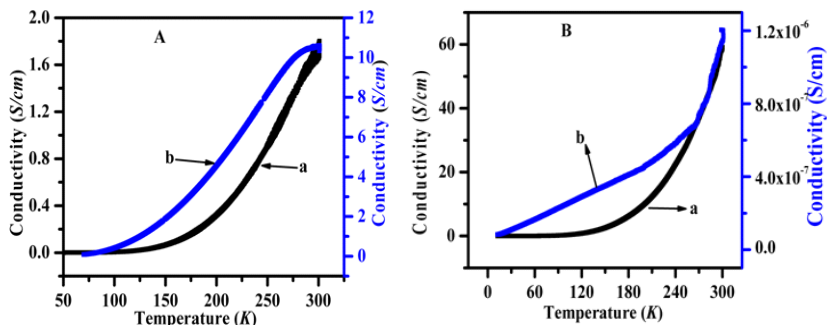


Figure 7. A: Temperature dependent DC conductivity of PANI-ES (a) and *in situ* nanocomposites (b); B: *core-shell* nanocomposites (a) and *ex situ* nanocomposites (b)

$$\sigma = \sigma_0 \exp\left(-\frac{T_0}{T}\right)^r \dots\dots\dots (2)$$

Where T_0 is the Mott characteristic temperature and σ_0 the limiting value of conductivity at infinite temperature and the exponent 'r' is related to the dimensionality of the transport process via the expression $r = [1/(1+d)]$, where $d=1, 2$ and 3 for one, two and three dimensional conduction process, respectively. The Mott's 3D VRH plots are presented in **Fig. 8 (A and B)**.

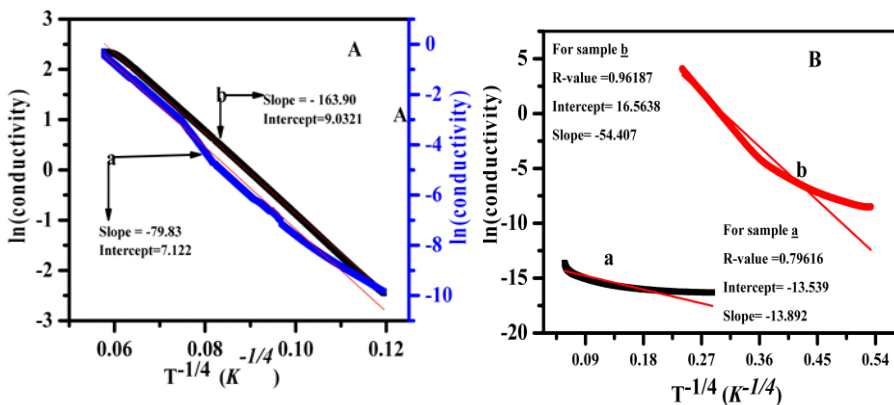


Figure 8. A: Logarithmic variation of DC conductivity of PANI-ES (a) and *in situ* nanocomposites (b); B: *core-shell* nanocomposites (a) and *ex situ* nanocomposites (b)

As another possibility, it may satisfy the Arrhenius model and this was used to measure the activation energy. **Fig. 9** shows the Arrhenius plot of measured DC conductivity as a function of reciprocal temperature. In Arrhenius model, the temperature dependent DC conductivity follows [29,30] the equation (3)

$$\sigma = \sigma_0 \exp\left(-\frac{E_a}{kT}\right) \dots \dots \dots (3)$$

Where E_a is the thermal activation energy of the electrical conduction and σ_a is a parameter depending on the semiconducting nature. The better linear dependency, *i.e.*, regression value (after linear fit) of conductivity vs temperature (Mott's VRH model and Arrhenius model) follows that the transport process corresponds either Mott's VRH model or Arrhenius model [30-32]. The regression values (both Mott's VRH model and Arrhenius model) are presented in **Table 5**. Accordingly, the better regression value was found in Mott's 3D-VRH model (0.99856 for PANI-ES and 0.99098 for *in situ* nanocomposite, 0.96187 for *core-shell* nanocomposite and 0.79616 for *ex situ* nanocomposite). Hence, it follows the Mott's 3D-VRH model which is consistent with the results reported in the literature [30-32]. This suggests that charge carrier can hop both in between the chains, *i.e.*, interchain hopping and along the chain, *i.e.*, intrachain hopping as PANI-ES has chain structure [30-32].

Table 5. Regression value (R-value) of PANI-ES, in situ nanocomposites, ex situ nanocomposites and core-shell nanocomposites from linearly fitted data (3D-VRH and Arrhenius model)

R-values	PANI-ES	<i>in situ</i> nanocomposite	<i>core-shell</i> nanocomposite	<i>ex situ</i> nanocomposite
3D-VRH	0.99856	0.9984	0.96187	0.79616
Arrhenius model	0.97381	0.97026	0.75038	0.61723

According to 3D-VRH model, the temperature dependence of DC conductivity can be presented in equation (4) as follows [30-34]

$$\sigma = \sigma_0 \exp\left(-\frac{T_0}{T}\right)^{\frac{1}{4}} \dots \dots \dots (4)$$

T_0 and σ_0 were also calculated from VRH plot $\ln \sigma$ vs $T^{-1/4}$ of prepared nanocomposites along with PANI-ES and is presented in **Table 3.6**. All nanocomposites show higher localization length (nanometer) than pure PANI-ES. This effect may be due to the presence of nanoclays in the PANI-ES chains [18]. These are partially block the conductive path [18]. Therefore, charge carriers could not hop easily from one chain to another chain. On the other hand, the clay based nanocomposites prepared by *core-shell* route indicates higher localization length than

other prepared nanocomposites. This has happened due to the presence of more clay particles in the PANI-ES chains and which affect the localisation length (L_{loc}).

We analyzed the resistivity data by the 3D-VRH model among localized states as described in the literature [32,33]

$$\rho(T) = \rho_0 e^{\left(\frac{T_{Mott}}{T}\right)^{\frac{1}{4}}} \dots\dots\dots(5)$$

$$T_{Mott} = \left[\frac{16}{K_B N(E)_F L_{loc}^3} \right] \dots\dots\dots(6)$$

Where K_B is the Boltzmann constant; $N(E)_F$ is the density of states at the Fermi level; and L_{loc}^3 ; the localization length. We plotted $\ln \sigma$ vs $T^{-1/4}$. This plot exhibits a straight line after linear fit for all prepared materials as shown in **Fig. 8**. T_{Mott} can be evaluated from slope of the straight line and listed in **Table 6**. The localization length L_{loc} can be calculated from temperature dependent conductivity at particular magnetic field (0.5 T) data as shown in **Fig. 10**. From the Mott expression, the resistivity at different temperatures at a particular magnetic field can be written as [30-32]

$$\ln \left[\frac{\rho(H)}{\rho_0} \right] = t (L_{loc} / L_H)^4 \left(\frac{T_{Mott}}{T} \right)^{\frac{3}{4}} \dots\dots\dots(7)$$

Where, $t = 5/2016$, $L_H = (hc/2\pi eH)^{1/2}$ = magnetic length, c = velocity of light (3×10^{10} cm/s), h = Planck's constant (6.62×10^{-27} erg.sec), e = electronic charge (1.6×10^{-19} C) and $H = 0.5$ tesla (T) is the applied magnetic field. **Fig. 10** shows the plot of $\ln [\rho(H, T)/\rho(0)]$ against $T^{-3/4}$, which is a straight line for each sample. From the slope, we determined the values of L_{loc} and are listed in **Table 6**. Using the values of T_{Mott} and L_{loc} for each sample in equation (6), the values of $N(E)_F$ was calculated and are presented in **Table 6**.

$$R_{hop,Mott} = \left(\frac{3}{8} \right) \left(\frac{T_{Mott}}{T} \right)^{\frac{1}{4}} L_{loc} \dots\dots\dots(8)$$

$$\Delta_{hop,Mott} = \left(\frac{1}{4} \right) (k_B T) \left(\frac{T_{Mott}}{T} \right)^{\frac{1}{4}} \dots\dots\dots(9)$$

Using the values of $T_{0,Mott}$, L_{loc} and $N(E_F)$, we calculated the mean hopping distance ($R_{hop,Mott}$) and the energy difference between sites ($\Delta_{hop,Mott}$) from the equation 8 and 9 and the data are presented in **Table 3.6** [30-32].

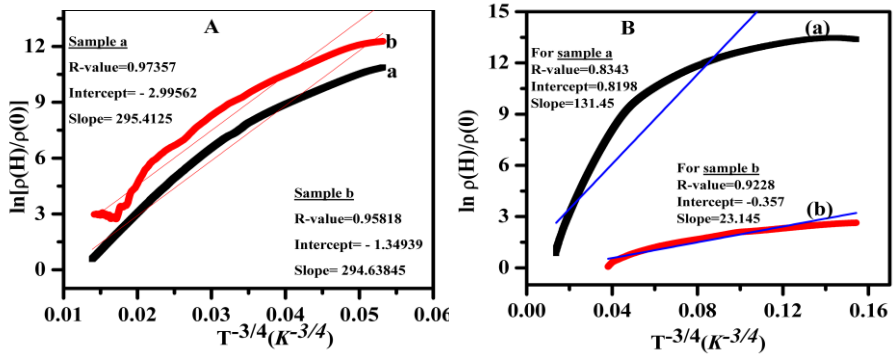


Figure 10. A: Plots of $[\ln \rho(H)/\rho(0)]$ vs $T^{-4/3}$ for PANI-ES (a) and *in situ* nanocomposite (b) at 0.5 T; B: Plots of $[\ln \rho(H)/\rho(0)]$ vs $T^{-4/3}$ for *core-shell* nanocomposite (a) and *ex situ* nanocomposite (b) at 0.5 T

Table 6. Conduction parameters obtained by analysing low temperature resistivity/conductivity with and without field data of PANI-ES, *in situ* nanocomposites, *ex situ* nanocomposites and *core-shell* nanocomposites

Conducting parameters	PANI-ES	<i>in situ</i> nanocomposite	<i>core-shell</i> nanocomposite	<i>ex situ</i> nanocomposite
Slope (without field)	-80.6126	-79.83	-54.4071	-13.5396
Intercept (without field)	22.4947	7.1224	16.538	13.892
Slope (with field)	295.4125	294.6384	131.4528	23.1452
σ_0	5.87×10^9	1.239×10^3	1.56×10^7	1.079×10^6
T_{Mott} (K)	4.22×10^7	4.0613×10^7	8.7×10^6	3.355×10^4
L_{loc} (nm)	274.68	277.18	301.24	549.28
$N(E_F)$ (no. states/eV/cm ³)	2.12×10^{19}	2.15×10^{17}	7.8×10^{17}	3.33×10^{19}
Temperature (K) at M-I transition	100	104	90	100
$R_{hop, Mott}$ ($^{\circ}A$)	262.5	259.8	199.2	88.15
$\Delta_{hop, Mott}$ (meV) at M-I transition	54.9	56.01	34.19	9.22
k (eV/K)	8.62×10^{-5}	8.62×10^{-5}	8.62×10^{-5}	8.62×10^{-5}

Using the parameters in the above expression, the values of $R_{hop,Mott}$ and $\Delta_{hop,Mott}$ were calculated at metal-insulator (M-I) transition point. At particular temperature, this transition is possible. The temperature is estimated at M-I transition and is presented in **Table 6**. In addition, the obtained hopping parameters helped to understand the 3D-VRH mechanism of as prepared materials.

Thermogravimetric (TG) analysis

Fig. 11 shows the typical TGA curves of Cloisite 20A, HCl-treated Cloisite 20A, HCl doped PANI-ES and PANI-ES/Cloisite 20A (4 wt%) nanocomposites (*in situ*, *core-shell* and *ex situ*), as measured under a nitrogen (N_2) atmosphere. From the above TGA curves, it is seen that the HCl doped PANI-ES starts degradation at 110 °C (12% weight loss), but the nanocomposites degrades at 128 °C (6% weight loss) for loading of 4 wt% Cloisite 20A nanoclays. The residual weight was also found to be higher than that of pure PANI-ES. This certainly indicates the release of bound water molecule from PANI-ES and its corresponding nanocomposites. The moisture content of 4 wt% PANI-ES/Cloisite 20A nanocomposites (*in situ*, *core-shell* and *ex situ*) is less due to the presence of Cloisite 20A, *i.e.*, hydrophobicity of PANI-ES increases. This was followed by rapid weight loss (up to 500 °C) of neat PANI-ES and as prepared nanocomposites (*in situ*, *core-shell* and *ex situ*). This is due to the release of HCl molecule (up to 500 °C) when the third stage degradation started. Final stage degradation occurred for neat PANI-ES and nanocomposites prepared by *in situ*, *core-shell* and *ex situ* method to complete degradation and decomposition of PANI-ES backbone. TGA curves clearly indicate that prepared nanocomposites are thermally stable than HCl doped PANI-ES due to the presence of Cloisite 20A nanoclays. Here, the Cloisite 20A platelets act as barriers to heat flow due to their high aspect ratio and hindered the degradation process [28].

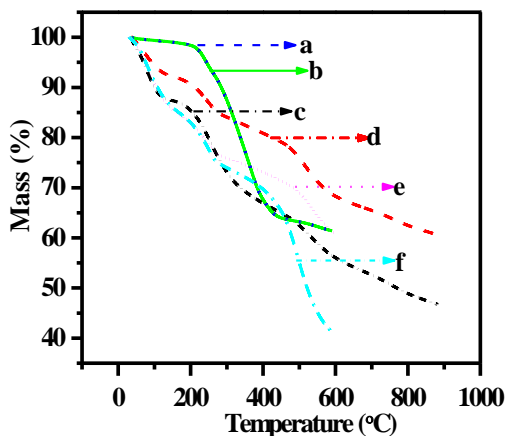


Figure 11. TGA plots of Cloisite 20A (a), HCl-treated Cloisite 20A (b), pure PANI-ES (c), *in situ* nanocomposites (d), *ex situ* nanocomposites (e), and *core-shell* nanocomposites (f)

Differential scanning calorimetric (DSC) analysis

The crystallinity of polymer is typically calculated by DSC analysis and equation 10 as follows [33,34]

$$\% \text{ Crystallinity} = \frac{\Delta H^m}{\Delta H^m_0} \times 100 \quad \dots\dots\dots(10)$$

Where ΔH^m is the enthalpy of fusion of the polymer samples which is determined by area of the peak at melting temperature and ΔH^m_0 is enthalpy of fusion of the totally crystalline polymer measured at equilibrium melting temperature in degree centigrade ($^{\circ}\text{C}$). The enthalpy of fusion is estimated are 447.097 for PANI-ES, 324.25 for *in situ*, 859.296 for *core-shell* and 227.19 for *ex situ* nanocomposites, respectively. The neat PANI-ES as well as PANI-ES/Cloisite 20A nanocomposites (*in situ*, *core-shell* and *ex situ*) is presented in **Fig. 12**. According to the equation 10, % crystallinity is directly related to the ΔH^m . Higher the enthalpy of fusion at melting temperature more be the crystallinity. Hence, % crystallinity of PANI-ES/Cloisite 20A (4 wt%) nanocomposites (*in situ*, *core-shell* and *ex situ*) shows higher crystallinity than pure PANI-ES. Since Cloisite 20A can be attributed in closer chain arrangements and hence, increases the compactness, *i.e.*, more is the crystallinity [33,34].

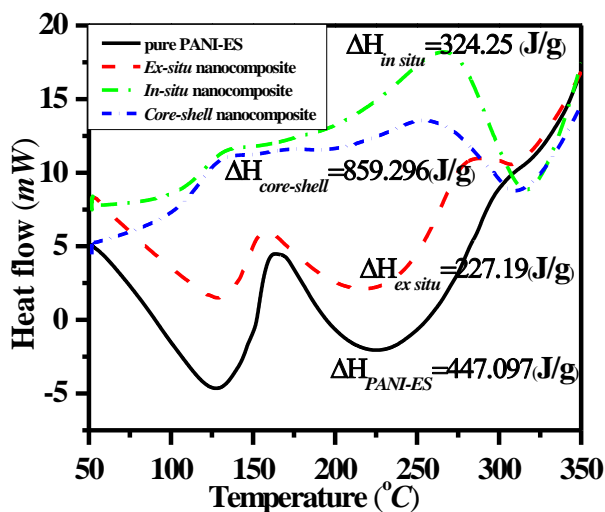


Figure 12. DSC thermograms of PANI-ES, *in situ* nanocomposites, *core-shell* nanocomposites and *ex situ* nanocomposites

2.4. Response Of Nitrogen Dioxide (I.E., NO₂ Gas Sensor)

Nitrogen dioxide (NO₂) is one of the important compositions of vehicle exhaust, emissions of the thermal power plant, and chemical production industries [35, 36]. The main sources of NO₂ are acid rain and photochemical smog. It is very harmful

to the plant, structural components, and equipments [37, 38]. NO₂ is a colorless, flammable, and dangerous gas even at very low concentration. It is a reddish-brown color gas at high temperature. Additionally, the reaction between NO₂ and CO in the presence of sunlight is to produce ozone (O₃). Ozone acts as a oxidizing agent and is believed to be harmful to plants and the respiratory system of human beings and animals. Due to the toxic nature of NO₂ gas, it causes some serious problems of human being *i.e.*, heart failure, arrhythmia and other cardiovascular. if the humans inhaled in large amounts, it may cause death [39]. Hence, from the protection of public health and environmental, the detection of nitrogen dioxide is great scientific challenge. Implication of monitoring and measuring system for NO₂ gas, it has great support to decrease the damage level and keep humane health safe. So far, scientific community have been put there lots of efforts for developing a variety of NO₂ gas sensor systems (such as semiconductor sensor [40], capacitive type sensor [41], and Surface acoustic wave (SAW) sensor [42]). Till to discovery of conducting polymers, the metal oxides based films have been used extensively for detecting the gas. The sensors have lack high sensitivity and have operated at high temperature (300–500 °C) [43, 44].

The conducting polymers have many potential applications for making different devices with their combined properties such as optical, electrochemical, and electrical properties [45]. In the conducting polymer family, polyaniline (PANI) is one of the member and has received attention widespread. This is due to mechanical flexibility, high environmental stability, ease of processing, simple and reversible doping/dedoping chemistry, and modifiable electrical conductivity [46-49].

Polyaniline based gas sensors have been taking significant consideration in last few decades [50, 51]. It has unique electrical conductivity. PANI has ability to transport charge carriers in both ways *i.e.*, inter polymer chain and intra polymer chains. Therefore, polyaniline can willingly react with reductive and oxidative agents, to change their electrical performance at room temperature.

Nanostructured polyanilines *i.e.*, nanowires, nanofibers, and nanorods, have been shown better performance due to their high aspect ratio's. This helps the fast diffusion of gas molecules into the structures. Some reports are available for synthesizing of polyaniline nanofiber [52-54]. The diameter of polyaniline nanofibers are obtained with nearly uniform diameters between 30 and 120 nm.

There are different forms of polyaniline. Emeraldine salt form (half-oxidization and half-de oxidization state) of polyaniline has the highest conductivity in the PANI family. The conductivity of polyaniline decreases with increase the extent of oxidization [55]. Particularly, NO₂ gas (oxidizing character) was exposed on polyaniline, the degree of oxidization of polyaniline would increase. Consequently, its conductivity decreases. Therefore, the experimental results are shown in Figure 13. It can be explained by the extent of oxidation state of polyamine. When exposed NO₂ gas on polyaniline, the conductivity decreases. This is due to increase the extent of oxidation. Brief summary of NO₂ detection is presented in Table 7.

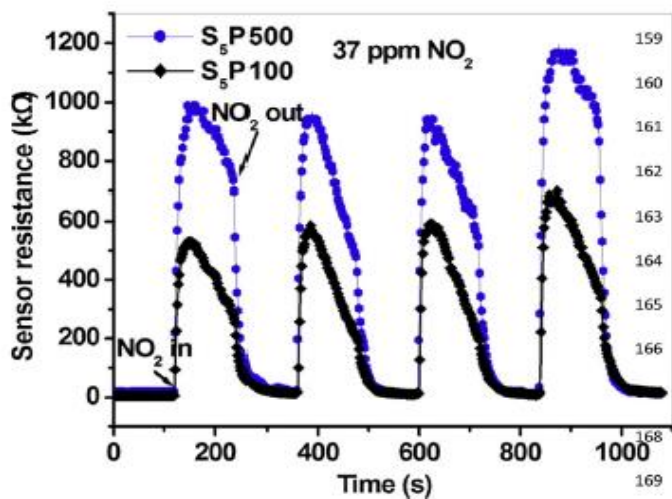


Figure 13. [56] The response nitrogen dioxide (NO₂) of PANI-ES based sensor measured at 37 ppm NO₂ gas concentrations at ambient condition-

Table 7. Brief summary of NO₂ detection

Study	Materials	Perporfamce	Optimum temperature (°C)	Limitation
Yan et al. [57]	polyaniline nanofibers	Response time xxx s	Room Temperature	Medium NO2 concentration
Kim et al. [58]	An organic conductive nanocomposite	Sensitivity xxx %	Room Temperature	High NO2 concentration
Kumar et al. [59]	Plasma Polymerized Nanostructure Polyaniline Thin Film	Response time xxxx s	Room Temperature	Medium NO2 concentration
Surwade et al. [60]	poly-o-toluidine	Response time 5 s	Room Temperature	Low-Medium NO2 concentration
Xie et al. [61]	Polyaniline based ultra-thin film	Response time xxx s	Room Temperature	Low NO2 concentration
Rozemarie et al. [62]	Polyaniline based electrospun	Sensitivity 45 %	Room Temperature	High NO2 concentration
Haynes et al. [63]	Polyaniline		Room Temperature	High NO2 concentration

2.5. Conclusions

We have successfully prepared PANI-ES/Cloisite 20A nanocomposites in *in situ*, *core-shell* and *ex situ* polymerization routes. The silicate layers of the clay platelets were delaminated after addition of Cloisite 20A in aqueous HCl medium during the synthesis of PANI-ES and nanocomposites. The PANI-ES/Cloisite 20A nanocomposites (*in situ*, *core-shell* and *ex situ*) exhibited remarkable improvement of DC electrical conductivity, thermal stability and enthalpy of fusion compared to pure PANI-ES. We described the concurrent improvement the properties like electrical DC conductivity, thermal stability and enthalpy of fusion of the prepared nanocomposites. Temperature dependent DC conductivity of prepared nanocomposite samples was observed. The linear fit data favoured to the Mott's 3D-VRH mechanism. The resistivity with magnetic field 0.5 T of HCl doped PANI-ES, PANI-ES/Cloisite 20A (4 wt%) nanocomposites (*in situ*, *core-shell* and *ex situ* polymerization route) were performed in the range of 77–300 K to estimate the L_{loc} of 274.68 nm, 277.18 nm, 301.24 nm and 549.28 nm for HCl doped PANI-ES and PANI-ES/Cloisite 20A (4 wt%) nanocomposites (*in situ*, *core-shell* and *ex situ* polymerization route), respectively. The resistivity at 0.5 T of prepared materials follows the Mott's expression. Varieties of physical parameters such as $N(E_F)$, T_{Mott} , L_{loc} , R_{hop} , and Δ_{hop} corresponds to transport mechanism are estimated in the presence and absence of magnetic field. The nitrogen dioxide gas responses and mechanism of polyaniline based materials were studied in details.

3.0. Acknowledgments

The author conveys their sincere thanks to the CRF, IIT Kharagpur for their providing testing facilities and Materials Science Centre to do the research work. I would like to thank Prof. Debabrat Pradhan for their invaluable guidance, advices, constant inspiration and technical support throughout the entire research program.

4.0. References

- [1] Saini, P., Choudhary, V., Vijayan, N., and Kotnala, R. K. 2012, Improved Electromagnetic Interference Shielding Response of Poly(aniline)-Coated Fabrics Containing Dielectric and Magnetic Nanoparticles, Journal of Physical Chemistry C, Vol. 116, pp. 13403-13412.
- [2] Burroughes, J. H., Bradley, D. D. C., Brown, A. R., Marks, R. N., Mackay, K., Friend, R. H., Burns, P. L., and Homes, A. B. 1990, Light-emitting Diodes Based on Conjugated Polymers, Nature, Vol. 347, pp. 539-541.
- [3] Frackowiak, E., Khomenko, V., Jurewicz, K., Lota, K., and Be'guin F. 2006, Supercapacitors Based on Conducting Polymers/Nanotubes Composites, Journal of Power Sources, Vol. 153, pp. 413-418.
- [4] Wu, F., Chen, J., Chen, R., Wu, S., Li, L., Chen, S., and Zhao, T. 2011,

- Sulfur/Polythiophene with a Core/Shell Structure: Synthesis and Electrochemical Properties of the Cathode for Rechargeable Lithium Batteries, *Journal of Physical Chemistry C*, Vol. 115, pp. 6057-6063.
- [5] Yu, L., Jin, X., and Zeng, X. 2008, Methane Interactions with Polyaniline/ Butylmethylimidazolium Camphorsulphonate Ionic Liquid Composite, *Langmuir*, Vol. 24, pp. 11631-11636.
- [6] Racicot, R., Richard Brown, R., and Yang, S. C. 1997, Corrosion Protection of Aluminium Alloys by Double-strand Polyaniline, *Synthetic Metals*, Vol. 85, pp. 1263-1264.
- [7] MacDiarmid, A. G., Chang, J. C., Richter, A. F., and Epstein, A. J. 1987, Polyaniline: A New Concept in Conducting Polymers, *Synthetic Metals*, Vol. 18, pp. 285-290.
- [8] Yue, J., Epstein, A. J., Zhong, Z., Gallagher, P. K., and MacDiarmid, A. G. 1991 Thermal Stabilities of Polyaniline, *Synthetic Metals*, Vol. 41, pp. 765-768.
- [9] Cao, Y., Smith, P., and Heeger, A. J. 1992, Counter-ion Induced Processability of Conducting Polyaniline and of Conducting Polyblends of Polyaniline in Bulk Polymers, *Synthetic Metals*, Vol. 48, pp. 91-97.
- [10] Alexandre, M., and Dubois, P. 2000, Polymer-Layered Silicate Nanocomposites: Preparation, Properties and Uses of a New Class of Materials, *Materials Science Engineering, and R*, and Vol. 28, pp. 1-63.
- [11] Mott, C. J. B. 1988, Clay Cinerals-an Introduction, *Catalysis Today*, Vol. 2, pp. 199-208.
- [12] Olad, A. 2011, Polymer/Clay Nanocomposites, *Advances in Diverse Industrial Applications of Nanocomposites*, Dr. Boreddy Reddy (Ed.), and ISBN: 978-953-307-202-9, InTech.
- [13] Maiti, P., Yamada, K., Okamoto, M., Ueda, K., and Okamoto, K. 2002, New Polylactide/Layered Silicate Nanocomposites: Role of Organoclay, *Chemistry of Materials*, Vol. 14, and pp. 4654-4661.
- [14] Tang, Z., Liu, P., Guo, J., and Su Z. 2009, Preparation of Polyaniline/Vermiculite Clay Nanocomposites by *in situ* Chemical Oxidative Grafting Polymerization, *Polymer International*, Vol. 58, pp. 552-556.
- [15] Kalaivasan, N., and Shafi, S. S. 2010, Synthesis of Various Polyaniline/clay Nanocomposites Derived from Aniline and Substituted Aniline Derivatives by Mechanochemical Intercalation Method, *E-Journal of Chemistry*, Vol. 7, pp. 1477-1483.
- [16] Garai, A., Kuila, B. K., and Nandi, A. K. 2006, Montmorillonite Clay Nanocomposites of Sulfonic Acid Doped Thermoreversible Polyaniline Gel: Physical and Mechanical Properties, *Macromolecules*, Vol. 39, pp. 5410-

- 5418.
- [17] Song, D. H., Lee, H. M., Lee, K.-H. and Choi, H. J. 2008, Intercalated Conducting Polyaniline–clay Nanocomposites and their Electrical Characteristics, *Journal of Physics and Chemistry Solids*, Vol. 69, pp. 1383-1385.
- [18] Kim, B. H., Jung, J. H., Hong, S. H., Joo, J. S., Epstein, A. J., Mizoguchi, K., Kim, J. W., and Choi, H. J. 2002, Nanocomposite of Polyaniline and Na⁺-montmorillonite Clay, *Macromolecules*, Vol. 35, pp. 1419-1423.
- [19] Yeh, J. M., Liou, S. J., Lai, C. Y., and Wu, P. C. 2001, Enhancement of Corrosion Protection Effect in Polyaniline via the Formation of Polyaniline-clay Nanocomposite Materials, *Chemistry of Materials*, Vol. 13, pp. 1131-1136.
- [20] Nascimento, G. M. do, Constantino, V. R. L., and Temperini, M. L. A. 2002, Spectroscopic Characterization of New type of Conducting Polymer-clay Nanocomposite, *Macromolecules*, Vol. 35, pp. 7535-7537.
- [21] Mansoori, Y., Hemmati, S., Eghbali, P., Zamanloo, M. R., and Imanzadeh, G. 2013, Nanocomposite Materials Based on Ascribed Methacrylate/Cloisite 20A, *Polymer International*, Vol. 62, pp. 280-288.
- [22] Panigrahi, M., Singh, N. K., Gautam, R. K., Banik, R. M., and Maiti, P. 2010, Improved Biodegradation and Thermal Properties of Poly (lactic acid)/Layered Silicate Nanocomposites, *Composite Interfaces*, Vol. 17, pp. 143-158.
- [23] Crosa, M., Boero, V., and Franchini-Angela, M. 1999, Determination of Mean Crystallite Dimensions from X-ray Diffraction Peak Profiles: a Comparative Analysis of Synthetic Hematites, *Clays Clay Miner*, Vol. 47, pp. 742-747.
- [24] Li, L., Qin, Z., Liang, X., Fan, Q., Lu, Y., Wu, W., and Zhu, M. F. 2009, Facile Fabrication of Uniform Core-shell Structured Carbon Nanotube-Polyaniline Nanocomposites, *Journal of Physical Chemistry C*, Vol. 113, pp. 5502-5507.
- [25] Wu, T., Xie, T., and Yang, G. 2009, Characterization of Poly (vinylidene fluoride)/Na-MMT Composites: An Investigation Into the β -Crystalline Nucleation Effect of Na-MMT, *Journal of Polymer Science, Part B: Polymer Physics*, Vol. 47, pp. 903-911.
- [26] Ciric-Marjanovic, G., Dondur, V., Milojevic, M., Mojovic, M., Mentus, S., Radulovic, A., Vukovic, Z., and Stejskal, J. 2009, Synthesis and Characterization of Conducting Self-assembled Polyaniline Nanotubes/Zelite Nanocomposite, *Langmuir*, Vol. 25, pp. 3122-3131.
- [27] Olad, A., and Rashidzadeh, A. 2008, Preparation and Anticorrosive

- Properties of PANI/Na-MMT and PANI/O-MMT Nanocomposites, Progress in Organic Coatings, Vol. 62, pp. 293-298.
- [28] Sengupta, P. P., Kar, P., and Adhikari, B. 2009, Influence of Dopant in the Synthesis, Characteristics and Ammonia Sensing Behavior of Processable Polyaniline, Thin Solid Films, Vol. 517, pp. 3770-3775.
- [29] Kapil, A., Taunk, M., and Chand, S. 2010, Preparation and Charge Transport Studies of Chemically Synthesized Polyaniline, Journal of Materials Science-Materials Electronics, Vol. 21, pp. 399-404.
- [30] Li, J., Fang, K., Qiu, H., Li, S., and Mao, W. 2004, Micromorphology and Electrical Property of the HCl-doped and DBSA-doped Polyaniline, Synthetic Metal, Vol. 142, pp. 107-111.
- [31] Ghosh, M., Barman, A., Meikap, A. K., De, S. K., Chatterjee, S., and Chattopadhyay, S. K. 2000, Electrical Resistivity and Magnetoresistivity of Protonic Acid (H₂SO₄ and HCl)-doped Polyaniline at Low Temperature, Journal of Applied Polymer Science, Vol. 75, pp. 1480-1486.
- [32] Chakraborty, G., Gupta, K., Rana, D., and Meikap, A. K. 2012, Effect of Multiwalled Carbon Nanotubes on Electrical Conductivity and Magnetoconductivity of Polyaniline, Advance in Natural Science, Nanoscience and Nanotechnology, Vol. 3, pp. 035015-035023.
- [33] Kong, Y., and Hay, J. N. 2002, The Measurement of the Crystallinity of Polymers by DSC, Polymer, Vol. 43, pp. 3873-3878.
- [34] Abdelkader, R., Amine, H., and Mohammed, B. 2012, Thermally Stable forms of Pure Polyaniline Catalyzed by a Acid-exchanged Montmorillonite Clay called Maghnite-H⁺ as an Effective Catalyst, International Journal of Polymer Science, Vol. 2012, pp. 1-7.
- [35] Zamboni, G., Capobianco, M., and Daminelli, E. 2009, Estimation of Road Vehicle Exhaust Emissions from 1992 to 2010 and Comparison with Air Quality Measurements in Genoa, Italy, Atmospheric Environment, Vol. 43, pp. 1086-1092.
- [36] Hawe, E., Fitzpatrick, C., Chambers, P., Dooly, G., and Lewis, E. 2008, Hazardous Gas Detection using an Integrating Sphere as a Multipass Gas Absorption Cell, Sensors and Actuators A, Vol. 141, pp. 414-421.
- [37] Richter, A., Burrows, J.P., Nuc, H., Granier, C., and Niemeier, U. 2005, Increase in Tropospheric Nitrogen dioxide over China Observed from Space, Nature, Vol. 437 pp. 129-132.
- [38] Jeong, O.C., and Konishi, S. 2008, Three-Dimensionally Combined Carbonized Polymer Sensor and Heater, Sensor and Actuators A, Vol. 143 pp. 97-105.
- [39] Hoek, G., Brunekreef, B. Fischer, P., and Wijnen, J.V. 2001, The Association

- Between Air Pollution and Heart Failure, Arrhythmia, Embolism, Thrombosis, and other Cardiovascular Causes of Death in a Time Series Study, *Epidemiology*, Vol. 12, pp. 355-357.
- [40] Wierzbowska, K., Bideux, L., Adamowicz, B., and Pauly, A. 2008, A novel III-V Semiconductor Material for NO₂ Detection and Monitoring, *Sensor and Actuators A*, Vol. 142, pp. 237-241.
- [41] Zamani, C., Shimanoe, K. and Yamazoe, N. 2005, A New Capacitive-Type NO₂ Gas Sensor Combining An MIS with a Solid Electrolyte, *Sensor and Actuators B*, Vol. 109, pp. 216-220.
- [42] Venema, A., Nieuwkoop, E., Vellekoop, M.J., Ghijsen, W.J., Barendsz, A.W., and Nieuwenhuizen, M.S. 1987, NO₂ Gas-Concentration Measurement with a SAW-Chemosensor, *IEEE transection on Ultrasonic Ferroelectric Frequence Control*, Vol. 34, pp. 149-156.
- [43] Ricco, A.J. and Martin, S.J. 1991, Thin Metal Film Characterization and Chemical Sensors: Monitoring Electronic Conductivity, Mass Loading and Mechanical Properties with Surface Acoustic Wave Devices, *Thin Solid Films* Vol. 206 pp. 94-101.
- [44] Auld, B.A. *Acoustic Fields and Waves in Solid*, New York: Wiley, 1973.
- [45] Skotheim, T.A. Elsenbaumer, R.L. and Reynolds, J.R. *Handbook of Conducting Polymers*, 2nd ed., Marcel Dekker, New York, 1997.
- [46] Anderson, M.R., Mattes, B.R., Reiss, H., and Kaner, R.B. 1991, Conjugated Polymerfilms for Gas Separations, *Science*, Vol. 252, pp. 1412–1415.
- [47] Cao, Y., Smith, P., and Heeger, A.J. 1993, Counterion Induced Processibility of Conducting Polyaniline, *Synthetic Metals*, Vol. 57, pp. 3514-3519.
- [48] Chiang, J.C., and MacDiarmid, A.G. 1986, Polyaniline-Protonic Acid Doping of the Emeraldine from to the Metallic Regime, *Synthetic Metals*, Vol. 13, pp. 193-205.
- [49] Huang, W.S., Humphrey, B.D., and MacDiarmid, A.G. 1986, Polyaniline, a Novel Conducting Polymer-Morphology and Chemistry of its Oxidation and Reduction in Aquwous-Electrolytes, *Journal of the Chemical Society, Faraday Transections*, Vol. 82, pp. 2385.
- [50] Agbor, N.E., Petty, M.C., and Monkman, A.P., 1995, Polyaniline Thin-Films for Gas Sensing, *Sensor and Actuators B: Chemical*, Vol. 28 pp. 173-179.
- [51] Kang, E.T., Neoh, K.G., and Tan, K.L. 1998, A Polymer with many Interesting Intrinsic Redox States, *Progress in Polymer Science*, Vol. 23 pp. 277-324.
- [52] Huang, J.X., Virji, S., Weiller, B.H., and Kaner, R.B., 2003, Polyaniline Nanofibers: Facile Synthesis and Chemical Sensors, *Journal of American*

- Chemical Society, Vol. 125 pp. 314-315.
- [53] Huang, J.X., and Kaner, R.B. 2004 A General Chemical Route to Polyaniline Nanofibers, *Journal of American Chemical Society*, Vol. 126 pp. 851-855.
- [54] Huang, J.X., and Kaner, R.B. 2004, Nanofiber Formation in the Chemical Polymerization of Aniline: A Mechanistic Study, *Angewandte Chemie International Edition*, Vol. 43 pp. 5817-5821.
- [55] Ram, M.K., Yavuz, O., and Aldissi, M. 2005, NO₂ Gas Sensing Based on Ordered Ultrathin Films of Conducting Polymer and its Nanocomposite, *Synthetic Metals*, Vol. 151 pp. 77-84.
- [56] H. Xu, D. Ju, W. Li, H. Gong, J. Zhang, J. Wang, B. Cao, 2016, Low-working-Temperature, Fast-Response-Speed NO₂ sensor with Nanoporous-SnO₂/Polyaniline Double-Layered Film, *Sensor and Actuators B*, Vol. 224 pp. 654-660.
- [57] Yan, X., Han, Z.J., · Yang, Y.K.K., and Tay, B.K. NO₂ Gas Sensing with Polyaniline Nanofibers Synthesized by a Facile Aqueous/Organic Interfacial Polymerization, *Sensor and Actuators B Chemical*, Vol. 123, pp. 107-113.
- [58] Kim, S.G., Jun, J., Lee, J.S., and Jang, J. 2019, A Highly Sensitive Wireless Nitrogen Dioxide Gas Sensor Based on an Organic Conductive Nanocomposite Paste, *Journal of Materials Chemistry A*, Vol. 7, pp. 8451-8459.
- [59] Kumar, R., Singh, S., and Mishra, A.K. 2010, Development of NO₂ Gas Sensor Based on Plasma Polymerized Nanostructure Polyaniline Thin Film, *Journal of Minerals & Materials Characterization & Engineering*, Vol. 9, No.11, pp.997-1006.
- [60] Surwade, S.P., Rao Agnihotra, S., Dua, V., and Manohar, S.K., 2009, Nitrogen Dioxide Vapor Detection using Poly-o-Toluidine, *Sensor and Actuators B*, 143, 454-457.
- [61] Xie, D., Jiang, Y., Pan, W., Li, D., Wu, Z., and Li, Y. 2002, Fabrication and Characterization of Polyaniline based Gas Sensor by Ultrathin Film Technology, *Sensor and Actuators B*, Vol. 81, pp. 158-164.
- [62] Rozemarie, M.L., Andrei, B., Liliana, H., Cramariuc, R. and Cramariuc, O. 2017, Electrospun Based Polyaniline Sensors – A Review, *International Conference on Innovative Research — ICIR EUROINVENT 2017*, IOP Conf. Series: Materials Science and Engineering Vol. 209, pp. 012063 (doi:10.1088/1757-899X/209/1/012063).
- [63] Haynes, A., and Gouma, P.-I. Polyaniline-Based Environmental Gas Sensors, *Sensors for Environment, Health and Security* pp. 451-459.

Chapter 4

Acrylic Acid (AA) Based Polyaniline Composite for Liquefied Petroleum Gas (LPG) Sensors

Muktikanta Panigrahi ^{1,*}, Basudam Adhikari ¹

¹ Materials Science Centre, Indian Institute of Technology, Kharagpur, West Bengal, India

*Corresponding author: muktikanta2@gmail.com

Abstract

N-substituted PANI-ES was obtained from N-phenyl- β -alanine (N-substituted aniline). N-phenyl- β -alanine was synthesized chemically from methyl acrylate and aniline precursor. ESI-MS, ¹H NMR spectroscopy and FTIR spectroscopy are employed to characterise the N-phenyl- β -alanine for structure elucidation. The structure and properties of corresponding polymers were investigated by X-ray diffraction, FTIR, UV-Visible, ¹H NMR, FESEM, solubility, and DC conductivity. On the basis of experimental results of prepared N-substituted aniline monomer and its corresponding polymer is proposed. At room temperature, the average DC conductivity of as-prepared PANI polymers was found in semiconducting range, which is 0.153 S/cm for poly (3-methyl (phenyl amino) propionic acid). We also were analysed temperature dependent DC conductivity with and without magnetic field of as prepared PANI polymers to understand the conduction mechanism and it was followed variable-range hopping (VRH) process. In addition, we were discussed the response of liquefied petroleum gas (LPG) with polyaniline based sensor materials.

Keywords: Dopant, Amorphous, Electrical conductivity, Conduction mechanism, Thermal stability, Solubility

1.0 Introduction

Now days, scientific communities have taken much more interest towards electronically conducting polymers due to their potential applications in emerging fields such as rechargeable batteries, electrochromic windows, biosensor and antistatic coating materials [1-6]. Particularly, PANI is an important conducting polymer in the conducting polymeric group because of its ease of synthesis *via* chemical and

electrochemical routes, good environmental stability, unique oxidation reduction chemistry and low cost synthesis, etc [7-9]. However, the conducting form of PANI is insoluble in common organic solvents even in N-methyl-2-pyrrolidone (NMP) and dimethyl sulphoxide (DMSO). The limitation has impeded not only its practical applications but also a complete understanding of the polymer structure [10]. To solve this problem, researchers are devoted to improve the processability, solubility and electronic properties of PANI for their performance. Great effort has been devoted to design acid doped polymer to improve their solubility and processability by the development of synthetic route. Generally, organic and inorganic acid dopants are used in the conducting polymers. These are small molecules and can evaporate at room or higher temperature which affects the conductivity of the PANI. The limitation can be overcome by using bigger size dopants, polymeric acid dopants, and substituted form in conducting PANI polymeric backbone. In case of polymeric acid dopants, the dopant has lower glass transition temperature (T_g) (lower than that of PANI) and then can enhance the flexibility of the PANI film. There are several reports on polymeric acids dopants. These are mentioned as poly (ethenesulfonic acid) [10], poly (acrylic acid) [10,11], poly (styrene sulfonic acid) [10-14], poly (2-(acrylamido)-2-methylpropanesulfonic acid) [15], and poly (amic acid) [16]. These dopants can be used during the synthesis by chemical or electrochemical polymerization of aniline in aqueous solution through oxidative polymerization method [17,18]. Due to the presence of protonic acid groups on polymer chains of the polymeric dopant and to the conformational hindrance created by the flexible chain, it is expected that not all of the acid groups are capable of doping PANI and there should be nonuniform distribution. Consequently, the experimental results of the polymeric acid doped PANI should be different from that of non polymeric protonic acid doped PANI [17,18].

Substitution at nitrogen of PANI backbone is another kind to assist the improvement of processability along with hydrophilicity and compatibility. Several reports show that alkyl group-, alkyl ring- are attached to N-atom of PANI. The polymers have been formed directly from aniline monomers, which are soluble in common organic solvents [19,20]. Incorporation of the side groups into PANI has changed its properties. Other than the above approach, co-polymerization of aniline with suitable substituted aniline to produce co-polymers is possible to improve its solubility in organic solvents [21,22]. Utilizing a functionalized acid, *e.g.*, dodecyl benzenesulphonic acid or 10-camphorsulphonic acid, to protonate the base form of PANI improved the processability [23].

Doped conjugated polymers exhibit characteristic properties of the metallic state, which is showing high electrical conductivity. Usually, highly doped conducting polymers do not show the metallic transport, *i.e.*, resistivity (ρ) is not proportional to the temperature. Now a days, the quality of the conjugated polymers has been improved by doping process and results the in-homogeneity in the doping level. Also, the processability has assisted to enhance the quality of conjugated polymer. The doped conjugated polymeric chains are often disordered and structurally amorphous. In the conjugated polymer, some regions are crystalline and other regions are amorphous in nature. The amorphous regions can dominate the electrical transport.

Consequently, the characteristic metallic features in the bulk electrical transport properties are severely limited by strong disorder [24].

Presence of partially filled bands in the doped polymers, the electronic structure will be the similar to that of metal. It is well known that disorder can result in localization of states. If all states become localized, the system will be an insulator. In such an insulator, there is no gap in the density of states, *i.e.*, Fermi level (E_F) lies in an energy interval in which all states are localized, called Fermi glass. In this system, the conductivity is influenced by temperature. At high temperatures, the activation energy is measured by the energy difference between E_F (which lies in the region of localized states) and the mobility edge and at lower temperatures, variable-range-hopping (VRH) transport is resulted from the existence of unoccupied localized electronic states near E_F . Transition from metal to insulator (M-I) occurs when the disorder is sufficiently weak that means mobility edges move away from the center of the band toward the band tails such that E_F lies in a region of extended states. To understand the transport phenomena of conducting polymer, it is important to quantify the disorder by estimating/calculating the transport parameters and to establish the M-I transition [24].

Several reports are found on transport phenomena of conducting polymers. Li and co-workers [25] proposed a variable range of hoping (VRH) model which described the transport mechanism of HCl doped and DBSA doped PANI. Kapil *et al.* [26] analyzed transport mechanism of p-toluene sulphonic acid (PTSA) doped PANI by Arrhenius model, Variable range hoping (VRH) model and Kivelson model in the temperature range of 30-300K. The conduction mechanism of PANI organic film and metal particles embedded in an insulating material and PANI was also explained by using VRH and charge energy limited tunnelling (CELT) models [26]. The conductivity measurements were also done in the presence of magnetic field to measure the magnetoresistance (MR). Several conducting polymers such as PANI [24,26-31], polypyrrole [32-34], PEDOT films [35], and PANI composites have shown positive MR at low temperature (<10 K).

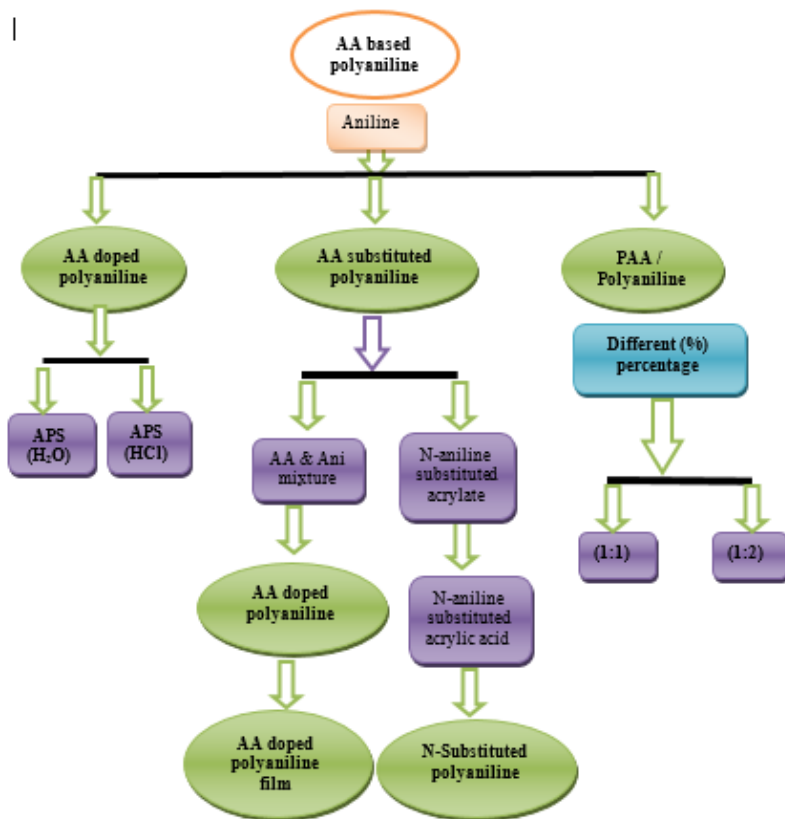
This work was undertaken to study the synthesis, spectroscopic analysis, measurement of electronic properties, microstructure and thermal stability of the AA doped, substituted AA and polymeric protonic acid, *i.e.*, PAA/PANI. Its electronic properties at the temperature range and optical band of the doped PANI were also investigated. Acrylic acid is taken as three forms, *viz.*, doped form, substituted form, polymeric form, *i.e.*, PAA. We present the results of a comprehensive study of the transport in AA based PANI polymer. In the system, DC conductivity as a function of temperature and resistivity in the presence of magnetic field was studied in temperature range 70-300 K. We have observed variable-range-hopping behaviour due to the presence of extent of disorder in the prepared materials. Magnetic fields of 0.4 T induced a transition from the critical regime of M-I transition to the insulating region where the states near E_F are localized and the transport took place *via* variable-range hopping. Various transport parameters of AA based PANI polymers were calculated for understanding the conduction mechanism. An understanding of the

system should also be applicable to systems with other polymeric protonic acid dopant and would provide valuable information for applications of the doped PANI in different applications like electromagnetic interference shielding, in conductive coatings, and as positive electrodes of electroluminescence diode.

2.0 Experimental

2.1 Synthesis of AA Based Pani Polymer

Materials. Acrylic acid (AA), aniline (Ani), dichloromethane (DCM), ammonium persulfate (APS), N,N-dimethyl formamide (DMF), Dimethylsulphoxide (DMSO), methyl acrylate, sodium hydroxide (NaOH), n-hexane, and HCl, ethyl acetate were procured from Merck. All the chemicals are synthesis grade. Distilled water is used in the synthesis.



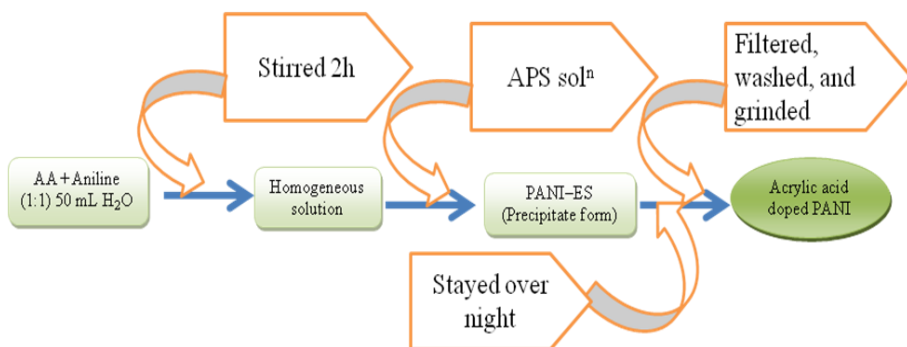
Scheme 1. Design of AA based polyaniline: AA doped polyaniline, substituted PANI and PAA/PANI composite

Synthesis of AA based PANI polymer. The design of AA based PANI polymer is mentioned as follows in **Scheme 1**. In the synthesis **Scheme 1**, acrylic acid

used in three different ways *viz.*, AA is used as doping in the synthesis of PANI polymer [36], AA is employed as substitution on N-atom (NH_2) of aniline, called monomer [37] and it is polymerised to form the PANI [38]. N-substituted aniline monomers was synthesised in two ways *viz.*, one is direct mixing of AA and aniline and another way of synthesis was used the reference 37. PAA and PANI are used during the preparation of PAA/PANI composite [38]. The design of AA based polyaniline is presented in **Scheme 1**. We have employed chemical routes to synthesize acrylic acid (AA) based PANI polymer. The details synthesis procedures have been described.

Synthesis of acrylic acid (AA) based PANI polymer

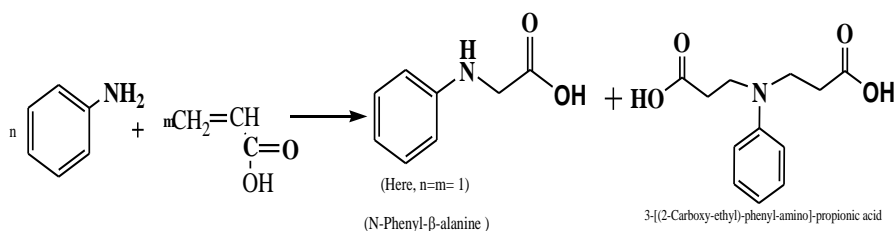
Synthesis of acrylic acid (AA) doped PANI from aniline precursor. AA doped PANI was synthesised following the method in literature [36] and occurred by chemical oxidation process. In this method, AA (2 mL) was added to 50 mL of distilled water and stirred slowly to form AA solution. Then, aniline (2.66 mL) was added slowly to AA solution in stirring condition. Before addition of APS, temperature of system was maintained at 5 °C with continuous stirring. Then, an aqueous solution of APS (2.76 g in 50 mL of distilled water) was added slowly to the above AA solution for 1 h under continuous stirring. The polymerization reaction was carried out. During the polymerization, slight green precipitate was formed in initial stage of polymerization and green precipitate was formed when polymerization proceeds which is followed to stand overnight to complete the polymerization. After filtration, the precipitate was washed adequate amount of distilled H_2O till the precipitate becomes neutral. This washing step removed the unreacted AA and APS. The product was dried under vacuum at 60 °C for 12 h. After that, the solid mass was grinded using mortar and pastel and finally, we got powder. Schematically, the flow chart for synthesis of AA doped PANI polymer is presented in **Scheme 2**.



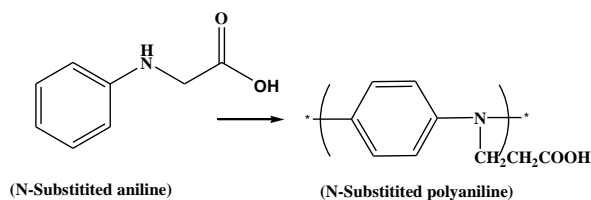
Scheme 2. Schematic flow chart for the synthesis of AA doped PANI polymer

Synthesis of N-substituted aniline monomer and N-substituted PANI polymer from aniline (Ani) and AA/methyl acrylate precursors. Initially, N-substituted aniline monomer was synthesized using AA and Ani predecessors and then

it was polymerizes by chemical-oxidation method. Equivalent amount (mili-equivalent) of both colorless liquid **Ani** and **AA** were mixed together with continuous (45 min) stirring at 5 °C. At last, colorless viscous mixture was formed with the evolution of heat. The reaction was exothermic in nature. During the reaction, different color transitions were observed. The obtained mass became viscous, the color of which changed from colorless to light pink then to light greenish-yellow. Such viscous mass was purified using co-precipitation technique. At first, the mixture was dissolved in dichloromethane (**DCM**) followed by n-hexane in the ratio 1:5. It was preserved in a refrigerator for 12 h. After that, the mass formed two layers in the flask (gel in bottom part and liquid in upper part). The upper liquid part was discarded carefully. Appropriate amount of water was added to the prepared gel and shacked for 15 min. **APS** (0.045 moles) as oxidant was dissolved in 60 mL of water to make oxidant solution. The oxidant solution was added drop wise into deep-end of the purified gel solution through injection syringe with continuous stirring. At this stage, temperature was maintained (10 to 0 °C) using ice bath. After 2 h, the reaction mixture was brought to room temperature in stirring condition for 10 h more. The change of color of the solution was observed, which was from colorless to deep greenish and the polymer was formed as deep green solid lump, which is floated on the solution. The solid polymer was dissolved in **DMF** and distilled water was poured into the solution from which the polymer precipitated out and thus we got polymer without any inorganic impurity. From the spectroscopic analysis is confirmed the formation of mixture of monomer. Accordingly, the reaction Scheme for synthesis of prepared monomer and its corresponding polymer are shown in **Schemes 3** and **4**, respectively.



Scheme 3. Synthesis of mixture of N-substituted aniline monomer

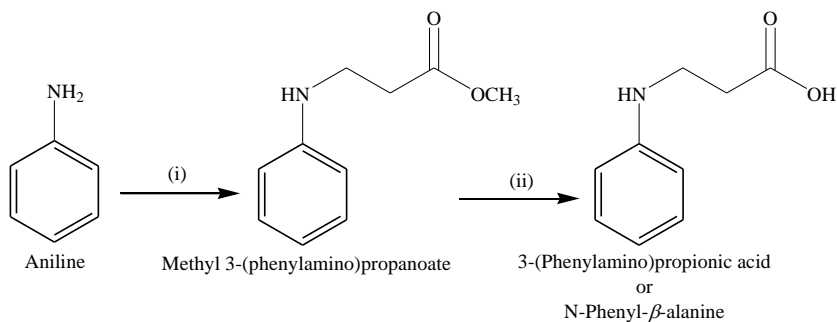


Scheme 4. Synthesis of N-substituted polyaniline

Our aim was to synthesize 3-methyl (phenylamino) propanoic acid (N-Phenyl- β -alanine), which is 100% abundance. This was used to polymerize to form poly (3-methyl (phenylamino) propanoic acid). Poly (3-methyl (phenylamino)

propanoic acid) was further used for different characterizations and analysis. 3-methyl (phenylamino) propanoic acid was synthesized as reported earlier [37]. It is a two step reaction: aniline was first converted to β -amino ester (**Scheme 5**). For this synthesis, 1.623 g aniline (17.43 mill mole) was added slowly to 1.5 g methacrylate (17.43 mill mole) in 6 mL of dry toluene. HCl-treated MMT (0.3 g, 10 wt%, used as catalyst) was added to the reaction mixture. The reaction was carried out in dry condition. The reaction temperature was maintained at 90 °C using oil bath and was continued for 2 h with vigorous stirring. During the reaction, the transition of color of compound was observed from colorless to light brown. Finally, the solvent was evaporated using rotary evaporator to obtain a densed brown product, methyl 3-(phenylamino) propionate. Without further purification, the crude product was used for the next step.

In the second step, the synthesized 3-methyl (phenylamino) propanoate was converted to 3-methyl (phenylamino) propanoic acid (β -amino acid) (**Scheme 5**). For this, 2.89 g (17.49 mill mole) β -amino ester was added to 10 mL methanol in a round bottom flask, followed by the addition of 0.699 g NaOH (17.49 mill mole). The reaction mixture was stirred vigorously for 2 h and the temperature was maintained at 05 °C using ice-bath. After that, methanol was evaporated using vacuum rotary evaporator to get viscous mass. The product was neutralized by the addition of 6 M HCl in cold condition and the pH was adjusted to ~4. Finally, the product was extracted with ethyl acetate several times. Then the solvent was evaporated using vacuum rotary evaporator. The product was precipitated using n-hexane. The product was dried under vacuum to obtain light brown mass. Reaction Scheme for synthesis single N-substituted aniline monomers is presented in **Scheme 5**.



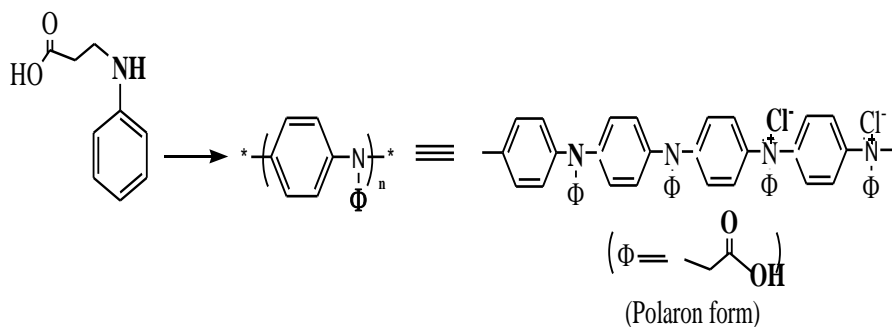
Reagent and conditions:

(i) Methyl acrylate, Toluene, 90 °C, 2 h; (ii) MeOH, NaOH, 0-5 °C, 2 h

Scheme 5. Synthesis of 3-methyl (phenylamino) propanoate and 3-methyl (phenylamino) propanoic acid single monomer

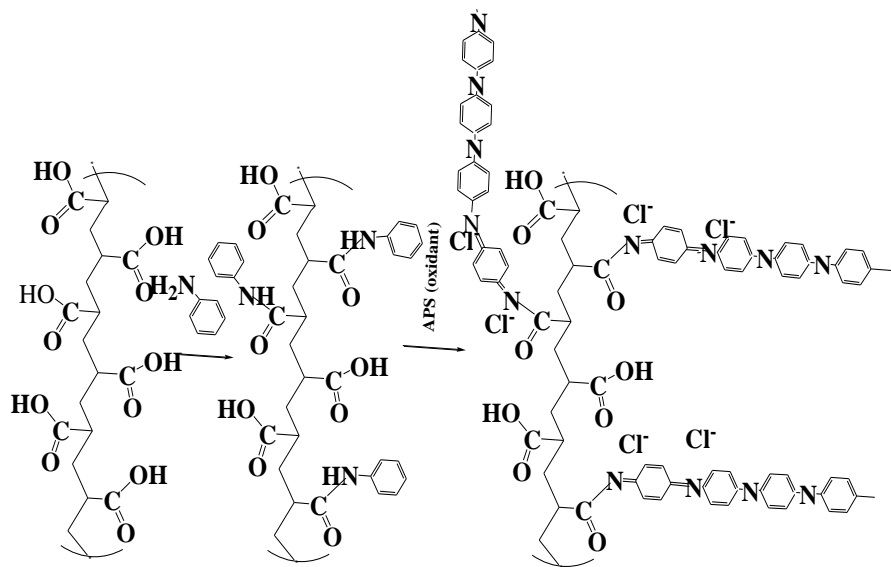
The nanostructures of poly (3-methyl (phenylamino) propanoic acid) doped with HCl were synthesized by a chemical oxidation method. Poly (3-methyl (phenylamino) propanoic acid) doped with HCl was synthesized as follows: Aniline (0.165 g) was mixed with in 10 mL distilled water in the ice bath to form N-substituted aniline solution. Then, an aqueous solution of APS (0.001 mol) in 25 mL of 0.01 M

HCl solution was added drop wise to the above solution. The polymerization was carried out for 12 h in the ice bath. A green solid of HCl doped poly (3-methyl (phenylamino) propanoic acid) was obtained after rinsing with H_2O , CH_3OH , and CH_3OCH_3 for three times [38]. The reaction scheme for synthesis of HCl doped poly (3-methyl (phenylamino) propanoic acid) polymers are shown in following **Scheme 6**.



Scheme 6. Synthesis of HCl doped poly (3-methyl (phenylamino) propanoic acid)

Synthesis of PAA/PANI composites. The **PAA/PANI** composites were prepared by chemical oxidation process in aqueous medium [38]. The **PANI/PAA** composites were prepared as follows: aniline was added to the **PAA** (commercially available, $M_w \sim 1800$) solution with constant stirring at room temperature and solution becomes colorless.



Scheme 7. Reaction scheme for synthesis of HCl doped **PAA/PANI** composite

The ratio **PAA** and aniline was 1.0:0.5 (w/w). Next, the reaction mixture was

cooled to 5 °C and stirred for 1 h. During this time, freshly prepared APS solution (0.01 mol **APS** in 0.001 M HCl) was added slowly to the reaction mixture. After 2 h, the mixture was brought to the room temperature and stirred continuously for 6 h to complete the polymerization of aniline. The color of the mixture changed from colorless to deep green. The obtained product was kept 12 h for complete the polymerization after which the polymer was filtered with Buckner funnel. After that, these products were washed with distilled water several times (pH ~7) and dried under vacuum at 60 °C for 6 h to get composites. The reaction for synthesis of HCl doped **PAA/PANI** polymer is presented in **Scheme 7**.

2.2. Characterization Techniques

FTIR spectra were recorded on a Thermo Nicolt Nexus 870 spectrophotometer in the range 400-4000 cm^{-1} . The instrument settings were kept constant (50 scan at 4 cm^{-1} resolution, transmittance mode). **Ani, AA, AA and Ani mixture, β -amino acid, PAA and AA based PANI samples** were used. Before running the samples, a background spectrum was collected. Then samples were put in a sample holder and data were collected. **^1H NMR** of AA and Ani mixture, **β -amino acid** and its **corresponding polymer** are recorded using **Bruker DRX500 MHz** spectrometer at IIT Kharagpur (Chemistry Dept.). These were dissolved separately in **$\text{d}_6\text{-DMSO}/\text{CDCl}_3$** and **$\text{CDCl}_3$** . The chemical shifts of the groups are recorded in the range 10-200 Hz for monomer and 10-400 Hz for prepared polymer with a delay of 2.5 sec. Identification of the product ions formed during **ESI-MS** analyses were performed on **AXIMACFR** laser desorption ionization flying time spectrometer (**COMPACT**). In order to identify these product ions, structure of prepared compound were created. Gel as well as solid granules materials were analysed and are fine aerosol. It helps to evaporate solvent easily. Typical solvents for electrospray ionization are prepared by mixing water with volatile organic compounds like methanol and acetonitrile. Acetic acid is added to prepared typical solvent. X-ray diffraction (**XRD**) experiments were performed using a Phillips PW-1710 Advance wide angle X-ray diffractometer, **Phillips PW-1729** X-ray generator, and Cu $\text{K}\alpha$ radiation (wavelength, $\lambda = 0.154 \text{ nm}$). The generator was operated at 40 kV and 20 mA. The powder samples were placed on a quartz sample holder at room temperature and were scanned at diffraction angle 2θ from 5° to 60° at the scanning rate of 2 °/min. Acrylic acid based PANI samples was taken for XRD analysis. The **UV-Visible** spectra of aniline, acrylic acid, acrylic acid based monomers and its corresponding polymer(s) were recorded by using a **Micropack UV-VIS-NIR, DH 2000** in the wave length region 200-800 nm. The samples were dissolved in N-methyl pyrrolidone (**NMP**). Base line was corrected before recording the spectra. This technique was performed for studying the variety of electronic transitions. Surface morphologies of acrylic acid based PANI polymer as well as N-substituted aniline (monomer) were analyzed by field emission scanning electron microscopy (**FESEM**) using **Carl Zeiss Supra 40** scanning electron microscope. Before FESEM experiment, gold coating was needed. Operating voltage was 4 kV. The enthalpy of fusion of prepared AA based PANI polymer was calculated from differential scanning calorimetry (**DSC**)

experiment. The parameters such as heating rate = 10 °C/min, temperature range = 50 to 350 °C were set. The thermal stability of the prepared materials was determined by thermogravimetric (TG) analysis using a **NETZSCH TG-209 F1 analyzer** at a heating rate of 10 °C/min in nitrogen environment from 50-700 °C.

The **room temperatures** as well as **temperature** dependent **DC conductivity** of the prepared acrylic acid based PANI polymer were measured using linear four-probe technique. Four contacts were made with nonconducting silver paste.

A constant current (I) from a current source (Keithley 2400 programmable current source) was allowed to pass through two terminal leads of the four probe and the voltage (V) across the other two leads was measured using a multimeter (Keithley 2000 digital multimeter). According to four point probe method, the resistivity (ρ) was calculated using the relation [39]

$$\rho = 2\pi S \left(\frac{V}{I} \right) \dots\dots\dots (1)$$

where S is the probe spacing in centimetres (cm), which was kept constant, (I) is the supplied current in mill-amperes (mA) and the corresponding voltage (V) was measured in mili-volts (mV). The conductivity (σ) was calculated using the relation as follows [39]

$$\sigma = \frac{1}{\rho} \dots\dots\dots (2)$$

For temperature variation resistivity measurement, the chamber pressure was maintained at 10⁵ torrs. The Lakeshore (model 331) temperature controller was connected. Then, we measured DC resistivity. A constant current is passed through the two side probes and measured voltage in the two middle probes. A DC current source (Keithley 220 programmable) was taken. Different millampere/nanoampere current was applied and corresponding voltage was measured. Voltage across the terminals was measured using Keithley nanovoltmeter (model 2182). For In addition, the resistivity measurement with a particular magnetic field is a function of temperature which is important for calculating localisation length (L_{loc}). Determination of other different transport parameters [28] such as Density of states at Fermi level ($N(E_F)$), Mott's characteristics temperature in Kelvin (T_{Mott}), Mott's hopping distance ($R_{Hop, Mott}$ in nm at 300 K) and the energy difference ($\Delta_{Hop, Mott}$) between the sites in the Mott's limits is calculated using L_{loc} . These are the important parameters to understand the conduction mechanism.

2.3. Results And Discussion

The outcomes obtained from different experiments of monomer synthesis

and polymerizations are described separately.

Monomer synthesis

The mixture of aniline and acrylic acid (gel-like monomer) was purified using DCM and n-Hexane solvents. The purpose was to remove excess of unreacted monomers. Such process is called co-precipitation method. Particularly, for this monomer synthesis, colorless liquid aniline (2 mL) was added directly on colorless acrylic acid (2 mL) to form impure monomer. During the formation, a different color was observed as shown in **Fig. 1**. There may be an interaction between the two materials. The excesses individual precursors were removed using precipitation technique. Impure monomers were dissolved by DCM and followed by n-Hexane. Such solution was kept at low temperature (0-5 °C) for 12 h. The purpose of using DCM and n-Hexane was to remove excess of precursors. Color transition during the preparation of gel like monomer is shown in **Fig. 1**.

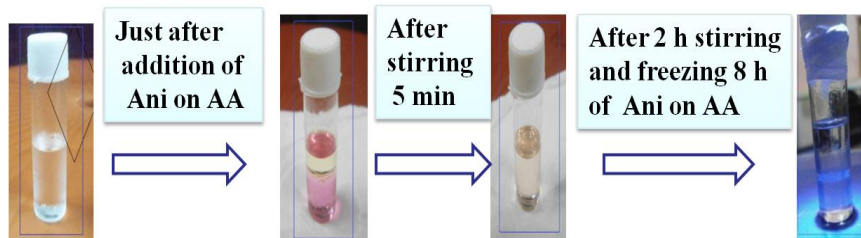


Figure 1. Color change during the synthesis of N-substituted anilinic monomer (aniline and acrylic acid mixture)

For the synthesis of N-Phenyl- β -alanine, aniline and methyl acrylate were taken in dry toluene [36]. HCl-treated MMT was used as catalyst to the reaction mixture. The reaction was carried out in dry condition. The reaction temperature (90 °C) was maintained using an oil bath. During the reaction, the transition of color was observed from colorless to light brown. After solvent evaporation, a dense brown product was obtained. This product was used for the next step. For the conversion of ester to acid, crude product (prepared from first step) was added to methanol followed by addition of NaOH and 6 M HCl. Finally, the product was extracted with ethyl acetate several times. After solvent evaporation, precipitation by n-hexane and drying, a light brown mass was obtained.

ESI-MS, ^1H NMR, and FTIR techniques were used for structural elucidation of substituted aniline monomer.

ESI-MS analysis

For structural analysis, the masses of adducts formed from these compounds via the attachment of various different species ($[\text{P} + (\text{M})n]n+$, where P represents a target compound; M represents a solvent molecule or sodium, potassium, lithium,

silver, hydrogen, or ammonium cations; and $n = 1$ for singly charged ions or $n = 2$ for doubly charged ions) were calculated [37]. The exact masses calculated for these adduct species are used in the assignment of peaks generated in the ESI-MS experiments. To assign chemical structures of acrylic acid and aniline mixture, 3-methyl (phenyl amino) propanoate and 3-methyl (phenyl amino) propionic acid were investigated by ESI-MS and it is presented in **Fig. 2, 3** and **4**. The spectra were generated using the normal scan mode. The spectra were taken (zoom scan) over representative m/z areas of the region dominated by ideal star peaks (**Fig. 2, 3** and **4**). In **Fig. 2**, by comparing theoretical m/z values to these peaks, the adduct species are able to be found and these are mechanistically feasible. In **Fig. 2**, the observed m/z value of small peak (below 100 % abundance) matches with the theoretical m/z of hydrogen adducts formed from the products (substituted anilinic monomer obtained from aniline and acrylic acid) and most intense peak (100%) corresponds to hydrogen adducts of N,N-disubstituted anilinic product (100 % abundance). Other than these peaks, a significant number of non-reproducible and/or non-periodic peaks were observed in these spectra, which were not unexpected. Thus, it is not mechanistically feasible and disregarded.

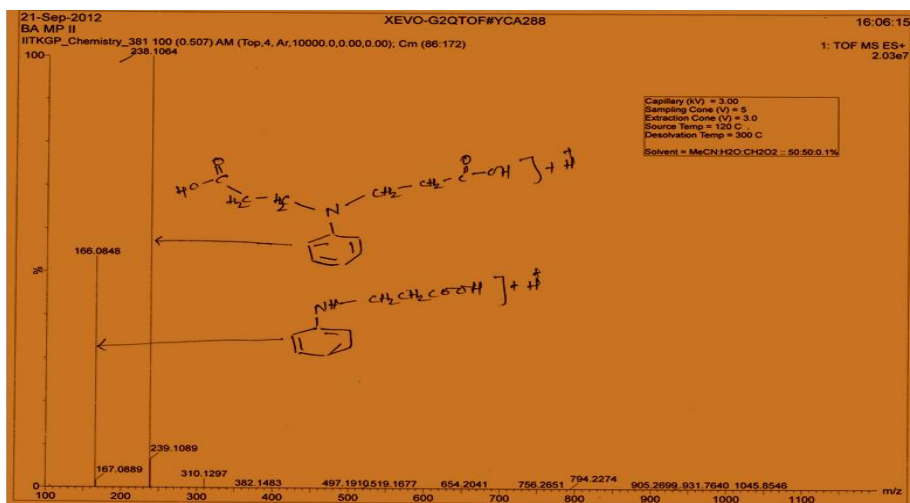


Figure 2. ESI-MS spectrum of monomer obtained from AA and Ani mixture

In **Fig. 3**, 100 % abundant peak matched with hydrogen adduct, which has arisen from 3-methyl (phenyl amino) propionate product (mentioned the chemical structure of product). No oxidation products are formed. The assignment is mechanistically feasible. Other peaks in the spectrum (**Fig. 3**) are not matched to any adducts. Thus, it can be seen that there is an ambiguity in the assignment of products.

Also, ESI-MS technique is used to characterize the 3-methyl (phenyl amino) propionic acid. In **Fig. 4**, we observed single peak, which is 100% (relative abundance). This peak indicates to 3-methyl (phenyl amino) propionic acid adduct. No oxidation products are formed. The assignment is mechanistically feasible. Other

peaks in the spectrum are not matched to any adducts.

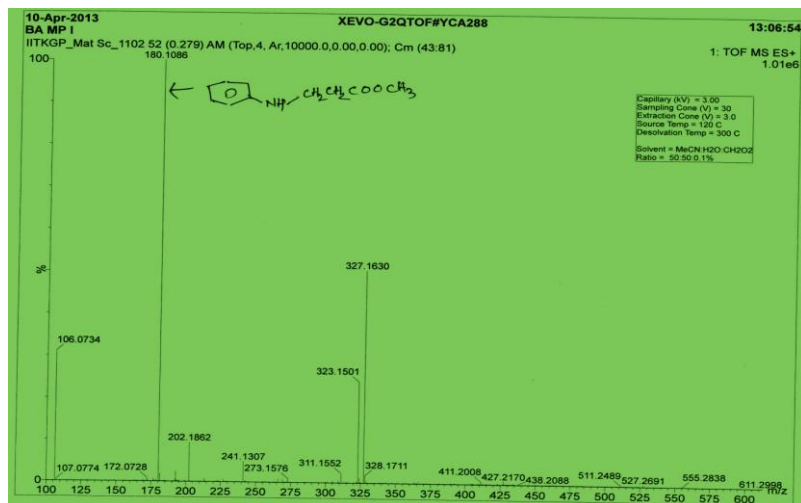


Figure 3. ESI-MS spectrum of anilinic monomer (3-methyl (phenyl amino) propionate) prepared from methyl acrylate and aniline

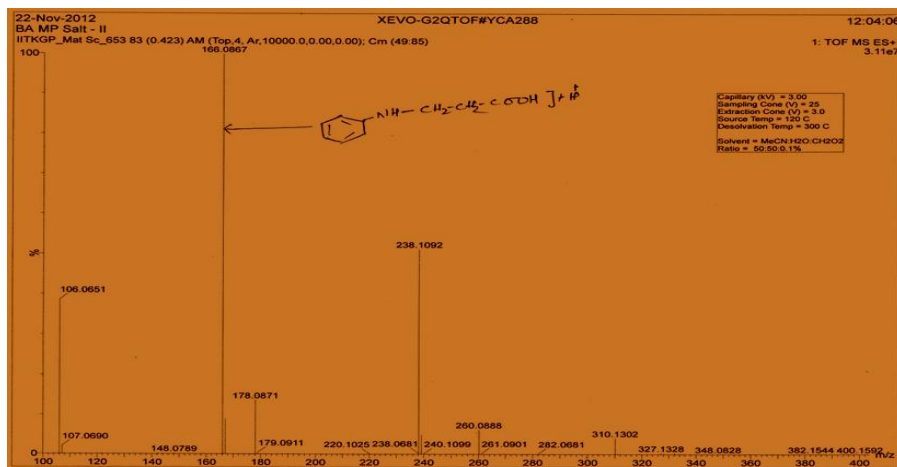


Figure 4. ESI-MS spectrum of 3-methyl (phenyl amino) propionic acid monomer obtained from 3-methyl (phenyl amino) propionate

H¹NMR analysis

Spectroscopic characterizations such as H¹NMR, FTIR and ESI-MS, etc. were employed to elucidate the chemical structure of materials. Out of them, H¹NMR is one of the important spectroscopic characterizations to explore the molecular

[illegible]

In a similar fashion, the 3-methyl (phenyl amino) propionic acid has been characterized by H^1NMR technique and the spectrum is displayed in **Fig. 6**.

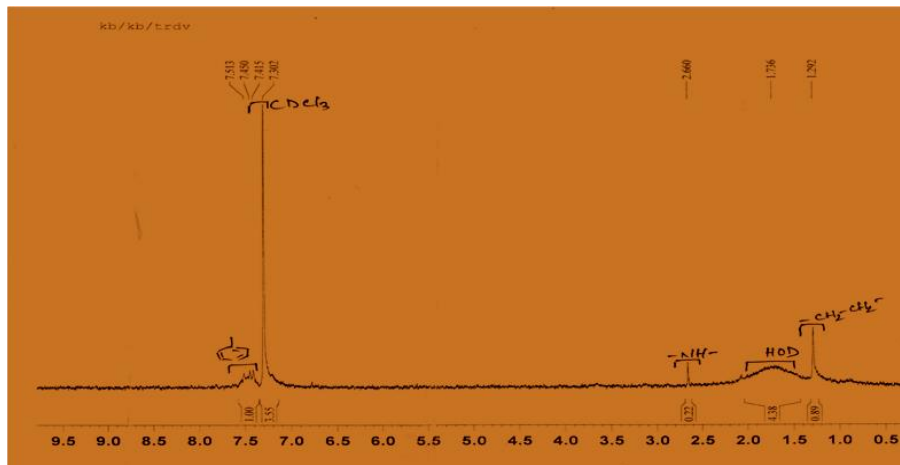


Figure 6. ^1H NMR spectrum of 3-methyl (phenyl amino) propionic acid monomer)

From this spectrum analysis, the peak positions and their assignments are presented in **Table 1**. In **Table 1** various protonic groups such as phenyl protons ($-\text{C}_6\text{H}_5$) at 7.302-7.513 [38], amine proton ($-\text{NH}-$) at 2.66 ppm [38] and ethylenic proton ($-\text{CH}_2\text{CH}_2-$) 1.292 ppm, CDCl_3 (7.3 ppm) [39] were assigned. Thus, it supports a possible structure of repeat unit (3-methyl (phenyl amino) propionic acid).

FTIR analysis

Fig. 7 shows the FTIR spectra of (AA), aniline (Ani) and synthesised anilinic monomers. The characteristic peak positions and their assignments are given in **Table 1**. From **Fig. 7**, the major bands of **AA** at 3062, 1706, 1431 and 1238 cm^{-1} have been attributed to C–H stretching, C=O stretching, and C–O stretching vibration of acid group, respectively [40]. This indicates that the characters of AA are retained. The peaks of **Ani** (**Fig. 7**) are found at 3365, 3034, 1496, and 1173 cm^{-1} corresponding to $-\text{NH}$ -, $-\text{CH}$ -, benzenoid and C=N stretching, respectively [41]. From our observation in **Fig. 7** and **Table 1**, the main bands are $-\text{NH}-$ (3403 cm^{-1}), benzenoid ring (1502 cm^{-1}), $-\text{CH}-$ (2952 cm^{-1}), $-\text{OH}$ (2600 cm^{-1}), $-\text{C}=\text{O}$ (1619 cm^{-1}) and C–O (1241 cm^{-1}), which indicated the presence of both AA and aniline. Also, main bands of prepared substituted monomers of mixture of AA and Ani are found at 3046 cm^{-1} , 1718 cm^{-1} , 3370 cm^{-1} , 1415 cm^{-1} , and 1211 cm^{-1} corresponding to $=\text{C}-\text{H}$ stretching, C=O stretching of ester, N–H stretching, C=C stretching of aromatic ring, C–N stretching, respectively.

Table 1: FTIR, ^1H NMR, and ESI-MS peak positions and their assignments

	Peak positions and their assignments of anilinic monomer from acrylic acid and aniline					
FTIR Peak Positions (cm^{-1})	3403	2952	2600	1619	1502	1241
Its peak assignments	NH	CH	OH	C=O	Benzene ring	=C-N
^1H NMR peak positions	2.575-271	3.444-3.638	4.336-4.422	6.658-6.842	7.094-7.269	
Its peak assignments	CH_2CH_2	NH	impurities	CDCl_3	Benzene proton	
ESI-MS	166	238				

peak positions						
Its peak assignments	N-mono substituted monomer	N,N-di substituted monomer				
FTIR Peak Positions (cm^{-1})	3482	2952	2610	1735	1525	1107
Its peak assignments	NH	CH	OH	C=O	Benzene ring	=C-N
^1H NMR peak positions	7.3-7.5	7.3	2.6	1.7	1.3	1.0
Its peak assignments	Benzene proton	CDCl_3	NH	HOD	CH_2CH_2	TMS
ESI-MS peak positions	180 (100%)	166	---	---	---	---
Its peak assignments	N-substituted Methyl ester	N-substituted Methyl ester	---	---	---	---

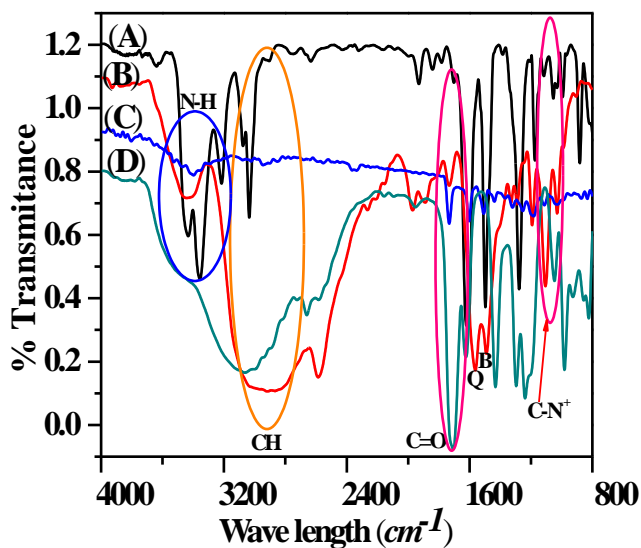


Figure 7. FTIR spectra of Aniline (A), 3-methyl (phenyl amino) propionic acid (B), anilinic monomer (AA and Ani mixture) (C), and AA (D)

Considering the entire peak assignments and peak intensity obtained from the FTIR spectra, the bands of 3-methyl (phenyl amino) propionic acid are found at 2952 cm^{-1} , 1735 cm^{-1} , 3482 cm^{-1} , 1525 cm^{-1} , 2610 cm^{-1} , and 1107 cm^{-1} for C-H stretching, C=O stretching of acid, N-H stretching, C=C stretching of aromatic ring, -OH stretching of carboxylic acid, and C-N stretching, respectively.

XRD analysis

X-ray Diffraction (XRD) was used to study the structure of synthesised 3-methyl (phenyl amino) propionic acid monomeric product and shown in **Fig. 8**. From this **Fig. 8**, we observed sharp peaks, which indicated the crystalline nature of 3-methyl (phenyl amino) propionic acid (monomer) [42].

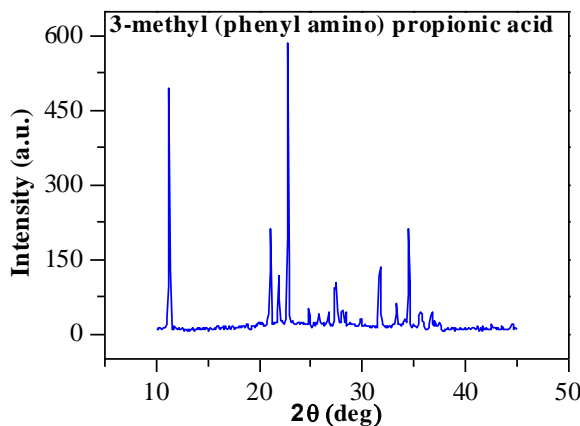


Figure 8. XRD plot of prepared 3-methyl (phenyl amino) propionic acid monomer (methyl acrylate and aniline)

Synthesis of AA based PANI polymer

FTIR, ^1H NMR, UV-Visible, and X-ray diffraction (XRD) spectral analysis of synthesised AA based PANI polymer were done for chemical structure analysis of synthesized AA based PANI.

Synthesis of AA based PANI polymer

For carrying the polymerization, both monomers and oxidant (APS) were taken in water phase. The oxidative coupling polymerizations of the both monomers were mediated at the aqueous medium. As compared to the experimental condition to synthesize substituted PANI, oxidative coupling polymerization was conducted between oxidant and monomers. From FESEM experiment, morphology of

synthesised polymeric product was analysed and it is shown in **Fig. 9**. The FESEM images (**Fig. 9**) show the crystals-like morphology of 3-methyl (phenyl amino) propionic acid, net-like structure of poly (3-methyl (phenyl amino) propionic acid, crystal plates of PAA, cauliflowers like morphology of PAA/PANI composites, globular shapes of AA doped PANI (APS in H₂O), and nanofibers of AA doped PANI (APS in 1 M HCl). In net-like structure, it may be believed that substituted PANI chains are inter-linked, whereas small cauliflowers image shows that PANI chains are interacting with carboxylic group in PAA chains. The interaction is non-uniform. In case of fiber-like morphology, the average diameters of fiber is more than 50 nm, known as nanofiber. Conducting polymers were first nucleated at the interface through oxidative coupling between monomer of PANI and APS (oxidant) in the aqueous layer. These polymers were grown in the aqueous medium. A variety of FESEM images were found in morphology study as shown in **Fig. 9**.

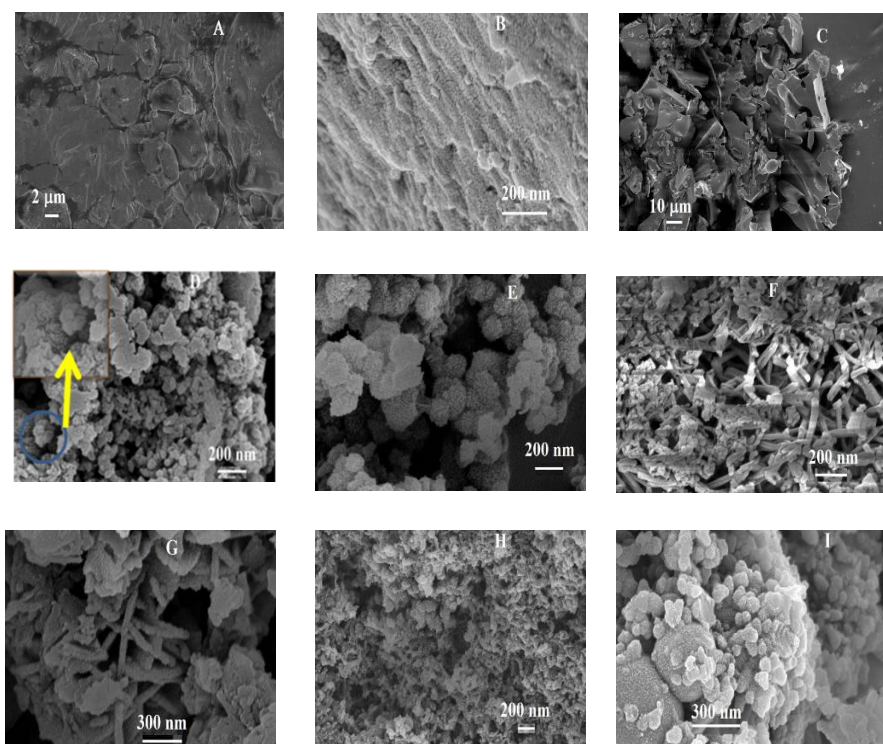


Figure 9. FESEM images of 3-methyl (phenyl amino) propionic acid (A), Poly (3-methyl (phenyl amino) propionic acid) (B), PAA (C), PAA/PANI (PAA : aniline (w/w) = 1 : 0.5) composite (D), PAA/PANI (PAA : aniline (w/w) = 1 : 0.5) composite (E), AA doped PANI (APS in 1 M HCl) (F), AA doped PANI (APS in 0.5 M HCl) (G), HCl doped PANI (H) and AA doped PANI (APS in water) (I)

X-ray diffraction (XRD) analysis

In this work, X-ray diffraction (XRD) was done to exploit the crystalline/amorphous nature of synthesized AA based PANI polymer. From XRD patterns, AA doped PANI (APS in water), AA doped PANI (APS in 1 M HCl), PAA, PAA/PANI composite and HCl doped PANI are shown in **Fig. 10**. Broad peaks in **Fig. 10** indicate the amorphous nature of the polymer [43]. In case of HCl doped PANI, several diffraction peaks are observed in **Fig. 10**. This shows that PANI chains become more ordered after the doping [44]. On the contrary, two peaks at 19° and 25° are found in the patterns of AA based PANI. It indicates the presence of two polymers (PANI and PAA). This might happen during the polymerization process. Some of the acrylic acid was converted to PAA (polyacrylic acid). Similar pronounced diffraction peaks (at 19° and 25°) of PAA/PANI composite are found in the pattern with high intensity. This indicates the presence of more PAA in the PAA/PANI composite.

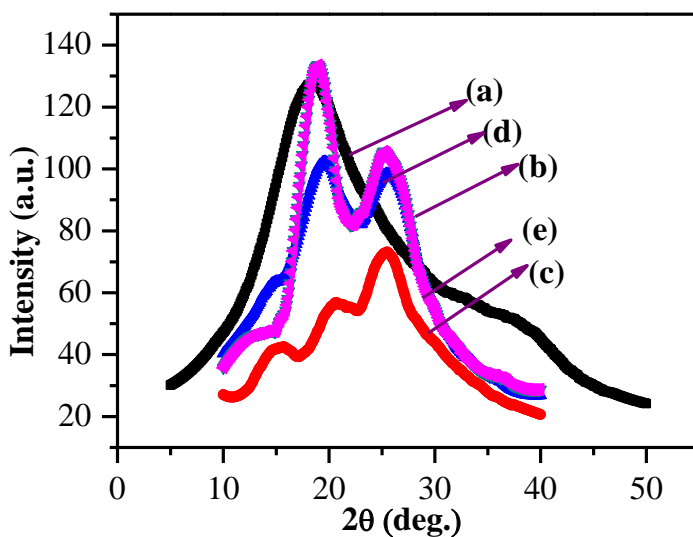


Figure 10. XRD pattern of the PAA (a), PAA/PANI (b), HCl doped PANI (c), AA doped PANI (APS in 1 M HCl) (d) and AA doped PANI (APS in water) (e)

FTIR analysis

FTIR spectra of AA acid based PANI (APS in water), AA acid based PANI (APS in 1 M HCl), poly (3-methyl (phenyl amino) propionic acid), PAA/PANI composite and HCl doped PANI are shown in **Fig. 11**. The different band positions and their assignments are presented in **Table 2**. The most important bands of AA acid doped PANI (APS in water) at 3445 , 2919 , 1550 , 1457 , 1125 and 1269 cm^{-1} have been attributed to N-H, C-H, quinoid, benzenoid, C=N and C-O stretching vibration of acid group, respectively [45]. This indicates that the required characters of the PANI are retained. The main features of AA acid based PANI (APS in 1 M HCl) are found at 3450 , 1595 , 1435 , 1115 , and 2924 cm^{-1} corresponding to N-H, quinoid, benzenoid, C=N stretching and C-H, respectively [45]. From our observation, quinoid (1595

cm^{-1}) and benzenoid ring (1435 cm^{-1}) vibrations are indicated for the AA doped PANI [45]. Also, main bands of prepared poly (3-methyl (phenyl amino) propionic acid) are found at $3450, 1568, 1473, 1120, 2932, 1685, 3681, 1294,$ and 1237 cm^{-1} corresponding to N-H stretching, quinoid, C=C stretching of aromatic ring, C-N stretching, C-H stretching, C=O stretching of acid, O-H stretching and C-O stretching, respectively. The band positions of PAA/PANI composites are found at $3450, 1582, 1491, 1120, 2932, 1710, 3693, 1377,$ and 1288 cm^{-1} for N-H stretching, quinoid stretching, C=C stretching of aromatic ring, C-N stretching, C-H stretching, C=O stretching of acid, O-H stretching and C-O stretching, respectively [46]. The characteristic band positions of HCl doped PANI are found at $3289, 1533, 1453, 1067, 2965, 1375$ and 1262 cm^{-1} for N-H stretching, quinoid stretching, C=C stretching of aromatic ring, C-N stretching, C-H stretching, C=O stretching of acid and C-O stretching, respectively [47].

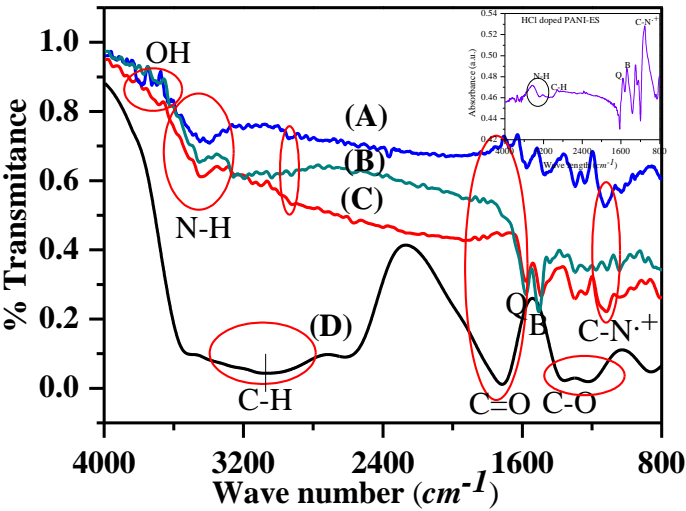


Figure 11. Poly (3-methyl (phenyl amino) propionic acid) (A), AA doped PANI (B), PAA/PANI composite (C), PAA (D)

Table 2. FTIR Peak positions and their assignment of AA doped PANI, Poly (3-methyl (phenyl amino) propionic acid), HCl doped PANI, PAA, PAA/PANI composite

Peak assignments	Peak positions (cm^{-1})				
	AA doped PANI	N substituted PANI	HCl doped PANI	PAA	PAA/PANI composite
NH stretch.	3445	3450	3289	---	3450
Quinoid	1550	1568	1533	---	1582

stretch.					
Benzenoid stretch.	1457	1473	1453	---	1491
C=N stretch.	1125	1120	1067	---	1120
C-H stretch.	2919	2932	2965	3037	2932
C=O stretch.	---	1685	1728	1722	1710
OH stretch.	---	3681	---	---	3693
CH (def.)	---	1294	1375	1364	1377
CH (bending)	1269	1237	1262	1217	1288

H¹NMR analysis

Careful analysis of the H¹NMR characterization of N-substituted PANI polymer [48] obtained from aniline monomer (AA and Ani mixture) product provides insight into the structure of the material. The H¹NMR plot is shown in **Fig. 12**. In the repeat unit, various proton containing groups are presented. The characteristic C-H proton of phenyl ring are found at 6.635-6.915 and 7.019-7.751 ppm, 10 ppm (O-H), 5.740 ppm, and 2.493 and 3.244-3.844 ppm (methylene proton linked to -COOH and -N-), respectively.

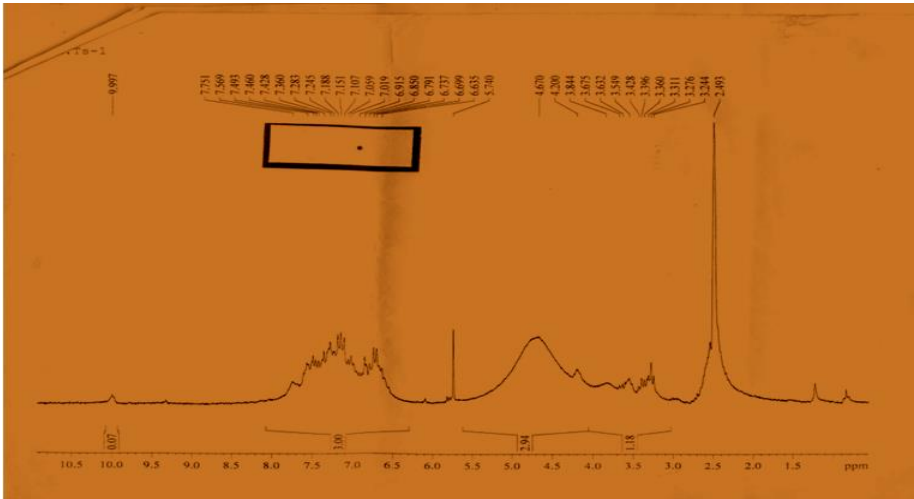


Figure 12. H¹NMR spectrum of N-substituted PANI polymer from acrylic acid and aniline mixture

UV-Visible spectroscopic analysis

It is reported that AA, Ani, 3-methyl (phenyl amino) propanoic acid, poly (3-

methyl (phenyl amino) propanoic acid), AA doped PANI and PAA/PANI composite are shown in **Fig. 13 (a)** and **(b)** in the range (250-800 nm). The type of UV-Visible band positions and their assignments are presented in **Table 3**. The $\pi-\pi^*$ transition was observed at 258 nm due to the presence of π -bond (ethylenic group and C=O) in acrylic acid [49]. The $\pi-\pi^*$ band at 293 nm appeared in the aniline unit [**Fig. 13 (a)**] [50]. Two types of electronic transitions (band) were found at 276 nm and 317 nm in synthesised anilinic monomer (AA and Ani). The assignment may be due to the presence of combined aniline unit and acrylic acid unit in the as prepared salt. This signifies the absence of anilinic unit and excitation band. In the **Fig. 13**, no band is observed in PAA spectrum. PAA/PANI composite shows bands at 272 nm, 294 nm and 564 nm as shown in **Fig. 13 (b)**. The peak observed at 564 nm is due to electronic excitation [46]. This signifies the formation of oxidation state, *i.e.*, salt form of PANI [46]. Also, other two peaks (272 nm, 294 nm) are assigned for $\pi-\pi^*$. These indicate the presence of aniline unit of PANI [46]. As well, AA doped PANI shows two types of bands ($\pi-\pi^*$ and excitation band). This signifies aniline unit and oxidation state of PANI, respectively [51]. Salt forms of PANI contain both amine groups and imine groups. Imine group represents the doped state of PANI, *i.e.*, the N atoms in the imine groups are protonated, N and its neighbouring quinoid ring become a semiquinoid radical cation [52]. The different absorption bands are observed in **Fig. 13 (b)**. This may be happened due to the different rate of doping as well as synthetic procedure [52].

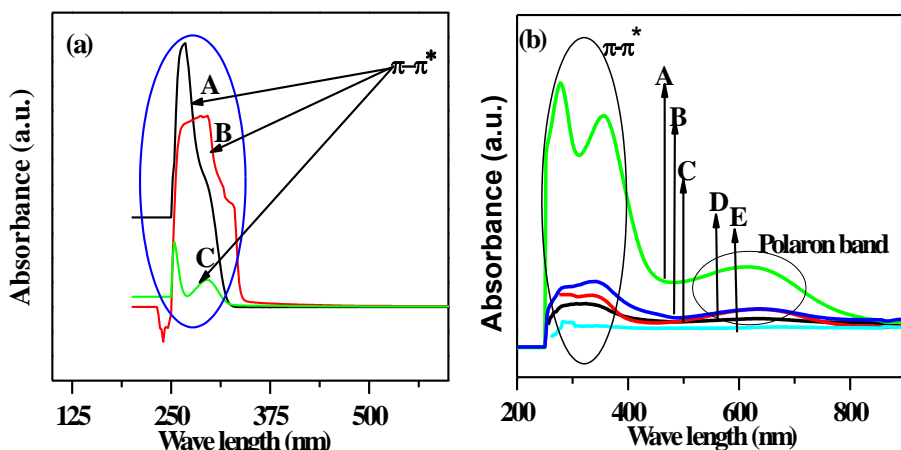


Figure 13. UV-Visible spectra of AA (A), Ani (B), 3-methyl (phenyl amino) propanoic acid (C) in (a), whereas HCl doped PANI (A), AA doped PANI (B), PAA/PANI composites (C), 3-methyl (phenyl amino) propanoic acid (D), and PAA (E) in (b)

Table 3. UV-Visible peak positions and assignments for acrylic acid (AA) based PANI polymers (^aAPS in H₂O, ^bAPS in 1 M HCl)

Peak	Peak positions (nm)
------	---------------------

assignments	AA based PANI ^a	AA doped PANI ^b	HCl doped PANI	N-substituted PANI	PAA/PANI composite
π - π^*	268 & 347	276 & 369	277 & 360	310	338
Polaron band	580	706	614	625	630

The electronic transitions were observed between two bands, which happened after photon absorption. Photon absorption (UV-Visible) semiconductor is followed by Tauc expression [53].

$$(\alpha h\nu) = A (h\nu - E_g)^n \dots\dots\dots (1)$$

Where α = optical absorption co-efficient, $h\nu$ = photon energy, E_g = energy gap calculated from graph, A = absorption constant, n = represents the types of transition. Here, $n = 2$ indicates allowed indirect transitions and $n = 1/2$ indicates allowed direct transitions. The optically (direct) allowed transitions of AA doped PANI, Poly (3-methyl (phenyl amino) propanoic acid), and PAA/PANI composite are shown in **Fig. 13 (c)** and its value is presented in **Table 4**. For direct transition, we can

plot $(\alpha h\nu)^2$ vs. $h\nu$ and extrapolate the linear portion of it to $\alpha = 0$ value to obtain corresponding direct band gap. We estimated two E_g values corresponding to two types of transitions observed from **Fig. 13 (c)**. This band gap values are 3.65 and 2.79 eV for HCl doped PANI, 3.08 eV for PAA/PANI composite, 2.90 eV for AA doped

PANI and 2.83 eV for poly (3-methyl (phenyl amino) propanoic acid). There E_g values correspond to the wide band gap of the inorganic semiconductor [53]. This variation is probably due to the formation of PANI polymeric structure using different monomers [53], which means that the different polymeric structures have produced various electronic environments. This environment produces different repulsive electron-electron interactions between two electrons on the same monomer unit or on neighbouring carbons along the backbone. That's why; we got various optical (direct) bands of prepared AA based PANI polymer [54].

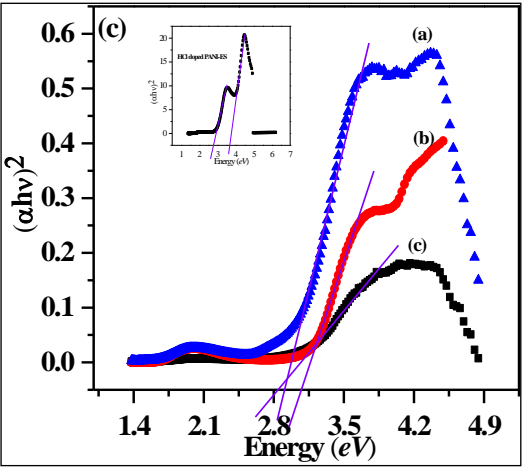


Figure 13(c). Optical (direct) band gap of AA doped PANI (a), PAA/PANI composite (b), poly (3-methyl (phenyl amino) propanoic acid) (c), HCl doped PANI at left corner

DC conductivity

Conductivity is the inherent property of intrinsically conducting polymers (ICPs). To work out the room temperature DC conductivity of using the relation

$$\sigma = \frac{1}{\rho}$$

, where, ρ is resistivity [43]. The resistivity was measured using the relation

$$\rho = 2\pi S \left(\frac{V}{I} \right)$$

, where S is the probe spacing (0.2 cm), I be the applied current in

the four probe system (micro amp regime) and V be the corresponding obtained voltage in (V). At room temperature, the average DC conductivity was found to be 4.79×10^{-4} S/cm for AA doped PANI (APS in water), 0.825 S/cm for AA doped PANI (APS in HCl), 0.135 S/cm for (poly (3-methyl (phenyl amino) propanoic acid) palette), 0.1004 S/cm for PAA/PANI composites, 1.35×10^{-4} S/cm for HCl doped PANI, respectively. The DC conductivity values are indicating the semiconducting material range [43]. The reason may be due to the different strengths of acid dopants as well as monomer unit and that forms different oxidation states in PANI polymer backbone. Dopant helps to extend the conjugation of PANI polymeric structure evolved in the polymerization mechanism. Structural ordering is possible in the polymers and that may be happened due to the incorporation of the charged species [54]. There are signatures supporting these changes in the UV-Vis results. Estimated average DC conductivity at room temperature for AA based PANI is mentioned in **Table 4**.

Table 4. Estimated average DC conductivity at room temperature and optical (direct) band gap of AA based PANI polymer

Parameters	Materials name				
	AA doped PANI ^a	AA doped PANI ^b	Poly (3-methyl (phenyl amino) propanoic acid	PAA/PANI composite	HCl doped PANI
DC (av.) Conductivity	4.79×10^{-4}	0.8625	0.153	0.1004	1.35×10^{-4}

(S/cm)					
Optical (direct band gap (eV)	2.56 & 3.663	2.90	2.74	3.09	2.82 & 3.76

The variation of DC conductivity with temperature is presented in **Fig. 14(a)** and **(b)** for the prepared materials. It is seen that the conductivity of the prepared materials is increased with the increase of temperature from 70 to 300 K. This behaviour is similar to the behaviour of inorganic semiconductor [25].

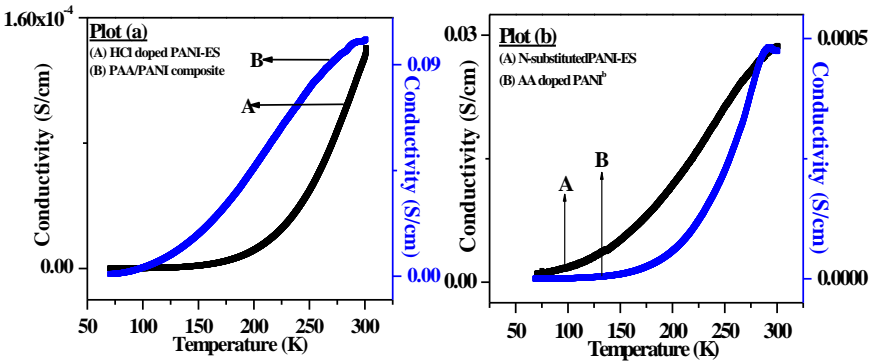


Figure 14. Variation of DC conductivity with temperature of HCl doped PANI (A) and PAA/PANI composite (B) in plot (a), whereas Poly (3-methyl (phenyl amino) propanoic acid (A) and AA doped PANI (APS in 1 M HCl) in plot (b)

DC conductivity of the prepared materials was measured at temperature from 70-300 K in the presence and absence of magnetic field (0.4 T) for better understanding of the conduction mechanism. Several reports have described the metal-insulator (M-I) transition behaviour that occurred in the semiconducting polymeric materials. In this transition, three different regions are identified such as metallic ($\rho_r < 2$), critical ($2 < \rho_r < 6$) and insulating ($\rho_r > 6$) depending on resistivity ratio [28]. Since the resistivity ratio of our prepared materials are more than 2 and then, it is treated as insulating region [28].

Some reports have mentioned about Anderson transition in three dimensional (3D) electronic systems [24]. In this system (3D), fluctuation increases due to random potential. That is why transition occurred from metal to insulator. Because of this transition, the nature of the electron wave functions changes under the influence of the disorder. Particularly in an insulating phase, a potential fluctuation is more and the wave is localised in the region of space [24]. When the Fermi energy lies in a region of localized states and the system is a Fermi glass insulator. In this region, the low temperature transport is possible by variable-range hopping (VRH) [24]. Thermally activated or hopping behaviour is studied by temperature dependent DC conductivity without magnetic field and it is shown in **Fig. 14** (Arrhenius model) and **Fig. 15** (3D VRH model). With the help of Mott's expression (equation 2) and Arrhenius equation,

the more prominent transport behaviour was shown to occur either by thermally activated or hopping process in conducting polymer [25]. Mott’s expression and Arrhenius equation are shown in equation 2 and 3, respectively, whereas R-values are presented in **Table 5**.

$$\sigma = \sigma_0 \exp \left(-\frac{T_0}{T} \right)^r \dots\dots\dots(2)$$

where T_0 is the Mott characteristic temperature and σ_0 the limiting value of conductivity at infinite temperature and the exponent ‘r’ is related to the dimensionality of the transport process via the expression $r = [1/(1+d)]$, where d = 1, 2 and 3 for one-, two- and three-dimensional conduction process, respectively.

Arrhenius equation is obtained from rearrangement of Mott’s expression (equation 3). In Arrhenius plot (**Fig. 14**), we plotted $\ln \sigma$ vs $1000/T$.

$$\ln \sigma = \ln \sigma_0 + \left[(-rT_0) \left(\frac{1000}{T} \right) \right] \dots\dots\dots(3)$$

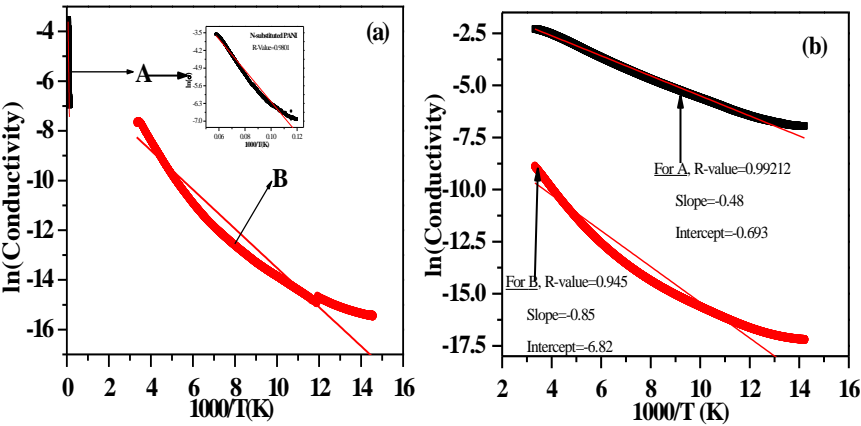


Figure 15. (a): \ln (Conductivity) vs reciprocal Temperature of HCl doped PANI (A) and PAA/PANI composite (B); (b): AA acid doped PANI (APS in 1 M HCl) (A) and poly (3-methyl (phenyl amino) propanoic acid (B)

Arrhenius model (**Fig. 15**) or Mott’s variable range hopping (Mott’s VRH) model (**Fig. 16**) was fitted linearly. The outcomes of regression values are presented in **Table 5**. According to the regression value, the as prepared materials satisfies Mott VRH in three dimensions (3D) except for PAA/PANI composite (followed Mott 1D-VRH). Mott 3D VRH (equation 4) and Mott 1D VRH (equation 5) equations are shown below.

$$\sigma = \sigma_0 \exp \left(-\frac{T_0}{T} \right)^{\frac{1}{4}} \dots\dots\dots(4)$$

$$\sigma = \sigma_0 \exp \left(-\frac{T_0}{T} \right)^{\frac{1}{2}} \dots\dots\dots(5)$$

Table 5. Regression values (R-values) after linear fitting of 3D-VRH, 1D-VRH and Arrhenius model of AA based PANI polymer

Models	Regression values (R-values) of various materials				
	AA doped PANI ^a	AA doped PANI ^b	N-substituted PANI	PAA/PANI composite	HCl doped PANI
VRH (3D) model	0.99048	0.997	0.99508	0.99208	0.99599
VRH (1D) model	0.97859	0.9926	0.99001	0.99712	0.9905
Arrhenius model	0.93928	0.9682	0.97226	0.99212	0.9724

PANI ^a: APS in distilled water, PANI^b: APS in 1 M HCl, N-substituted PANI: poly (3-methyl (phenyl amino) propanoic acid

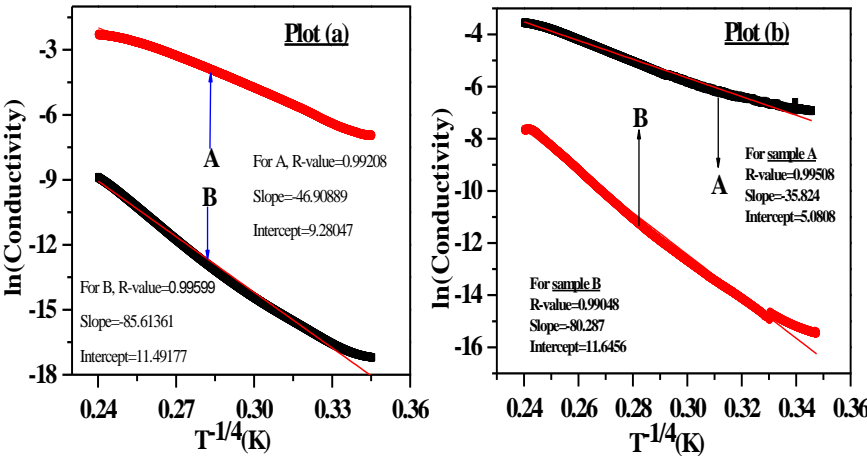


Figure 16. 3D VRH model for temperature variations of DC conductivity of PAA/PANI composite (A) and HCl doped PANI (B) in plot (a), whereas plot (b) Poly (3-methyl (phenyl amino) propanoic acid (A) and AA doped PANI (APS in 1 M HCl) (B) in plot (b)

Since the temperature dependence of DC conductivity is characteristic of variable-range hopping, the densities of states are localized near the Fermi energy. Using Mott's 3D-VRH (equation 4) and Davis expression (equation 6) and analysing resistivity data, we estimated density of states $[N(E_F)]$ at localised region.

$$T_{\text{Mott}} = \left[\frac{16}{K_B N(E_F) L_{\text{loc}}^3} \right] \dots \dots \dots (6)$$

Where K_B is the Boltzmann constant, $N(E_F)$ is the density of states at the Fermi level, L_{loc} is the localization length [28] and Mott's temperature. In Mott's 3D VRH, we plotted $\ln(\text{Conductivity})$ vs. $T^{-1/4}$ and it is fitted linearly. From the slope and intercept of the straight line, we found T_{Mott} and σ_0 which are presented in **Table 6**.

It was reported earlier that possible transitions also occur from the critical regime to insulating regime through variable-range hopping by the application of an external magnetic field [28]. Therefore, magnetic field would be required to achieve the localization of charge carrier [28]. The localization length (L_{loc}) can be done from resistivity data with magnetic field (0.4 T). According to the VRH theory, the resistivity with magnetic field can be expressed as [28]

$$\ln \left[\frac{\rho(H)}{\rho_0} \right] = t (L_{\text{loc}} / L_H)^4 \left(\frac{T_{\text{Mott}}}{T} \right)^{\frac{3}{4}} \dots \dots \dots (7)$$

Where, $t = 5/2016$, $L_H = (hc/2\pi eH)^{1/2}$ = magnetic length, c = velocity of light (3×10^{10} cm/s), h = Planck's constant (6.62×10^{-27} erg.sec), e = electronic charge (1.6×10^{-19} C) and $H = 0.4$ T is the applied magnetic field. **Fig. 17** shows the plot of $\ln [\rho(H)/\rho(0)]$ against $T^{-3/4}$ and fitted linearly. From the slope, we estimated the values of L_{loc} and are listed in **Table 6**.

The transport occurs *via* variable-range hopping among localized states on the insulating side of the M-I transition (where $\ln(\text{Conductivity})$ vs $T^{-1/4}$ is a straight line in zero field). By taking the values of T_{Mott} and L_{loc} for each sample from equation (6), the density of state values $[N(E_F)]$ was calculated. The values are presented in **Table 6**. Furthermore, the M-I transition temperature was found from plot of resistivity (ρ) vs temperature (T) and shown in **Fig. 18**. Using T_{Mott} , L_{loc} and M-I transition temperature, we estimated hopping distance ($R_{\text{hop, Mott}}$) and hopping energy ($\Delta_{\text{hop, Mott}}$), *i.e.*, the energy difference between the sites from the following equations (8) and (9) [28] and mentioned in **Table 6**.

$$\Delta_{hop,Mott} = \left(\frac{1}{4}\right) (k_B T) \left(\frac{T_{Mott}}{T}\right)^{\frac{1}{4}} \dots\dots\dots(8)$$

$$R_{hop,Mott} = \left(\frac{3}{8}\right) \left(\frac{T_{Mott}}{T}\right)^{\frac{1}{4}} L_{loc} \dots\dots\dots(9)$$

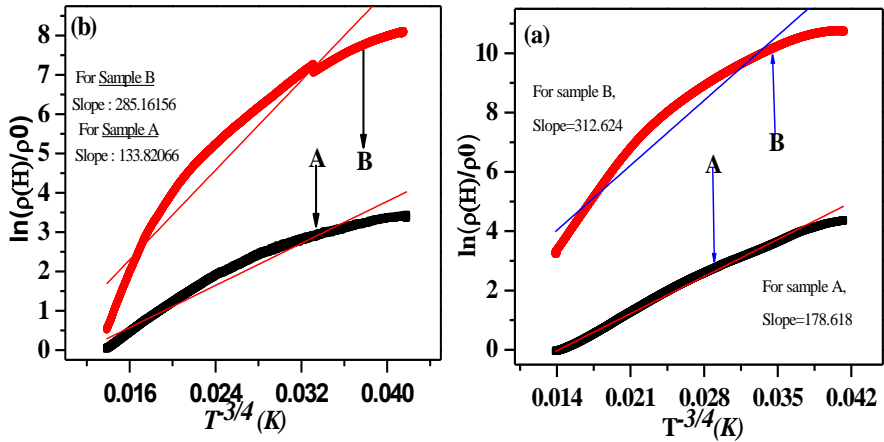


Figure 17 (a). Plots of $[\ln \rho(H)/\rho(0)]$ vs $T^{-4/3}$ for HCl doped PANI (A) and PPA/PANI composite (B) at 0.4 T; (b): Plots of $[\ln \rho(H)/\rho(0)]$ vs $T^{-4/3}$ for poly (3-methyl (phenyl amino) propanoic acid (A) and AA doped PANI (B) at 0.4T with temperature range (70–300 K)

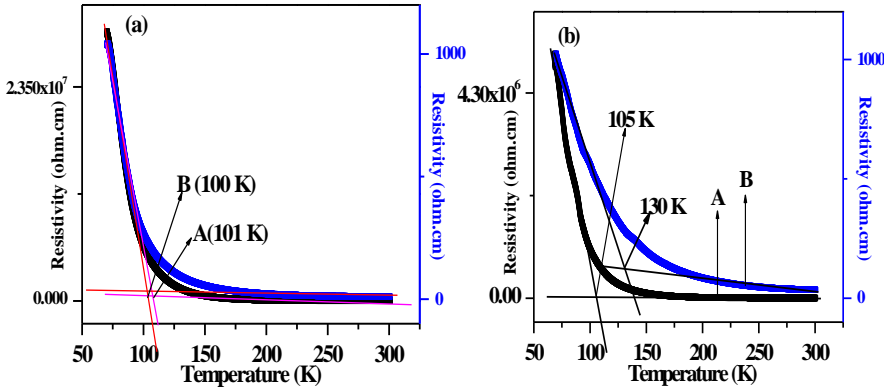


Figure 18:(a). Plots of resistivity (\square) vs temperature (T) for HCl doped PANI (A) and PPA/PANI composite (B); (b): Plots of resistivity (\square) vs temperature (T) for poly (3-methyl (phenyl amino) propanoic acid (A) and AA doped PANI (B) with

temperature range (70-300 K)

From overall results of DC conducting data as a function of temperature, it is concluded that HCl doped PANI shows lower localisation length (L_{loc}) and higher density of states $[N(E_F)]$ than other prepared PANI materials presented in this work. That indicates that PANI chains are compacted, *i.e.*, very close to each other. This implies that the wave (electron) is localised more in the region of space in the insulating phase.

Table 6. Conduction parameters obtained by analyzing the low temperature resistivity (with and without magnetic field) data of AA doped PANI

Conducting parameters	N substituted PANI	AA doped PANI ^a	HCl doped PANI	AA doped PANI ^b	PAA/PANI
σ_0	160.9	1.14×10^5	9.79×10^4	1355.6	13.91
M-I transition temp. (K)	144	96	100	125	103
T _{Mott} (K)	1.647×10^6	4.155×10^7	5.37×10^7	8.5×10^5	6.697×10^3
L_{loc} (nm)	231.4	25.49	24.88	40.7496	117.49
N (E_F) (no. states/eV/cm ³)	9.095×10^{18}	2.697×10^{25}	2.244×10^{25}	3.227×10^{21}	1.747×10^{22}
R _{Hop, Mott} (nm)	897.34	245.168	252.73	138.75	124.17
$\Delta_{Hop, Mott}$ (meV)	32.09	53.06	58.37	24.45	6.3
k (eV/K)		8.62×10^{-5}	8.62×10^{-5}	8.62×10^{-5}	8.62×10^{-5}

PANI^a: APS in distilled water, PANI^b: APS in 1 M HCl, N substituted PAN: Poly (3-methyl (phenyl amino) propanoic acid

Thermogravimetric (Tg) Analysis

Fig. 19 shows typical TGA curves of (a) PAA powder (Mol. weight ~1800), (b) PAA/PANI composite, (c) HCl doped PANI (aqueous APS solution), (d) 3-methyl (phenyl amino) propanoic acid, (e) poly (3-methyl (phenyl amino) propanoic acid) and (f) AA doped PANI measured under a nitrogen atmosphere from 28-700 °C. Various

percentages (%) of weight loss are presented in **Table 7**. For PAA powder, the weight losses (about 5 %) before 94 °C of these samples are due to losses of adsorbed moisture [55]. The weights of these samples remain unchanged before 185 °C [55]. Total PAA mass is lost at 520 °C and that is observed from **Fig. 19**. From the TGA curve (e) and **Table 7**, it is clear that the PAA/PANI composite film indicates the four stages of weight loss. First stage shows 9 % weight loss due to the loss of moisture and 9 % weight loss occurs in the second stage. This happened due to the loss of HCl molecules. Weight loss at the third stage (7 %) may be due to the loss of low molecular weight PAA. Weight loss at fourth stage (25 %) is due to the decomposition of PANI chain [46,56]. In case of HCl doped PANI, 9 % initial weight loss was observed. This may be happened due to the loss of moisture. PANI chain was lost upto 34 % [57]. 3-methyl (phenyl amino) propanoic acid profile shows two main weight loss steps. It is well known that the first (56 °C) is due to the residual water in the prepared monomer.

Table 7. Thermogravimetric (TG) analyses of 3-methyl (phenyl amino) propanoic acid (monomer), poly (3-methyl (phenyl amino) propanoic acid (polymer), AA doped PANI (APS in water), AA doped PANI (APS in 1 M HCl), PAA, PAA/PANI composite

Different stages (%) of weight loss	N-substituted aniline	N substituted PANI	AA doped PANI ^a	AA doped PANI ^b	PAA	PAA/PANI composite
1 st stage	6	10	12	13	6	9
2 nd stage	75	10	18	11	78	9
3 rd stage	---	5	4	4	---	7
4 th stage	---	20	22	22	---	25
5 th stage	---	5	10	11	---	---

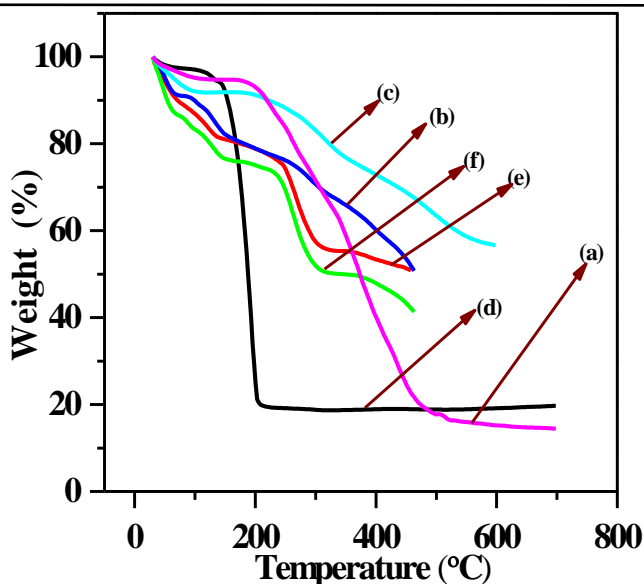


Figure 19. Thermogravimetric (TG) analysis of 3-methyl (phenyl amino) propanoic acid (a), poly (3-methyl (phenyl amino) propanoic acid) (b), AA doped PANI (APS in 1 M HCl) (c), PAA (d), PAA/PANI composite (e) and HCl doped PANI (f)

The second (56–207 °C) indicates the mass loss of the prepared monomer. This loss is attributed to the complete decomposition of the prepared monomer. TGA curve of poly (3-methyl (phenyl amino) propanoic acid) is also shown in **Fig. 19**. Gradual weight losses over the wide temperature in the polymer can be attributed to moisture, HCl, side chains attached to this polymer and finally complete decomposition of PANI polymer which shows better thermal stability than AA doped PANI chain. From overall TGA results, it is concluded that HCl doped PANI (aqueous APS solution) shows better thermal stability than other prepared PANI materials presented in this work.

DSC Analysis

Our major interest was to study the effect of different form of acrylic acid on the thermal behavior of these acrylic acid based PANI and HCl doped PANI. Few reports are found on thermal properties like enthalpy energy and cross-linking temperature of the pristine polyaniline is presented in **Table 8**. Thermal behaviours of the prepared AA based PANI polymeric materials and AA substituted aniline monomer, *i.e.*, 3-methyl (phenyl amino) propanoic acid have been compared with those of HCl doped PANI (aqueous APS solution) was investigated by DSC and plotted in **Fig. 21** for study of enthalpy energy (ΔH). DSC curve of PAA shows two endothermic peaks [55]. The peaks are observed at 172 and 235 °C. At this position, the sample consumes energy values of 98.48 and 48.64 J/g. In addition, the curve

shows two exothermic peaks at 164.38 °C with emitted heat values of 437.1963 J/g, respectively. It signifies the stability of prepared HCl doped PANI polymer [57].

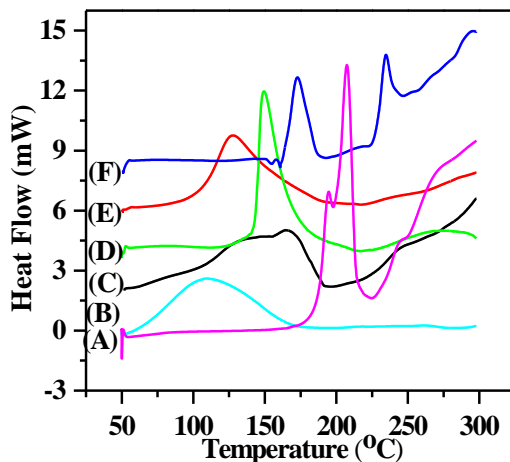


Figure 21. Differential scanning calorimetry (DSC) thermograms of 3-methyl (phenyl amino) propanoic acid (A), poly (3-methyl (phenyl amino) propanoic acid (B), AA doped PANI (APS in water) (C), PAA/PANI composite (D), AA doped PANI (APS in 1 M HCl) (E), and PAA (F)

Table 8. Differential scanning calorimetry (DSC) analyses of 3-methyl (phenyl amino) propanoic acid (monomer), poly (3-methyl (phenyl amino) propanoic acid (polymer), AA doped PANI (APS in water), AA doped PANI (APS in 1 M HCl), PAA, and PAA/PANI composite

Parameters	N-substituted aniline	N substituted PANI	AA doped PANI ^a	AA doped PANI ^b	PAA	PAA/PANI composite
ΔH (J/g)	$\Delta H_1=300.3$ $\Delta H_2=8.02$	$\Delta H_1=345.4$ $\Delta H_2=0$	$\Delta H_1=437.2$ $\Delta H_2=0$	$\Delta H_1=236.5$ $\Delta H_2=0$	$\Delta H_1=91.5$ $\Delta H_2=48.6$	$\Delta H_1=251.7$ $\Delta H_2=0$
Temp. at 1 st peak (°C)	207.34	109.86	164.38	127.69	172.66	149.40
Temp. at	243.04	---	---	---	234.58	---

2nd peak (°C)						
-------------------------------------	--	--	--	--	--	--

Solubility

Many reports have mentioned the solubility of conducting polymers by incorporation of side chains in the polymer backbone [59-61]. For poly (3-alkylthiophene), both solubility and fusibility have been reached due to the attachment of relatively long, flexible hydrocarbon side groups without changing the π -electronic structure. The qualitative solubility of the N-substituted polymers is summarized in **Table 9**. In contrast to polyaniline (without substitution), N-alkylated polyaniline bearing more than eight carbons of alkylated units already exhibit satisfactory solubilities in different solvents such as chloroform, toluene, THF, and also other common organic solvents. Polyanilines containing longer side chains like PANI-16, and PANI-18, may even be dissolved in hexane and methylene chloride. The main concept is “solvent bound” in the rigid polymers with flexible side chains. In addition, the solubility may affect the stiffness of polymeric chains and that is discussed later. On the other hand, polar solvents such as NMP, DMSO, and DMF are no longer good solvents for these heavily substituted polyanilines because they formed strong hydrogen-bonding interaction and contribute to the dissolution of polyaniline emeraldine base in NMP, DMSO, and m-cresol. Now as a consequence of the side chains, the substituted polyaniline contains the functional groups (-COOH) that can form hydrogen bonding and solvation occurred. In that way their solubility is increased with strong polar solvents. The solubility of the substituted polyaniline depends on the presence of the side chain with a certain concentration as well as the size of the pendant side chain [59-61].

Table 9. Solubility of AA based polyaniline in different solvents

Materials	NMP	DMSO	THF	n-Hexane	Water	CHCl₃
N-substituted aniline	++	++	++	-	++	++
N-substituted PANI	+	+		-	-	-
AA doped PANI (APS in water)	+	+	+	-	+	-
AA doped PANI (APS in 1 M HCl)	+	+	+	-	+	-
PAA/PANI composite	+	+	+	-	+	-
PANI	+	+	-	-	-	-
PAA	++	++	++	-	++	+

^a Key: ++, well soluble; +, partially soluble; -, slightly soluble or insoluble,

2.4 Response of Liquefied Petroleum Gas (LPG) (i.e., LPG SENSOR)

LPG is one of the flammable gases. It is also called a hazards gas, which is create in both *i.e.*, humans and an environment. It has highly flammable characteristics at ppm level of concentration. It poses a serious threat to humans and an environment. LPG is used in various sectors such as house hold, automotive industries, etc. With the progressive global population, many more peoples are being endangered by the effect due to the exposure of LPG. One of the potential uses of LPG is automotive fuel for vehicles or as a propellant for aerosols. In addition to automotive fuel, of LPG is widely used in cooking. Therefore, it urgent requires detecting precisely, fast and selectively for preventing the occurrence of accidental explosions. Till to date, good LPG sensor has not been found. Now, the problem is vital to industry as well as general public. To meet the requirement, significant research for new sensors is ongoing with enhancing the performance, compared with traditional sensors *i.e.*, resistive metal oxide sensors. Metal oxide based LPG sensors is allowed to detect lower level LPG concentration and their selectivity low. The other important sensor operating parameter is temperature. High temperature is requires for their operation [62-64]. So, power consumption is more, which is reducing the sensor life. Room temperature sensor operation is an important parameter, which is supported to achieve intrinsically safe performance in potentially hazardous situations. This sensors exhibit a fast, reversible response at room temperature [65-67].

In current years, conducting polymer based materials have been used to detect various gas analytes [68-71]. The sensors work on the principle of barrier mechanism [72, 73]. Conversely, LPG response is pronounced at 473 K. For this response, it is required high power consumption and complexities in integration. For meeting the requirements, researchers put their effort to develop new sensor materials. The developed materials are used to analyse LPG gas and other poisoning species. It has better stability, selectivity and lower fabrication costs. The developed novel material is conducting polymer based one *i.e.*, thin films, blends, or heterojunction. Polyaniline is potential member in the conducting polymer family. It is p-type semiconducting material and is used in junction devices [74, 75]. It showed high electrical conductivity in doping state. In the sensor material, I-V characteristic measured the LPG response at different LPG concentration exposure in room temperature. Exposure of LPG gas on sensor materials, current drastically decreased with increase in their concentration. This is due to the change in work function of the polyaniline. Therefore, the resistance of the polyaniline is increased. Hence, current decreases. **Brief summary of LPG gas detection is presented in Table xxx.**

Table. xxx Brief summary of LPG gas detection

Study	Materials	Perporfamce	Optimum temperature (°C)	Limitation
-------	-----------	-------------	--------------------------	------------

Kumar et al. [76]	ZnO/ polyaniline	Response time 25 s	Room Temperature	High LPG concentration
Singh et al. [77]	PANI–Co3O4 nanocomposite	Sensitivity 40%	Room Temperature	High LPG concentration
Taheri et al. [78]	Reduced Graphene Oxide/Gold Nano-hybrid	Response time 5 s	Room Temperature	High LPG concentration
Joshi et al. [79]	n-CdSe/p- polyaniline junction	Response time 50 and 100 s	Room Temperature	High LPG concentration
Dhawale et al. [80]	p-polyaniline/n- TiO2 heterojunction	Response 63 %	Room Temperature	High LPG concentration
Dhawale et al. [81]	n-CdS/p- polyaniline heterojunction	Response 80%	Room Temperature	High LPG concentration

3.0 Conclusions

Flexible PAA/PANI composite was synthesised using chemical oxidation method of aniline in an aqueous solution of PAA. Its morphology and structure show fiber like and amorphous nature. Retaining of chemical groups in the composite backbone is observed from FTIR spectrum. Also, due to the presence of polaron band emeraldine form of PAA/PANI composite is indicated. Room temperature DC conductivity is calculated. Different parameters of conduction mechanism support to understand the transport process. Thermal stability shows better results than HCl doped PANI.

A new bifunctional monomer, *i.e.*, 3-methyl (phenyl amino) propanoic acid incorporating both aniline and acrylic acid, was synthesized and fully characterized. In conjugated poly (3-methyl (phenyl amino) propanoic acid backbone, it is bearing an acrylic acid as side group produced by chemical oxidation polymerization method using ammonium persulfate as oxidant. FTIR, ^1H NMR, and ESI-MS spectroscopic characterizations have supported the prepared 3-methyl (phenyl amino) propanoic acid. FTIR shows the presence of various organic groups in the prepared monomer and polymeric backbone. UV-Visible spectrum indicates the emeraldine form of Poly (3-methyl (phenyl amino) propanoic acid. Calculated average DC conductivity was observed in the semiconducting range. Different transport parameters support to better understand the conduction mechanism. In this study, thermal stability of poly (3-methyl (phenyl amino) propanoic acid shows better results than HCl doped PANI. AA

doped PANI results show feasible data to other AA based PANI polymer. In particular, liquefied petroleum gas responses and mechanism of polyaniline based materials were discussed.

4.0 Acknowledgements

The author conveys their sincere thanks to the CRF, IIT Kharagpur for their providing testing facilities and Materials Science Centre to do the research work. I would like to thank Prof. Debabrat Pradhan for their invaluable guidance, advices, constant inspiration and technical support throughout the entire research program.

5.0 References

- [1] Burroughes, J.H., Bradley, D.D.C., Brown, A.R., Marks, R.N., Mackay, K., Friend, R.H., Burns, P.L., and Homes, A.B. (1990), Light-Emitting Diodes Based on Conjugated Polymers, *Nature*, Vol. 347, pp. 539-541.
- [2] Frackowiak, E., Khomenko, V., Jurewicz, K., Lota, K., and Beguin F. (2006), Supercapacitors Based on Conducting Polymers/Nanotubes Composites, *J. Power Sources*, Vol. 153, pp. 413-418.
- [3] Wu, F., Chen, J., Chen, R., Wu, S., Li, L., Chen, S., and Zhao T. (2011), Sulfur/Polythiophene with a Core/Shell Structure: Synthesis and Electrochemical Properties of the Cathode for Rechargeable Lithium Batteries, *Journal of Physical Chemistry C*, Vol. 115, pp. 6057-6063.
- [4] Yu, L., Jin, X., and Zeng, X. (2008), Methane Interactions with Polyaniline/Butylmethylimidazolium Camphorsulphonate Ionic Liquid Composite, *Langmuir*, Vol. 24, pp. 11631-11636.
- [5] Racicot, R., Brown, R.R., and Yang, S.C. (1997), Corrosion Protection of Aluminium Alloys by Double-strand Polyaniline, *Synthetic Metals*, Vol. 85, pp. 1263-1264.
- [6] Saini, P., Choudhary, V., Vijayan, N., and Kotnala, R. K. (2012), Improved Electromagnetic Interference Shielding Response of Poly(aniline)-Coated Fabrics Containing Dielectric and Magnetic Nanoparticles, *Journal of Physical Chemistry C*, Vol. 116, pp. 13403-13412.
- [7] MacDiarmid, A.G., Chang, J.C., Richter, A.F., and Epstein, A.J. (1987), Polyaniline: a New Concept in Conducting Polymers, *Synthetic Metals*, Vol. 18, pp. 285-290.
- [8] Yue, J., Epstein, A.J., Zhong, Z., Gallagher, P.K., and MacDiarmid, A.G. (1991), Thermal Stabilities of Polyaniline, *Synthetic Metals*, Vol. 41, pp. 765-768.
- [9] Cao, Y., Smith, P., and Heeger, A.J. (1992), Counter-ion Induced

-
- Processability of Conducting Polyaniline and of Conducting Polyblends of Polyaniline in Bulk Polymers, *Synthetic Metals*, Vol. 48, pp. 91-97.
- [10] Hwang, J.H., and Yang, S.C. (1989), Morphological Modification of Polyaniline Using Polyelectrolyte Template Molecules, *Synthetic Metals*, Vol. 29, pp. 271-276.
- [11] Liu, J.-M., and Yang, S.C. (1991), Novel Colloidal Polyaniline Fibrils Made by Template Guided Chemical Polymerization, *Journal of chemical society, chemical communication*, Vol. 0, pp. 1529- 1531.
- [12] Li, S., Dong, H., and Cao, Y. (1989), Synthesis and Characterization of Soluble Polyaniline, *Synthetic Metals*, Vol. 29, pp. 329 -336.
- [13] Malhotra, B.D., Ghosh, S., and Chandra, R. (1990), Polyaniline/ Polymeric Acid Composite, a Novel Conducting Rubber, *Journal of Applied Polymer Science*, Vol. 40, 1049-1052.
- [14] Kang, Y., Lee, M.-H., and Rhee, S.B. (1992), Electrochemical Properties of Polyaniline Doped with Poly(styrenesulfonic acid), *Synthetic Metals*, Vol. 52, pp. 319-328.
- [15] Lapkowski, M. (1993) Electrochemical Synthesis of Polyaniline/ Poly (2-acryl-amido-2- methyl-1-propane-sulfonic acid) Composite, *Synthetic Metals*, Vol. 55-57, pp. 1558-1563.
- [16] Angelopoulos, M., Patel, N., and Saraf, R. (1993), Amic Acid Doping of Polyaniline: Characterization and Resulting Blends, *Synthetic Metals*, Vol. 55-57, pp. 1552-1557.
- [17] Angelopoulos, M., Patel, N., Shaw, J.M., and Labianca, N.C. 1994, Water Soluble Polyanilines: Properties and Applications, *Materials Research Society Symposium Proceeding*, Vol. 328, pp. 173-xxx.
- [18] Angelopoulos, M., Patel, N., Shaw, J.M., Labianca, N.C., and Rishton, S.A. (1993), Water Soluble Conducting Polyanilines: Applications in Lithography, *Journal of Vacuum Science and Technology B*, Vol. 11(6), pp. 2793-2191.
- [19] Chevalier, J.-W., Bergeron, J.-Y., and Dao, L.H. (1992), Synthesis, Characterization, and Properties of Poly (N-alkylanilines), *Macromolecules*, Vol. 25, pp. 3325-3331.
- [20] Wei, Y., Focke, W.W., Wnek, G.E., Ray, A., and MacDiarmid, A.G. (1989), Synthesis and Electrochemistry of Alkyl Ring-Substituted Polyanilines, *Journal of Physical Chemistry*, Vol. 93, pp. 495-499.
- [21] Wei, Y., Hariharan, R., and Patel, S.A. (1990), Chemical and Electrochemical Copolymerization of Aniline with Alkyl Ring-Substituted Anilines, *Macromolecules*, Vol. 23, pp. 158-164.

-
- [22] Bergeron, J.-Y., and Dao, L.H. (1992), Electrical and Physical Properties of New Electrically Conducting Quasi Composites. Poly (aniline-co-N-butylaniline) copolymers, *Macromolecules*, Vol. 25, pp. 3332-3337.
- [23] Cao, Y., Smith, P., and Heeger, A.J. (1993), Counter-ion Induced Processibility of Conducting Polyaniline, *Synthetic Metals*, Vol. 55-57, pp. 3514-3519.
- [24] Menon, R., Yoon, C.O., Moses, D., Heeger, A.J., and Cao, Y. (1993), Transport in Polyaniline near the Critical Regime of the Metal-insulator Transition, *Physical Review B: Condensed Matter*, Vol. 48, pp. 17685-17694.
- [25] Li, J., Fang, K., Qiu, H., Li, S., and Mao, W. (2004), Micromorphology and Electrical Property of the HCl-doped and DBSA-doped Polyaniline, *Synthetic Metal*, Vol. 142, pp. 107-111.
- [26] Kapil, A., Taunk, M., and Chand, S. (2010), Preparation and Charge Transport Studies of Chemically Synthesized Polyaniline, *Journal of Materials Science: Materials in Electronics*, Vol. 21 pp. 399-404.
- [27] Mukherjee, A.K., and Reghu, M. (2005), Magnetotransport in Doped Polyaniline, *Journal of Physics: Condensed Matter*, Vol. 17, pp. 1947-1960.
- [28] Ghosh, M., Barman, A., De, S.K., and Chatterjee, S. (1998), Electrical Resistivity and Magnetoresistivity of Protonic Acid (H_2SO_4 and HCl)-Doped Polyaniline at Low Temperature, *Journal of Applied Physics*, Vol. 84, pp. 806-811.
- [29] Aleshin, A.N., Mironkov, N.B., Suvorov, A.V., Conklin, J.A., Su, T.M., and Kaner, R. B. (1996), Transport Properties of Ion-implanted and Chemically Doped Polyaniline Films, *Physics Review B*, Vol. 54, pp. 11638-11643.
- [30] Tzamalīs, G., Zaidi, N.A., and Monkman, A.P. (2003), Applicability of the Localization-interaction Model to Magnetoconductivity Studies of Polyaniline Films at the Metal-insulator Boundary, *Physics Review B*, Vol. 68, pp. 245106-245111.
- [31] Long, Y., Chen, Z., Wang, N., Li, J., and Wan, M. (2004), Electronic Transport in PANI-CSA/PANI-DBSA Polyblends, *Physica B*, Vol. 344, pp. 82-87.
- [32] Yoon, C.O., Reghu, M., Moses, D., and Heeger, A.J. (1994), Transport near the Metal-insulator Transition: Polypyrrole Doped with PF_6 , *Physics Review B*, Vol. 49, pp. 10851-10863.
- [33] Sutar, D., Mithra, M., Reghu, M., and Subramanyam, S.V. (2001), Conductivity and Magnetoresistance in Polypyrrole- PF_6 at Various Doping Level, *Synthetic Metal*, Vol. 119, pp. 455-456.
- [34] Chauvet, O., Paschen, S., Forro, L., Zuppiroli, L., Bujard, P., Kai, K., and

- Wernet, W. (1994), Magnetic and Transport Properties of Polypyrrole Doped with Polyanions, *Synthetic Metal*, Vol. 63, pp. 115-119.
- [35] Aleshin, A.N., Kiebooms, R., Reghu, M., and Heeger, A.J. (1997), Electronic Transport in Doped Poly (3,4-ethylenedioxythiophene) Near the Metal-insulator Transition, *Synthetic Metal*, Vol. 90, pp. 61-68.
- [36] Joseph, T., Shanbhag, G.V., Sawant, D.P., and Halligudi, S.B. (2006), Chemoselective anti-Markovnikov Hydroamination of σ,β -Ethylenic Compounds with Amines using Montmorillonite Clay, *Journal of Molecular Catalysis A: Chemical*, Vol. 250, pp. 210-217.
- [37] Gene, H.-S., Hugh, C.-M., and Christopher, B.-K. (2008) Living Star Polymer Formation: Detailed Assessment of Poly (acrylate) Radical Reaction Pathways via ESI-MS, *Macromolecules*, Vol. 41, pp. 3023-3041.
- [38] Zheng, L., Zhang, S., Yu, X., Zhao, L., Gao, G., Yang, X., Duan, H., and Cao, S. (2006), Enhancement of Enantioselectivity in Lipase-Catalyzed Resolution of N-(2-Ethyl-6-Methylphenyl) Alanine by Additives, *Journal of Molecular Catalysis B: Enzymatic*, Vol. 38, pp. 17-23.
- [39] Cambridge Isotope Laboratories, Inc. 50 Frontage Road, Andover MA 01810, NMR Solvent Data Chart.
- [40] Max, J.-J., and Chapados, C. (2004), Infrared Spectroscopy of Aqueous Carboxylic Acids: Comparison between Different Acids and Their Salts, *J. Phys. Chem. A*, Vol. 108, pp. 3324-3337.
- [41] Ilic, M., Koglin, E., Pohlmeier, A., Narres, H.D., and Schwuger, M.J. (2000), Adsorption and Polymerization of Aniline on Cu (II)-Montmorillonite: Vibrational Spectroscopy and ab Initio Calculation, *Langmuir*, Vol. 16, pp. 8946-8951.
- [42] Sridevi, D., and Rajendran, K.V. (2009), Synthesis and Optical Characteristics of ZnO nanocrystals, *Bulletin of Materials Science*, Vol. 32, pp. 165-168.
- [43] Sengupta, P.P., Kar, P., and Adhikari, B. (2009), Influence of Dopant in the Synthesis, Characteristics and Ammonia Sensing Behavior of Processable Polyaniline, *Thin Solid Films*, Vol. 517, pp. 3770-3775.
- [44] Pawar, S.G., Patil, S.L., Chougule, M.A., Achary, S.N., and Patil, V.B. (2011), Microstructural and Optoelectronic Studies on Polyaniline: TiO₂ Nanocomposites, *International Journal of Polymeric Materials*, Vol. 60, pp. 244-254.
- [45] Athawale, A.A., and Chabukswar, V.V. (2001), Acrylic Acid-Doped Polyaniline Sensitive to Ammonia Vapors, *Journal of Applied Polymer Science*, Vol. 79, pp. 1994-1998.
- [46] Chen, S.-A., and Lee, H.-T. (1995), Structure and Properties of Poly (acrylic

- acid)-Doped Polyaniline, *Macromolecules*, Vol. 28, pp. 2858-2866.
- [47] Liu, R., Qiu, H., Zong, H., and Fang, C. (2011), Fabrication and Characterization of Composite Containing HCl-Doped Polyaniline and Fe Nanoparticles, *Journal of Nanomaterials*, Vol. 2012, pp. 1-8.
- [48] Kavitha, B., Prabakar, K., Kumar, K.S., Srinivasu, D., Srinivas, Ch., Aswal, V.K., Siriguri, V., and Narsimlu, N. (2012), Spectroscopic Studies of Nano Size Crystalline Conducting Polyaniline, *IOSR Journal of Applied Chemistry (IOSRJAC)*, Vol. 2, pp. 16-19.
- [49] Chabukswar, V., and Bhavsar, S. (2010), Synthesis and characterization of organically soluble and electrically conducting acids doped polyaniline, *Chemistry and Chemical Technology*, Vol. 4, pp. 277-280.
- [50] Valle, M.A.D., Gacitúa, M.A., Borrego, E.D., Zamora, P.P., Díaz, F.R., Camarada, M.B., Antilén, M.P., and Soto, J.P. (2012), Electro-Synthesis and Characterization of Aniline and o-Anisidine Oligomers, *International Journal of Electrochemical Science*, Vol. 7, pp. 2552-2565.
- [51] Athawale, A.A., Kulkarni, M.V., and Chabukswar, V.V. (2002), Studies on Chemically Synthesized Soluble Acrylic Acid Doped Polyaniline, *Materials Chemistry and Physics*, Vol. 73, pp. 106-110.
- [52] Furukawa, Y., Ueda, F., Hyodo, Y., Harada, I., Nakajima, T., and Kawagoe, T. 1988, *Vibrational Spectra and Structure of Polyaniline*, *Macromolecules*, Vol. 21, pp. 1297-1305.
- [53] Sajeev, U.S., Mathai, C.J., Saravanan, S., Ashokan, R.R., Venkatachalam, S., and Anantharaman, M. R. (2006), on the Optical and Electrical Properties of rf and a.c. Plasma Polymerized Aniline Thin Films, *Bulletin of Materials Science*, Vol. 29, pp. 159-163.
- [54] Patil, A.O., Heeger, A.J., and Wudl, F. (1988), Optical Properties of Conducting Polymers, *Chemistry Review*, Vol. 88, pp. 183-200.
- [55] Moharram, M.A., and Allam, M.A. (2007), Study of the Interaction of Poly (acrylic acid) and Poly (acrylic acid)-Poly (acrylamide) Complex with Bone Powders and Hydroxyapatite by Using TGA and DSC, *Journal of Applied Polymer Science*, Vol. 105, pp. 3220-3227.
- [56] HAN, M.G., and IM, S.S. (1999), Electrical and Structural Analysis of Conductive Polyaniline/Polyimide Blends, *Journal of Applied Polymer Science*, Vol. 71, pp. 2169-2178.
- [57] Gomes, E.C., and Oliveira, M.A.S. (2012), Chemical Polymerization of Aniline in Hydrochloric Acid (HCl) and Formic Acid (HCOOH) Media. Differences between the Two Synthesized Polyanilines, *American Journal of Polymer Science*, Vol. 2, pp. 5-13.
- [58] Cardoso, M.J.R., Lima, M.F.S., and Lenz, D.M. (2007), Polyaniline

-
- Synthesized with Functionalized Sulfonic Acids for Blends Manufacture, Materials Research, Vol. 10, pp. 425-429.
- [59] Zheng, W.-Y., Levon, K., Laakso, J., and Bterholm, J.-E. (1994), Characterization and Solid-state Properties of Processable N-Alkylated Polyaniline in the Neutral State, *Macromolecules*, Vol. 27, pp. 7754-7768.
- [60] Bergeron, J.-Y., Chevalier, J.-W., and Dao, L.H. (1990), Water-soluble Conducting Poly (aniline) Polymer, *Journal of Chemical Society: Chemical Communications*, Vol. xxx, pp. 180-182.
- [61] Kim, Y.H., and Calabrese, J.C. (1991), N-Alkylated Aromatic Polyamides, *Macromolecules*, Vol. 24, pp. 2951-2954.
- [62] More, A.M., Gunjekar, J.L., and Lokhande, C.D. 2008, Liquefied Petroleum Gas (LPG) Sensor Properties of Interconnected Web-Like Structured Sprayed TiO₂ Films, *Sensor and Actuators B*, Vol. 129 pp. 671-677.
- [63] Gunjekar, J.L., More, A.M., and Lokhande, C.D. 2008, Chemical Deposition of Nanocrystalline Nickel Oxide from Urea Containing Bath and its Use in Liquefied Petroleum Gas Sensor, *Sensor and Actuators B*, Vol. 131, pp. 356-361.
- [64] Salunkhe, R.R., Shinde, V.R., and Lokhande, C.D. 2008, Liquefied Petroleum Gas (LPG) Sensing Properties of Nanocrystalline CdO Thin Films Prepared by Chemical Route: Effect of Molarities of Precursor Solution, *Sensor and Actuators B*, Vol. 133, 296-301.
- [65] Fang, Q., Chetwynd, D.G., Covington, J.A., Toh, C.S., and Gardner, J.W. 2002, Microgas-Sensor with Conducting Polymers, *Sensor and Actuators B*, Vol. 84, pp. 66-71.
- [66] Xie, D., Jiang, Y., Pan, W., Li, D., Wu, Z., and Li, Y. 2002, Fabrication and Characterization of Polyaniline-based Gas Sensor by Ultra-Thin Film Technology, *Sensor and Actuators B*, Vol. 81, pp. 158-164.
- [67] Zee, F., and Judy, J.W. 2001, Micromachined Polymer-based Chemical Gas Sensor Array, *Sensor and Actuators B*, Vol. 72, pp. 120-128.
- [68] Traversa, E., Miyayama, M., and Yanagida, H. 1994, Gas Sensitivity of ZnO/La₂CuO₄ Heterocontacts, *Sensor and Actuators B*, Vol. 17, pp. 257-261.
- [69] Tamaki, J., Maekawa, T., Miura, N., and Yamazoe, N. 1992, CuO-SnO₂ Element For Highly Sensitive and Elective Detection of H₂S, *Sensor and Actuators B*, Vol. 9, pp. 197-203.
- [70] Zhou, X., Cao, Q., Hu, Y., Gao, J., and Xu, Y. 2001, Sensing Behavior and Mechanism of La₂CuO₄-SnO₂ Gas Sensors, *Sensor and Actuators B* Vol. 77, pp. 443-446.
- [71] Zhou, X., Cao, Q., Huang, H., Yang, P., and Hu, Y. 2003, Study on Sensing

- Mechanism of CuO-SnO₂ Gas Sensors, Materials Science & Engineering B, Vol. 99, pp. 44-47.
- [72] Hikita, K., Miyayama, M., and Yanagida, H. 1995, New Approach To Selective Semiconductor Gas Sensors using a de-based PN Heterocontact, Journal of American Ceramic Society, Vol. 78, pp.865-873.
- [73] Ling, Z., Leach, C., and Freer, R.2003, NO₂ Sensitivity of a Heterojunction Sensor based on WO₃ and Doped SnO₂, Journal of European Ceramic Society, Vol. 23, pp. 1881-1891.
- [74] Narasimhan, M., Hagler, M., Cammarata, V., and Thakur, M. 1998, Junction Devices based on Sulfonated Polyaniline, Applied Physics Letter, Vol. 72, pp. 1063-1065.
- [75] Xu, B., Ovchencov, Y., Bai, M., Caruso, A.N., Sorokin, A.V., Ducharme, S., Doudin, B., and Dowben, P.A. 2002, Heterojunction Diode Fabrication from Polyaniline and a Ferroelectric Polymer, Applied Physics Letter, Vol. 81, pp. 4281-4283.
- [76] Kumar, S., Kumar, L., and Sharma, V.K. 2020, Synthesis of ZnO/polyaniline Nanocomposite and its Application as Liquefied Petroleum Gas Sensor, International Journal on Emerging Technologies, Vol. 11, pp. 419-424.
- [77] Singh, N. Singh, P.K., Singh, M., Gangopadhyay, D., Singh, S.K., and Tandon, P. 2019, Development of a Potential LPG Sensor based on a PANI-CoO Nanocomposite that Functions at Room Temperature, New Journal of Chemistry, Vol. 43, pp. 17340-17350.
- [78] Taheri, M., Feizabadi, Z., and Mansour, N. Fast Response and High Sensitivity of Reduced Graphene Oxide/Gold Nano-hybrid for LPG Sensors at Room Temperature, Journal of Electronic Materials, vol.xxx, year, pp.
- [79] Joshi, S.S., Lokhande, C.D., and Han, S.-H. 2007, A Room Temperature Liquefied Petroleum Gas Sensor based on all-Electrodeposited n-CdSe/p-Polyaniline Junction, Sensors and Actuators B, Vol. 123, pp. 240-245.
- [80] Dhawale, D.S., Salunkhe, R.R., Patil, U.M., Gurav, K.V., More, A.M., and Lokhande, C.D. 2008, Room Temperature Liquefied Petroleum Gas (LPG) Sensor based on p-Polyaniline/n-TiO₂ Heterojunction, Sensors and Actuators B, Vol. 134, pp. 988-992.
- [81] Dhawale, D.S., Dubala, D.P., Jamadadea, V.S., Salunkhe, R.R., Joshi, S.S., and Lokhande, C.D. 2010, Room Temperature LPG Sensor based on n-CdS/p-Polyaniline Heterojunction, Sensors and Actuators B Vol. 145, pp. 205-210.

Chapter 5

DL-Polylactide (DL-PLA) Based Polyaniline Composite for Hydrogen Gas Sensors

Muktikanta Panigrahi ^{1,*}, Basudam Adhikari ¹

¹ Materials Science Centre, Indian Institute of Technology, Kharagpur, West Bengal, India

*Corresponding author: muktikanta2@gmail.com

Abstract

Different inorganic acids like HCl, HNO₃, H₂SO₄ and H₃PO₄-doped based DL-PLA/PANI-ES composites were synthesized by *in-situ* chemical oxidation polymerization technique using liquid aniline as precursors. The doped composite have observed fibril-like morphology with different average sized diameter (178 nm for HCl doped composite, 162 nm (H₂SO₄ doped composite), 153 nm (H₃PO₄ doped composite) and 163 nm (HNO₃ doped composite), respectively. Analysis of presence of functional groups and other chemical groups of as prepared composites was done by FTIR experiment in ATR mode. The optical (direct) band gap was estimated from UV-Visible absorption spectra. The estimated band gap values are to be 160 eV, 1.37 eV, 1.46 eV, and 1.69 eV for HCl, HNO₃, H₂SO₄ and H₃PO₄-doped DL-PLA/PANI-ES composite, respectively. The electrical conduction mechanism of HCl-, H₂SO₄- and H₃PO₄-doped DL-PLA/PANI-ES composites were taken to study the conduction mechanism in detail in the low temperature regime (77-300 K) with and without applied of the magnetic field. Different models such as variable range hopping (VRH) and Arrhenius model were taken to explain the conduction mechanism of as prepared composites. In the Mott type VRH model, the density of states at the Fermi level, which is constant in the temperature range of 77-300 K were estimated. In the absence of magnetic field, DC conductivity of HCl-, H₂SO₄- and HNO₃-, H₃PO₄- doped DL-PLA/PANI-ES composite was measured. Also, magnetoresistance (MR) was measured at room temperature for as prepared doped DL-PLA/PANI-ES composites and showed negative MR. In addition, we were discussed the response of hydrogen (H₂) gas with polyaniline-based sensor materials.

Keywords: Conducting polymer, Nanofibers, DC conductivity, VRH model, Activation energy, Magnetoresistance, Hydrogen gas response

© IOR INTERNATIONAL PRESS, 2021

Muktikanta Panigrahi & Basudam Adhikari, *DL-Polylactide (DL-PLA) Based Polyaniline Composite for Hydrogen Gas Sensors*

<https://doi.org/10.34256/ioriip2125>

1.0 Introduction

Conductivity is a main characteristic of polymeric materials for their potential applications in different fields such as light emitting diodes, supercapacitors, sensors, [1-3]. The preparation constraints can be changed in a precise mode to get desired conductivity of the polymeric materials. Two methods such as doping and structural modification are generally used to increase the conductivity of polymeric materials. Hence, appropriate doping agent and polymeric materials prerequisite to select for improving the conductivity. In the connection, polyaniline (PANI) is one of the polymeric materials. It is commonly known as intrinsically conducting polymer (ICP). Generally, ICP is not established under ambient circumstance. Different methods are adopted to improve the stability of PANI. One of the ways is to be used to make composite form using thermoplastic polymer as base materials, which act as a stabilizer [4]. A variety of PANI composites have been prepared using different types of thermoplastic polymers such as poly (methyl methacrylate), polyvinyl chloride, polystyrene and polyurethane [5-8] as base materials. The detail electrical behaviours were studied with and without magnetic field [9-12].

To realize the conducting behaviour of different doped conducting polymer, various models are anticipated. Predominantly, variable range hopping (VRH) model is employed to understand the transport phenomena. In the connection, Li and co-workers proposed a VRH model and explained the conduction mechanism of HCl- and DBSA- doped polyaniline [13]. Kapil and co-workers [14] studied conduction mechanism of p-toluene sulphonic acid (PTSA) doped polyaniline by VRH model, Arrhenius model, and Kivelson model in the temperature range of 30–300 K. The conduction mechanism of polyaniline organic film and embedded metal particles in an insulating material were also described by VRH and charge-energy-limited-tunnelling (CELT) models. Similarly, the conductivity is measured with the variation of magnetic field at constant temperature, which is called magnetoresistance (MR). It helps to realize the depth of transport phenomena.

A few conducting polymers have shown positive MR such as PANI [15-18], polypyrrole [19-21], PEDOT films [22], and PANI composites at low temperature ($0 < 10$ K). The positive MR of conducting polymer is ascribed to the shrinkage of localised wave functions of electron in the presence of magnetic field [23] or electron-electron interactions [24,25]. Moreover, there are also a few polymers which show negative MR. Lee et al. [26] reported the negative MR from highly conducting polyacetylene at low temperature (1.5 K), which was attributed to the weak localization effects.

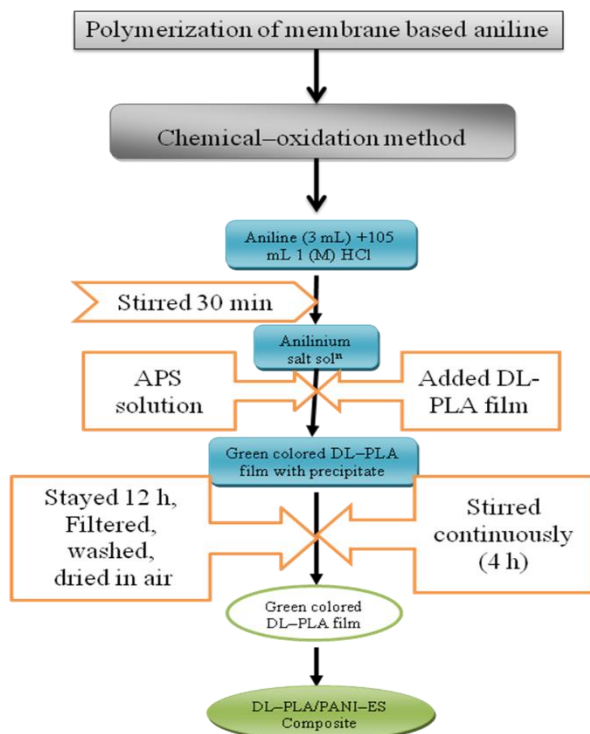
Our goal was to prepare an environmentally stable PANI-ES composite that would show better electrical properties and, therefore, can be potential for gas sensor and other electronic applications. We selected DL-PLA polymer in the composite preparation because of its high mechanical properties compared to other biodegradable polymer and strong interaction with ionic electroactive polymer such as PANI. Inorganic acids (HCl or H_2SO_4 or H_3PO_4) were doped into DL-PLA/PANI-ES to improve the electrical properties of the as prepared composites by *in situ*

polymerization technique. The low and room temperature conductivity of HCl , H_2SO_4 and H_3PO_4 doped DL-PLA/PANI-ES composite is investigated by DC conductivity measurement and possible conduction mechanism is proposed. Furthermore, MR of H_2SO_4 and H_3PO_4 doped DL-PLA/PANI-ES composite have been studied.

2.0 Experimental Details

2.1. Preparation Of DL-PLA Films and DL-PLA/PANI-ES Composites

During the synthesized of doped DL-PLA/PANI-ES COMPOSITES, small sized DL-PLA films were first prepared by solution casting method by taking DL-PLA beads and chloroform (CHCl_3) as polymer and polar solvent, respectively at room temperature. 2 g of DL-PLA polymer was added to 20 mL of CHCl_3 in a beaker (100 mL) and stirred continuously for 3 h. The transparent viscous soluble product was formed and poured into a 10 cm diameter petridish. It was left 10 h for solvent evaporation. After solvent evaporation in the petridish, DL-PLA film formed. The films removed from petridish and cut into small pieces having $1.5 \text{ cm} \times 1.5 \text{ cm}$ size. It was used for synthesizing composite and raw materials characterizations.



Scheme 1. The flow chart of preparation of HCl doped DL-PLA/PANI-ES composite [28]

During the doped DL-PLA/PANI-ES composites synthesized, *in situ* technique via chemical-oxidation polymerization technique was employed. The polymerization reaction was carried out at room temperature using aniline and DL-PLA film (1 cm²), which act as monomers and base material, respectively. During the polymerization process, 3 mL of liquid aniline was taken and was added to 105 mL of aqueous 1 M HCl solution. It was stirred for 0.5 h until slightly yellowish solution was formed and the solution was called **Solution 1**. After that, DL-PLA films (1.5 cm × 1.5 cm) were put in solution 1. It was stirred for 12 h. During the preparation of **solution 2**, 7.47 g of ammonium perdisulphate (APS) was added to 60 mL of 1 M HCl solution. The **solution 2** was added drop wise to the mixture which contained DL-PLA and solution 1 with continuous stirring for 1 h. The polymerization reaction was carried out. The color of the reaction solution and DL-PLA film was changed from white to light green and finally to dark green as polymerization continue to progress. The polymerization reaction was continued to stir constantly for 10 h to complete the polymerization reaction. HCl doped DL-PLA/PANI-ES composite was finally prepared and washed with deionised water several times followed by drying in the ambient conditions [27, 28].

Similar process was employed to synthesize other composites (HNO₃, H₂SO₄ and H₃PO₄ doped DL-PLA/PANI-ES composites). Schematic diagram of the flow chart of HCl doped DL-PLA/PANI-ES composites is exposed (**Scheme 1**). The prepared composites was used for different characterizations.

2.2. Characterization Techniques.

Fourier transformation infrared (FTIR) spectra were recorded in ATR mode on a Thermo Nicolet Nexus 870 spectrophotometer.

Ultra-violet visible (UV-Vis) spectra were recorded by using a Micropack UV-VIS-NIR, DH 2000.

Surface morphology was analysed by scanning electron microscopy (SEM) using Carl Zeiss Supra 40 scanning electron microscope. Gold coating was performed before doing SEM analysis.

I-V characteristics and DC conductivity was measured using linear four-probe technique at room temperature using Keithley 2400 programmable current source. According to four probe method, the resistivity (ρ) was calculated using the expression [29]

$$\rho = 2\pi S \left(\frac{V}{I} \right) \dots\dots\dots(1)$$

Here, S is the probe distance (cm), I is applied current (mA) and V is measured voltage (mV). Conductivity (σ) was calculated using the relation [29]

$$\sigma = \frac{1}{\rho} \dots\dots\dots (2)$$

Temperature variation resistivity with magnetic field was measured using a linear four-probe method for better understanding of transport mechanism of the prepared composite. During the measurement, helium compressor (HC) (model HC-4E1)-sumitomo cryostat (model Gains research CO, INC) equipped with 0.8 T superconducting magnet (Lake shore electromagnet) was employed temperature controller (Lake shore 331). Keithley 220 programmable current source was used as a current source.

2.3. Results and Discussion

Fig. 1 (a), (b and c) and (d), (e), (f) indicate the SEM images of DL-PLA film, HCl, H₂SO₄ (low and higher magnification), H₃PO₄, and HNO₃ doped DL-PLA/PANI-ES composites, respectively.

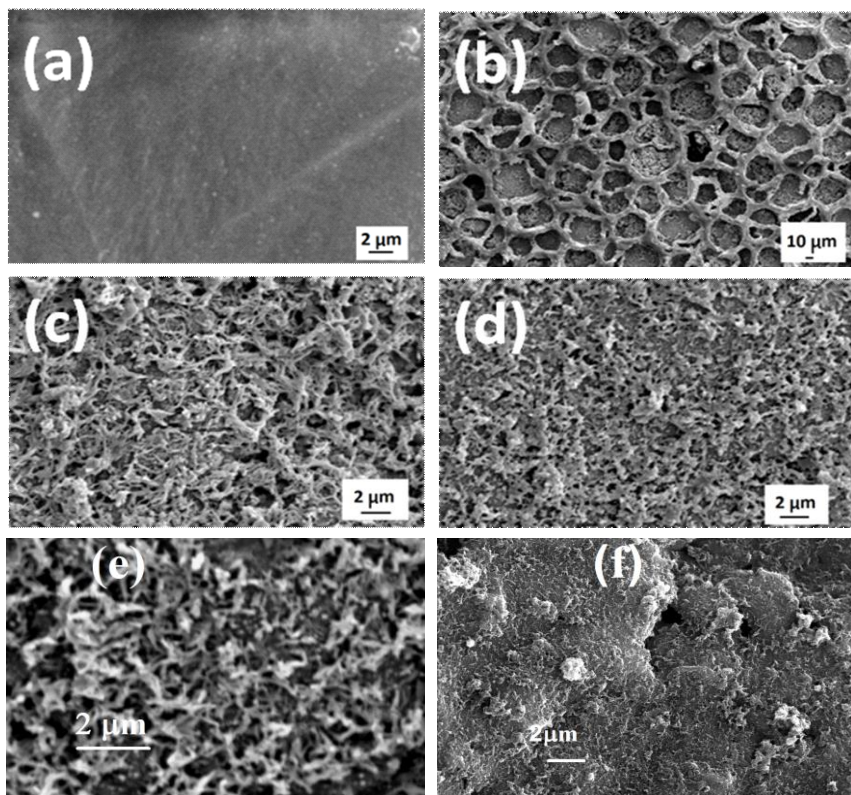


Figure 1. SEM images of (a) DL-PLA film, H₂SO₄ ((b) low and higher (c) magnification) H₃PO₄ (d), HNO₃ (e) and HCl (f) doped DL-PLA/PANI-ES composite [28]

The pure DL-PLA film appears quiet smooth (**Fig. 1a**) whereas doped DL-PLA/PANI-ES composites have fibrous morphology [**Fig. 1 (b-f)**]. **Fig. 1c and 1d** show the SEM images of H_2SO_4 doped DL-PLA/PANI-ES composite at two different type magnifications with a network type surface morphology (**Fig. 1c**) on the DL-PLA film. This network-type morphology is formed (**Fig. 1c**) after a DL-PLA film is put into the solution 1 (*i.e.*, before polymerization). The change in the surface morphology is believed to be due to the reaction of hydrogenium ion (from dopant) and anillium salt with ester group present in DL-PLA chain. After the polymerization (slow addition of solution 2 into the solution 1) the network type morphology remains with the formation of additional fibrous morphology all over the surface of DL-PLA film at lower magnification. The magnified image of [**Fig. 1(c)**] shows the fibrous morphology of H_2SO_4 doped DL-PLA/PANI-ES composite. The average diameter of as grown fibers was measured to be 153 nm. Similar type fibrous morphology is also obtained for H_3PO_4 , HCl and HNO_3 doped DL-PLA/PANI-ES [**Fig. 1(d), 1(e) and 1(f)**] film with average fiber diameter of 163 nm, 178 nm and 162 nm, respectively. The different sized diameter is formed and it may be due to the presence of various sized counter ions in the as prepared composites. The formation of fiber morphology is favorable for the sensor application due to the inherent increase in the surface area of composite film.

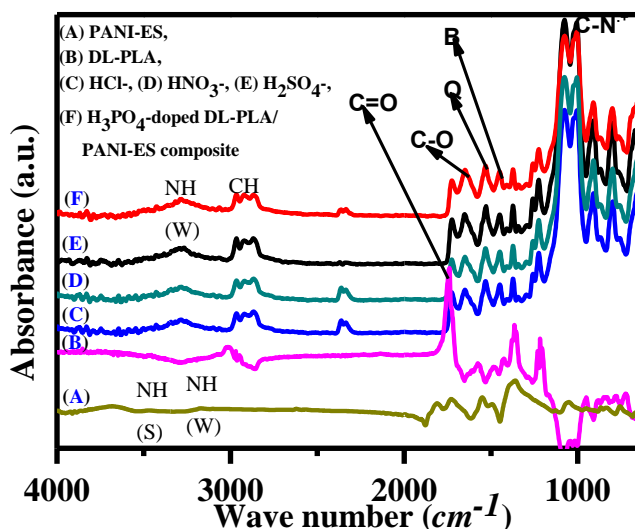


Figure 2. ATR-FTIR spectra of PANI-ES (A), DL-PLA (B), HCl (C), HNO_3 (D), H_2SO_4 (E), H_3PO_4 (F) doped DL-PLA/PANI-ES composites [28]

Fig. 2 indicates the ATR-FTIR spectra of DL-PLA, PANI-ES and HCl , H_2SO_4 , H_3PO_4 , HNO_3 doped DL-PLA/PANI-ES composites. All the characteristic bands and their corresponding assignments to prepare above materials are presented in **Table 1**. The absorption bands of DL-PLA at 2995, 1759, 1616 and 1216 cm^{-1} have been attributed to C-H stretching, C=O stretching, C-O stretching of ester and C-O-C

stretching vibration, respectively, whereas the bands at 1453, 1361 and 1363 cm^{-1} represent the stretching vibration of C-H deformation of DL-PLA polymer [27]. This indicates that the characteristic absorption features of DL-PLA polymer are retained in the prepared DL-PLA film. The main FTIR bands of PANI-ES are found at 1554, 1475 and 1108 cm^{-1} corresponding to quinoid, benzenoid and C=N stretching, respectively [29]. From our observation, the presence of quinoid and benzenoid ring vibrations are exhibited at 1475 and 1554 cm^{-1} respectively, indicating the presence of oxidation state of PANI-ES. The characteristic band obtained in the ATR-FTIR spectrum of DL-PLA/PANI-ES composite film indicates the formation of conducting DL-PLA/PANI-ES composite films. From **Table 1**, it is observed that N-H bands of HCl doped DL-PLA/PANI-ES, H_2SO_4 doped DL-PLA/PANI-ES, H_3PO_4 doped DL-PLA/PANI-ES appeared at 3289, 3291 and 3280 cm^{-1} respectively. The different N-H stretching peak positions represent the strong dependency on acid strength. The C=N, C=O, C-O and C-O-C stretching bands do not change significantly. The entire bands indicate that both PANI-ES and DL-PLA are retained in the composites.

Table 1. FTIR peak positions and their assignments of DL-PLA, PANI-ES, HCl, HNO_3 , H_2SO_4 , and H_3PO_4 doped DL-PLA/PANI-ES composites [28]

Peak assignments	Peak positions (cm^{-1})					
	DL-PLA	PANI-ES	HCl doped DL-PLA PANI-ES	HNO_3 doped DL-PLA PANI-ES	H_2SO_4 doped DL-PLA PANI-ES	H_3PO_4 doped DL-PLA PANI-ES
N-H (stretch.)	---	3217	3289	3291	3291	3280
Quinoid (stretch.)	---	1554	1533	1537	1530	1531
Benzoid (stretch.)	---	1475	1453	1450	1451	1454
C=N (stretch.)	---	1108	1067	1085	1077	1067
C-H (stretch.)	2995	2926	2965	2968	2965	2968
C=O	1759	---	1728	1720	1725	1724
C-O	1616	---	1652	1650	1656	1653
CH (def.)	1363	---	1375	1363	1374	1374
CH (bending)	1268	---	1262	1267	1259	1260
C-O-C	1216	---	1226	1223	1229	1226

It is found from literature that PANI-ES show $\pi-\pi^*$ of benzene ring, polaron to π^* , benzenoid to quinoid ring and polaron transition respectively [30]. It is noticed from **Fig. 3 (A)** that there is no transition in DL-PLA film [31]. Various transitions are observed in HCl, HNO₃, H₂SO₄ and H₃PO₄ doped DL-PLA/PANI-ES composites, which is shown in **Fig. 3**. Its peak positions with their assignments are mentioned in **Table 2**. From the **Fig. 3** and **Table 2**, we found two types of bands such as π to localised polaron band and $\pi-\pi^*$ band of benzenoid ring for HCl, HNO₃, H₂SO₄ and H₃PO₄ doped DL-PLA/PANI-ES composite. Both $\pi-\pi^*$ band of benzenoid ring and polaron band are suggested to the presence of anilinic unit and oxidation unit in emeraldine salt form of composite films [30, 32]. The different peak positions and also peak areas may be happened due to the presence of a variety of nano regime PANI-ES chains on DL-PLA polymer film. This indicates the conjugation lengths which affect the band gap energy. Hence, electrons are delocalised in the excitation band [32].

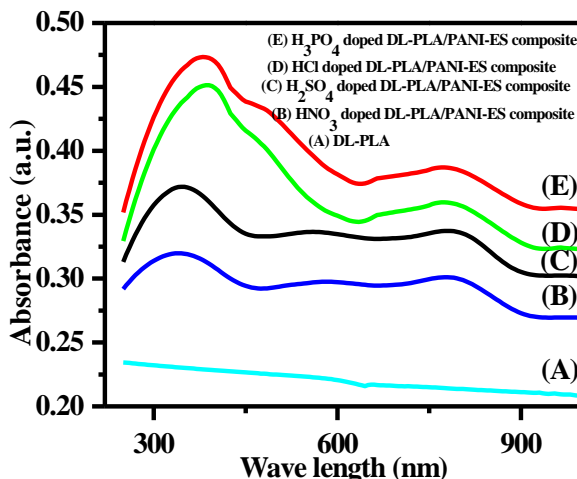


Figure 3. UV-Vis spectra of neat DL-PLA (A), HNO₃ (B), H₂SO₄ (C), HCl (D), and H₃PO₄ (E) doped DL-PLA/PANI-ES composites [28]

The photon absorption in UV-Vis region of semiconducting materials is observed by Tauc expression [33]

$$\alpha h\nu = A(h\nu - E_g)^n \dots\dots\dots(1)$$

Where α = Optical absorption co-efficient, $h\nu$ = photon energy, E_g = Energy gap calculated from graph, A = absorption constant, n = Represents types of transition occurs. $n = 2$ indicated allowed indirect transitions and $n = 1/2$ indicated allowed direct transitions. We have plotted $(\alpha h\nu)^2$ vs. $h\nu$ for direct band energy analysis of prepared samples and are shown in **Fig. 4**. It extrapolated the linear portion of it to $\alpha = 0$ value to obtain direct band gap energy. The band gap energy value is found to be 1.60 eV for HCl doped DL-PLA/PANI-ES composite, 1.69 eV for HNO₃ doped DL-PLA/PANI-ES composite, 1.46 eV for H₃PO₄ doped DL-PLA/PANI-ES composite

and 1.37 eV for H₂SO₄ doped DL-PLA/PANI-ES composite, respectively. The difference in band energy occurred due to the effect of acid strength during the formation of PANI-ES on DL-PLA polymer film. It is observed from **Table 2**, the H₂SO₄ doped DL-PLA/PANI-ES composite showed highest band gap value than other three prepared composites. It may be happened due to the higher strength of H₂SO₄. It forms higher conjugation of PANI-ES chains and affect the band gap energy [30-33].

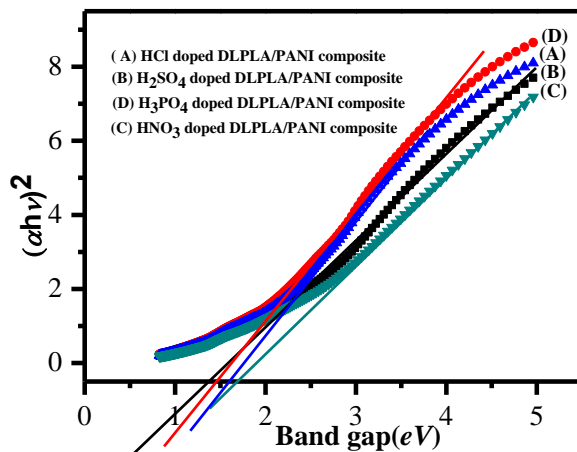


Figure 4. Optical (direct) band gap of HCl (A), H₂SO₄ (B), HNO₃ (C), H₃PO₄ (D) doped DL-PLA/PANI-ES composites [28]

Table 2. UV-Visible peak positions and their assignments and direct band gap of DL-PLA, HCl, HNO₃, H₂SO₄, H₃PO₄ doped DL-PLA/PANI-ES composites [28]

Materials	Polaron band	π - π^*	Band gap (eV)
DL-PLA	---	---	---
HCl doped DL-PLA/PANI-ES composite	780	383	1.60
H ₂ SO ₄ doped DL-PLA/PANI-ES composite	797	344	1.37
H ₃ PO ₄ doped DL-PLA/PANI-ES composite	787	381	1.46
HNO ₃ doped DL-PLA/PANI-ES composite	791	344	1.69

The DC conductivity of HCl, HNO₃, H₂SO₄, and H₃PO₄ doped DL-PLA/PANI-ES composites along with DL-PLA polymer film was measured at room temperature using linear four-probe technique. The used expression is $\sigma = 1/\rho$, ρ is resistivity. The resistivity was measured from the relation $\rho = 2\pi S (V/I)$, where

S is the probe spacing (0.15 cm) I is the supplied current (in nA) and V is the corresponding voltage (in mV). **Fig. 5** shows the I - V characteristics of HCl, HNO_3 , H_2SO_4 and H_3PO_4 doped DL-PLA/PANI-ES composites at room temperature. The measured I - V characteristics show the linear behaviour. The linear fit straight line passes through origin indicating the ohmic behavior. The conductivity measured from I - V data for the HCl, HNO_3 , H_2SO_4 and H_3PO_4 doped DL-PLA/PANI-ES composites is presented in **Table 3**. The conductivity of H_2SO_4 doped DL-PLA/PANI-ES composite (0.15×10^{-2} S/cm) is found to be higher than that of HCl, HNO_3 , and H_3PO_4 doped DL-PLA/PANI-ES composite (0.285×10^{-4} , 0.774×10^{-3} and 0.309×10^{-3} S/cm). This could be due to that stronger H_2SO_4 dopant, which exerts more force towards better ordering of PANI polymer chains leading to higher conjugation. The conjugation is a favorable factor for the intramolecular mobility of charged species along the chains and to some extent on the intermolecular hopping because of proper arrangement of polymeric chains [34]. Additionally, H_2SO_4 doped composite produces more semiquinone conducting group and PANI-ES as compared to HCl, HNO_3 and H_3PO_4 doped composite because of highly reactive nature of H_2SO_4 dopant [35, 36].

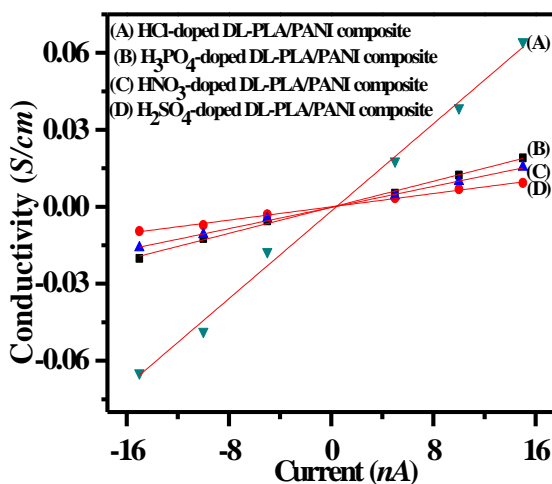


Figure 5. DC conductivity of HCl (A), H_2SO_4 (B), HNO_3 (C) and H_3PO_4 (D) doped DL-PLA/PANI-ES composites measured at room temperature [28]

The temperature dependent DC conductivity is shown in **Fig. 6**. It shows the conductivity of HCl, H_2SO_4 and H_3PO_4 doped DL-PLA/PANI-ES composites as a function of temperature. It is evident from **Fig. 6** that the composites showed increase in conductivity with increase in the temperature from 77 to 300 K, which is similar to an inorganic semiconductor. Hence, it can be called as organic semiconductor [37].

Various models including variable range hopping (VRH) were used as to understand the probable mechanism of current transport in the organic semiconductor [38-41].

Table 3. DC conductivity of HCl, H₂SO₄, HNO₃ and H₃PO₄ doped DL-PLA/PANI-ES composites at room temperature [28]

Materials Name	DC Conductivity (S/cm)
DL-PLA	6.05×10^{-15}
HCl doped DL-PLA/ PANI-ES composite	0.285×10^{-4}
H ₂ SO ₄ doped DL-PLA/ PANI-ES composite	0.162×10^{-2}
H ₃ PO ₄ doped DL-PLA/ PANI-ES composite	0.1097×10^{-3}
HNO ₃ doped DL-PLA/ PANI-ES composite	0.774×10^{-3}

According to VRH, the temperature (T) dependence of DC conductivity follows the Mott's expression [38-41].

$$\sigma = \sigma_0 \exp\left(-\frac{T_0}{T}\right)^r \dots\dots\dots(2)$$

Where T_0 is the Mott characteristic temperature and σ_0 the limiting value of conductivity at infinite temperature and the exponent ' r ' is related to the dimensionality of the transport process *via* the expression $r = 1/(1+d)$ here, $d = 1, 2$ and 3 for one-, two-, and three-dimensional (1D, 2D and 3D) conduction process, respectively. Out of three processes, three dimensional processes are more fitted.

Plot (a) and (b) in **Fig. 7** show the 3D-VRH plots and Arrhenius plots on measured conductivity in logarithmic scale for HCl, H₂SO₄ and H₃PO₄ doped DL-PLA/PANI-ES composites in the temperature range of 77–300 K, respectively. The conductivity data were carefully fitted linearly to both the 1D- and 3D-VRH as well as Arrhenius plots for conduction processes. The obtained regression values are presented in **Table 4**. It is clear from **Table 4** that Mott's 3D VRH model of as prepared composite fits better into the experimental data (Regression values) than that of 1D model and Arrhenius model. This suggests that charge carrier can hop both in between the chains, *i.e.*, interchain hopping and along the chain, *i.e.*, intrachain hopping as PANI has the chain structure [38-41].

In the 3D-VRH model, the temperature dependence of DC conductivity can be written as

$$\sigma = \sigma_0 \exp\left(-\frac{T_0}{T}\right)^{\frac{1}{4}} \dots\dots\dots(3)$$

Fig. 7 (a) shows that the linear dependence of $\ln \sigma$ vs $T^{-\frac{1}{4}}$ is better than that of $\ln \sigma$ vs $T^{-\frac{1}{2}}$. The estimated linear factor, i.e., regression values (R-values) for 3D-VRH model (0.9976) was better than that of 1D-VRH model (0.974), supporting the reported literature [42-45]. T_0 and σ_0 values were also calculated from the VRH plot of H_2SO_4 doped DL-PLA/PANI-ES composite and presented in Table 5. Unlike the H_2SO_4 doped, the regression value for H_3PO_4 doped DL-PLA/PANI-ES composite was measured to be almost same, i.e., 0.9937 and 0.993 from the 3D and 1D fitted VRH model, respectively. This indicates that 3D VRH model can be applied to describe the conduction mechanism in the H_3PO_4 doped DL-PLA/PANI-ES composite. In the H_2SO_4 doped DL-PLA/PANI-ES composite, sulphuric acid (H_2SO_4) is strong dopant which exerts stronger force leading to alignment of chains and increase in the compactness [34]. Therefore, charge carriers could hop easily from one chain to another chain obeying the 3D-VRH conduction mechanism model.

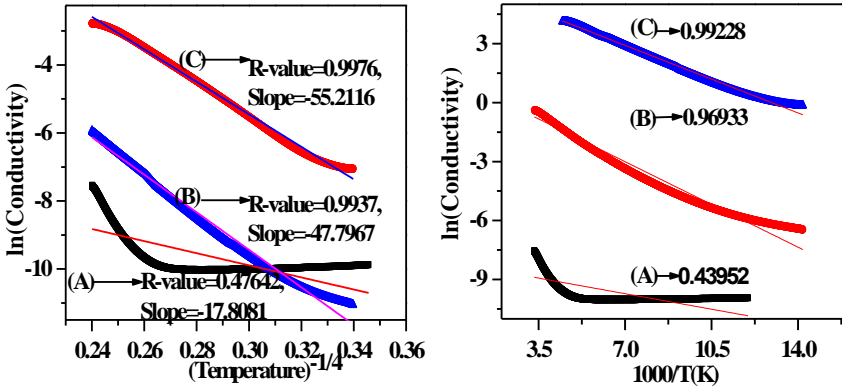


Figure 7. 3D VRH plot (left side) and Arrhenius plot (right side) of HCl (A), H_2SO_4 (B) and H_3PO_4 (C) doped DL-PLA/PANI-ES composites [28]

Other than the regression values, other parameters like density of states, hopping distance, hopping energy is supported to understand the conduction mechanism. Estimation of localisation length (L_{loc}) is an important parameter for the calculation of density of states, hopping distance, and hopping energy. Resistivity of HCl , H_2SO_4 and H_3PO_4 doped DL-PLA/PANI-ES composite was measured as a function of temperature in presence of magnetic field (0.4 T). We analyzed the resistivity data at 0.4 T (Fig. 8) along with the 3D-VRH model described by Mott's law [13] and given below and calculated localization length (L_{loc}) and density of states. Using these important parameters, we calculated hopping distance ($R_{hop, Mott}$) and hopping energy ($\Delta_{hop, Mott}$). The above estimated parameters help to understand the transport phenomenon.

$$\rho(T) = \rho_0 e^{\left(\frac{T_{Mott}}{T}\right)^{\frac{1}{4}}} \dots\dots\dots(4)$$

$$T_{Mott} = \frac{16}{[K_B N(E)_F L_{loc}^3]} \dots\dots\dots(5)$$

Where K_B is the Boltzmann constant, $N(E_F)$ is the density of states at the Fermi level, and L_{loc} is the localization length. The plot of $\ln \rho$ vs $T^{-\frac{1}{4}}$ exhibits a straight line for HCl, H₂SO₄ and H₃PO₄ doped DL-PLA/PANI-ES composites (**Fig. 8**). T_{Mott} can be evaluated from the slope of the straight line and is listed in **Table 5**.

The localization length L_{loc} can also be calculated from magnetoresistivity data as shown in **Fig. 8**. From the VRH model, the resistivity at different temperatures at a particular magnetic field can be written as [46]

$$\ln \left[\frac{\rho(H)}{\rho_0} \right] = t \left(L_{loc} / L_H \right)^4 \left(\frac{T_{Mott}}{T} \right)^{\frac{3}{4}} \dots\dots\dots(6)$$

Where $t = \frac{5}{2016}$, and $L_H = \left[\frac{hc}{2\pi eH} \right]^{\frac{1}{2}}$ is magnetic length, c = velocity of light (3×10^{10} cm/s), h = Planks constant (6.62×10^{-27} erg.sec), e = electronic charge (1.6×10^{-19} C) and H = 0.4 T is the applied magnetic field. From the slope of curves

in **Fig. 8**, we determined the L_{loc} values and listed in **Table 5**.

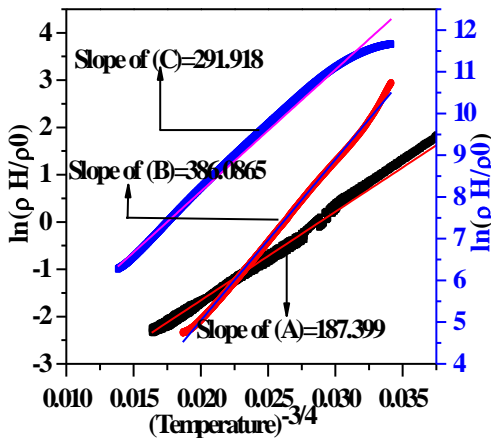


Figure 8. Plots of $[\ln(\rho(H)/\rho(0))]$ vs $T^{-4/3}$ for HCl (A), H₂SO₄ (B), H₃PO₄ (C) doped DL-PLA/PANI-ES composite at 0.4 T (77-300 K) [28]

Using the $T_{0,Mott}$ and L_{loc} of HCl, H₂SO₄ and H₃PO₄ doped DL-PLA/PANI-ES composite in equation (5), the density of states $(N(E_F))$ can be calculated.

The $T_{0,Mott}$, L_{loc} , and $(N(E_F))$ values were used to calculate the mean hopping distance R_{hop} and the energy difference between sites (Δ_{hop}) by using the following expression [13, 46] and presented in **Table 5**.

$$R_{hop,Mott} = \left(\frac{3}{8}\right) \left(\frac{T_{Mott}}{T}\right)^{\frac{1}{4}} L_{loc} \dots \dots \dots (7)$$

$$\Delta_{hop,Mott} = \left(\frac{1}{4}\right) (k_B T) \left(\frac{T_{Mott}}{T}\right)^{\frac{1}{4}} \dots \dots \dots (8)$$

By putting required parameters in the above expressions, the $R_{hop,Mott}$ and $\Delta_{hop,Mott}$ values were calculated at M-I transition temperature (125 K), which is presented in **Table 5**. In addition, the obtained hopping parameters were found to satisfy the 3D-VRH criteria.

Table 5. VRH conduction parameters obtained by analyzing the low temperature resistivity (with and without magnetic field) data of HCl, H₂SO₄, H₃PO₄ doped DL-PLA/PANI-ES composites [28]

Conducting parameters	L _H (Magnetic Length in °A)	HCl doped DL-PLA / PANI-ES composite	H ₂ SO ₄ doped DL-PLA / PANI-ES composite	H ₃ PO ₄ doped DL-PLA/ PANI-ES composite
Slope at 0 T (3D-VRH)	49.39	-17.8081	-55.21167	-47.7966
Slope at 0.4T		187.399	386.08	291.918
T _{Mott} (K)		1.005 × 10 ⁵	9.29 × 10 ⁶	5.21 × 10 ⁶
L _{loc} (°A)		95.11	48.48	50.28
N (E _F) (no. states/eV/cm ³)		2.14 × 10 ¹⁸	1.755 × 10 ¹⁷	2.08 × 10 ¹⁷
R _{Hop, Mott} (°A) at 125 K		189.74	300.18	269.47
Δ _{Hop, Mott} (meV at 125 K)		19.34	44.48	38.49
Temp. at M-I (K)		125	125	125

Newly, the negative MR of hopping systems has been explored and various possible way of hopping path was interpreted by quantum interference effect of spins in presence of magnetic field [47-50]. This effect is ascribed to the statistics of self-crossed trajectories in conductors, *i.e.*, phase coherence of the electron's wave function between different conduction paths is destroyed in presence of magnetic field [26]. In the present work, the low temperature conductivity has indicated the hoping conduction mechanism but not the weak localization system. The concept of weak localisation effect is valid for diffusive motion of current carriers, and can be extended to hopping conduction [47, 48]. In the weak field region, the negative MR can be expressed as [47, 48].

$$MR = \left[\frac{R(H) - R(0)}{R(0)} \right] \propto -H^x T^{-y} \dots \dots \dots (9)$$

Where the exponent $x = 1$ [47] or $x = 2$ [48] $y = \frac{3}{4}$ for 3D – and $y = \frac{3}{2}$ for 1D–VRH. The interesting observation was found by Sivan et al. [47] and predicted quadratic field dependence over most of the weak-field range. Also, Nguyen et al. [48] reported the negative MR, which is linear in the field. Using equation (9), MR values of H_2SO_4 and H_3PO_4 doped DL–PLA/PANI-ES composites was calculated at room temperature. **Fig. 9** shows the plot of negative MR as a function of magnetic field (H). In the case of H_2SO_4 doped DL–PLA/PANI-ES composites, MR were found to linearly decrease with increase in the magnetic field whereas in case of H_3PO_4 doped DL–PLA/PANI-ES composites, the MR value was found to slightly increase above 0.4T. The above negative MR results are in qualitative agreement with the predicated features [47, 48].

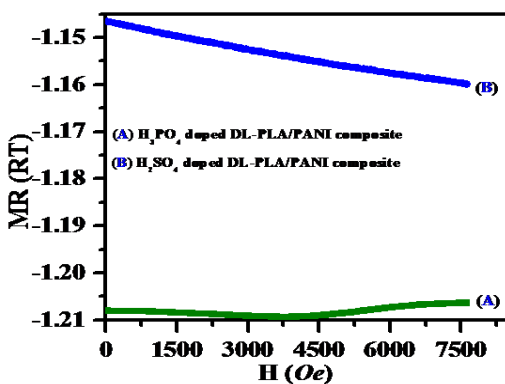


Figure 9. Magnetoresistance (MR) of H_3PO_4 (A) and H_2SO_4 (B) doped DL-PLA/PANI-ES composites at room temperature [28]

2.4. Response Of Hydrogen (H₂) Gas (i.e., H₂ Gas Sensor)

Hydrogen (H₂) is one of the flammable gases. Also, H₂ gases are found to be highly explosive. It is becoming the fuel of the next generation of automobiles. Therefore, the detection of low concentration i.e., ppm level of H₂ is highly essential in houses, vehicles, or industrial places is potentially important. The prominence of environmental gas monitoring system is well understood and much research has focused on the development of suitable sensor material [49]. In addition, Hydrogen is the cleanest, sustainable and renewable energy carrier for future fuel. Hydrogen gas is flammability when H₂ gas comes in presence 4% air or more [50]. Hence monitoring systems are essential to sense hydrogen gas at room temperature. Most of the monitoring systems available on the market are metal oxide semiconductor based sensors, which is operated at high temperature. The obtained sensor sensitivity and selectivity is significant [51-53]. The researcher is focused much more on room temperature operated sensor system. Some reports are available on conducting polymer based sensors.

Table 6. Brief summary of H₂ detection

Study	Materials	Perporfa mce	Optimum temperat ure (°C)	Limitation
Conn et al. [65]	polyaniline-platinum oxide	Response time 25 s	Room Temperature	High H ₂ Concentration
Sadek et al. [66]	Polyaniline (PANI) nanofiber	Response time xxx	Room Temperature	High H ₂ concentration
Conn et al. [49]	Polyaniline	Response time 20 s	Room Temperature	High H ₂ concentration
Sadek et al. [67]	Polyaniline Nanofiber	Response time 28 s	Room Temperature	High H ₂ concentration
Al-Mashat et al. [68]	Graphene/Polyaniline Nanocomposite	Sensitivity 1 %	Room Temperature	High H ₂ concentration
Arsat et al. [68]	Ordered polyaniline nanofibers		Room Temperature	High H ₂ concentration
Sandarwan et al. [70]	Polyaniline/palladiumnano hybrids	Frequency change	Room Temperature	High H ₂ concentration

The benefits of the conducting polymers have sensitive layer of gases, intrinsic conductivity, fast response, low cost, light weight, ease of synthesis, stability in air and particularly, their sensitivity at the room temperature [54-56]. Few reports

are mentioned that conducting polymers may have ability to store hydrogen [57, 58]. Polyaniline is one of the members of conducting polymer family. Since, it has chemically stable and easy to synthesize. Polyaniline can exist as two different emeraldine forms. One is called polyaniline emeraldine base, which is insulating ($\sigma \sim 10^{-5}$ S/cm) and other one is polyaniline emeraldine salt, which is metallic in nature ($\sigma < 1000$ S/cm). The metallic nature is obtained by doping process [59-64]. Both classes are completely different with their own chemical and physical properties. The unique nature of this attractive class of polyaniline highlights its potential importance in a new type of H_2 reaction. Due to versatile nature of polyamine, it is used as an active layer for H_2 gas sensors. Brief summary of H_2 gas detection is presented in Table 6.

2.4 Conclusions

HCl, H_2SO_4 , HNO_3 , and H_3PO_4 doped DL-PLA/PANI-ES composites were synthesized successfully by *chemical-oxidation* polymerization process. The composites showed different diameter sized fibrous morphology. Presences of preferred groups of the composites are observed from ATR-FTIR spectra. Emeraldine salt form of the composites is found from UV-Visible spectra. Room temperature I-V characteristics of the doped composites have shown ohmic behaviour. Among the composites, H_2SO_4 doped DL-PLA/PANI-ES composite (0.15×10^{-2} S/cm) was found to be higher room temperature DC conductivity than that of HCl (0.285×10^{-4} S/cm) and H_3PO_4 doped (0.309×10^{-3} S/cm) DL-PLA/PANI-ES composite. Also, the DC conductivity of as prepared composites was observed to increase as a function of temperature. In Mott's 3D-VRH model, the temperature variation DC conductivity data's are more fitted and explained the conduction mechanism of the doped composites. The temperature variation (77-300 K) resistivity measurement of HCl, H_2SO_4 and H_3PO_4 doped DL-PLA/PANI-ES composites with magnetic field (0.4 T) were performed. The L_{loc} was estimated and found to be 95.11, 48.48 and 50.28 °A for HCl, H_2SO_4 and H_3PO_4 doped DL-PLA/PANI-ES composites, respectively. Using the resistivity at 0.4 T data's and 3D-VRH model data's of as prepared composites,

different conduction mechanism parameters such as $N(E_F), T_{Mott}, L_{loc}, R_{hop}$, and Δ_{hop} were estimated. In particulars, hydrogen gas responses and mechanism of polyaniline based materials were studied.

3.0 Acknowledgments

The author conveys their sincere thanks to the CRF, IIT Kharagpur for their providing testing facilities and Materials Science Centre to do the research work. I would like to thank Prof. Debabrat Pradhan for their invaluable guidance, advices, constant inspiration and technical support to the work.

4.0 References

- [1] Burroughes, J.H., Bradley, D.D.C., Brownn, A.R., Marks, R.N., Mackay, K., Friend, R. H., Burns, P. L., and Homes, A. B. (1990), Light-emitting Diodes Based on Conjugated Polymers, *Nature*, Vol. 347, pp. 539-541.
- [2] Frackowiak, E., Khomenko, V., Jurewicz, K., Lota, K., and Beguin F. (2006), Supercapacitors Based on Conducting Polymers/Nanotubes Composites, *Journal of Power Sources*, Vol. 153, pp. 413-418.
- [3] Conn, C., Sestak, S., Baker, A.T., and Unsworth. J. (1998), A Polyaniline-Based Selective Hydrogen Sensor, *Electroanalysis*, Vol. 10, pp. 1137-1141.
- [4] Abdelkader, R., Amine, H., and Mohammed, B. (2012), Thermally Stable Forms of Pure Polyaniline Catalyzed by Acid-exchanged Montmorillonite Clay called Maghnite- H^+ as an Effective Catalyst, *International Journal of polymer science*, Vol. 2012, pp. 1-7.
- [5] Yang, S., and Ruckenstein, E. (1993), Processable Conductive Composites of Polyaniline/Poly (alkyl methacrylate) Prepared via an Emulsion Method, *Synthetic Metals*, Vol. 59, pp. 1-12.
- [6] Singh, V., Mohan, S., Singh, G., Pandey, P.C., and Prakash, R. (2008), Synthesis and Characterization of Polyaniline-carboxylated PVC Composites: Application in Development of Ammonia Sensor, *Sensors and Actuators, B*, Vol. 132, pp. 99-106.
- [7] Okubo, M., Fujii, S., and Minami, H. (2001), Production of Electrically Conductive, Core-shell Polystyrene/Polyaniline Composite Particles by Chemically Oxidative Seeded Dispersion Polymerization, *Colloid and Polymer Science*, Vol. 279, pp. 139-145.
- [8] Spirkova, M., Stejskal, J., and Quadrat, O. (1999), Electrically Anisotropic Polyaniline-Polyurethane Composites, *Synthetic Metals*, Vol. 102, pp. 1264-1265.
- [9] Aleshin, A., Kiebooms, R., Menon, R., and Heeger, A.J. (1997), Electronic Transport in Doped Poly (3,4-ethylenedioxythiophene) Near the Metal-Insulator Transition, *Synthetic Metals*, Vol. 90, pp. 61-68.
- [10] Shklovskii, B.I. and Efros, A.L. (1984), *Electronic Properties of Doped Semiconductors*, (Berlin: Springer).
- [11] Long, Y.Z., Yin, Z.H., and Chen, Z.J. (2008), Low-Temperature Magnetoresistance Studies on Composite Films of Conducting Polymer and Multiwalled Carbon Nanotubes, *Journal of Physical Chemistry C*, Vol. 112, pp. 11507-11512.
- [12] Zuppiroli, L., Bussac, M.N., Paschen, S., Chauvet, O., and Forro. L. (1994), Hopping in Disordered Conducting Polymers, *Physical Review B*, Vol. 50, pp. 5196-5203.

- [13] Li, J., Fang, K., Qiu, H., Li, S., and Mao, W. (2004), Micromorphology and Electrical Property of the HCl-doped and DBSA-doped Polyaniline, *Synthetic Metals*, Vol. 142, pp. 107-111.
- [14] Kapil, A., Taunk, M., and Chand, S. (2010), Preparation and Charge Transport Studies of Chemically Synthesized Polyaniline, *Journal of Materials Science: Materials in Electronics*, Vol. 21, pp. 399-404.
- [15] Reghu, M., Yoon, C.O., Moses, D., Smith, P., Heeger A. J., and Cao, Y. (1995), Magnetoresistance in Polyaniline Networks Near the Percolation Threshold, *Synthetic Metals*, Vol. 69, pp. 271-272.
- [16] Clark, J.C., Ihas, G.G., Rafanello, A.J., Meisel, M.W., Reghu M., Yoon, C.O., Cao, Y., and Heeger, A.J. (1995), Resistivity and Magnetoresistance of Metallic Polyaniline and Polypyrrole at Millikelvin Temperatures, *Synthetic Metals*, Vol. 69, pp. 215-216.
- [17] Long, Y., Chen, Z., Zhang, X., Zhang, J., and Liu, Z. (2004), Synthesis and Electrical Properties of Carbon Nanotube Polyaniline Composites, *Applied Physics Letters*, Vol. 85, pp. 1796-1798.
- [18] Sangeeth, C.S.S., Jiménez, P., Benito, A.M., Maser, W.K., and Menon, R. 2010, Charge Transport Properties of Water Dispersible Multiwall Carbon Nanotube-Polyaniline Composites, *Journal of Applied Physics*, Vol. 107, pp. 103719-103723.
- [19] Abou-Elazab, T.F., Migahed, M.D., Park, H., Park, Y.W., MacNeillis, P., and Rabenau, T. (1996), Magnetoresistance of Polypyrrole and Polyacetylene, *Synthetic Metals*, Vol. 76, pp. 281-284.
- [20] Mativetsky, J.M., and Datars, W.R. (2002), Morphology and Electrical Properties of Template-synthesized Polypyrrole Nanocylinder, *Physica B*, Vol. 324, pp. 191-204.
- [21] Park, J.G., Lee, S.H., Kim, B. and Park, Y.W. (2002), Electrical Resistivity of Polypyrrole Nanotube Measured by Conductive Scanning Probe Microscope: The Role of Contact Force, *Applied Physics Letters*, Vol. 81, pp. 4625-4627.
- [22] Aleshin, A., Kiebooms, R., Menon, R., and Heeger, A.J. (1997), Electronic Transport in Doped Poly (3,4-ethylenedioxythiophene) near the Metal-Insulator Transition, *Synthetic Metals*, Vol. 90, pp. 61-68.
- [23] Nath, C., and Kumar, A. (2013), Effect of Temperature and Magnetic Field on the Electrical Transport of Polyaniline Nanofibers, *Journal of Applied Physics*, Vol. 113, pp. 093707-0937010.
- [24] Long, Y., Chen, Z., Shen, J., Zhang, Z., Zhang, L., Huang, K., Wan, M., Jin, A., Gu, C., and Duvail, J.L. (2006), Magnetoresistance Studies of Polymer Nanotube/Wire Pellets and Single Polymer Nanotubes/Wires,

- Nanotechnology Vol. 17, pp. 5903-5911.
- [25] Long, Y., Huang, K., Yuan, J., Han, D., Niu, L., Chen, Z., Gu, C., Jin, A., and Duvail, J.L. (2006), Electrical Conductivity of a Single Au/Polyaniline Microfiber, *Applied Physics Letters*, Vol. 88, pp. 162113-162116.
- [26] Lee, P.A., and Ramakrishnan, T.V. (1985), *Disordered Electronic Systems*, *Reviews of Modern Physics*, Vol. 57, pp. 287-337.
- [27] Panigrahi, M., Singh, N.K., Gautam, R.K., Banik, R.M., and Maiti, P. (2010), Improved Biodegradation and Thermal Properties of Poly(lactic acid)/Layered Silicate Nanocomposites, *Composite Interfaces*, Vol. 17, pp. 143-158.
- [28] Panigrahi, M., Pradhan, D., Majumdar, S.B., and Adhikari, B. 2017, Investigation of DC Conductivity, Conduction Mechanism and CH₄ Gas Sensor of Chemically Synthesized Polyaniline Nanofiber Deposited on DL-PLA Substrate, Edited by Sanjay K. Nayak, Smita Mohanty, Lakshmi Unnikrishnan, pp. 101 -126, *Trends and Applications in Advanced Polymeric Materials* [https:// doi.org/10.1002/9781119364795.ch6](https://doi.org/10.1002/9781119364795.ch6).
- [29] Mathai, C.J., Saravanan, S., Anantharaman, M.R., Venkitachalam, S., and Jayalekshmi, S. (2002), Effect of Iodine Doping on the Band Gap of Plasma Polymerized Aniline Thin Films, *Journal of Physics D:Applied Physics*, Vol. 35, pp. 2206-2210.
- [30] Nascimento, do G.M., Constantino, V.R.L., and Temperini, M.L.A. , 2002, Spectroscopic Characterization of New Type of Conducting Polymer-Clay Nanocomposite, *Macromolecule*, Vol. 35, pp. 7535-7537.
- [31] Bocchini, S., and Frache, A. 2013, Comparative Study of Filler Influence on Polylactide Photooxidation, *e-XPRESS Polymer Letters* Vol.7, pp. 431-442.
- [32] Shi, J., Wu, Q., Li, R., Zhu, Y., Qin, Y., and Qiao, C. (2013), The pH-Controlled Morphology Transition of Polyaniline from Nanofibers to Nanospheres, *Nanotechnology*, Vol. 24, 175602-17569.
- [33] Ansari, A.A., Khan, M.A.M., Khan, M.N., Alrokayan, S., Alhoshan, A.M., and Alsalhi, M.S. 2011, Optical and Electrical Properties of Electrochemically Deposited Polyaniline/CeO₂ Hybrid Nanocomposite Film, *Journal of Semiconductors*, Vol. 32, pp. 043001-043006.
- [34] Lux, F. (1994), Properties of Electronically Conductive Polyaniline: A Comparison Between Well-known Literature Data and Some Recent Experimental Findings, *Polymer*, Vol. 35, pp. 2915-2936.
- [35] Langer, J. J., Krzyminiowski, R., Krucznski, Z., Gibinski, T., Czajkowski, I., and Framski, G. (2001), EPR and Electrical Conductivity in Microporous Polyaniline, *Synthetic Metals*, Vol. 122, pp. 359-362.
- [36] Li, J., Fang, K., Qiu, H., Li, S., and Mao, W.J. (2004), Micromorphology and

- Electrical Property of the HCl-doped and DBSA-doped Polyaniline, *Synthetic Metals*, Vol. 142, pp. 107-111.
- [37] Chakraborty, G., Gupta, K., Meikap, A.K., and Jana, P.C. (2010), Direct Current Electrical Transport and Magneto Transport Properties of Polyaniline Nanocomposites, *Journal of Physical Science*, Vol. 14, pp. 207-218.
- [38] Long, Y., Chen, Z., Shen, J., Zhang, Z., Zhang, L., Huang, K., Wan, M., Jin, A., Gu, C., and Duvail, J.L. (2006), Magnetoresistance Studies of Polymer Nanotube/Wire Pellets and Single Polymer Nanotubes/Wires, *Nanotechnology*, Vol. 17 pp. 5903-5911.
- [39] Wang, Z.H., Javadi, H.H.S., Ray, A., Macdiarmid, A.G., and Epstein, A.J. (1990), Electron Localization in Polyaniline Derivatives, *Physical Review B* (Rapid communication), Vol. 42, pp. 5411-5414.
- [40] Li, W., and Wan, M. (1998), Porous Polyaniline Films with High Conductivity, *Synthetic Metals*, Vol. 92, pp. 121-126.
- [41] Chakraborty, G., Gupta, K., Rana, D., and Meikap, A.K. (2012), Effect of Multiwalled Carbon Nanotubes on Electrical Conductivity and Magnetoconductivity of Polyaniline, *Advance Nature Science: Nanoscience Nanotechnology*, Vol. 3, pp. 035015-035023.
- [42] Ghosh, M., Barman, A., Meikap, A.K., De, S.K., Chatterjee, S., and Chattopadhyay, S. K. (2000), Electrical Resistivity and Magnetoresistivity of Protonic Acid (H_2SO_4 and HCl)-Doped Polyaniline at Low Temperature, *Journal of Applied Polymer Science*, Vol. 75, pp. 1480-1486.
- [43] Faran, O., and Ovadyaho, Z. (1998), Magnetoconductance in the Variable-Range-Hopping Regime due to a Quantum-Interference Mechanism, *Physical Review B*, Vol. 38, pp. 5457-5465.
- [44] Baumgartner, G., Carrard, M., Zuppiroli, L., Bacsá, W., Heer, W. A., and Forro, L. (1997), Hall Effect and Magnetoresistance of Carbon Nanotube Films, *Physical Review B*, Vol. 55, pp. 6704-6707.
- [45] Yosida, Y. and Oguro, I. (1999), Variable Range Hopping Conduction in Bulk Samples Composed of Single-Walled Carbon Nanotubes, *Journal of Applied Physics*, Vol. 86, pp. 999-1003.
- [46] Fuhrer, M. S., Holmes, W., Richards, P.L., Delany, P., Louie, S.G., Zettl, A. (1999), Nonlinear Transport and Localization in Single-Walled Carbon Nanotubes, *Synthetic Metals*, Vol. 103, pp. 2529-2532.
- [47] Nguyen, V.L., Spivak, B.Z., and Shklovskii, B.I. (1985), Aharonov-Bohm Oscillation with and Superconductivity Flux-Quanta in Hopping Conduction, *Soviet Physics-Journal of Experimental and Theoretical Physics*, Vol. 62, pp. 1021-xxx.

- [48] Sivan, U., Entin-Wohlman, O., Imry, Y. (1988), Orbital Magnetoconductance in the Variable-Range-Hopping Regime. *Physical Review Letter*, Vol. 60, pp. 1566-1569.
- [49] Conn,C., Sestak, S., Baker, A.T., and Unsworth, J. 1998, A Polyaniline-Based Selective Hydrogen Sensor; *Electroanalysis*, Vol. 10, pp. 1137-1141.
- [50] Samarasekara, P. 2009, Hydrogen and Methane Gas Sensors Synthesis of Multi-Walled Carbon Nanotubes, *Chinese Journal of Physics*, Vol. 47, pp.361-369.
- [51] Sadek, A.Z., Wlodarski, W., Kalantar-Zadeh, K., Baker, C., and Kaner, R.B. 2007, Doped and Dedoped Polyaniline Nanofiber based Conductometric Hydrogen Gas Sensors; *Sensors and Actuators A* Vol. 139, pp.53-57.
- [52] Sadek, A.Z., Wlodarski, W., Shin, K., Kaner, R.B., and Kalantar-zadeh, K. 2008, A Polyaniline/WO₃ Nanofiber Composite-based ZnO/64° YX LiNbO₃; SAW Hydrogen Gas Sensor; *Synthetic Metals*, Vol.158, pp. 29-32.
- [53] Arsata, R., Yu, X.F., Li, Y.X., Wlodarski, W., and Kalantar-zadeh, K.2009, Hydrogen Gas Sensor based on Highly Ordered Polyaniline Nanofibers, *Sensors and Actuators B*, Vol. 137, pp.529-532.
- [54] Atashbara, M.Z., Sadek, A.Z., Wlodarski, W., Sriram, S., Bhaskaran, M., Cheng, C.J., Kaner, R.B., and Kalantar-zadeh, K. 2009, Layered SAW Gas Sensor based on CSA Synthesized Polyaniline Nanofiber on AlN on 64° YX LiNbO₃ for H₂ Sensing, *Sensors and Actuators B*, Vol. 138, pp. 85-89.
- [55] Srivastavaa, S., Sharmaa, S.S., Agrawal, S., Kumar, S., Singh, M., and Vijay, Y.K. 2010, Study of Chemiresistor type CNT Doped Polyaniline Gas Sensor, *Synthetic Metals* Vol. 160, pp. 529-534.
- [56] Srivastava, S., Sharma, S.S., Kumar, S., Agrawal, S., Singh, M., and Vijay, Y.K. 2009, Characterization of Gas Sensing Behavior of Multi-Walled Carbon Nanotube Polyaniline Composite Films, *International Journal of Hydrogen Energy*, Vol. 34, pp. 8444- 8450.
- [57] Srinivasan, S.S., Ratnadurai, R., Niemann, M.U., Phani, A.R., Goswami, D.Y., and Stefanakos, E.K. 2010, Reversible Hydrogen Storage in Electrospun Polyaniline Fibers, *International Journal of Hydrogen Energy*, Vol. 35, pp. 225-230.
- [58] Yang, L.-Y., and Liaua, W.-B. 2010, Environmental Responses of Polyaniline Inverse Opals: Application to Gas Sensing; *Synthetic Metals*, Vol. 160, pp. 609-614.
- [59] Sadek, A. Z., Trinch, A., Wlodarski, W., Kalantar-zadeh, K., Galatsis, K., Baker, C. and Kaner, R.B. 2005, A Room Temperature Polyaniline Nanofiber Hydrogen Gas Sensor, in *SENSORS 2005: Proceedings of the 2005 IEEE Sensors conference*, IEEE, Piscataway, N.J., pp. 207-210..

- [60] Yadav, J.B., Jadhav, S.V., Puri, R.K., and Puri, V. 2008, Properties of Vacuum Evaporated Vapour Chopped Polyaniline Thin Film: Effect of Synthesis Method, *Journal of Physics Conference Series*, Vol. 114, pp. 012037-xxx.
- [61] Mylvaganam, K., and Zhang, L.C. 2007, Fabrication and Application of Polymer Composites Comprising Carbon Nanotubes, *Recent Patents Nanotechnol.* Vol. 1, pp. 59-65.
- [62] Bai, H., and Shi, G. 2007, Gas Sensors Based on Conducting Polymers, *Sensors*, Vol. 7, pp. 267-307.
- [63] Genies, E.M., Boyle, A., Lapkowski, M., and Tsintavis, C. 1990, Polyaniline: A Historical Survey, *Synthetic Metals*, Vol. 36, pp. 139-182.
- [64] Negi, Y.S., and Adhyapak, P.V., 2002, Development in Polyaniline Conducting Polymers, *Journal of Macromolecular Science-part-C polymer Review*, Vol. 42, pp. 35-53.
- [65] Conn, C., Sestak, S., Baker, A.T., and Unsworth, J. 1999, A Polyaniline-Based Selective Hydrogen Sensor, *An International Journal devoted to Electronanalysis, Sensors, Bioelectronic device.* 1999, Vol. 10, pp. 1137-1141.
- [66] Sadek, A.Z., Trinchì, A., Wlodarski, W., Kalantar-zadeh, K., and Galatsis, K. 2006, A Room Temperature Polyaniline Nanofiber Hydrogen Gas Sensor, *IEEE Xplore*, Print ISBN:0-7803-9056-3, DOI: 10.1109/ICSENS.2005.1597672.
- [67] Sadek, A.Z. Wlodarski, W., Kalantar-Zadeh, K., Baker, C., and Kaner, R.B. Doped and Dedoped Polyaniline Nanofiber Based Conductometric Hydrogen Gas Sensors, *Sensors and Actuators A: Physical*, Vol. 139, pp. 53-57.
- [68] Laith Al-Mashat, Koo Shin, Kourosh Kalantar-zadeh, Johan D. Plessis, Seung H. Han, Robert W. Kojima, Richard B. Kaner, Dan Li, Xinglong Gou, Samuel J. Ippolito, Wojtek Wlodarski, 2010, Graphene/Polyaniline Nanocomposite for Hydrogen Sensing, *J. Phys. Chem. C* Vol. 114, pp. 16168-16173.
- [69] Arsat, R., Yu, X.F., Li, Y.X., Wlodarski, W., and Kalantar-Zadeh, K. 2009, Hydrogen Gas Sensor Based on Highly Ordered Polyaniline Nanofibers, *Sensors and Actuators B: Chemical* Vol. 137, pp. 529-532.
- [70] Sandaruwan, C., Herath, H.M.P.C.K., Karunaratne, T.S.E.F., Ratnayake, S.P., Amaratunga, G.A.J., and Dissanayake, D.P. 2018, Polyaniline/Palladium Nanohybrids for Moisture and Hydrogen Detection, *Chemistry Central Journal*, Vol. 93, pp. 1742-xxx.

Chapter 6

Poly Methyl Methacrylate (Pmma) Based Polyaniline Composite for Ammonia (Nh3) Gas Sensors

Muktikanta Panigrahi ^{1,*}, Basudam Adhikari ¹

¹ Materials Science Centre, Indian Institute of Technology, Kharagpur, West Bengal, India

*Corresponding author: muktikanta2@gmail.com

Abstract

Inorganic acids (HCl, H₂SO₄, and H₃PO₄) doped-PMMA/PANI composites are prepared by *in-situ* technique via oxidation-polymerization process. Different techniques such as XRD, FTIR, UV-Visible, four-probe method are used to characterize the composite. Presence of different chemical group of the doped composites is analysed by ATR-FTIR spectroscopic analysis. Charge carrier behaviour of the doped composite is analyzed by UV-Visible spectroscopy. Band gap (E_g) of the doped composites is determined from UV-Visible absorption analysis using Tauc expression. The estimated direct band gap energy (E_g) is found to be 1.93 eV (for HCl doped PMMA/PANI composite), 1.19 eV (for H₂SO₄ doped PMMA/PANI composite), and 1.71 eV (for H₃PO₄ doped PMMA/PANI composite), respectively. DC-conductivity is measured with and without magnetic field. Temperature dependent DC conductivity is also measured. In addition, we were discussed the response of ammonia (NH₃) gas with polyaniline-based sensor materials.

Key Words: PMMA, PANI-ES, Dopant, UV-Visible, Band Gap, Conductivity (with and without) magnetic field, Organic Semiconductor

Introduction

Conducting polymers with extended π -electrons conjugation are highly susceptible to chemical or electrochemical oxidation or reduction. Conducting polymers have established to have suitable properties for technological applications such as electroluminescent device [1], field effect transistor [2], chemical sensor [3], electrode [4], metal anticorrosion [5], marine fouling prevention [6].

© IOR INTERNATIONAL PRESS, 2021

Muktikanta Panigrahi & Basudam Adhikari 1, *Poly Methyl Methacrylate (Pmma) Based Polyaniline Composite for Ammonia (Nh3) Gas Sensors*,

<https://doi.org/10.34256/ioriip2126>

In the conducting polymer family, polyaniline (PANI) occupies an important position in the family, which is inherently present conductivity. The conducting polymer is called intrinsic conducting polymer (ICP). PANI is synthesized by different routes such as chemical and electrochemical method. It has low cost of synthesis with good environmental stability and unique acid-base doping-dedoping [7-9]. In spite of its several desirable properties, there is some limitations *viz.* insolubility in conventional solvents for processing [10] and poor mechanical strength [4,5]. One of the ways to overcome these demerits that is to prepare conducting composites using an insulating polymer matrix [11]. Researchers have devoted to prepare polyaniline composite with insulating polymers. The composite show enhanced structural and electronic stability in different atmospheres. Several popularly used matrix polymers employed are poly (vinyl acetate) [12], poly (vinyl chloride) [13], poly(methyl methacrylate) [14], polystyrene [15], poly urethane [16], polylactide [17], and poly(vinyl pyrrolidone) (PVP) [18]. PVP surface can adsorb the electroactive polymer, forming a solvated steric barrier around individual particles, thus preventing aggregation and increasing dispersion [18]. If PANI is encapsulated, PVP can enhance the electrical conductivity of polyaniline by trapping gases inside its matrix, thus allowing increased gas surface interactions between the analytes and PANI particles. Guixin et al. [19] prepared electrically conductive biodegradable composite from polypyrrole and poly (D,L-lactide) by emulsion polymerization followed by precipitation. Huang and his co-workers [20] synthesized a block copolymer having polylactide covalently bonded to an electroactive polymer, such as PANI which could exhibit improved solubility, and processibility of electroactive materials.

To investigate the optical properties of conducting polymer composite have attracted great attention because of their technological applications such as optical sensors [21], antireflective coatings [22]. Both optical band gap and refractive index are the key parameter of an optical material. Since, these are closely related to the electronic properties of materials.

In the current work, author is reported synthesis of doped PMMA/PANI composites using liq. aniline as precursor *via in situ* polymerization route. HCl, H₂SO₄, and H₃PO₄ are used as dopants, which is inorganic in nature. We analyzed the effect of dopants *i.e.*, HCl, H₂SO₄, H₃PO₄ on crystallinity, charge transfer spectra, band gap and room temperature DC conductivity with and without magnetic field in doped PMMA/PANI composite(s). Also, estimated temperature variation DC conductivity.

Experimental Details

Chemicals and Materials

Reagent grade chemicals such as aniline liquid, ammonium persulfate, hydrochloric acid, sulphuric acid, ortho-phosphoric acid, diethyl ether are procured from Merck, India. Poly (methylmethacrylate) (PMMA) is used as base materials, which is purchased from local market as sheet. This is used during the preparation of

PMMA/PANI composite.

Pmma/Pani Composite Preparation (*In-Situ*)

Both polymer (*i.e.*, PMMA polymer piece, small) and chloroform (*i.e.*, CHCl_3) are taken In a 100 mL beaker. The mixture is stirred (upto 3 h) to form a transparent mass solution. The mass solution is poured and cast into a flat petridis (diameter= 5 inches). The film (*i.e.*, cast mass) is removed from petridis after solvent evaporation. The film is cut into small pieces (1.5 ×1.5 cm) and is used during the preparation of composite.

PMMA/PANI composite is prepared by chemical-oxidation method using liquid aniline (conducting polymeric material) and PMMA film (base materials). The composite preparation is carried out at room temperature [23]. The composite is prepared in **three steps**. In **step one**; dopant solution is prepared by taking distilled water and concentrated HCl in appropriate proportion. In **step two**, oxidant solution is taken into account. 7.47 g of ammonium persulphate (APS) is added slowly to 60 mL of 1(M) HCl solution with shaking (5 minutes). 3 mL of liquid aniline and PMMA films (1.5 cm × 1.5 cm) are put into the 500 mL conical flask contained 105 mL of 1 (M) HCl solution. It is stirred (with 600 rpm) up to 12 h in a magnetic stirrer. To this solution, APS solution is added drop wise with continuous stirring. The polymerization is carried out and is mentioned in **third step**. The reaction mixture is stirred for 10 h. The color of transparent PMMA films became light green to dark green. The composites are washed with distilled water several times followed by dry up in air for 6 h. For comparison, H_2SO_4 , doped PMMA/PANI composite and H_3PO_4 doped PMMA/PANI composites are also prepared under same conditions.

Characterization Techniques

X-ray diffraction experiments PMMA film, PANI, and doped PMMA/PANI composite are executed using a Phillips PW-1710 advance wide angle X-ray diffractometer, Phillips PW-1729 X-ray generator, $\text{CuK}\alpha$ radiation, $\lambda = 0.154$ nm. The generator is operated at 40 kV and 20 mA. The film/powder samples are tested. Samples are placed on a quartz sample holder at room temperature. The scanned diffraction angle is 10° to 50° (2θ) with scanning rate ($2^\circ/\text{min}$).

ATR-FTIR spectra are recorded on a Thermo Nicolt Nexus 870 spectrophotometer (from 400 to 4000 cm^{-1}). ATR-FTIR spectrometer settings are kept constant (50 scan at 4 cm^{-1} resolution, Absorbance measurement mode). Film/powder samples are tested. For powder samples particularly PANI, palate is prepared using potassium Bromide (KBr) through compression molding with pelletizer. Before running the samples, a background spectrum is collected. Then samples are put in a sample holder and data are collected.

Doped PMMA/PANI composite is used during UV-Visible analysis. The spectra of the composites are recorded by using a Micropack UV-VIS-NIR, DH 2000.

The wave length region of the analysis is 250-1000 nm. Base line is corrected before recording the spectra. Optical band gaps are determined from UV-Visible analysis.

Raman spectra are noted on a Renishaw Raman imaging microscope (System 3000) containing a Olympus metallurgical microscope and a CCD detector (cooled by a Peltier) using 632.8 nm exciting radiation (He-Ne laser, Spectra Physics, model 127). 457.9, 488.0, and 514.5 nm exciting radiations (Ar⁺ laser, Omnichrome model 543-AP) are done. The laser beam is focused on the sample in a roughly 1 μ m spot by a \times 80 lens. The laser power is always kept below 0.7 mW for avoiding sample degradation. FT-Raman spectra of the samples are recorded in an RFS 100 FT-Raman Bruker spectrometer with the 1064 nm radiation (Nd:YAG laser). Solid samples are taken for Raman study.

Surface morphology of PMMA polymer film, PANI, and PMMA/PANI composite are analyzed by scanning electron microscopy (Carl Zeiss Supra 40). Samples are coated with gold before the measurement.

DC-conductivity of the doped composite (with and without magnetic field) at room temperature is measured using a linear four-probe technique. DC-conductivity are calculated using the relation $\rho = 2\pi S (V/I)$ where S is the probe spacing (mm), ' I ' is the supplied current (nA) and ' V ' is the corresponding voltage (mV). The conductivity (σ) is calculated using the expression $\sigma = 1/\rho$ [23].

Magneto-resistivity is investigated using a Helium Compressor (HC) (model HC-4E1) –sumitomo cryostat (model Ganis research CO, INC) equipped with 0.8T superconducting magnet (Lake shore electromagnet). Lake Shore 331 temperature controller is used. The measurement(s) are performed in the temperature range 77-300 K using a computer-controller measuring system.

Results and Discussion

XRD patterns for HCl doped PMMA/PANI composite, H₂SO₄ doped PMMA/PANI composite, and H₃PO₄ doped PMMA/PANI composite are shown in **Figure 1**. The PMMA film show a highly broaden peak, indicating their amorphous nature [24]. But, doped PMMA/PANI composites show certain peaks which is due to crystalline structure exhibit well defined crystalline peaks at 2θ of 22.4°, 30°, and 42°, respectively. It is also observed that the peak area is reduced and is slightly shifted to higher angle in the composites. Therefore, This may be happened due to the combined effect of polyaniline and presence of dopant (HCl or H₂SO₄ or H₃PO₄) with retaining PMMA structure [25].

The typical absorption peaks of PMMA film, PANI-ES and doped PMMA/PANI composites are shown in **Figure 2**. The bands of PMMA film are observed at 2965, 1751, 1626, 1221 cm^{-1} in the **Figure 2** [25]. It is attributed to C-H stretching, C=O stretching, C-O stretching of ester, and C-O-C stretching vibration respectively. The bands at 1448, 1364, 1358 cm^{-1} represent the stretching vibration of C-H deformation of PMMA film. The peaks at 1253, 1184, 1134, 1047 cm^{-1}

correspond to aliphatic $-C-H$ in plane bending of PMMA [25]. These indicate that the characteristic absorption features of PMMA film are retained in the prepared PMMA films. FTIR bands of PANI are found at 1554, 1475, 1108 cm^{-1} . This is corresponded to quinoid, benzenoid, and $C=N$ stretching respectively [25].

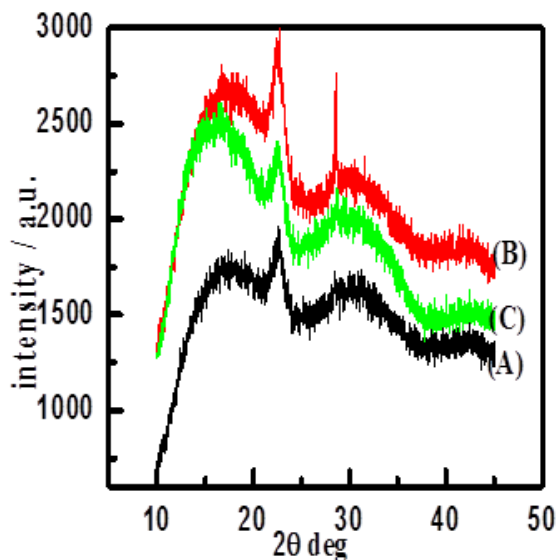


Figure 1. XRD pattern of HCl (A), H_2SO_4 (B), and H_3PO_4 (C) doped PMMA/PANI composites

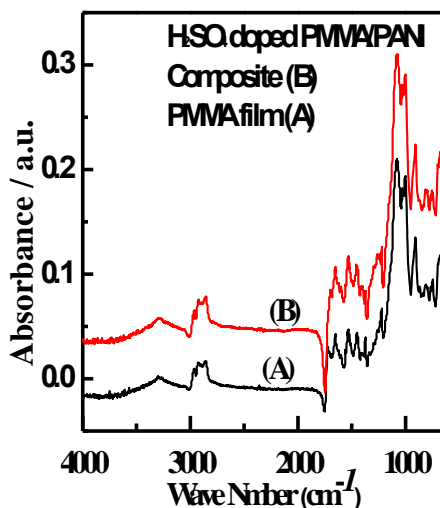


Figure 2. ATR-FTIR spectra of PMMA film (A) and H_2SO_4 doped PMMA/PANI-ES composites (B)

From our remark, spectrum of H₂SO₄ doped PMMA/PANI composites are exhibited the presence of quinoid and benzenoid ring vibrations at 1475, and 1554 cm⁻¹ respectively. This is indicated the occurrence of oxidation state of PANI [24]. This indicates the formation of conducting PMMA film.

In the literature, PANI shows different electronic transitions such as π - π^* of benzene ring, polaron to π^* , benzenoid to quinoid ring and polaron transition, respectively [26, 27]. No polaron transition is found in spectrum of PMMA film [24]. H₂SO₄ doped PMMA/PANI composite is conducted optical studies with the use of a UV-visible (UV-VIS) spectroscopic technique and is shown in **Figure 3**. Results show that the absorption of photon energy by organic molecules in the UV-VIS region caused an upward transition of electrons in the n, σ , and π orbitals. Various electronic transitions correspond to the different bands present in the samples. In **Fig. 3**, bands like π to localized polaron band of H₂SO₄ doped PMMA/PANI composite is observed. Polaron band is suggested to the presence of oxidation unit *i.e.*, formed emeraldine salt [26, 27]. Hence, electrons are delocalized in the excitation band [26, 27]

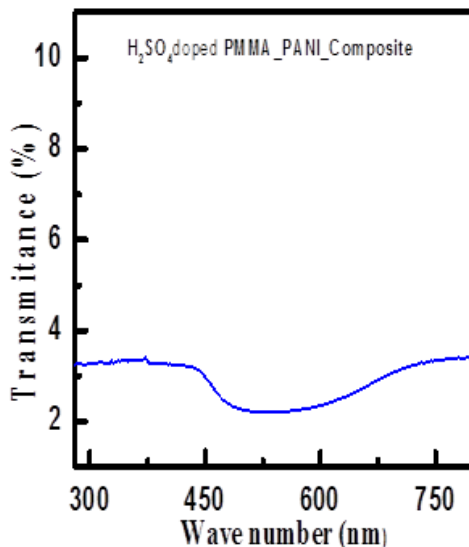


Figure 3. UV-Vis spectrum of H₂SO₄ doped PMMA/PANI composites

The photon absorption of organic semiconductor is observed by Tauc expression [28, 29].

$$(\alpha h\nu) = A (h\nu - E_g)^n \dots\dots\dots (1)$$

Where α = optical absorption co-efficient, $h\nu$ =photon energy, E_g =Energy gap calculated from graph, A = absorption constant, n = represents the type of transition occurs. If $m = 2$ indicated allowed indirect transitions and $m = 1/2$ indicated allowed direct transitions [28, 29].

$$A = \alpha bc = -\ln T \dots\dots\dots (2)$$

$$\alpha = -\ln T / bc \dots\dots\dots (3)$$

Substituting 'α' in equation (1),

Then, $[(-\ln T / bc) hv] = A (hv - E_g)^m$

$[(-\ln T) (hv)] = B(hv - E_g)^m$

Where;

b= thickness of samples

c=concentration of samples

T=transmittance

B=another constant.

Table 1 Direct and indirect band gap of doped PMMA/PANI Composites

Prepared materials name	Direct allowed band gap (eV)	Indirect allowed band gap (eV)
H ₂ SO ₄ doped PMMA_PANI_Composite	1.19	0.17
H ₃ PO ₄ _ doped PMMA_PANI_Composite	1.71	0.65
HCl_ doped PMMA_PANI_Composite	1.93	0.853

For direct transition can plot $(\alpha hv)^2$ vs hv, and extrapolate the linear portion of it to $\alpha=0$ value to obtained corresponding direct band gap. Similarly, the intercept of these curves on the photon energy axis (hv) gives the indirect band gap [28, 29]. The direct and indirect allowed transitions energies of three prepared composites are listed in **Table xxx**. To estimated direct band gap of doped PMMA/PANI (1M H₂SO₄), doped PMMA/PANI (1M H₃PO₄) and doped PMMA/PANI (1M HCl) are found to be 1.19 eV, 1.71 eV, and 1.93 eV respectively. The variations of band gap values are due to the incorporation of used dopants into the polymer chain. The dopants strength is in the order of HCl < H₃PO₄ < H₂SO₄. The lower strength dopant exerts less force against ordering and closing of the polymer chains leading to a lower density of states into the visible region [28, 29].

The morphologies of PMMA film and PMMA/PANI composite are evaluated with Raman spectrophotometer and is shown Figure 4. Figure 4A *i.e.*, morphologies of PMMA film shows different sizes speherical domains. Magnification of the image is 10X. The morphology of H₂SO₄ doped PMMA/PANI composite is indicated in Figure 4B with 10X magnification. H₂SO₄ doped PMMA/PANI composite is getting solid fibers or rods. This is happened due to reaction of H₂SO₄

dopants and polyaniline salt with PMMA films.

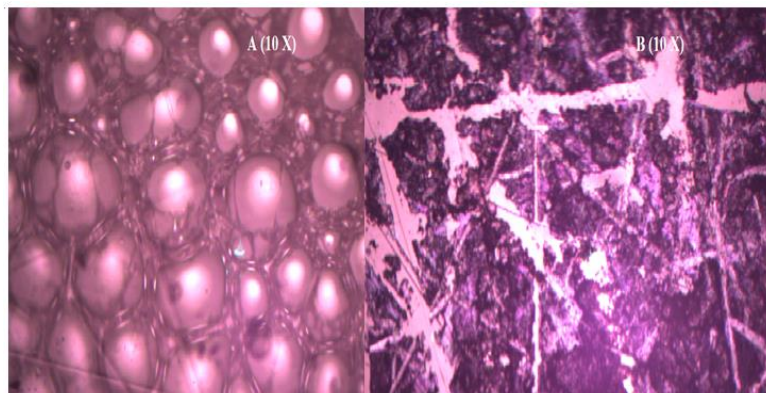


Figure 4. Image of PMMA flim (A) and H₂SO₄ doped PMMA/PANI Composite (B)

SEM images for pure PMMA polymer film and doped PMMA/PANI Composites are shown in Figure 1.

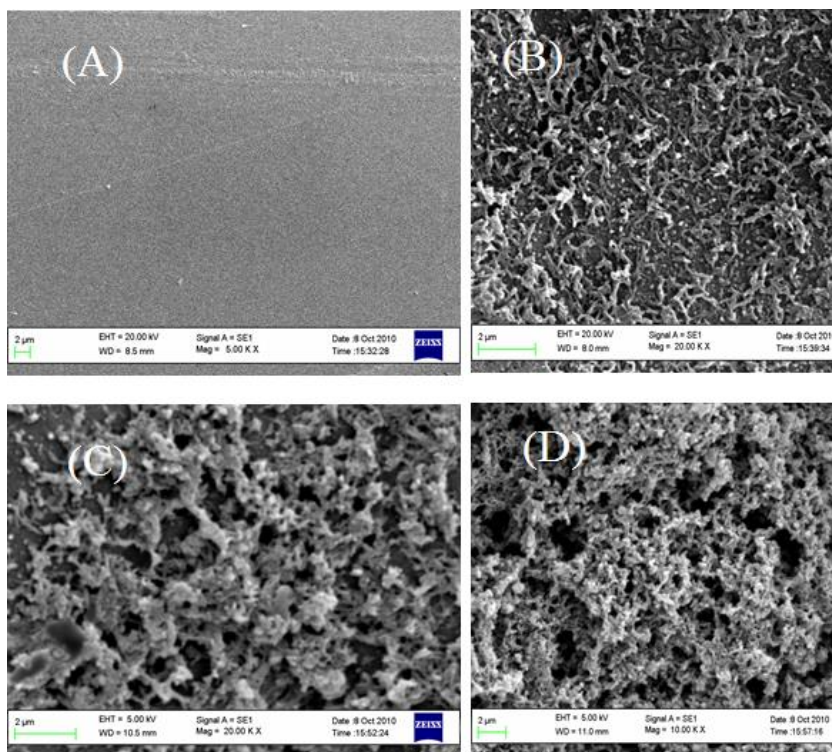
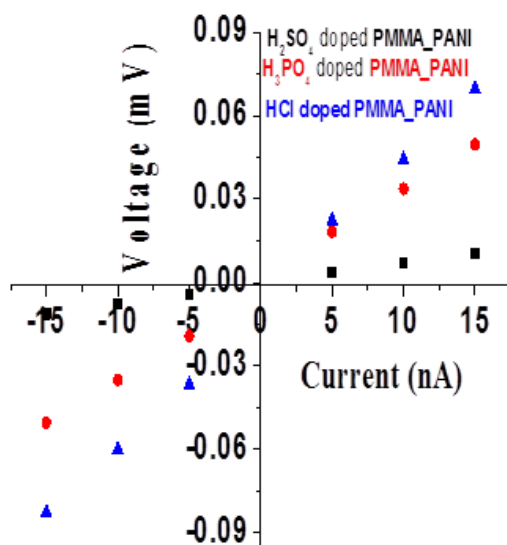


Figure 1 FESEM images of PMMA polymer film (A), 1 M HCl doped

PMMA PANI composite (B), 1 M H₃PO₄ doped PMMA PANI composite (C), and 1 M H₂SO₄ doped PMMA PANI composite (D)

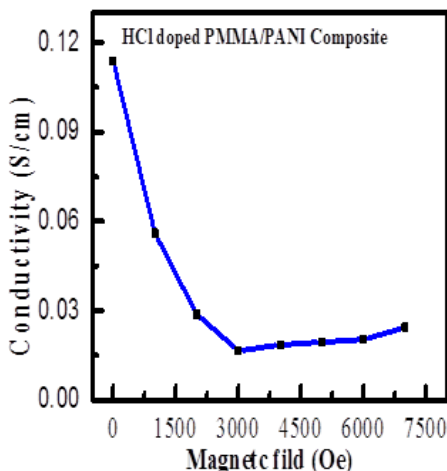
Smooth texture is observed in Fig.1A, whereas fibrous structures are showed in all doped PMMA/PANI Composites. Three dopants viz., HCl, H₂SO₄ and H₃PO₄ are used to prepare doped PMMA/PANI Composites. It is also found that size and formation probability of PANI is strongly dependent on dopant strength, structure and reaction conditions. Moreover, the diameter size of PANI nano-fibrous is affected by dopant structure. Average (av.) diameters of PMMA/PANI composites are found to be 178 nm, 152 nm, and 165 nm, respectively. The diameter is related to aspect ratio *i.e.*, surface area/volume. The surface area of nanofibers increases as the average diameter of nanofibers decreases. it could be important, particularly for gas sensor application.

The plot of room temperature DC-conductivity of HCl-, H₂SO₄- and H₃PO₄-doped PMMA/PANI composites are shown in **Figure 5**. It is observed from the **Figure 5**; the voltage (mV) is linearly related with current (nA) and passes through origin, indicating that the ohmic behaviour. The conductivity of prepared conductive composite is presented in Table 1, it is clear from the Table, the conductivity of H₂SO₄-doped PMMA/PANI composite showed 0.1497×10^{-2} S/cm at 0 Tesla which is higher than other two as-prepared doped PMMA/PANI composite at 0 tesla. This is due to higher strength dopant. The higher strength dopants exert less force against ordering and closing of polymer chains leading to higher compactness of polymer chains. The compactness is a favorable factor for intramolecular mobility of charged species along the chain and some extent inter molecular hopping because of better and closer packing and hence, higher conductivity than the later one [8]. Also, The DC conductivity is observed for H₂SO₄-doped PMMA/PANI composite (0.1421×10^{-2} S/cm) at 0.4 tesla.



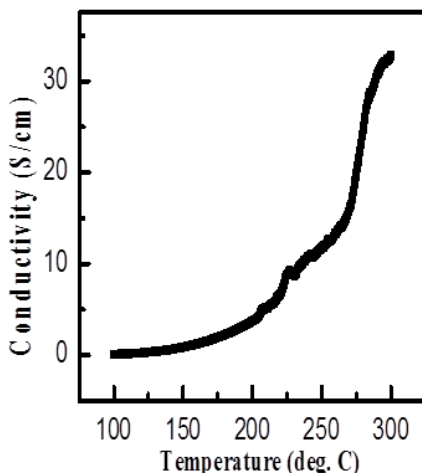
Figurer 5 DC conductivity of HCl (A), H₂SO₄ (B), and H₃PO₄ (C) doped PMMA/PANI composites measured at room temperature without magnetic field

The plot of room temperature DC-conductivity with magnetic field (from 0 Oe to 7500 Oe) of HCl-doped PMMA/PANI composites is shown in **Figure 6**. It is observed from the **Figure 6** that the DC conductivity decreases with increase in magnetic field. This is due to electron-scattering mechanisms of the composite [31].



Figurer 6. DC conductivity of HCl doped PMMA/PANI composites measured at room temperature with magnetic field

Figure 7 indicates temperature variation DC conductivity of HCl doped PMMA/PANI composite. It is evident from the **Figure 7**, DC conductivity of composite increases with increase in temperature.



Figurer 7. Temperature dependent DC conductivity of HCl doped PMMA/PANI composites measured at 0 Oe magnetic field

It means that prepared conductive composite represent a temperature dependent conductivity, which is similar behaviour to a inorganic semiconductor. Henceforth, it is termed as organic semiconductor [8].

Response of Ammonia (Nh3) Gas

Monitoring of ammonia gases is a vital issue in the environment due to their high toxic nature of the gas. The toxicity limit of ammonia for human exposure is found to be 25 ppm for 8 h [31]. Traditional method for detecting ammonia gas by chemical analysis is a time-consuming and complicated process. This method is not suitable for analyzing the NH_3 gas. Hence, there is an increasing mandate for a sensor, which has fast, non-destructive and reliable. Metal oxide based sensors such as SnO_2 or Fe_2O_3 are sensitive to detect low levels of concentration. The operation of sensors requires high temperatures, which increases cost and complexity of these devices [32]. Researchers put their effect to discover monitoring system, which is operated at ambient temperature. The new type of sensor materials are conducting polymer based materials and it is operated at room temperature [33] at lower concentration level.

Conducting polymers are a new class of sensors material due to their diversity, ease of synthesis, doping/de-doping behaviour and sensitivity at ambient temperature [34-36]. The gas sensor performance of a conducting polymer based sensor materials is depended on electrical or optical properties. The changes of electrical properties are directly related to the adsorption of analytes concentration at ppm levels on sensor materials surface [37, 38]. Some reports on specificity and sensitivity of conducting polymer based sensors are available even at low concentration (ppm) of analytes gases. It is achieved either by incorporating functional groups or doping to the main chain of conducting polymer [39, 40]. A few works are reported on the ammonia gas sensing of polyaniline, polypyrrole, Polythiophene and their composites [41-43]. Conducting polymer films devices have been used to sense ammonia gas in the range of 10–5000 ppm concentration. Sensor characteristics such as fast response, rapid recovery and detection at low concentration level i.e., ppm level are still key concerns to commercialize the conducting polymer-based sensor. Conducting polymer thin films based sensor materials are projected to give better response and recovery than conducting polymer based sensor. The schematic diagram of possible ammonia sensing mechanism is shown in Figure 8.

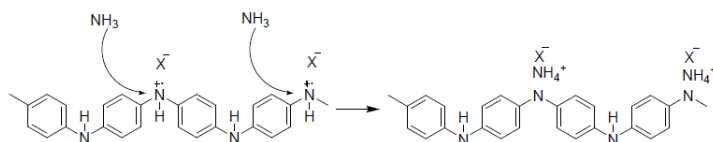


Figure 8. Possible polyaniline with ammonia sensor mechanism [44]

Particularly, polyaniline is one of the conducting polymer families. It is controlled by acid/base reactions in doped state. Therefore, polyaniline is extensively used to detect acidic and basic gases. When exposed ammonia gas on polyaniline, it undergoes dedoping by deprotonation [45-50]. The protons on –NH– groups of polyaniline backbone are transferred to NH₃ molecules and formed ammonium ions. Polyaniline itself formed base. The process is reversible. When ammonia atmosphere is removed, the ammonium ion can be decomposed to ammonia gas and proton.

The extent of response and rapid recovery is dependent on the methods used to prepare thin film. Ultra-thin films of conducting polymers have very high aspect ratio. It can allow the gas molecules on the film surface to produce large and rapid change of the chemical or physical properties, which is leading to enhance sensitivity of the device [51].

Table 2. Brief summary of CO detection

Study	Materials	Perporfamce	Optimum temperature	Limitation
Yadav et al. [54]	PANI-DBSA	Response time 329 s	Room temperature	Contact potential suddenly increased
Lv et al.[55]	PSS-PANI/PVDF composite	Response 70%	Room temperature	Low NH ₃ concentration
Sutar et al. [56]	Polyaniline nanofiber	Response time 1-5 s	Room temperature	Low NH ₃ concentration
Crowley et al.[57]	polyaniline nanoparticles	Response 15 s	Room temperature	Humidity dependency Humidity dependency and conductivity decreases on exposing ammonia gas
Matsuguchi et al. [58]	PANI–PMMA blend film	RH 68%	Room temperature	High concentration of NH ₃ gas (600 ppm)
Matsuguchi et al.[59]	PANI–PMMA blend film		Room temperature	High concentration of NH ₃ gas (500 ppm)
Deshpande et al.[60]	Polyaniline SnO ₂ nanocomposite	Response 37%	Room temperature	

Tai et al.[61]	PANI/TiO ₂ thin film	Room temperature	High concentration of NH ₃ gas (2500 ppm)
----------------	---------------------------------	------------------	--

In this perspective, one of the thin film technologies is Langmuir–Blodgett technique. It can be used to produce very regular multilayers, and well-defined molecular orientation [52, 53]. The sensor materials fabricated using this technique is expected to have higher sensitivity, faster response time and good reproducibility. The brief summary carbon monoxide detection is presented in Table 2.

Fig. 9 shows the relative response of a typical material as a function of NH₃ concentration. Relative response is estimated using $(R-R_0)/R_0$, where R_0 is the initial resistance in the absence of NH₃ and R is the saturation value of resistance measured on exposure to gas. It is saturate at higher concentrations. This is due to the availability of a limited number of reactive species in the layer of sensing materials. The fast response is accredited to high aspect ratio, which is offered by nanofibrous morphology. Hence, nanostructures help to easy diffusion of NH₃ gas. The different ammonia concentration exposure vs time of polyaniline based martials is shown in Figure 9.

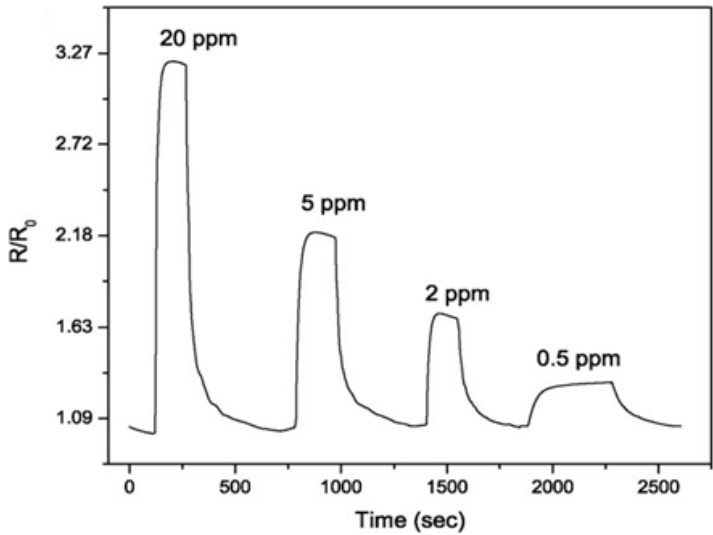


Figure 9. Plot of different ammonia concentration exposure vs time of polyaniline based martials [56]

Conclusions

PMMA/PANI composite films are prepared by *insitu* polymerization technique. HCl, H₂SO₄, and H₃PO₄ are used dopants, separately, during the

polymerization reaction. Different desired chemical groups of PMMA film, PANI and PMMA/PANI composites are confirmed from ATR-FTIR spectroscopy. Polaron band is shown in UV-Visible data and are confirmed the formation of emeraldine salt (ES). A drastic increment of band gap of the doped samples is found. I-V characteristics without magnetic field of doped PMMA/PANI composites are revealed ohmic behaviour at room temperature. Highest DC conductivity without magnetic field is found to be 0.1421×10^{-2} S/cm for H₂SO₄ doped PMMA/PANI composite. Decreased DC conductivity data with increased magnetic field is observed. Temperature dependent DC conductivity data of HCl doped composite is indicated the semiconducting behaviour. In particulars, ammonia gas responses and mechanism of polyaniline-based materials are discussed.

Acknowledgments

The author conveys their sincere thanks to the CRF, IIT Kharagpur for their providing testing facilities and Materials Science Centre to do the research work.

References

- [1] Burroughes, J.H., Bradley, D.D.C., Brown, A.R., Marks, R.N., Mackay, K., Friend, R.H., Burns, P.L., and Holmes, A.B. 1990, Light-emitting Diodes Based on Conjugated Polymers, *Nature*, Vol. 347, pp. 539-541.
- [2] Frackowiak, E., Khomenko, V., Jurewicz, K., Lota, K., and Beguin, F. 2006, Supercapacitors Based on Conducting Polymers/Nanotubes Composites, *Journal of Power Sources*, Vol. 153, pp. 413-418.
- [3] Conn, C., Sestak, S., Baker, A.T., and Unsworth, J. 1998, A Polyaniline-Based Selective Hydrogen Sensor, *Electroanalysis*, Vol. 10, pp. 1137-1141.
- [4] Abdelkader, R., Amine, H., and Mohammed, B. 2012, Thermally Stable Forms of Pure Polyaniline Catalyzed by Acid-exchanged Montmorillonite Clay called Maghnite-H⁺ as an Effective Catalyst, *International Journal of polymer science*, Vol. 2012, pp. 1-7.
- [5] Yang, S. and Ruckenstein, E. 1993, Processable Conductive Composites of Polyaniline/Poly (alkyl methacrylate) Prepared via an Emulsion Method, *Synthetic Metals*, Vol. 59, pp. 1-12.
- [6] Singh, V., Mohan, S., Singh, G., Pandey, P.C., and Prakash, R. 2008, Synthesis and Characterization of Polyaniline-carboxylated PVC Composites: Application in Development of Ammonia Sensor, *Sensors and Actuators B: Chemical* Vol. 132, pp. 99-106.
- [7] Spirkova, M., Stejskal, J., and Quadrat, O. 1999, Electrically Anisotropic Polyaniline-Polyurethane Composites, *Synthetic Metals*, Vol. 102, pp. 1264-1265.

- [8] Panigrahi, M.K., Majumdar, S.B., and Adhikari, B. 2011, H₃PO₄-doped DL-PLA/PANI composite for Methane gas sensing", IEEE explorer, Vol. 97, pp. 1-7. ISBN: 978-1-4577-2035-2, 8-10 Dec. 2011, Nanoscience, Technology and Societal Implications (NSTSI), 2011 International Conference.2011, Vol. 97 (12), pp. 1-7.
- [9] Kumar, A., Jangir, L.K., Kumari, Y., Kumar, M., Kumar, V., and Awasthi, K., 2015, Optical and Structural Study of Polyaniline/Polystyrene Composite Films, Macromolecular symposia (Special Issue: Soft Materials.), Vol. 357, pp 229-234.
- [10] Gu, L., Zhao, X., Tong, X., Ma, J., Chen, B., Liu, S., Zhao, H., Yu, H., and Chen, J. 2016, Facile Preparation of Polyaniline Nanoparticles and Their Dispersion for Waterborne Anticorrosion Coatings, International Journal of Electrochemical Science, Vol. 11, pp. 1621-1631.
- [11] Shi, G., Rouabhia, M., Wang, Z., Dao, L.H., and Zhang, Z. 2004, A Novel Electrically Conductive and Biodegradable Composite Made of Polypyrrole Nanoparticles and Polylactide, Biomaterials, Vol. 25, pp. 2477-88.
- [12] Ruiz, J., Gonzalo, B., Dios, J.R., Laza, J.M., Vilas, J.L., and León, L.M. 2013, Improving the Processability of Conductive Polymers: The Case of Polyaniline, Advances in polymer Technology, Vol. 32, pp. 180-188.
- [13] Pozo-Gonzalo, C., Mecerreyes, D., Pomposo, J.A., Salsamendi, M., Marcilla, R., Grande, H., Vergaz, R., Barrios, D., and Sánchez-Pena, J.M., 2008, All-Plastic Electrochromic Devices based on PEDOT as Switchable Optical Attenuator in the Near IR, Solar Energy Materials: Solar Cells, Vol. 92, pp. 101-106.
- [14] Nguyen, T., Rendu, P. Le, Long, P., and Vos, S. De 2004, Chemical and Thermal Treatment of PEDOT: PSS Thin Films for Use in Organic Light Emitting Diodes, Surface Coating Technology, Vol. 180-181, pp. 646-649.
- [15] Hu, Z., Zhang, J., and Zhu, Y.2014, Effects of Solvent-Treated PEDOT:PSS on Organic Photovoltaic Devices, Renewable Energy, Vol. 62, pp. 100-105.
- [16] Bernards, D., Macaya, D., Nikolou, M., Defranco, J., Takamatsu, S., and Malliaras, G. 2008, Enzymatic Sensing with Organic Electrochemical Transistors, Journal of Materials Chemistry, Vol. 18, pp.116-120.
- [17] Li, J., Fang, K., Qiu, H., Li, S., and Mao, W. 2004, Micromorphology and Electrical Property of the HCl-Doped and DBSA-Doped Polyaniline, Synthetic Metals, Vol. 142, pp. 107-111.
- [18] Kapil, A., Taunk, M., and Chand, S. 2010, Preparation and Charge Transport Studies of Chemically Synthesized Polyaniline, Journal of Materials Science: Materials in Electronics, Vol. 21, pp. 399-404.

- [19] Bohli, N. Gmati, F., Mohamed, A.B., Vigneras, V., and Miane, J.-L. 2009, Conductivity Mechanism of Polyaniline Organic Films: The Effects of Solvent type and Casting Temperature, *Journal of Physics D Applied Physics*, Vol. 42, pp. 205404-xxx.
- [20] Long, Y.Z. Yin, Z.H., and Chen, Z.J. 2008, Low-Temperature Magnetoresistance Studies on Composite Films of Conducting Polymer and Multiwalled Carbon Nanotubes, *Journal of Physical Chemistry C*, Vol. 112, pp. 11507-11512.
- [21] Patil, A.O., Heeger, A.J., and Wudl, F. 1988, Optical Properties of Conducting Polymers, *Chemistry of Reviews*, Vol. 88, pp. 183-200.
- [22] Joshi, D.N., Atchuta, S.R., Reddy, L., Kumar, Y.N., and Sakthivel, A. 2019, Super-Hydrophilic Broadband Anti-reflective Coating with High Weather Stability for Solar and Optical Applications, *Solar Energy Materials and Solar Cells*, Vol. 200, pp. 110023-xxx.
- [23] Panigrahi, M.K. 2021, Investigation of Dc-Conductivity and Morphology of PMMA/PANI Composite, *International Research Journal of multidisciplinary Technovation*, Vol. 3, pp. 49-53.
- [24] Shobhana, E. 2012, X-Ray Diffraction and UV-Visible Studies of PMMA Thin Films, *International Journal of Modern Engineering Research (IJMER)*, Vol.2, pp-1092-1095.
- [25] Tomara, A.K., Mahendi, S., and Kumar, S. 2011, Structural Characterization of PMMA Blended with Chemically Synthesized PANi, *Advances in Applied Science Research*, Vol. 2, pp. 327-333.
- [26] Patricia L.B. Araujo, Katia A.S. Aquino, Elmo S. Araujo, (2007), Effects of Gamma Irradiation on PMMA/Polyaniline Nanofibre Composites, *Raman, International Journal of Low Radiation*, Vol. 4, pp. 149-160.
- [27] K.A. Ibrahim, (2017), Synthesis and Characterization of Polyaniline and Poly(aniline-co-o-Nitroaniline) using Vibrational Spectroscopy, *Arabian Journal of Chemistry*, Vol. 10, pp. 2668-2674.
- [28] Salma M. Hassan, (2013), Optical Properties of Prepared Polyaniline and Polymethylmethacrylate blends, *International Journal of Application or Innovation in Engineering & Management (IJAIEEM)*, Vol. 2, pp. 19-22.
- [29] S. H. Deshmukh, D.K. Burghate, S.N. shilaskar, G.N. Chaudhan, P.T. Deshmikh, (2008), Optical Properties of Polyaniline Doped PVC-PMMA Thin Film, *Indian Journal of pure & applied physics*, Vol. 46, pp.344-348.
- [30] D. Farka, Andrew O.F. Jones, R. Menon, N. S. Sariciftci, P. Stadler, (2018), Metallic Conductivity Beyond the Mott Minimum in PEDOT: Sulphate at Low Temperatures, *Synthetic Metals*, Vol. 240, pp.59-66.
- [31] Timmer, B., Olthuis, W., and Van den Berg, A. Ammonia Sensors and Their

- Applications-A Review, 2005, Sensor and Actuators B: Chem., Vol. 107, pp. 666-677.
- [32] Dubbe, A. 2003, Fundamentals of Solid State Ionic Micro Gas Sensor, Sensor and Actuators B: Chemical, Vol. 88, pp. 138-148.
- [33] Mount, G.H., Rumburg, B., Havig, J., Lamb, B., Westberg, H., Yonge, D., Johnson, K., and Kincaid, R. 2002, Measurement of Atmospheric Ammonia at a Dairy using Differential Optical Absorption Spectroscopy in the Mid-Ultraviolet, Atmospheric Environment, Vol. 36, pp. 1799-1810.
- [34] Bidan, G. 1992, Electroconducting Conjugated Polymers: New Sensitive Matrices to Build up Chemical or Electrochemical Sensors – A Review, Sensor and Actuators B, Vol. 6, pp. 45-46.
- [35] de Lacy Costello, B.P.J., Evans, P., Guernion, N., Ratcliffe, N.M., Sivanand, P.S., and Teare, G.C. 2000, The Synthesis of a Number of 3-Alkyl and 3-Carboxy Substituted Pyrroles; Their Chemical Polymerisation onto Poly(Vinylidene Fluoride) Membranes, and Their Use as Gas Sensitive Resistors, Synthetic Metals, Vol. 114, pp. 181-188.
- [36] Riul Jr., A., Soto, A.M.G., Mello, S.V., Bone, S., Taylor, D.M., and Mattoso, L.H.C. 2003, An Electronic Tongue using Polypyrrole and Polyaniline, Synthetic Metals, Vol. 132, pp. 109-116.
- [37] Guernion, N., Ewen, R.J., Pihlainen, K., Ratcliffe, N.M., and Teare, G.C. 2002, The Fabrication and Characterization of a Highly Sensitive Polypyrrole Sensor and its Electrical Response to Amines of Differing Basicity at High Humidities, Synthetic Metals, Vol. 126, pp. 301-310.
- [38] Penza, M., Milella, E., Alba, M.B., Quirini, A., and Vasanelli, L. 1997, Selective NH₃ Gas Sensor based on Langmuir–Blodgett Polypyrrole Film, Sensor and Actuators B, Vol. 40, pp. 205-209.
- [39] Anitha, G., and Subramanian, E. 2003, Dopant Induced Specificity in Sensor Behaviour of Conducting Polyaniline Materials with Organic Solvents, Sensor and Actuators, Vol. 92, (2003) pp. 49-59.
- [40] Sakurai, Y., Jung, H.-S., Shimanouchi, T., Inoguchi, T., Morita, S., Kuboi, R., and Natsukuwa, K. 2002, Novel Array-Type Gas Sensors using Conducting polymers, and Their Performance for Gas Identification, Sensor and Actuators B, Vol. 83, pp. 270-275.
- [41] Lin, C.W., Hwang, B.J., and Lee, C.R. 1999, Sensing Behaviors of the Electrochemically Co-Deposited Polypyrrole-Poly(Vinylalcohol) Thin Film Exposed to Ammonia Gas, Materials Chemistry and Physics, Vol. 58, pp. 114-120.
- [42] Lee, Y.-S., Joo, B.-S., Choi, N.-J., Lim, J.-O., Huh, J.-S., and Lee, D.-D. 2003, Visible Optical Sensing of Ammonia based on Polyaniline Film,

Sensor and Actuators B, Vol. 93, pp. 148-152.

- [43] Rella, R., Siciliano, P., Quaranta, F., Primo, T., Valli, L., and Schenetti, L., 2002, Poly[3-(butylthio)thiophene] Langmuir–Blodgett Films as Selective Solid State Chemiresistors for Nitrogen Dioxide, *Colloids Surface A: Physicochemical Engineering Aspects*, Vol. 198, pp. 829-833.
- [44] Bai H., and Shi, G. 2007, Review Gas Sensors Based on Conducting Polymers, *Sensors*, Vol. 7, pp. 267-307.
- [45] Jin, Z., Su, Y.X., and Duan, Y.X. 2001, Development of a Polyaniline-based Optical Ammonia Sensor, *Sensor and Actuators B*, Vol. 72, pp. 75-79.
- [46] Nicho, M.E., Trejo, M., Garcia-Valenzuela, A., Saniger, J.M., Palacios, J., and Hu, H. 2001, Polyaniline Composite Coatings Interrogated by a Nulling Optical-Transmittance Bridge for Sensing Low Concentrations of Ammonia Gas, *Sensor and Actuators B*, Vol. 76, pp. 18-24.
- [47] Hu, H. Trejo, M., Nicho, M.E., Saniger, J.M., and Garcia-Valenzuela, A. 2002, Adsorption Kinetics of Optochemical NH₃ Gas Sensing with Semiconductor Polyaniline Films, *Sensor and Actuators B* Vol. 82, pp. 14-23.
- [48] Bekyarova, E., Davis, M., Burch, T., Itkis, M.E., Zhao, B., Sunshine, S., and Haddon, R.C. 2004, Chemically Functionalized Single-Walled Carbon Nanotubes as Ammonia Sensors, *Journal of Physical Chemistry B*, Vol. 108, pp. 19717-19720.
- [49] Hong, K.H., Oh, K.W., and Kang, T.J. 2004, Polyaniline-Nylon-6 Composite Fabric for Ammonia Gas Sensor, *Journal of Applied Polymer Science*, Vol. 92, pp. 37-42.
- [50] Liu, H.Q., Kameoka, J., Czaplewski, D.A., and Craighead, H.G. 2004, Polymeric Nanowire Chemical Sensor, *Nano Letter*, Vol. 4, pp. 671-675.
- [51] Honey Bourne, C.L., 1987, Solid Thin Films of Extended--Systems: Deposition, Characterization and Application, *Journal of Physics and Chemistry of Solids*, Vol. 48, pp. 109-141.
- [52] Liang, B., Yuan, C., and Wei, Y., 1997, Semiconducting, Gas Sensing Properties of Europium Bisphthalocyanine Langmuir–Blodgett Thin Films, *Journal of Vacuum Science & Technology B* Vol. 15, pp. 1432-1436.
- [53] Riul Jr., A., Mattoso, L.H.C., Melo, S.V., Telles, G.D., and Oliveria Jr., O.N., 1995, Langmuir and Langmuir–Blodgett Films of Parent Polyaniline Doped with Functionalized Acids, *Synthetic Metals*, Vol. 71, pp. 2067-2068.
- [54] Yadav, A., Agarwal, A., Agarwal, P.B., and Saini, P., 2015, Ammonia Sensing by PANI-DBSA Based Gas Sensor Exploiting Kelvin Probe Technique, *Journal of Nanoparticles* Vol. 2015, pp. 1-6.

- [55] Lv, D., Wenfeng D.L., Chen, S.W., Tan, R., Xu, L., and Song, W. 2021, PSS-PANI/PVDF Composite based Flexible nh Sensors with Sub-ppm Detection at Room Temperature, *Sensors and Actuators B: Chemical*, Vol. 328, pp. 129085-xxx.
- [56] Sutar, D.S., Padma, N., Aswal, D.K., Deshpande, S.K., Gupta, S.K., and Yakhmi, J.V., 2007, Preparation of Nanofibrous Polyaniline Films and Their Application as Ammonia Gas Sensor, *Sensors and Actuators B*, Vol. 128, pp. 286-292.
- [57] Crowley, K., Morrin, A., Hernandez, A., Malley, E.O., Whitten, P.G., Wallace, G.G., Smyth, M.R., and Killard, A.J. 2008, Fabrication of an Ammonia Gas Sensor using Inkjet-Printed Polyaniline Nanoparticles, *Talanta*, Vol. 77, pp. 710-717.
- [58] Matsuguchi, M., Io, J., Sugiyama, G., Sakai, Y. 2002, Effect of NH₃ Gas on the Electrical Conductivity of Polyaniline Blend Films, *Synthetic Metals*, Vol. 128, pp. 15-19.
- [59] Matsuguchi, M., Okamoto, A., Sakai, Y. 2003, Effect of Humidity on NH₃ Gas Sensitivity of Polyaniline Blend Films, *Sensors and Actuators B*, Vol. 94, pp. 46-52.
- [60] Deshpande, N.G., Gudage, Y.G., Sharma, R., Vyas, J.C., Kim, J.B., and Lee, Y.P. 2009, Studies on Tin Oxide-Intercalated Polyaniline Nanocomposite for Ammonia Gas Sensing Applications, *Sensors and Actuators B*, Vol. 138, pp. 76-84.
- [61] Tai, H., Jiang, Y., Xie, G., Yu, J., Chen, X., and Ying, Z. 2008, Influence of Polymerization Temperature on NH₃ Response of PANI/TiO₂ Thin Film Gas Sensor, *Sensors and Actuators B*, Vol. 129, pp. 319-326.

Chapter 7

Inorganic Doped DL-Polylactide Polyaniline Based Composite for Methane (CH₄) Gas Sensing

Muktikanta Panigrahi ^{1,*}, Basudam Adhikari ¹

¹ Materials Science Centre, Indian Institute of Technology, Kharagpur, West Bengal, India

*Corresponding author: muktikanta2@gmail.com

Abstract

Polyaniline (PANI) nonofibriles have been successfully synthesised by simple chemical-oxidation polymerization method using aniline as a predecessor at room temperature. It was synthesized using H₃PO₄ dopants. The structure, chemical groups, and electronic transition were investigated by SEM, FTIR, and UV Visible. We present the methane gas response of as-prepared H₃PO₄ doped DL-PLA/PANI-ES composite film at different concentration. The percentage (%) methane gas response was found to be 9 % at 500ppm.

Keywords: Polyaniline, Polylactide, Doping, Composite, Methane gas sensing

Introduction

Methane is the chief constituent of natural gas which is hazardous for both human and environment. Due to its highly flammable and explosive characteristics, even at low level (5–14%) concentration poses a serious threat. With the global population boom, more and more human lives are being endangered by the effect of CH₄ gas exposure [1]. That creates a demand for monitoring CH₄ gas for making the safety environments in homes, industries and mines. It is in great need of development of sensors for detecting methane gas quickly and accurately in the coal mine at ambient condition. Generally, metal oxide-based gas sensors such as ZnO [2], MoO₃ [3], SnO₂ [4], TiO₂ [5], ZrO₂ [6], spinel compounds [7] etc. have been used. All the above sensors require high temperature for sensor operation, which is expensive. Researchers have put their effort for making room temperature-based sensors. In spite of considerable efforts, room temperature-based sensors for CH₄ gas sensing has not been found hitherto, the problem being of vital to industry as well as general public.

© IOR INTERNATIONAL PRESS, 2021

Muktikanta Panigrahi, Basudam Adhikari, *Inorganic Doped DL-Polylactide Polyaniline Based Composite for Methane (CH₄) Gas Sensing*,

<https://doi.org/10.34256/ioriip2127>

To meet this demand, a new class of sensor materials is underway, including efforts to prepare the sensor, such as conducting polymer based sensor, which can work at ambient condition. In the conducting polymer family, PANI is one of the members with good environmental and thermal stability coupled with ease of processability [8] and doping-dedoping features [9]. In spite of above advantages, PANI film is brittle and highly moisture sensitive. This is due to the ionic electroactive nature of PANI polymer and it makes the limits for commercial applications. The stability of PANI polymer can be improved by making in composite with thermoplastic polymer such as poly (methyl methacrylate) (PMMA), polyvinyl chloride (PVC), polystyrene (PS), and polyurethane (PU) as stabilizer [10–13]. The stability of PANI polymer could be enhanced by covalently grafting with polymers [14,15]. We selected DL-PLA polymer in the composite preparation because of its strong interaction with ionic electroactive polymer such as PANI polymer. This interaction can change potentially the surface properties such as surface charge, wettability, conformational and dimensional changes on bioactive materials. Despite of all above mentioned properties, one of the most important issues related to the applications of biodegradable polymer in electronic engineering is to reduce the degradation of conducting polymers. There are some reports on the use of PLA with multiwalled carbon nanotubes (MWCNT) [16], conducting polymers such as PANI [17], and polypyrrole [18] to form composites. That showed improved surface resistance/conductivity properties compared with neat one. Therefore, the use of biodegradable polymer with conductive polymers is a very important and challenging task. Our goal was to prepare an environmental stable PANI composite having better electrical properties for sensor and other electronic applications.

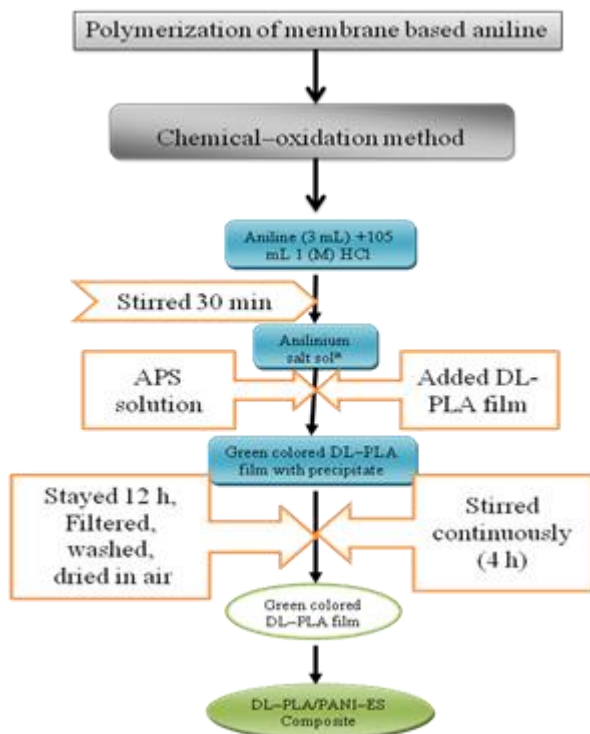
In this chapter, we have reported the methane gas sensing characteristics of H₃PO₄ doped DL-PLA/PANI-ES composite. Such characteristics of H₃PO₄ doped DL-PLA/PANI-ES composite we have demonstrated first time to achieve CH₄ gas response at room temperature.

Experimental Details

At first, DL-PLA films were prepared by solution casting technique. During the DL—PLA preparation, DL-PLA and CHCl₃ were used as polymer and solvent, respectively. 2 g DL-PLA was put to 20 mL of CHCl₃ in a 100 mL beaker. It is continuously stirred for 3 h at room temperature. The transparent soluble product was poured into a petridish having diameter 10 cm. It is left in air for the solvent evaporation. After solvent evaporation, DL-PLA film formed. The films removed from petridish and cut into small pieces, which are used for their characterizations and preparation of composites.

Room temperature H₃PO₄ doped DL-PLA/PANI-ES composites was prepared by *in situ* technique through chemical oxidation polymerization method. During the composite preparation, aniline and DL-PLA film (1 cm²) was taken as monomer and base material, respectively. In this composite preparation, 3 mL of aniline was added to 105 mL of aqueous 1 M H₃PO₄ solution. The solution was stirred

continuously for 0.5 h and slightly yellowish solution (**Solution 1**) was obtained. Then a DL-PLA film (1 cm²) was put into solution 1. It is also stirred continuously for 12 h. **Solution 2** was prepared by adding 7.47 g of ammonium perdisulphate (APS) in 60 mL of 1 M H₃PO₄. Then **solution 2** was added drop wise to the DL-PLA mixed solution 1 for 1 h for the polymerization to occur. The color of DL-PLA film was observed to change from white to light green and finally to dark green as polymerization continue to proceed. The reaction mixture was maintained under constant stirring for 10 h to complete the polymerization. The resulting H₃PO₄ doped DL-PLA/PANI-ES composite was finally washed with deionised water several times and dried in the ambient atmosphere [19]. The flow chart of preparation of HCl doped DL-PLA/PANI-ES composites is shown in **Scheme 1**.



Scheme 1. The flow chart of preparation of H₃PO₄ doped DL-PLA/PANI-ES composite

Characterization Techniques

Surface morphologies of DL-PLA film and H₃PO₄ doped DL-PLA/PANI composites were analyzed using scanning electron microscope (SEM, Carl Zeiss Supra 40). Samples were needed gold coating before start SEM measurements.

In ATR-FTIR analysis, DL-PLA film and H₃PO₄ doped DL-PLA/PANI

composites were characterized by Thermo Nicolet Nexus 870 spectrophotometer in the range 400–4000 cm⁻¹.

The prepared material in the UV–Visible region was studied by UV–Visible (Micropack UV–VIS–NIR, DH 2000) spectroscopy.

For gas sensing studies, the prepared doped composite film (~25 °C) was taken. For this measurement, the surface of the material is electroded with silver paste strip of 8 mm length, 1.5 mm width, and separated from each other by 4 mm. The methane gas sensing behaviour was estimated by measuring the resistance change before and after gas exposure. This measurement was done using The CH₄ gas sensing performances of these materials are characterized by DC resistance measurements. From this measurement, the response (S) is estimated through the resistance change between air (R_a) and in test gas environment (R_g), using the following relations [19]:

$$\text{Response (\%)} = \frac{R_a - R_g}{R_a} \times 100$$

Results and Discussion

Figure 1 shows SEM images of DL–PLA film (A) and H₃PO₄ doped DL–PLA composite (B). In Figure 1 (a), it is observed that no nanowires were deposited on DL–PLA film at room temperature. Smooth surface was observed for neat DL–PLA film. H₃PO₄ doped composite film [Figure 1 (b)] indicates fibrous-like morphology. The diameter of the fibre was found in nano regimes. The nanofiber appears to be non-uniform as distributed over the DL–PLA film. The average diameter was estimated and was 131 nm. This might occur after establishing the polymerization reaction. Because of high surface area of polyaniline, it is favorable for the sensor application.

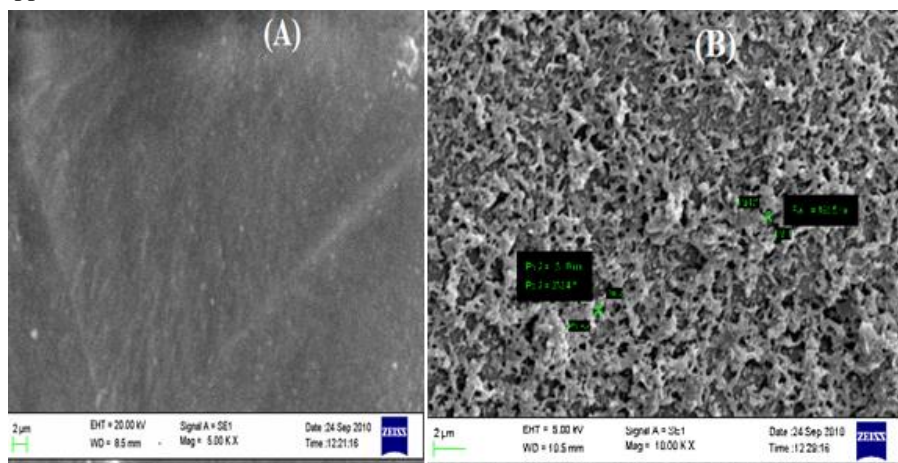


Figure 1. SEM image of DL-PLA film (A) and H₃PO₄ doped DL-PLA/PANI Composite (B) [19]

ATR-FTIR spectra of DL-PLA, H₃PO₄ doped PANI composite were shown in Figure 2. The absorption band position(s) and its assignments of as two materials such as DL-PLA, H₃PO₄ doped PANI composite were specified in Table 1. Absorption bands of DL-PLA was found at 2995, 1759, 1616 and 1216 cm⁻¹ and have been attributed to C-H stretching, C=O stretching, C-O stretching of ester and C-O-C stretching vibration, respectively. The other bands were observed at 1453, 1361 and 1363 cm⁻¹ and has been represented the stretching vibration of C-H deformation [19]. This signifies that all the bands of DL-PLA polymer are retained. The important absorption band positions and it assignments of H₃PO₄ doped PANI were found at 1554, 1475 and 1108 cm⁻¹ corresponding to quinoid, benzoid and C=N stretching, respectively [19]. The presence of quinoid (1475 cm⁻¹) and benzoid ring (1554 cm⁻¹) vibrations, these groups are indicated the salt form of polyaniline (PANI-ES) [19]. From Table 1, it is observed that N-H bands of H₃PO₄ doped DL-PLA/PANI composite appeared at 3289 cm⁻¹. The N-H stretching bands appeared. This is due to the existence of amine group on DL-PLA polymer film. The C=N, C=O, C-O and C-O-C stretching bands do not change considerably.

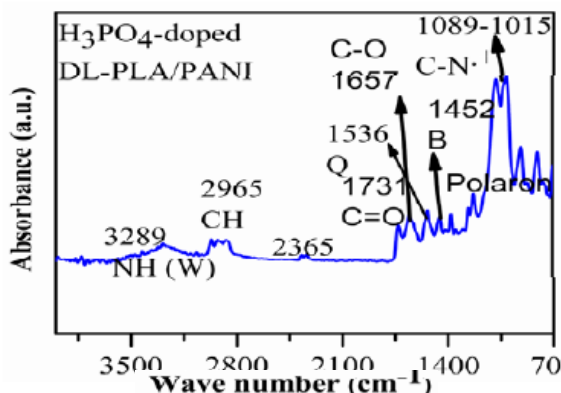


Figure 2. FTIR spectrum of H₃PO₄ doped DL-PLA/PANI composite [19]

Figure 3 is shown UV Visible spectrum of H₃PO₄ doped DL-PLA/PANI Composite. PANI-ES shows mainly two type of electronic transitions *i.e.*, π - π^* and polaron transitions, respectively within the range of 250–1000 nm of UV Visible spectrum [19].

There is no such transitions are found in DL-PLA film [19]. This indicates the absence of conducting sites in DL-PLA film. Both π - π^* , and polaron band types transitions were found in H₃PO₄ doped PANI salt film. This indicates the oxidation form of aniline [19].

The H₃PO₄ doped DL-PLA/PANI-ES composite was prepared for testing the CH₄ gas in different concentrations and balanced with synthetic air. During this gas sensing testing, the different gas concentrations (50 ppm, 100 ppm, 200 ppm, and 500 ppm) are used.

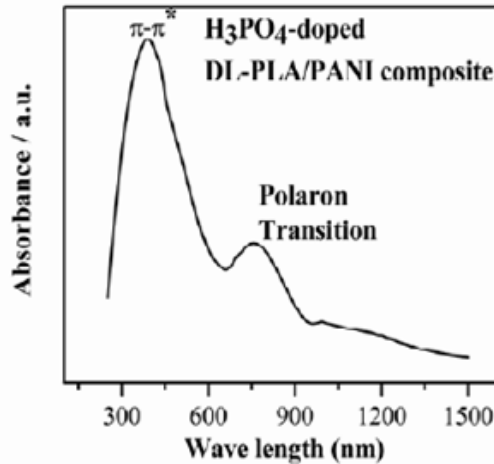


Figure 3. UV-Visible spectrum of H₃PO₄ doped DL-PLA/PANI composite [19]

The sensing measurement is operated at room temperature. Some have reported that PANI polymeric nanofibers are a well-known sensing material for hydrocarbon gases such as CH₄, H₂ [19, 20]. H₃PO₄ doped DL-PLA/PANI-ES composite is employed for sensor performance against a well-known polymer system.

Fig. 4 shows the dynamic responses of methane gas using H₃PO₄ doped DL-PLA/PANI sensor material as film. The sensor response is recorded typical resistance transients of the tested materials. From the **Fig. 4**, it is clear that the test gas *i.e.*, CH₄ gas is on, the resistance of sensor materials is decreased. During the recovery (*i.e.*, when the synthetic air is on), the resistance is increased. This means that the base resistance is regained. The percentage of response is assessed at room temperature using the expression

$$\text{Response (\%)} = \frac{R_a - R_g}{R_a} \times 100$$

Here, (R_a) and (R_g) are the sensor resistance, which is measured by the exposure of air and test gas respectively. Using the above expression, the percentage of response (%) was estimated to be 0.00288 %, 0.4255 %, 3.5 % and 9 % for 50 ppm, 100 ppm, 250 ppm and 500 ppm concentration of methane, respectively. Minimal base-line is drifted, which is indicated in the Figure 4. It is observed when the sensing element is switched back and forth between air and test gas environment. In addition, the base line is found to be shifted downward as indicated in Fig. 4 and 5. From the Figure 4 and 5, it is clear that the % response increases with the increase in CH₄ gas concentration. Also, it is found to be non-linear in nature [20- 22]. The resistance change in sensor materials is due to the interaction between the used materials surface

and CH₄ gas molecules [23,24]. The highest resistance is found to be 1.174 K Ω at 500 ppm CH₄ gases. Also, the lowest resistance is measured to be 0.0384 K Ω at 50 ppm CH₄ gases. It is believed that the smaller number of methane gas (*i.e.*, at 50 ppm) molecules are expected to interact with prepared sensor materials surface *i.e.*, PANI surface. It results poor response, *i.e.*, small change in the resistance [25].

During the exposure to 50 ppm of CH₄ gas balanced in synthetic air, the prepared sensor responded negligibly (0.00288 %). Different concentration exposers, *i.e.*, 50 ppm to 100 ppm, 250 ppm, and 500 ppm of CH₄ gas, the sensor materials response differently. J. D. Fowler et al. [26] suggested that the chemically absorbed H₂ gas molecules can react with oxygen molecule, which is present in the environment to form H₂O. They also exposed that the occurrence of H₂O molecules ruins the ability of PANI to sense CH₄ gas analytes. Presence of H₂O molecules in the sensing environment, it might also deteriorate the polyaniline-based sensor materials at high CH₄ gas concentrations (**Fig. 4 and 5**). This is due to the existence of 21 % oxygen in used synthetic air. Also, it was noticed that the diameter of the polyaniline nanofibers has a direct effect on their sensing performance [23].

CH₄ is a reducing gas. The interactions with the sensing materials are largely governed by the chemical properties of each material. CH₄ gas sensing mechanism for polyaniline-based sensor materials is still not understood. Chemisorption may occur between CH₄ gas molecules and the charged amine nitrogen sites of the polyaniline chain. The dissociation of the CH₄ bond leads to the formation of new N-H bonds with the amine nitrogen in the polyaniline chain. Consequently, the charge transfer between neighbouring nitrogen atom of amine. This signifies the polaronic form of polyaniline, *i.e.*, called doped state of polyaniline. After removal of the methane gas from the gas source, synthetic air expose to the sensor materials (contained polyaniline chains).

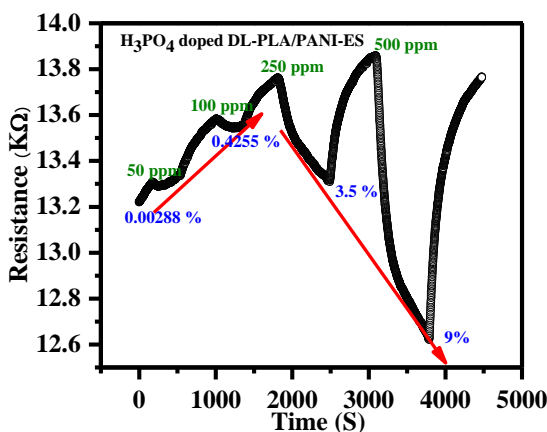


Figure 4: The resistance transient of H₃PO₄ doped DL-PLA/PANI-ES composite film measured at various CH₄ gas concentrations (ppm) in ambient condition [19]

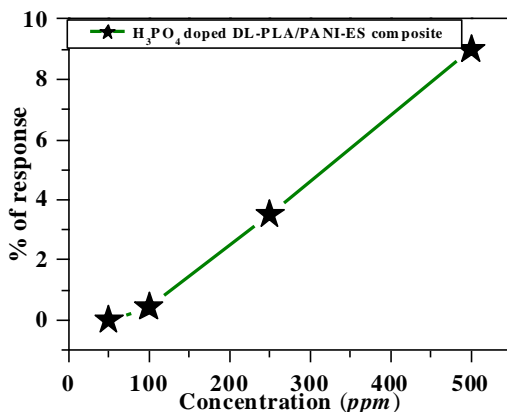


Figure 5: The % response with different concentration of H₃PO₄ doped DL-PLA/PANI-ES composite [19]

It is a completely reversible reaction [21]. The doped state of polyaniline is the highest conducting state and hence, conductivity is more. Therefore, during the exposure of test gas, the PANI film resistance is decreased (as observed from **Fig.4 and 5**). The methane gas molecules diffuse more because the polyaniline nanofibers provide more surface area for gas diffusion. PANI nanofibers have been observed in SEM image, which is presented in **Figure 1**. Therefore, the charged amine nitrogen sites on the PANI backbone are largely accessible to CH₄ gas molecules resulting in the dominant PANI CH₄ gas sensing mechanism.

Conclusions

H₃PO₄ doped DL-PLA/PANI-ES composite have successfully prepared by chemical-oxidation polymerization process. We have investigated the CH₄ gas sensing performance at room temperature of H₃PO₄ doped DL-PLA/PANI-ES composite. We have found that the H₃PO₄ doped DL-PLA/PANI-ES composite based gas sensor response (%) is 9 % at 500 ppm of CH₄ gas. The response (%) was calculated to be 0.00288 %, 0.4255 %, 3.5 % and 9 % for 50 ppm, 100 ppm, 250 ppm and 500 ppm concentration of methane, respectively.

Acknowledgments

The author conveys their sincere thanks to the CRF, IIT Kharagpur for their providing testing facilities and Materials Science Centre to do the research work. I would like to thank Prof. Subasis Basu Majumdar for their invaluable guidance, advices, constant inspiration and technical support throughout the entire research program.

References

- [1] Borowski, W. S. 2004, A Review of Methane and Gas Hydrates in the Dynamic, Stratified System of the Blake Ridge Region, Offshore South-eastern North America, *Chemical Geology*, Vol. 205 pp. 311-346.
- [2] Jun, J. H., Yun, J., Cho, K., Hwang, I.-S., Lee, J.-H., and Kim, S. 2009, Necked ZnO Nanoparticles-based NO₂ Sensors with High and Fast Response, *Sensors and Actuators B*, Vol. 140, pp. 412-417.
- [3] Barazzouk, S., Tandon, R. P., and Hotchandani, S. 2006, MoO₃-based Sensor for NO, NO₂ and CH₄ Detection, *Sensors and Actuators B*, Vol. 119, pp. 691-694.
- [4] Xi, L., Qian, D., Tang, X., and Chen, C. 2008, High Surface Area SnO₂ Nanoparticles: Synthesis and Gas Sensing Properties, *Materials Chemistry and Physics*, Vol. 108, pp. 232-236.
- [5] Hu, P., Du, G., Zhou, W., Cui, J., Lin, J., Liu, H., Liu, D., Wang, J., and Chen, S. 2010, Enhancement of Ethanol Vapor Sensing of TiO₂ Nanobelts by Surface Engineering, *Applied Materials & Interface*, Vol. 2, pp. 3263-3269.
- [6] Fidelus, J.D., Lojkowski, W., Millers, D., Grigorjeva, L., Smits, K., and Piticescu, R. R. 2007, Zirconia Based Nanomaterials for Oxygen Sensors-Generation, Characterisation and Optical Properties, *Solid State Phenomena*, Vol. 128, pp. 141-150.
- [7] Satyanarayana, L., Reddy, C.V.G., Manorama, S. V., and Rao, V. J. 1998, Liquid- Petroleum-Gas Sensor Based on a Spinel Semiconductor, ZnGa₂O₄, *Sensors and Actuators B* Vol. 46, pp. 1-7.
- [8] Macdiarmid, A.G., Chiang, J.C., Richter, A.F., and Epstein, A.J. 1987, Polyaniline: a New Concept in Conducting Polymers, *Synthetic Metals*, Vol. 18, pp. 285-290.
- [9] Focke, W.W., Wnek, G.E., and Wei, Y. 1987, Influence of Oxidation State, pH, and Counter ion on the Conductivity of Polyaniline, *Journal of Physical Chemistry*, Vol. 91, pp. 5813-5818.
- [10] Omastova, M., Pavlinec, J., Pionteck, J., Simon, F., and Kosina, S. 1998, Chemical Preparation and Characterization of Conductive Poly (methyl methacrylate)/Polypyrrole Composites, *Polymer*, Vol. 39, pp. 6559-6566.
- [11] Singh, V., Mohan, S., Singh, G., Pandey, P. C., and Prakash, R. 2008, Synthesis and Characterization of Polyaniline-carboxylated PVC Composites: Application in Development of Ammonia Sensor, *Sensors and Actuators B*, Vol. 132, pp. 99-106.
- [12] Cairns, D. B., Armes, S. P., Chehimi, M. M., Perruchot, C., and Delamar, M.

- 1999, X-ray Photoelectron Spectroscopy Characterization of Submicrometer-Sized Polypyrrole-Polystyrene Composites, *Langmuir*, Vol. 15, pp. 8059-8066.
- [13] Njuguna, J., and Pielichowski, K. 2004, Review: Recent Developments in Polyurethane-based Conducting Composites, *Journal of Materials Science*, Vol. 39, pp. 4081-4094.
- [14] Peng Wang, P., Tan, K.L., Zhang, F., Kang, E.T., and Neoh, K.G. 2001, Synthesis and Characterization of Poly (ethylene glycol)-Grafted Polyaniline, *Chemistry of Materials*, Vol. 13, pp. 581-587.
- [15] Chen, Y., Kang, E.T., Neoh, K.G., and Tan, K.L. 2000, Chemical Modification of Polyaniline Powders by Surface Graft Co-polymerization, *Polymer*, Vol. 41, pp. 3279-3287.
- [16] Yoon, J.T., Lee, S.C., and Jeong, Y.G. 2010, Effects of Grafted Chain Length on Mechanical and Electrical Properties of Nanocomposites Containing Polylactide-grafted Carbon Nanotubes, *Composites Science and Technology*, Vol. 70, pp. 776-782.
- [17] Yang, J., Wang, X., Wang, X., Jia, R., and Huang, J. 2010, Preparation of Highly Conductive CNTs/Polyaniline Composites Through Plasma Pretreating and *in situ* Polymerization, *Journal of Physics and Chemistry of Solids*, Vol. 71, pp. 448-452.
- [18] Lee, Y.K., Lee, K.J., Kim, D. S., Lee, D.J., and Kim, J.Y. 2010, Polypyrrole-carbon Nanotube Composite Films Synthesized Through Gas-phase Polymerization, *Synthetic Metals*, Vol. 160, pp. 814-818.
- [19] Panigrahi, M, Majumdar, S.B, and Adhikari, B. 2011, H₃PO₄-doped DL-PLA/PANI composite for Methane gas sensing, *IEEE explorer*, Vol. 97, pp. 1-7 (ISBN No.= 978-1-4577-2035-2, 8-10 Dec. 2011, Nanoscience, Technology and Societal Implications (NSTSI), 2011 International Conference)
- [20] Wu, Z., Chen, X., Zhu, S., Zhou, Z., Yao, Y., Quan, W., and Liu, B. 2013, Room Temperature Methane Sensor Based on Graphene Nanosheets/Polyaniline Nanocomposite Thin Film, *IEEE Sensors Journal*, Vol. 13, pp. 777-782.
- [21] Al-Mashat, L., Shin, K., Kalantar-zadeh, K., Plessis, J. D., Han, S. H., Kojima, R. W., Kaner, R. B., Li, D., Gou, X., Ippolito, S. J., and Wlodarski, W. 2010, Graphene/ Polyaniline Nanocomposite for Hydrogen Sensing, *Journal of Physical Chemistry C*, Vol. 114, pp. 16168-16173.
- [22] Lu, G., Ocola, L. E., Chen, J. 2009, Reduced Graphene Oxide for Room-temperature Gas Sensors, *Nanotechnology*, Vol. 20 pp. 445502-445511.
- [23] Fowler, J. D., Allen, M. J., Tung, V. C., Yang, Y., Kaner, R. B., and Weiller,

- B. H. 2009, Practical Chemical Sensors from Chemically Derived Graphene, ACS Nano, Vol. 3, pp. 301-306.
- [24] Virji, S., Kaner, R. B., and Weiller, B. H. 2006, Hydrogen Sensors Based on Conductivity Changes in Polyaniline Nanofibers, Journal of Physical Chemistry B, Vol. 110, pp. 22266-22270.
- [25] Fowler, J. D., Virji, S., Kaner, R. B., and Weiller, B. H. 2009, Hydrogen Detection by Polyaniline Nanofibers on Gold and Platinum Electrodes, Journal of Physical Chemistry C, Vol. 113, pp. 6444-6449.
- [26] Sadek, A. Z., Baker, C. O., Powell, D. A., Wlodarski, W., Kaner, R. B., Kalantar-zadeh, K. 2007, Polyaniline Nanofiber Based Conductometric Acoustic Wave Gas Sensors-effect of Nanofiber Diameter on H₂ Response, Journal of IEEE Sensor, Vol. 7, pp. 213-218.

Chapter 8

Inorganic Acid Doped Polyaniline Based Carbon Monoxide (Co) Sensor

Muktikanta Panigrahi ^{1,*}, Basudam Adhikari ¹

¹ Materials Science Centre, Indian Institute of Technology, Kharagpur, West Bengal, India

*Corresponding author: muktikanta2@gmail.com

Abstract

Simple *in situ* chemical oxidation method was employed to prepare different molar of HCl doped DL-PLA/PANI composites using AnHCl as precursor. Surface morphology, ATR-FTIR, UV-Visible, and band gap were studied. PANI nanowires with different diameter and smooth surface were observed for composites. The lowest direct band gap was found to be 1.68 eV for 2 (M) HCl doped DL-PLA/PANI. DC conductivity at room temperature was measured and followed the ohmic behaviour. The calculated highest DC conductivity at room temperature was found to be 0.1628×10^{-2} (S/cm) for 2 (M) HCl doped DL-PLA/PANI. Temperature variation (70–300 K) DC conductivity without magnetic field of as prepared composites was analysed using linear four probe techniques and showed semiconducting nature. The conductivity in the range of temperature (70–300 K) follows 3D VRH hopping mechanism. In kivelson model, the exponents are increased with increasing dopant concentration and was obeyed the power law. MR of the prepared DL-PLA/PANI composite films is strongly dependent on temperature, magnetic field, and concentration of HCl dopant. Negative MR is discussed in terms of a wave function-shrinkage effect on hopping conduction. In addition, we were discussed the response of carbon monoxide (CO) gas with polyaniline-based sensor materials.

Keywords: Composite, Nanofiber, Band gap, DC conductivity, Magnetoconductivity, Carbon monoxide Sensor

Introduction

The past few decades has witnessed rapid growth in research on conjugated polymer nanostructures, which has been driven by their unique electrochemical and

© IOR INTERNATIONAL PRESS, 2021

Muktikanta Panigrahi, Basudam Adhikari, *Inorganic Acid Doped Polyaniline Based Carbon Monoxide (Co) Sensor*,

<https://doi.org/10.34256/ioriip2128>

electronic properties as well as by the processing advantages of polymers relative to other electronic materials. The applications of conducting polymer nanostructures have been recently reviewed [1, 2]. Recently, conducting polymer nanowire and nanotube have been proposed as active materials for various potential commercial applications such as antistatic shielding, light emitting diodes (LED), supercapacitors, rechargeable batteries, artificial muscles, corrosion inhibitors and sensors [3-11].

In the conducting polymer family, PANI is one of the members with good environmental and thermal stability along with easy processing and oxidation–reduction mechanism, high conductivity [12-14]. Notwithstanding above advantages, PANI film has certain limit such as brittleness and moisture sensitivity that creates problems for its commercial applications. In various ways, researcher was tried to improve their stability. One of the effective ways was found in literature to improve the stability of PANI salt by making in composite form with thermoplastic polymer act as stabiliser [13]. A variety of doped PANI composite have been prepared using many types of thermoplastic polymers such as poly (methyl methacrylate), polyvinyl chloride, polystyrene and polyurethane and their conductivity was studied with and without magnetic field at room temperature and temperature variation (50–300 K) [15-18].

For future prospectus, researchers are introduced biodegradable polymers into the preparation conducting films with conducting polymer like PANI and polypyrrole (PPy). This is because biodegradable polymers have polar character (presence of polar groups) and conducting polymers have also polar character. The covalent interaction may be happened after composite preparation. Few reports are reported on composite that was made from biodegradable polymer and conducting polymers [19-21]. DL-PLA is one of the biodegradable polymers in biodegradable family. We chose DL-PLA biodegradable thermoplastic polymer has reported to the comparable good mechanical, bioresorbable, compatibility, surface properties with other biodegradable polymer and covalent interaction with conducting polymers. These materials can be used in different fields such as biosensor [21], intelligent scaffold materials [19], biochips [20] and gas sensing materials (present work).

It is well known that conductivity is key parameter for conducting polymer throughout its back bone. Conductivity was occurred only for charge transport phenomena in intra – and inters chains of the conducting polymer. For gas sensing applications, conductivity in terms of resistance change plays vital role and therefore, it is important to understand the charge transport in nanofibers because the charge transport mechanisms can have important consequences in term of the sensor signal to noise ratio. Some reports of thin film [22] and nanowires [23] are reported the complex electronic behaviour. The present scenario comes from structure of polymer. The polymeric structure mainly depends on synthetic condition, doping level, and balancing counter ions. Till now, the research is going on the study of transport behaviour throughout the conducting polymer. Such behaviour are found to be variety ways as electrical conductivity, magnetoresistance, frequency dependent conductivity, magnetic susceptibility, thermoelectric power have been intensively explored in the

last two decades [24, 25]. Out of above electrical properties, magnetoresistance is one important electrical property and that has been used to apply in various fields such as magnetic field sensor for studying high T_c – superconductor taps [26], vibration measurements in MEMS [26], manufacturing magnetocoupler device [26], detecting DNA or Protein binding to capture molecules in a surface layer [26]. Various reports have been studied magnetoresistance with temperature variation at particular magnetic field [27-29] or various magnetic fields at particular temperature [27-29] studying conducting behaviour. Different important parameters such as density of states (N_F), localization length (L_{loc}), characteristic temperature (T), hopping distance (R_{hop}) and hopping energy (Δ_{hop}) related to conduction mechanism were estimated for studying magnetoresistance with temperature variation at particular magnetic field.

Our purpose is to prepare an environmentally stable PANI composite that would show considerable good electrical properties. Also, it can be potential for sensor and other electronic applications. Looking for the above properties, biodegradable polymer such as poly (lactide) (DL-PLA) polymer is one of the thermoplastic polymers, which is used to prepare novel conductive material. It has good electrical conductivity, good durability, good environmental stability and easy processability.

In this input, author investigates the ethanol sensing of 2M HCl doped DL-PLA/PANI composites (different sized nanofibers) are prepared by *in situ* polymerization method. Also, the DC conductivity at room temperature and with temperature variation (presence and absence of magnetic field), response of CO, ATR-FTIR spectra, and UV-Visible with direct band gap has been studied.

Experimental Section

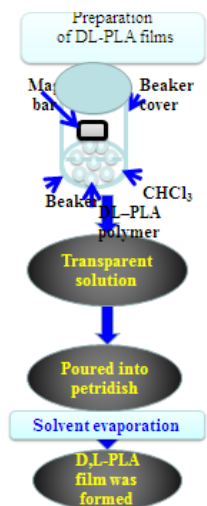
Chemicals And Materials

Laboratory grade chemicals such as aniline hydrochloride (AnHCl), hydrochloric acid (HCl), chloroform ($CHCl_3$), and ammonium perdisulphate (APS) are purchased from Merck, India. DL-PLA polymer is procured from Cargill Dow Bair; US-NE. Distilled water is used throughout the preparation of doped PANI composites.

DL-PLA films are prepared by solution casting technique. Both DL-PLA polymer (3 g) and $CHCl_3$ (30 mL) are taken as components during the DL-PLA film preparation. DL-PLA polymers are put in $CHCl_3$ contained beaker (100 mL). The mixture is stirred (3 h) by magnetic stirrer. It is observed that transparent soluble product is formed. The products are poured into ptdish (10 cm diameter). After $CHCl_3$ evaporation, films are removed from ptdish and cut into small pieces (1.5 cm \times 1.5 cm). The schematic representation of DL-PLA film preparation is mentioned as flow chart and presented in Scheme A.

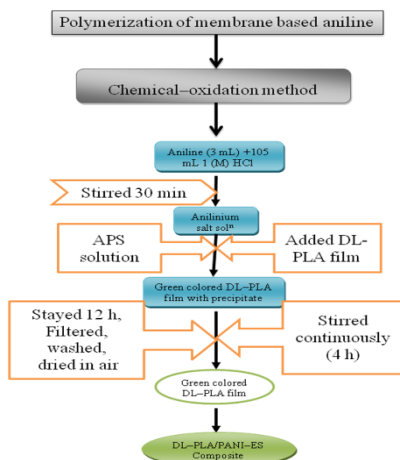
At ambient condition, various molar of HCl doped DL-PLA/PANI composites are prepared by *in situ* method through chemical oxidation polymerization route from AnHCl (monomer) and DL-PLA film as substrate. 0.03 moles (2.59 g)

AnHCl is added to 50 mL of 1 (M) HCl in 250 mL conical flask, called “solution A”.



Scheme A. The schematic representation of detail preparation of DL–PLA film is mentioned as flow chart and presented in Scheme A

DL–PLA films (1 cm × 1 cm) is dipped to “solution A” and stirred for 12 h. 0.045 moles (10.24 g) of APS was put to 50 mL of 1(M) HCl to form “solution B”. To the “solution A”, “solution B” is added drop wise for 1 h to form “solution C” and continued the stirring to 4 h. The polymerization is carried out in “solution C”. The color of “solution C” and DL–PLA films became light green to dark green. The reaction mixture is stayed overnight. The resulting composites are washed with deionised water several times followed by dried in air for 6 h [30].



Scheme B. The flow chart of preparation of HCl doped DL-PLA/PANI-ES composite

For comparison study, 2(M) –, and 3(M) – HCl doped DL-PLA/PANI composites are also prepared under similar conditions to those mention above. The flow chart of the preparations is illustrated in Scheme B.

Characterization Section

Surface morphologies of the as prepared materials are analyzed by scanning electron microscope (SEM, Carl Zeiss Supra 40). All samples are needed gold coating before doing SEM measurements.

For studying electronic transitions of all the prepared materials are needed UV-Visible (Micropack UV-VIS-NIR, DH 2000) spectral analyses. Band gap is estimated by Tauc expression.

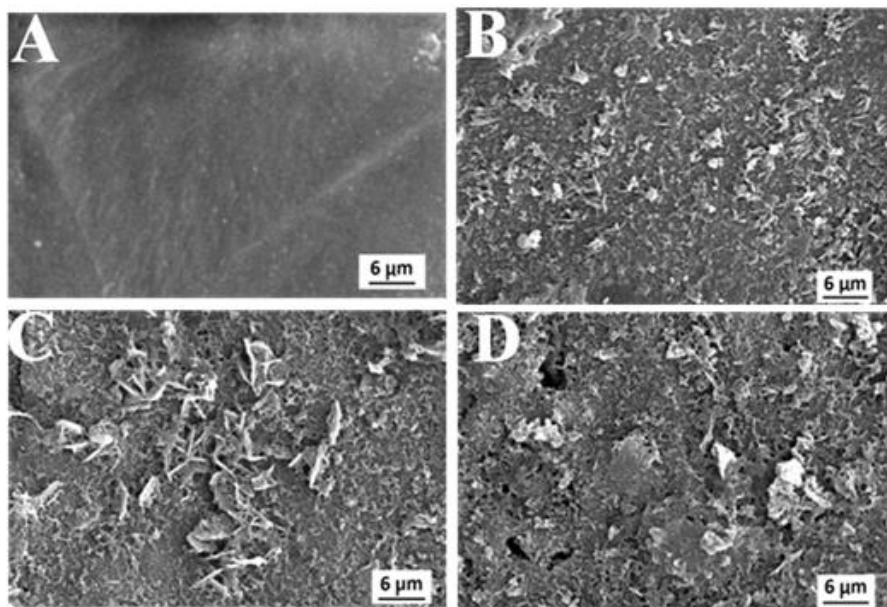
In support of ATR-FTIR spectra, functional groups of all as prepared materials are recorded on a Thermo Nicolet Nexus 870 spectrophotometer in the range 400-4000 cm^{-1} .

Both room- and low temperature DC conductivity of all as prepared composites are measured using a linear four probe technique. Also, Magnetoresistivity is measured using a linear four probe technique. Magnetoresistivity is investigated using a helium compressor (HC) (model HC-4E1)-sumitomo cryostat (Model Gains Research CO, INC) equipped with 0.8 T superconducting magnet (Lake shore electromagnet). Lake shore 331 temperature controller is used. Magnetoresistivity measurements are performed at 0.5T with varying temperature 50-300 K temperatures range using a computer controlling measuring system. In above electrical experiments, prepared film samples (thickness-0.51 mm) are contacted with conducting silver paste. A constant current (I) from a current source (Keithley 220 programmable current source) is allowed to pass through two terminals leads of four probe and the voltage (v) across the other two leads is measured using a multimeter (2182 NANO-VOLTMETER Keithley).

Results and Discussion

Figure 1 shows the variety of SEM images of prepared materials such as neat DL-PLA, neat 1 (M) HCl-doped PANI films, and PANI nanowires on DL-PLA film at room temperature. Smooth surface was observed in neat DL-PLA film (Figure 1 A) below 1 kX magnification whereas neat PANI and all HCl doped composites (Figure 1 B, C, D and E) have fibrous structure was observed in magnified SEM images having diameter in nanoregime, so called nanofiber. Non-uniformly distribution of nanofiber was observed in HCl doped composites and HCl doped PANI salt film. The average diameter of as prepared HCl doped materials was found to be 185.3 nm for HCl doped 1(M) DL-PLA/PANI composite, 165.1 nm for HCl doped 2(M) DL-PLA/PANI composite, and 211. 3 nm for HCl doped 3(M) DL-PLA/PANI

composite, respectively. The fiber like morphology was observed after polymerization start. This may be happened due to the reaction of hydrogenium ion from HCl and anillium salt with ester group present in DL-PLA film with drop wise addition of APS (oxidant) solution on a solution that contain anillium salt with DL-PLA (monomer and HCl treated) film. The formation of Nanofiberic structure is favourable for the sensor application due to increase in surface area of PANI. This



high surface area provides fast diffusion of gas molecules into the PANI nanofibers.

Figure 1. shows the variety of SEM images of prepared materials such as neat DL-PLA, 1 (M) HCl-doped DL-PLA/PANI composite (B), 2 (M) HCl-doped DL-PLA/PANI composite (C), and 3 (M) HCl-doped DL-PLA/PANI composite (D) films

Chemical structure of prepared materials was observed by analysis of ATR-FTIR spectra. Figure 2 indicates the ATR-FTIR spectra of DL-PLA, PANI-ES (1 M) and all prepared conductive composites. All the characteristic absorption peak positions of all prepared materials and its assignments are given in Table 1. The ATR-FTIR spectra of DL-PLA film was presented in Figure 2 (A). The variety of absorption bands of DL-PLA was found at 2995, 2944, 1759, 1616 and 1216 cm^{-1} , respectively. That bands have been attributed to C-H stretching, C=O stretching, C-O stretching of ester and C-O-C stretching vibration, respectively. The stretching vibration of C-H deformation band of DL-PLA polymer was found at 1453, 1361 and 1363 cm^{-1} [31]

This represents the characteristic absorption features of DL-PLA polymer and that are retained in the prepared DL-PLA film. An ATR-FTIR spectrum of HCl

doped PANI was observed in Figure 2 (C).

Table 1 for ATR–FTIR peak positions and peak assignments of as–prepared materials

Peak positions (cm ⁻¹)					
DL–PLA	PANI	DL–PLA/PANI	DL–PLA/PANI	DL–PLA/PANI	Peak
ES		1 (M) HCl	2 (M) HCl	3 (M) HCl	assignments
2995		2995	2969, 2968	2968	
2944	---	2944	2922	2925	CH stret.
---	3227 (W)	3287	3289	3295	NH stret.
---	3429 (S)	---	---	---	NH stret.
1759	---	1739	1725	1725	C=O stret.
1616	---	1616	1652	1652	C–O stret.
---	1564	1570	1530	1530	Quinoid stret.
---	1479	1482	1451	1454	Benzoid stret.
---	1116	1042	1070	1070	C=N stret.
1216	---	1214	1226	1226	C–O–C stret.
1453	---	1434	1411	1411	
1363	---	1361	1451	1454	
1361	---	---	1371	1373	
			1338	1345	CH – deform.

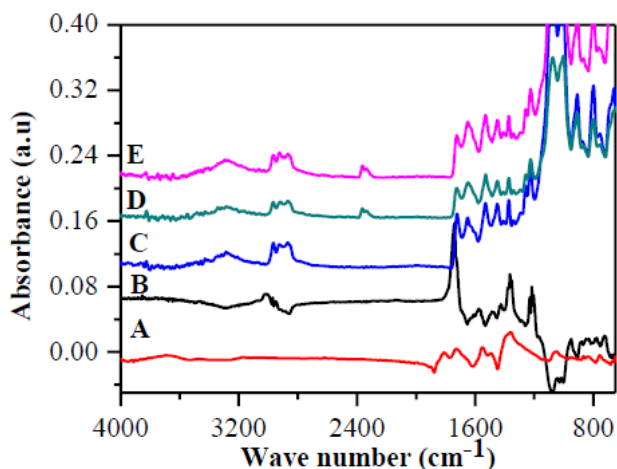


Figure 2. ATR–FTIR spectra of pristine DL–PLA ‘A’, PANI ES film ‘B’, DL–PLA/PANI 1 (M) HCl ‘C’, DL–PLA/PANI 2 (M) HCl ‘D’, and DL–PLA/PANI 3 (M) HCl ‘E’

The bands are found at 1554 cm⁻¹ for quinoid, 1475 cm⁻¹ for benzoid, and 1108 for C=N cm⁻¹ stretching, respectively [32]. This corresponds to the oxidation of PANI. The ATR–FTIR spectra of all composites are presented in Figure 2 (C), (D), and (E). Considering all the band features of as–prepared composites and comparing

with the band features of DL-PLA and HCl doped PANI, we conclude that salt form PANI is formed on DL-PLA film. From Table 1, it is observed that N-H bands of HCl-doped DL-PLA/PANI 1(M), HCl doped DL-PLA/PANI 2(M), HCl doped DL-PLA/PANI 3(M) appeared at 3291, 3289, and 3295 cm^{-1} , respectively. The variation of N-H stretching bands between prepared composites was strongly depended on concentration of HCl. The C=N, C=O, C-O and C-O-C stretching bands do not change significantly.

Variety of electronic transitions of as-prepared materials was established by studying UV-Visible spectra. This spectrum was existed in Figure 3. The band positions and band assignments of each prepared materials are mentioned in Table 2. From Figure 3 (A), it is noticed that no electronic transitions are found in DL-PLA film [33].

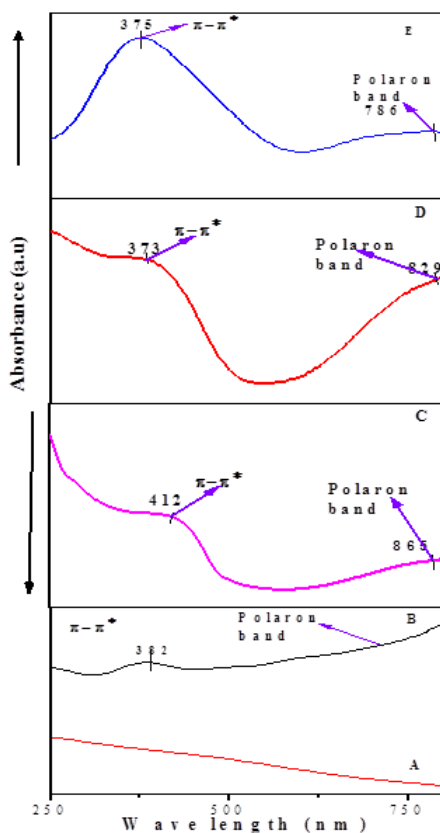


Figure 3 UV-Visible spectra of pristine DL-PLA 'A', PANI ES film 'B', DL-PLA/PANI 1 (M) HCl 'C', DL-PLA/PANI 2 (M) HCl 'D', and DL-PLA/PANI 3 (M) HCl 'E'

It is mentioned from literature that PANI-ES shows various types of

electronic transitions such as $\pi-\pi^*$ of benzene ring, polaron to π^* , benzoid to quinoid ring and polaron transition, respectively [34]. An UV–Visible spectrum of HCl doped PANI (1 M) film is indicated in Figure 3 (B). Polaron band and $\pi-\pi^*$ were found at 382 nm and >600 nm. This represented as the oxidation form PANI [27]. All the as prepared composites were generally showed in Figure 3 two types of transitions such as π to localised polaron band transition and $\pi-\pi^*$ transition of benzoid ring. The peak positions were found 865 nm and 412 nm for HCl doped DL–PLA/PANI (1 M), 829 nm and 373 nm for HCl doped DL–PLA/PANI (2 M), and 786 nm and 375 nm for HCl doped DL–PLA/PANI (3 M), respectively. Both $\pi-\pi^*$ transition of benzoid ring and polaron band are suggest to the presence of aniline unit and oxidation unit in emeraldine salt form of composite films.

Electronic transitions were occurred between two bands and that happened after photon absorption. From many literatures [35] was mentioned that the photon absorption of organic semiconductor is followed by Tauc expression as

$$(\alpha h\nu) = A(h\nu - E_g)^n \quad (2)$$

Where α = Optical absorption co-efficient, $h\nu$ = photon energy, E_g = Energy gap calculated from graph, A = absorption constant, n = Represents types of transition occurs. If n = 2 indicated allowed indirect transitions and $n = \frac{1}{2}$ indicated allowed direct transitions.

Table 2. UV–Visible band positions and its assignments of indicated materials.

Materials Identification	Peak positions (nm)		Band gap (Eg) in eV
	$\pi-\pi^*$	Polaron band	
DL–PLA	---	---	---
PANI ES film	382	>650	1.08
DL–PLA/PANI (1M HCl doped)	412	>865	>865
DL–PLA/PANI (2M HCl doped)	373	>829	1.68
DL–PLA/PANI (3M HCl doped)	375	>786	1.82

Note: ‘M’ stands for molar, ‘nm’ stands for nanometre and ‘eV’ stands for electron–volt

For direct electronic transition, plot was made between $(\alpha h\nu)^2$ and $h\nu$. From the plot, to extrapolate the linear portion of it to $\alpha = 0$ value to obtained corresponding direct band gap. Direct allowed transitions, all the prepared composites are shown in Figure 4 and its (band gap) values are presented in Table 3. It is observed from Table 3, 2 (M) HCl doped of DL–PLA/PANI composite have obtained lowest direct band gap value as compared to other HCl doped composites. The reduction in band gap

occurred due to the incorporation of H^+ ion concentration into the polymer chain; but there is certain limit and that affect the density of states, which is more into the visible region as compared to excess dopant used for composite preparation [35].

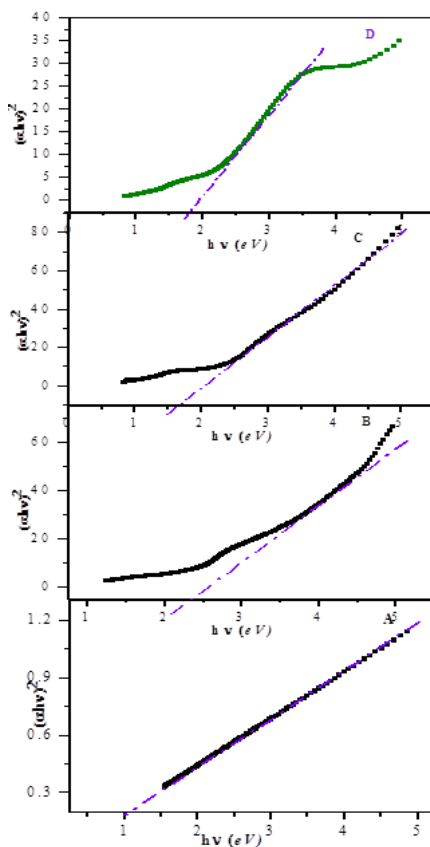


Figure 4. Estimation of direct band gap using Tauc expression of pristine PANI ES film ‘A’, DL-PLA/PANI 1 (M) HCl ‘B’, DL-PLA/PANI 2 (M) HCl ‘C’, and DL-PLA/ PANI 3 (M) HCl ‘D’

Conductivity is an important spirit for conducting materials. This character was measured by various ways. Linear four probe technique is one technique out of them and this technique was favoured for the researchers due to the minimization of voltage drop.

The DC conductivity of as prepared composites was measured using linear four probe technique and the expression is shown below [36].

$$\rho = 2\pi S \left(\frac{V}{I} \right) \quad (3)$$

$$\sigma = \frac{1}{\rho}$$

and (4)

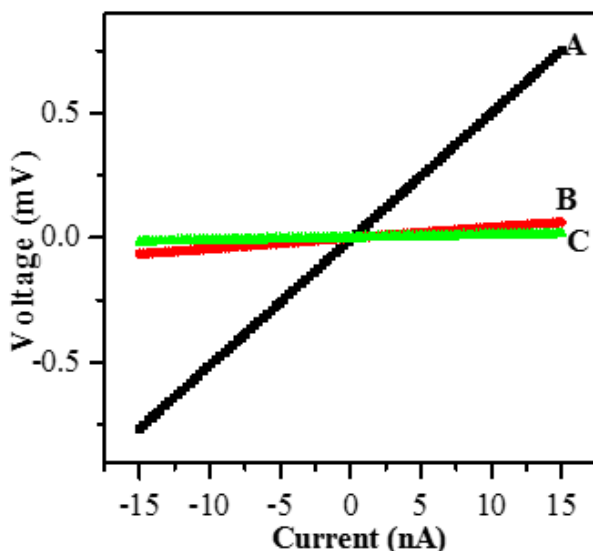


Figure 5. Room temperature DC conductivity of HCl doped 1 (M) ‘A’-, 2 (M) ‘C’-, 3 (M) ‘B’-DL-PLA/PANI composites, respectively.

ρ = resistivity, S = distance between two consecutive probes (0.15 cm), I be the applied current in the four probe system (nA) and V be the corresponding output voltage in (mV). The room temperature $I-V$ characteristics of HCl doped DL-PLA/PANI composites were shown in Figure 5. This indicates that the $I-V$ characteristics show linear behaviour (I and V) and passing through origin (after linear fit). This nature follows similar to the ohmic behaviour and is reported as [36]. The average (av.) DC conductivity values of HCl doped DL-PLA/PANI composites, and DL-PLA polymer film were presented in Table 3. It is cleared from the Table 3, the measured DC conductivity at room temperature of DL-PLA film are found to be 6.07×10^{-15} S/cm and it is pointing to an insulating materials [37]. Also, from Table 3 it is found that the av. DC conductivity of 2(M) HCl doped DL-PLA/PANI composites are found to be higher than rest of prepared composites. Conductivity may obtain due to the mobility of charge carrier. This carrier mobility mainly depends on the presence of reduced unit in PANI structure and that was happened due to the improvement of PANI salt structure at 2 (M) HCl doped prepared composite [38]. But excesses dopant concentration, that create a barrier for their charge transport in intra- and inter-PANI chains. Hence, the results are agreed with literature [38].

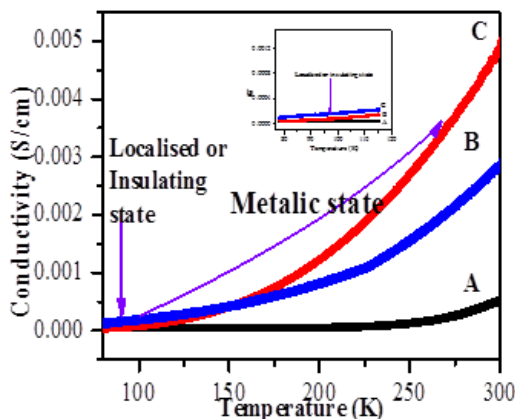


Figure 6. Temperature dependent DC conductivity of HCl doped 1(M) 'A', 3(M) 'B', 2(M) 'C'—DL—PLA/PANI composites, respectively and 70–115 K for localised state or insulating state and 115–300 K for metallic state are observed.

Until, charge transport process is difficult to understand of conducting materials. For understanding of conduction mechanism of as prepared composites, low temperature DC conductivity experiments were performed. Temperature variation (78–300 K) DC conductivity of HCl doped DL—PLA/PANI composites were showed in Figure 6. It is observed from Figure 6 that the conductivity of as prepared composites is proportionally increased with increase in temperature. Analogous nature was found from semiconducting materials [36].

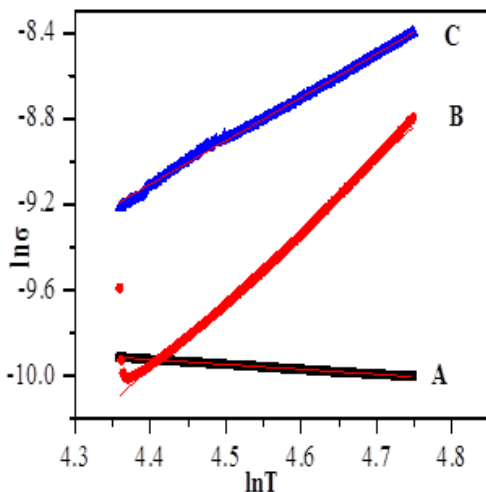


Figure 7. Temperature dependent DC conductivity in logarithmic scale following Kivelson model of HCl doped 1(M) 'A', 3(M) 'B', 2(M) 'C'—DL—PLA/PANI composites, respectively and slopes are corresponding to the exponent.

Hence, it is called as organic semiconductor. The temperature dependence of electronic conductivity was obtained from prepared nanofibers with different diameter. Figures 6 are shown the conductivity of all prepared composite samples and were exhibited two characters [27]. One is metallic character and that was observed in the temperature range 115–300 K. Other one is localised behaviour and that was found below 115 K. This behavior agrees with the Bloch–Grueneisen theory on the electron–acoustic phonon scattering mechanism. On the other hand, the smaller sample shows two distinct characteristics for the electron transport.

Different scattering mechanism was involved to determine the temperature dependence conductivity. At high temperatures ($T > 115$ K), the scattering mechanism seems to be predominant and the conductivity rises with increasing temperature (metallic phase) [27]. As the temperature is lowered, phonon scattering mechanisms become predominant [27], giving rise to a distinct temperature–dependent conductivity for $T < 115$ K, which explains in part the general features of the curve presented in Figure 6. At low temperature regime, the scattering mechanism can be related with the size of the nanofibers: as the nanofibers cross section decreases, the boundary scattering becomes relatively more important than for larger fibers because a larger portion of the carriers are located near the fibers boundary. Then (1) for small–dimension nanofibers, the disorder coming from processes like collisions with the boundaries [39, 40] provides the necessary disorder to randomize electron energy, resulting in a localized character for the transport; (2) this will increase the electron–electron interaction as well [41]. It is important to emphasize that the conductivity below 110 K is not related with strong localization: the disorder from boundary scattering, randomizing the electron potential, is not enough to promote strong localization. In fact, successive attempts in order to distinguish an activation law (Arrhenius model) or a variable range hopping (VRH) behaviour have failed [42–45].

In order to explain the current transport i.e. electron–electron or electron phonon or mixed charge carrier in localised state in the temperature range $T < 115$ K (below the solid line) was presented in Figure 7. The experimental data for $T < 115$ K was the best fitted, such model called Kivelson model [45]. According to this model, the temperature dependence conductivity is expressed as [45]

$$\sigma(T) = A(T^n) \quad (5)$$

Where A is some constant and n is the exponent. According to this model, we plotted $\ln \sigma$ vs. $\ln T$. The ‘ n ’ is equal to the slope of the straight line. The values of ‘ n ’ were found to be 0.229 eV, 2.72 eV, and 3.316 eV for 1 (M) DL–PLA/PANI composite, for 2 (M) DL–PLA/PANI composite, for 3 (M) DL–PLA/PANI composite, respectively. This value is deviate the values of one dimensional electron–electron scattering and this should be addressed mixed charge carrier below the 115 K [45].

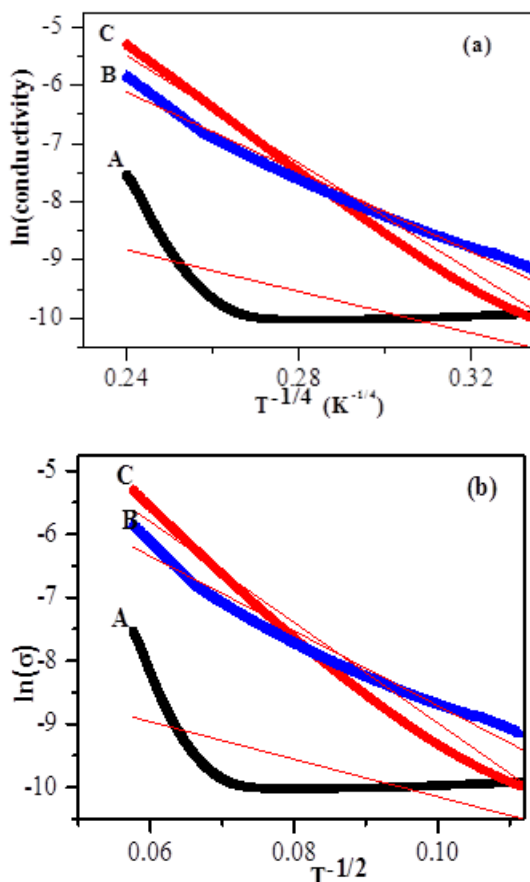


Figure 8. Temperature dependent DC conductivity of HCl doped 1 (M) 'A', 2 (M) 'B', 3 (M) 'C'—DL—PLA/PANI composite, respectively and showed (a) for 3D (a) – and 1D (b) –VRH model.

Variety of models was proposed to understand the conduction process of the conducting polymers. Generally, Mott's variable range hopping (Mott's VRH) model has been applied to organic semiconductor for understanding the hopping mechanism for conduction and that can be observed from temperature dependent conductivity. In this report, we mentioned the temperature dependence (78–300 K) conductivity (Figure 8) for studying Mott's VRH form of HCl doped DL—PLA/PANI composites. The temperature dependence DC conductivity as follows the eqⁿ (5) [42–45] and this is called Mott's expression.

$$\sigma = \sigma_0 \exp\left(-\frac{T_0}{T}\right)^x \quad (6)$$

Where T_0 is the Mott characteristic temperature and σ_0 the limiting value of conductivity at infinite temperature and the exponent 'r' is related to the dimensionality of the transport process using the relation $x = \frac{1}{(1+d)}$, where $d = 1, 2$ and 3 for one-, two- and three-dimensional (1D, 2D and 3D) transport process, respectively.

The 3D VRH plots on measured $\ln(\text{conductivity})$ vs. $T^{-1/4}$ for HCl doped DL-PLA/PANI composites in the temperature range 78–300 K were shown in Figure 8 (a). This conductivity data were well linearly fitted to the 3D conduction process. Similarly, 1D-VRH plots were shown in Figure 8 (b). It is cleared from all VRH plots, Mott's 3D VRH model of 2(M) HCl doped DL-PLA/PANI composite fits better into the experimental data than that of other VRH model. The linearly fit behaviour is observed from regression values and these values are presented in Table 3. Higher the regression values (i.e. close to unity) suggest the more charge carrier can hop in intra- and inter-hopping processes because of PANI chain structure, supporting the reported literatures [42–45]. In the 3D-VRH model, the temperature dependence of DC-conductivity can be presented in equation (2)

$$\sigma = \sigma_0 \exp \left[- \left(\frac{T_0}{T} \right)^{\frac{1}{4}} \right] \quad (7)$$

as can be seen in Figure 8 (a), the linear dependence of $\ln \sigma$ vs. $T^{-1/4}$ is well fitted. T_0 and σ_0 was also calculated from 3D-VRH plot of HCl-doped DL-PLA/PANI composites and presented in Table 3. It concluded that charge carriers could hop easily in 2 (M) HCl-doped as prepared composite than rest prepared and follow the conduction mechanism [43].

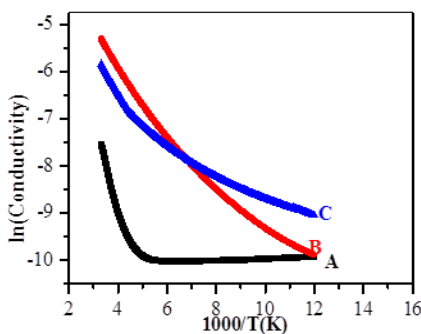


Figure 9. Plots on $\ln \sigma$ vs. $1000/T-1$ of HCl doped 1(M) 'A', 3(M) 'B', 2(M) 'C'-DL-PLA/PANI composites, respectively and Arrhenius models are followed.

Another important model i.e. Arrhenius model was employed to estimate the activation energy (minimum amount of energy needed to hop the inter chain) of prepared composite and this model is shown in Figure 9. Accordingly, Arrhenius eqⁿ. is represented as a function of temperature and the electronic conductivity is inversely

related i.e. $\sigma = f\left(\frac{10^3}{T}\right)$. The following expression is investigated from literature to Arrhenius model [44] in the temperature regime 78 to 300 K.

$$\sigma = \sigma_0 \exp\left(-\frac{E_a}{kT}\right) \quad (8)$$

Where E_a is the thermal activation energy of the electrical conduction, σ_a is a constant and that is depending on the semiconducting behaviour, T is the absolute temperature in Kelvin scale, and k is the Boltzmann constant and its value is 8.62×10^{-5} (eV/K).

From Figure 9 shows that the conductivity value does not exhibit linear dependency but markedly curved which indicates that the conductivity does not correspond to a thermally activated mechanism [44]. Taking slope value obtained from plot of $\ln \sigma$ vs. $10^3/T$ (after linear fit), the activation energy was calculated and its value is found to be 0.0195 eV for HCl doped DL-PLA/PANI 1(M) composite, 0.04974 eV for HCl doped DL-PLA/PANI 2(M) composite, and 0.0334 eV for HCl doped DL-PLA/PANI 3(M) composite, respectively. This different value of activation energy was observed and this may be happened due to the formation of different nanosized PANI chains.

In addition, the temperature variation (50–300 K) resistivity of HCl-doped DL-PLA/PANI composites in the presence of magnetic field (0.5 Tesla) was plotted in Figure 10.

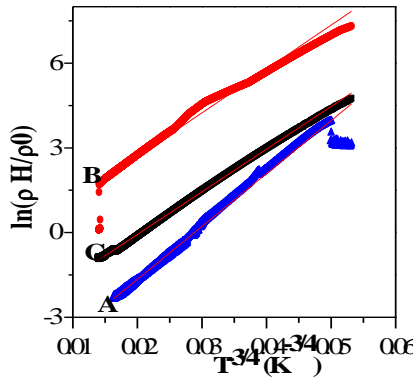


Figure 10. Plots of $\ln(\rho H/\rho_0)$ vs. $T^{-3/4}$ for HCl 1 (M) ‘A’–, 2 (M) ‘B’–, and 3 (M) ‘C’–doped DL-PLA/PANI composites at 0.5T in the temperature range of 50–300 K. Taking slopes (from these plots), Mott’s characteristic temperature (T_0), localization length, density of states, hopping distance, and hopping energy were estimated.

This characterization is very essential to support for better understanding of conduction mechanism. From this, we are calculated the important electrical parameters such as density of states $[N(E_F)]$, localization length (L_{loc}), hopping distance between the chains ($R_{hop, Mott}$), and hopping energy i.e. the energy required to

hop the electron ($\Delta E_{hop,Mott}$).

From resistivity data (3D–VRH model), Mott’s law is described [27] and the expression is given below.

$$\rho(T) = \rho_0 e^{\left(\frac{T_{Mott}}{T}\right)^{\frac{1}{4}}} \quad (9)$$

$$T_{Mott} = \frac{16}{[K_B N(E_F) L_{loc}^3]} \quad (10)$$

Where K_B is the Boltzmann constant; $N(E_F)$ is the density of states at the Fermi level; and L_{loc} , the localization length. T_{Mott} is an important parameter for calculation of $N(E_F)$, and L_{loc} . In 3D VRH model, we have plotted $\ln \sigma$ vs. $T^{-\frac{1}{4}}$ of HCl-doped DL–PLA/PANI composites and shown in Figure 8 (a). From slope of the straight line, T_{Mott} was estimated and listed in Table 3.

Table 3 Several parameters estimated from using the Band gap (direct), DC conductivity, VRH model, Power model, and Arrhenius model of prepared HCl doped DL–PLA/PANI Composite

Sample parameters	Symbol for materials identifications				
	A	B	C	D	E
σ (S/cm)	6.07×10^{-15}	0.910 $\times 10^{-3}$	0.3115×10^{-4}	0.1628×10^{-2}	0.410×10^{-3}
σ_0	---	---	0.01057	266.93	8.12049
L_H (nm)	---	---	0.0155	0.0155	0.0155
L_{loc} (nm)	---	---	31.20	146	87.80
$N(E_F)$ (no. states/ eV/cm ³)	---	---	3.41×10^{27}	2.845×10^{23}	5.847×10^{24}
$R_{hop,Mott}$ (nm) at 300 K	---	---	102.80	1582.8	654.66
$\Delta_{hop,Mott}$ (meV) at 300 (K)	---	---	56.80	186	128.54
T_{Mott} (K)	---	---	1.79×10^6	2.096×10^8	4.69×10^7

k = Boltzmann constant, T_{Mott} (K) = Mott’s characteristics temperature in Kelvin, σ_0 = intercept value obtained from 3D VRH model, σ be the conductivity at room temperature and unit can expressed as

S/cm. k (eV/K) = 8.62×10^{-5} , L_{loc} = the localization length in (nm), $N(E_F)$ = Density of states at

Fermi level (no. states per electron volt per centimetre cube), $R_{hop,Mott}$ (nm) at 300 K = Mott’s hoping distance in nanometre scale and the energy difference between the sites in the Mott’s limits.

A, B, C, D, and E are the symbol for prepared materials identification: DL–PLA = A, PANI film (0.61 mm) = B, DL–PLA/PANI (1 M HCl doped) = C, , DL–PLA/PANI (2 M HCl doped) = D,

DL-PLA/PANI (3 M HCl doped) = E.

From magnetoresistivity data, we have plotted $\ln\left[\frac{\rho(H)}{\rho(0)}\right]$ vs. $T^{-3/4}$. The equation for magnetoresistivity with varying temperature at a particular magnetic field was shown as follows [27]

$$\ln\left[\frac{\rho(H)}{\rho_0}\right] = t(L_{loc}/L_H)^4\left(\frac{T_{Mott}}{T}\right)^{\frac{3}{4}} \quad (11)$$

Where, $t = \frac{5}{2016}$ and $L_H = \left[\frac{h}{2\pi eH}\right]^{\frac{1}{2}}$ is magnetic length, h = Planks constant (6.62×10^{-34} joule.sec), e = electronic charge (1.6×10^{-19} C), $H = 0.5$ T is the applied magnetic field, $\rho(H)$ be the resistivity with magnetic field and $\rho(0)$ is the resistivity without magnetic field. The L_{loc} can be calculated from slope of the magneto-resistivity data is shown in Figure 10.

The obtained L_{loc} is presented in Table 4. Putting $T_{0,Mott}$ and L_{loc} values in eqⁿ (5), (7), and (8), $N(E_F)$, (R_{hop}) , and (Δ_{hop}) were calculated and was presented in Table 4. The eqⁿ (7) and (8), was found from literature as referred 27.

$$R_{hop,Mott} = \left(\frac{3}{8}\right)\left(\frac{T_{Mott}}{T}\right)^{\frac{1}{4}} L_{loc} \quad (12)$$

$$\Delta_{hop,Mott} = \left(\frac{1}{4}\right)(k_B T)\left(\frac{T_{Mott}}{T}\right)^{\frac{1}{4}} \quad (13)$$

By putting required parameters in the above expressions, the values of $R_{hop,Mott}$ and $\Delta_{hop,Mott}$ were calculated at 100 K and presented in Table 4. In addition, the obtained hopping parameters were found to satisfy the 3D-VRH criterions.

MC is a one of the important physical properties of conducting polymer. This property is informed to the disorderness of the materials in quantitatively. For this purpose, we performed MC measurements. Some reports are reported that weak disorder leads to a weak localization due to constructive quantum interference of time-reversed electron trajectories [46]. Below 115 K temperature, the localised character of prepared samples should be controlled by quantum interference effects, which in turn should be observed in the magnetoconductivity of the prepared nanofibers. Figure 11 shows the magnetoconductivity data obtained at 50K, 100K, 200K, and 300K temperatures, using the usual $B \perp I$ geometry (Taking $I = 50$ nA), with the magnetic field B ranging from 0 to 0.8 T. The presence of the electron quantum interference effects was then readily observed: (1) the increase of the conductivity with increasing magnetic field at 50K, 100K, and 200K temperature but the reverse effect was observed at 300K for HCl-doped DL-PLA/PANI (1M) composite in

Figure 11 (a)

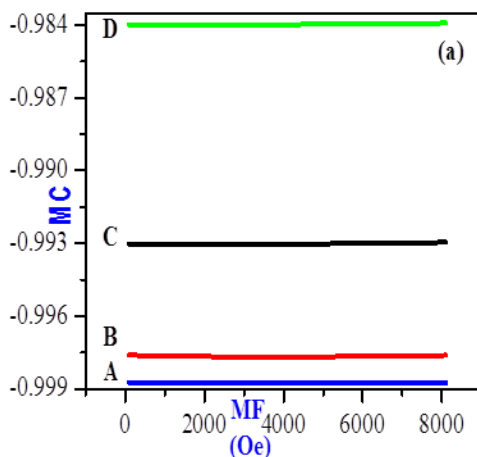


Figure 11(a) Plots on negative Magnetoconductivity vs. Magnetic field (MF) of HCl 3 (M)– ‘A’ at 50 K, 3 (M)– ‘B’ at 100 K, 3 (M)– ‘C’ at 200 K, and 3 (M)– ‘D’ at 300 K–doped DL–PLA/PANI composites, respectively.

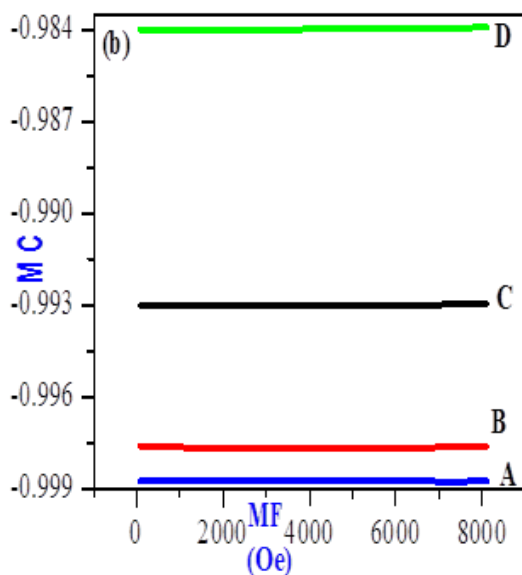


Figure 11(b) Plots on negative magnetoconductivity vs. Magnetic field (MF) of HCl 2 (M)– ‘A’ at 50 K, 2 (M)– ‘B’ at 100 K, 2 (M)– ‘C’ at 200 K, and 2 (M)– ‘D’ at 300 K–doped DL–PLA/PANI composites, respectively.

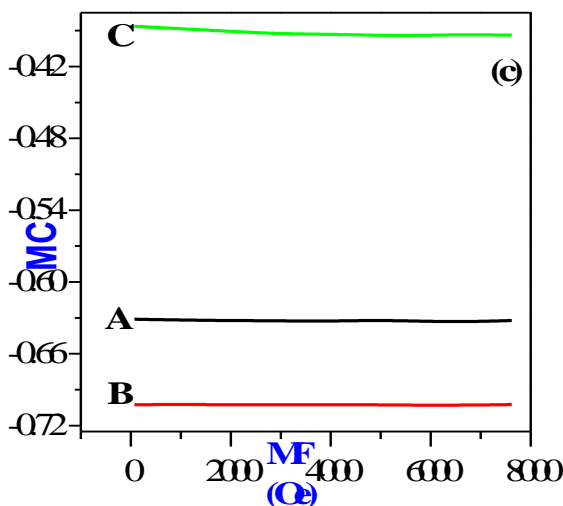


Figure 11(c) Plots on negative Magnetoconductivity vs. Magnetic field (MF) of HCl 1 (M)– ‘A’ at 100 K, 1 (M)– ‘B’ at 200 K, and 1 (M)– ‘C’ at 300 K–doped DL–PLA/ PANI composites, respectively.

In addition, the decrease of conductivity with increasing magnetic field at different temperature was observed in the Figure 11 (b and c) for 2 M– and 3M–HCl doped DL–PLA/PANI composites, respectively used for this experiments. The above negative MC results are agreement with the one–dimensional character of the samples [28].

Response of Carbon Monoxide (Co) Gas

Monitoring of Carbon monoxide (CO) is a key issue in the environment because of their toxic nature. Other than the toxic nature, CO is a colorless, colorless, and tasteless gas in the environment. CO is usually obtained in both sources such as natural sources and artificial sources. The major percentage of CO is come from indoors such as garages, kitchens, etc. Also, CO is produced during the combustion of engines, stoves, water heaters, generators, lanterns, and gas ranges or during burning charcoal and wood [47]. Huge amounts of CO are obtained from during the burning of any fossil fuel. Long-term with constant CO exposure is produced from automotive exhaust, smoke, and industrial sources (foundries, mills etc.) [48–52]. CO takes place following chemical reactions with hemoglobin. It can produce carboxyhemoglobin via bonding with hemoglobin, which is present in red blood cells. Due to the formation of carboxyhemoglobin, the extent of binding between the red blood cells and oxygen is reduced. Hence, the transport of oxygen in the human body decreases. This is resulted in the decrease in oxygen levels of the body and causes histotoxic hypoxia. Therefore,

it is resulting common health issues such as headache, nausea, vomiting, inertia, unconsciousness, weakness, hypotension, coma, inflammation of existing diseases, confusion, depression, hearing problems, etc. [48, 49]. Also, CO can cause for diabetes, parkinsonism, rhabdomyolysis, motion disorders. It may also cause the health issues of children and pregnant women. Inhalation of a small amount of CO over a long period of time or a large amount of CO in a short period of time can kill a person. Because of that, it is needed to monitor the toxic CO gas by best material and technology. Thus, researchers put their effort by taking many materials for their optimization. They are prepared materials using different methods and techniques. The prepared materials are used to detect this gas. The CO gas is also created in residential and household environments. So, it is very essential to develop mini or micro sensor, which is cost effective and efficient in these environments. It detects CO in parts per million (ppm) and parts per billion (ppb) levels.

Generally, Metal oxide semiconductor sensors are available on the market. The operational temperature of such sensor system is high. The performance (sensitivity and selectivity) of the sensor is significant [53-55]. The Scientific community is focused to work on room temperature operated sensor system. Some reports are available on conducting polymer based sensors. It is operated at room temperature. The advantages of the sensor materials are sensitive layer of gases, intrinsic conductivity, fast response, low cost, light weight, ease of synthesis, stability in air and particularly, their sensitivity at the room temperature [56-58]. In conducting polymer family, one of the members is polyaniline. It is exist in two forms. Former is called polyaniline emeraldine base and is insulating ($\sigma \sim 10^{-5}$ S/cm) nature. Later one is polyaniline emeraldine salt and is metallic nature ($\sigma < 1000$ S/cm). The metallic nature is acquired by doping process [59-64]. Two forms of polyaniline polymer are completely different their chemical and physical properties. Several reports are available to CO sensing mechanism of polyaniline based sensor materials [65-68]. There is a partial charge transfer from polyaniline nitrogen atom to carbon atom of CO molecules, which leads to an alternation in the conductivity of a conducting polymer [65-68]. So, the possible sensing mechanism is shown in the Figure 12 [66, 68].

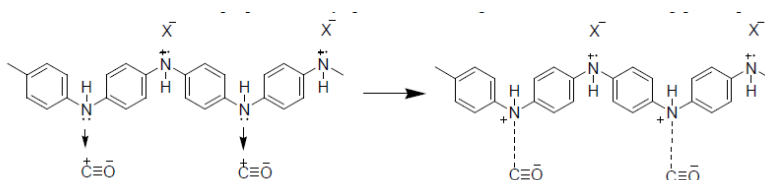


Figure 12. [78, 80] Possible carbon monoxide and polyaniline gas sensing mechanism

The chemistry of partial charge transfer from amine nitrogen: --NH-- which have lone pair of electrons to stable resonating structure of $+\text{C}\equiv\text{O--}$ having the positive charge at the carbon atom. Hence, the positive charge at the carbon atom is shifted to amine nitrogen atom. It results in a net increase in positive charge carriers on the polymer backbones. Therefore, conductivity of the material is increased. A summary

of health problems caused by exposure to CO is presented in Table 5 and brief summary of conducting polymer based CO detection is mentioned in Table 6.

Table 5. Health problems according to carbon monoxide (CO) concentration and exposure time

Concentration of CO (Exposure Time)	Created health problems
35 ppm (6-8 h), 100-200 ppm (2-3 h), 400 ppm (1-2 h), 800 ppm (45 min), 1600 ppm (20 min), 3200 ppm (5-10 min), 6400 ppm (1-2 min)	Headache, dizziness, nausea, loss of judgement and convulsions
1600 ppm (2h)3200 ppm (30min.), 6400 ppm (less than 20 min.), 12,800 ppm (less than 3 min.)	Respiratory arrest, severe conditions (coma) and death

Table 6. Brief summary of CO detection

Study	Materials	Perporfamce	Optimum temperature (°C)	Limitation
Zhao et al.[69]	Polyaniline coated nanofiber	Response time 20 s	Room temperature	Low concentration CO
Liu et al. [70]	polyaniline nanofiber	Response 400 s	Room Temperature	Low CO concentration
Jian et al. [71]	Polyaniline/SnO ₂ Nanocomposite	Response time 160 s	Room Temperature	Low CO concentration
Ram et al. [72]	Ultrathin conducting polymer/metal oxide (SnO ₂ and/or TiO ₂) films	Response time 60 s	Room Temperature	High CO concentration

Conclusions

At room temperature, HCl doped DL-PLA/PANI composites were successfully prepared by *in situ* polymerization technique. SEM characterization reveals that the prepared composites were showed fibrous morphology. ATR-FTIR spectroscopic experiment of DL-PLA polymer and PANI salt indicate that the main chemical structures are identical to those of DL-PLA polymer, the emeraldine salt form of PANI while DL-PLA/PANI nanofibers point to the combination of DL-PLA polymer and PANI salt. UV-Vis's spectra measurements show that the electronic transitions of prepared materials are indicated the emeraldine salt form of PANI on DL-PLA film. Room temperature DC conductivity of prepared composites has shown ohmic behaviour and its value was found to be higher for 2 (M) HCl doped DL-PLA/PANI composite (0.1628×10^{-2} S/cm) than prepared other composites. In addition, we measured DC conductivity as a function of temperature (70–300 K) of

HCl doped DL-PLA/PANI composites and obeyed semiconducting behaviour. Conduction mechanism was studied using temperature dependence of the DC conductivity experiment. In this experiments, metallic ($T > 110$ K) and localised systems ($T < 110$ K) were observed. The conductivity was found to be controlled by the electron–electron scattering and electron–phonon scattering in case of metallic and localised character, respectively. The temperature dependence magnetoresistivity of HCl doped DL-PLA/PANI composites were performed in the range of 70–300 K at 0.5 T to estimate the L_{loc} of 31.20 nm, 146 nm, and 87.80 nm for 1 (M)–, 2 (M)–, and 3 (M) HCl-doped DL-PLA/PANI composites, respectively. As well, we calculated important transports parameters like $N(E_F)$, T_{Mott} , L_{loc} , R_{hop} , and Δ_{hop} for better understanding of conducting process. The main results obtained from MC are summarized as follows: (1) The sign of MC in the prepared composite films is negative at different temperatures i.e. 50 K, 100 K, 200 K, 300 K in the range of magnetic field (0.1–0.7 tesla). The negative MC increases with lowering temperature. (2) The negative MC is discussed in terms of a quantum interference effect in hopping conduction process. These results suggest that the MC in the composite films made of is controlled by a random network of inter-fibril contacts. Moreover, the prepared composites show features of coherent transport of electrons that persist until high temperatures, making them attractive for further investigations aimed at development of novel devices. In summary, the present work reports the preparation, detailed morphological and spectral, electrical properties with mechanism of HCl doped DL-PLA/PANI composites. In particulars, carbon monoxide gas responses and mechanism of polyaniline-based materials were studied.

Acknowledgements

The author conveys their sincere thanks to the CRF, IIT Kharagpur for their providing testing facilities and Materials Science Centre to do the research work. I would like to thank Prof. Debabrat Pradhan for their invaluable guidance, advices, constant inspiration and technical support throughout the entire research program.

References

- [1] Abidian, M.R., Kim, D.H., and Martin, D.C. 2006, Conducting Polymer Nanotubes for Controlled Drug Release, *Advanced Materials*, Vol. 18, pp. 405-409.
- [2] Komarova, E., Aldissi, M., and Bogomolova, A. 2005, Direct Electrochemical Sensor for Fast Reagent-Free DNA Detection, *Biosensor and Bioelectronics*, Vol. 21, pp. 182-189.
- [3] Ohtani, A., Abe, M., Ezoe, M., Doi, T., Miyata, T., and Miyake, A., 1993, Synthesis and Properties of High-Molecular-Weight Soluble Polyaniline and its Application to the 4mb-Capacity Barium Ferrite Floppy Disks Antistatic Coating, *Synthetic Metals*, Vol. 57, pp. 3696-3701.

- [4] Gustafsson, G., Cao, Y., Treacy, G.M., Klavetter, F., Colaneri, N., and Heeger, A.J. 1992, Flexible Light-Emitting Diodes Made from Soluble Conducting Polymers, *Nature*, Vol. 357, pp. 477-479.
- [5] Rudge, A., Raistrick, I., Gottesfeld, S., and Ferraris, J.P. 1994, A Study of the Electrochemical Properties of Conducting Polymers for Application in Electrochemical Capacitors, *Electrochemical Acta*, Vol. 39, pp. 273-287.
- [6] Ryu, K.S., Kim, K.M., Kang, S.G., Lee, G. J., Joo, J., and Chang, S.H. 2000, Electrochemical and Physical Characterization of Lithium Ionic Salt Doped Polyaniline as a Polymer Electrode of Lithium Secondary Battery, *Synthetic Metas*, Vol.3, pp. 213-217.
- [7] MacDiarmid, A.G., and Zheng, W.G. 1997, Electrochemistry of Conjugated Polymers and Electrochemical Applications, *Materials Research Society Bulletin*, Vol. 22, pp. 24-30.
- [8] Sathiyarayanan, S., Dhawan, S.K., Trivedi, D.C., and Balakrishnan, K.1992, Soluble Conducting Poly Ethoxy Aniline as an Inhibitor for Iron in HCl, *Corrosion Science*, Vol. 33, pp. 1831-1841.
- [9] Kaneto, K., Kaneko, H., Takashima, W.J., 1995, Response of Chemomechanical Deformation in Polyaniline Film on Variety of Anions, *Japanese Journal of Applied Physics*, Vol. 34, pp. 837- 840.
- [10] Aliwi, S.M., Hassan, A.K., 2008, Interaction of Thin Films of Hydroxo-Oxobis (8-Quinolyloxo) Vanadium (V) with Ammonia Vapour, *Sensor and Actuators B*, Vol. 133, pp. 521-525.
- [11] M. S. Cho, S. Y. Park, J. Y. Hwang, H. J. Choi, 2004, Synthesis and Electrical Properties of Polymer Composites with Polyaniline Nanoparticles, *Materials Science and Engineering C*, Vol. 24, pp. 15-18.
- [12] Diaz, A.F., and Logan, J.A. 1980, Electroactive Polyaniline Films, *Journal of Electroanalytical Chemistry*, Vol. 111, pp. 111-114.
- [13] Cao, Y., Andreatta, A., Heeger, A.J., Smith, P. 1989, Influence of Chemical Polymerization Conditions on the Properties of Polyaniline, *Polymer*, Vol. 30, pp. 2305-2311.
- [14] Kingsborough, R.P., and Swager, T.M. 1998, Electroactivity Enhancement by Redox Matching in Cobalt Salen-Based Conducting Polymers, *Advanced Materials*, Vol. 10, pp. 1100-1104.
- [15] Omastova, M., Pavlinec, J., Pionteck, J., Simon, F., and Kosina, S. 1998, Chemical Preparation and Characterization of Conductive Poly(Methyl Methacrylate)/Polypyrrole Composites, *Polymer*, Vol. 39, 6559-6566.
- [16] Nikpour, M., Chaouk, H., Mau, A., Chung, D.J., and Wallace, G., 1999, Porous Conductive Films based on Polypyrrole-PMMA Composites, *Synthetic Metals*, Vol. 99, pp. 121-126.

- [17] Cairns, D.B., Armes, S.P., and Bremer, L.G.B. 1999, X-ray Photoelectron Spectroscopy Characterization of Submicrometer-Sized Polypyrrole-Polystyrene Composites, *Langmuir*, Vol. 15, pp. 8052-8058.
- [18] He, F., Omoto, M., Yamamoto, T., and Kise, H. 1995, Preparation of Polypyrrole-Polyurethane Composite Foam by Vapour Phase Oxidative Polymerization, *Journal of Applied Polymer Science*, Vol. 55, pp. 283-287.
- [19] Huang, L., Hu, J., Lang, L., Wang, X., Zhang, P., Jing, X., Wang, X., Chen, X., Lelkes, P.I., MacDiarmid, A.G., and Wei, Y. 2007, Synthesis and Characterization of Electroactive and Biodegradable ABA Block Copolymer of Polylactide and Aniline Pentamer, *Biomaterials*, Vol. 28, pp. 1741-1751.
- [20] Tuan VO-DINH, T. 2004, biosensors, nanosensors and biochips: Frontiers in Environmental and Medical Diagnostics, the 1st International Symposium on Micro & Nano Technology, 14-17 march, 2004, Honolulu, Hawaii, USA.
- [21] Shi, G., Rouabhia, M., Wang, Z., Dao, L.H., and Zhang, Z. 2004, A Novel Electrical Conductive and Biodegradable Composite Made of Polypyrrole and Polylactide, *Biomaterials*, Vol. 25, pp. 2477-2488.
- [22] Aleshin, A.N., Williams, S.R., and Heeger, A.J. 1998, Transport Properties of Poly(3, 4-ethylenedioxythiophene)/Poly(styrenesulfonate), *Synthetic Metals*, Vol. 94, pp. 173-177
- [23] Duvail, J.L., Retho, P., Garreau, S., Laurant, G., Godon, C., and Demoustier-Champagnon, S. 2002, Transport and Vibrational Properties of Poly(3,4-Ethylenedioxythiophene) Nanofibers, *Synthetic Metals*, Vol. 131, pp. 123-128.
- [24] Skotheim T.A., Elsenbaumer R.L., and Reynolds J.R. 1998 *Handbook of Conducting Polymers* 2nd edn (New York: Dekker) pp 27-121.
- [25] Kaiser, A.B. 2001, Electronic Transport Properties of Conducting Polymers and Carbon Nanotubes, *Reports on Progress in Physics*, Vol. 64, pp. 1-49.
- [26] Coehoorn, R. Lecture Notes 2003, Novel Magnetoelectronic Materials and Devices, Exchange-Biased Spin-Valves.
- [27] Ghosh, M., Barman, A., Meikap, A.K., De, S.K., Chatterjee, S. Chattopadhyay, S.K. 2000, Electrical Resistivity and Magnetoresistivity of Protonic Acid (H₂SO₄ and HCl)-Doped Polyaniline at Low Temperature, *Journal of Applied Polymer Science*, Vol. 75, pp. 1480-1486.
- [28] Chiquito, A.J., Lanfredi, A.J.C., Oliveira, R.F.M. de, Pozzi, L.P. and Leite, Ed. R. 2007, Electron Dephasing and Weak Localization in Sn Doped In₂O₃ Nanowires, *Nano letter*, Vol. 7, pp. 1439-1443.
- [29] Taunk, M., Kapil, A., and Chand, S. 2008, Synthesis and Electrical Characterization of Self-Supported Conducting Polypyrrole-Poly(vinylidene fluoride) Composite Films, *The Open Macromolecular Journal*,

Vol. 2, pp. 74-79.

- [30] Zhang, Z. , Wei, Z., Wa, M. 2002, Nanostructures of Polyaniline Doped with Inorganic Acids, *Macromolecules*, Vol. 35, pp. 5937-5942.
- [31] Mukherjee, K., Majumdar, S.B., 2009, Analyses of Response and Recovery Kinetics of Zinc Ferrite as Hydrogen Gas Sensor, *Journal of applied Physics*, Vol. 106, pp. 064912-064922.
- [32] Huang, J.W., Hung, Y.C., Wen, Y.L., Kang, C.C., and Yeh, M.Y. 2009, Polylactide/Nano and Microscale Silica Composite Films. I. preparation and characterization, *Journal of Applied Polymer Science*, Vol. 112, pp. 1688-1694.
- [33] Arenas, M.C., Andablo, E., and Castaño, V.M. 2010, Synthesis of Conducting Polyaniline Nanofibers from Single and Binary Dopant Agents, *Journal of Nanoscience and Nanotechnology*, Vol. 10, pp. 549-554.
- [34] Shameli, K., Ahmad ,M. Bin, Md Zin Wan Yunus, W., Ibrahim, N.A., Jokar, M., Darroudi, M. 2010, Synthesis and Characterization of Silver/Polylactide Nanocomposites, *World Academy of Science, Engineering and Technology*, Vol. 64, pp. 28-32.
- [35] Tzou, K., and Gregory, R.V. 1993, a Method to Prepare Soluble Polyaniline Salt Solutions—*in situ* Doping of PANI Base with Organic Dopants in Polar Solvents, *Synthetic Metals*, Vol. 53, pp. 365-377.
- [36] Lossy, R., Pappas, D.L., Roy, R.A., and Cuomo, J.J., and Sura, V.M. 1992, Filtered Arc Deposition of Amorphous Diamond, *Applied Physics Letter*, Vol. 61, pp. 171-173.
- [37] Li, J., Fang, K., Qiu, H., Li, S., and Mao, W. 2004, Micromorphology and Electrical Property of the HCl-Doped and DBSA-Doped Polyaniline, *Synthetic Metals*, Vol. 142, pp. 107-111.
- [38] Shameli, K., Ahmad, M. Bin, Wan Yunus, W. Md Zin, Ibrahim, N.A., Jokar, M., and Darroudi, M. 2010, Synthesis and Characterization of Silver/Polylactide Nanocomposites, *World Academy of Science, Engineering, and Technology.*, Vol. 64, pp. 28-32.
- [39] (50) Sinha, S., Bhadra, S., and Khastagir, D.J. 2009, Effect of Dopant Type on the Properties of Polyaniline, *Journal of Applied Polymer Science*, Vol. 112, pp. 3135-3140.
- [40] Thornton, T.J., Roukes, M.L., Scherer, A., and Van der Gaag, B.P. granular nanoelectronics; Ferry, D.K., and Baker, J R. Eds. C. Jacoboni, NATO ASI Series; Plenum Press: New York, 1991.
- [41] Berengue, O.M., Chiquito, J., Pozzi, L.P., Lanfredi, A.J. de Castro, and Leite, E.R. 2009, Electron-Phonon Scattering in Sn-Doped In₂O₃ FET Nanowires Probed by Temperature-Dependent Measurements,

- Nanotechnology, Vol. 20, pp. 245706-xxx.
- [42] Lin, J.J. and Bird, J.P. 2002, Recent Experimental Studies of Electron Dephasing in Metal and Semiconductor Mesoscopic Structures, *Journal of Physics: Condensed Matter*, Vol. 14, pp. R501–R596.
- [43] Chakraborty, G., Gupta, K., Meikap, A.K., and Jana, P.C. 2010, Direct Current Electrical Transport and Magneto Transport Properties of Polyaniline Nanocomposites, *Journal of Physical Science*, Vol. 14, pp.207-218.
- [44] Long, Y., Chen, Z., Shen, J., Zhang, Z., Zhang, L., Huang, K., Wan, M., Jin, A., Gu, C., and Duvail, J.L. 2006, Magnetoresistance Studies of Polymer Nanotube/Wire Pellets and Single Polymer Nanotubes/Wires, *Nanotechnology*, Vol. 17, pp. 5903–5911.
- [45] Wang, Z.H., Javadi, H.H.S., Ray, A., Macdiarmid, A.G., and Epstein, A. J. 1990, Electron Localization in Polyaniline Derivatives, *Physical Review B (Rapid communication)*, Vol. 42, pp. 5411-5414.
- [46] Li, W., and Wan, M. 1998, Porous Polyaniline Films with High Conductivity, *Synthetic Metals*, Vol. 92, pp. 121-126.
- [47] Beutler, D.E., and Giordano, N. 1988, Localization and Electron–Electron Interaction Effects in Thin Bi Wires and Films, *Physical Review, B*, Vol. 38, pp. 8-19.
- [48] Nandy, T., Coutu, R.A., and Ababei, C., 2018, Review Carbon Monoxide Sensing Technologies for Next-Generation Cyber-Physical Systems, *Sensors*, Vol. 18, p. 3443-3469.
- [49] Varon, J., Marik, P.E., Fromm, R.E., Jr. and Gueler, A. 1999, Carbon Monoxide Poisoning: a Review for Clinicians, *Journal of Emergency Medicine*, Vol. 17, pp. 87-93.
- [50] Raub, J.A., Mathieu-Nolf, M., Hampson, N.B., and Thom, S.R. 2000, Carbon Monoxide Poisoning-A Public Health Perspective, *Toxicology*, Vol. 145, pp. 1-14.
- [51] Respiratory Health–Air Pollution, Boston University School of Public Health. Available online:<http://sphweb.bumc.bu.edu/otlt/MPH-Modules/PH/RespiratoryHealth/RespiratoryHealth7.html> (accessed on 28 September 2018).
- [52] Harper, A. and Croft-Baker, J. 2004, Carbon Monoxide Poisoning: Undetected by both Patients and Their Doctors, *Age Ageing*, Vol. 33, pp. 105-109.
- [53] Goldstein, M. 2008, Carbon Monoxide Poisoning, *Journal of Emergency Nursing*, Vol. 34, pp. 538-542.

- [54] Pijolat, C., Pupier, C., Sauvan, M., Tournier, G., and Lalauze, R. 1999, Gas Detection for Automotive Pollution Control, Sensor and Actuators B, Vol. 59, pp. 195-202.
- [55] Meixner, H., Gerblinger, J., Lampe, U., and Fleischer, M. 1995, Thin-Film Gas Sensors based on Semiconducting Metal Oxides, Sensor and Actuators B, Vol. 23, pp. 119-125.
- [56] Lim, J.-W., Kang, D.-W., Lee, D.-S., Huh, J.-S., and Lee, D.-D. 2001, Heating Power-Controlled Micro-Gas Sensor Array, Sensor and Actuators B, Vol. 77, pp. 139-144.
- [57] Zhang, W., de Vasconcelos, E.A., Uchida, H., Katsube, T., Nakatsubo, T., and Nishioka, Y. 2000, A Study of Silicon Schottky Diode Structures for NO_x Gas Detection, Sensor and Actuators B, 65, pp. 154-156.
- [58] Rickerby, D.G., Horrillo, M.C., Santos, J.P., and Serrini, P. 1997, Microstructural characterization of nanograin tin oxide gas sensors, Nanostructured Materials, Vol. 9, pp. 43-52.
- [59] J. Melendez, A.J. de Castro, F. Lopez, J. Meneses, 1995, Spectrally Selective Gas Cell for Electrooptical Infrared Compact Multi-Gas Sensor, Sensor and Actuators A, Vol. 46-47, pp. 417-421.
- [60] McQuade, D.T., Pullen, A.E., and Swager, T.M., 2000, Conjugated Polymer based Chemical Sensors, Chemical Reviews, Vol. 100, pp. 2537-2574.
- [61] Monkman, A.P., Petty, M.C., Agbor, N.E., and Scully, M.T. Polyaniline Gas Sensor, US Patent 5536473, 16 July 1996.
- [62] Torsi, L., Pezzuto, M., Siciliano, P., Rella, R., Sabbatini, L., Valli, L., and Zambonin, P.G. 1998, Conducting Polymers Doped with Metallic Inclusions: New Materials for Gas Sensors, Sensor and Actuators B, Vol. 48, pp. 362-367.
- [63] Chiang, J.C., and MacDiarmid, A.G. 1986, Polyaniline: a New Concept in Conducting Polymers, Synthetic Metals, Vol. 13, pp. 193-xxx.
- [64] Dhawan, S.K., Kumar, D., Ram, M.K., Chandra, S., and Trivedi, D.C. 1997, Application of Conducting Polyaniline as Sensor Material for Ammonia, Sensor and Actuators Vol. 40, pp. 99-103.
- [65] Paddeu, S., Ram, M.K., and Nicolini, C. 1998, Langmuir-Schaefer Films of a Poly(O-Anisidine) Conducting Polymer for Sensors and Displays, Nanotechnology, Vol. 9, pp. 228-236.
- [66] Dixit, V., Misra, S.C.K., and Sharma, B.S. 2005, Carbon Monoxide Sensitivity Of Vacuum Deposited Polyaniline Semiconducting Thin Films, Sensor and Actuators B, Vol. 104, pp. 90-93.
- [67] Densakulprasert, N., Wannatong, L., Chotpattananont, D., Hiamtup, P.,

- Sirivat, A., and Schwank, J. 2005, Electrical Conductivity Of Polyaniline/Zeolite Composites and Synergetic Interaction with CO, Materials Science and Engineering B-Solid State for Materials Advanced Technology, 117, 276-282.
- [68] Misra, S.C.K., Mathur, P., and Srivastava, B.K. 2004, Vacuum-Deposited Nanocrystalline Polyaniline Thin Film Sensors for Detection of Carbon Monoxide, Sensor and Actuators A, Vol. 114, pp. 30-35.
- [69] Watcharaphalakorn, S., Ruangchuay, L., Chotpattahanont, D., Sirivat, A., and Schwank, J. 2005, Polyaniline/Polyimide Blends as Gas Sensors and Electrical Conductivity Response to CO-N₂ Mixtures, Polymer International, Vol. 54, pp. 1126-1133.
- [70] Zhao, J., Wu, G., Hu, Y., Liu, Y., Tao, X., and Chen, W. 2015, A Wearable And Highly Sensitive Co Sensor with a Macroscopic Polyaniline NanoFiber Membrane, Journal of Materials Chemistry A, Vol. 3, pp. 24333-24337.
- [71] Liu, C., Noda, Z., Sasaki, K., and Hayashi, K. 2012, Development of A Polyaniline Nanofiber-based Carbon Monoxide Sensor for Hydrogen Fuel Cell Application, International Journal of Hydrogen Energy, Vol. 37, pp. 13529-13535.
- [72] Jian, K.-S., Chang, C.-J., Wu, J.J., Chang, Y.-C., Tsay, C.-Y., Chen, J.-H., Horng, T.-L., Lee, G.-J., Karuppasamy, L., Anandan, S., and Chen, C.-Y. 2019, High Response CO Sensor Based on a Polyaniline/SnO₂ Nanocomposite, Polymers, Vol. 11, pp. 184-200.
- [73] Ram, M.K., Yavuz, O.Z., Lahsangah, V., and Aldissi, M. 2005, CO Gas Sensing from Ultrathin Nano-Composite Conducting Polymer Film, Sensors and Actuators B, Vol. 106, pp. 750-757.